Nonisothermal flows of viscoelastic fluids

Thermodynamics, analysis and numerical simulation

Nonisothermal flows of viscoelastic fluids

Thermodynamics, analysis and numerical simulation

De niet-isotherme stroming van visco-elastische vloeistoffen

Thermodynamica, analyse en numerieke simulatie

PROEFSCHRIFT

ter verkrijging van de graad van doctor
aan de Technische Universiteit Delft,
op gezag van de Rector Magnificus Prof. ir. K.F. Wakker,
in het openbaar te verdedigen ten overstaan van een commissie,
door het College van Dekanen aangewezen,
op maandag 26 februari 1996 te 16.00 uur

door

PETER WAPPEROM
wiskundig ingenieur,
geboren te Dordrecht.

Contents

Summary

Nonisothermal flows of viscoelastic fluids:
Thermodynamics, analysis and numerical simulation.

Peter Wapperom

Dependent on the time scale of the flow, viscoelastic materials mainly show viscous or elastic behaviour. In recent years much progress has been made with the numerical simulation of flows of viscoelastic materials. For example, it has become possible to calculate stationary flows with high Deborah numbers. Mostly this was restricted to isothermal flows. However, in practice many flows are nonisothermal. On the one hand due to the external cooling or heating, on the other hand due the internal production of heat, for example by the dissipation of mechanical energy.

Besides the usual balances of mass, linear momentum, angular momentum and energy, some equations are needed to describe the specific behaviour of the polymeric material. These so-called constitutive equations are necessary for the stress, the heat flux and the internal energy. General equations for these quantities will be derived from the thermodynamics, where internal (tensor) variables will be used to describe the relaxation phenomena. These internal tensor variables are a measure for the elastic deformation of a polymeric fluid. The resulting equations include the differential models for the stress that are commonly used in the literature. The resulting equation for the heat flux is an extension of the well-known Fourier law. The heat conduction tensor may depend on the (elastic) deformation of the material. With this dependence the experimentally observed anisotropy of the heat conduction tensor may be described, i.e. an increasing thermal conductivity in the direction of orientation and a decreasing thermal conductivity in the direction perpendicular to the orientation. Finally the balance of internal energy may be written as a temperature equation with the help of the thermodynamics. For this, it is important to distinguish the irreversible (dissipative) and reversible processes. This is possible with the help of the balance of entropy. Particularly, the temperature dependence of the density and the shear modulus appear to be important. Although these coefficients are relatively weak functions of the temperature, they do have a large influence on the reversible processes in the temperature equation. The temperature dependence of the density results in a cooling during expansion and a heating during compression. The temperature dependence of the shear modulus determines whether the reversible energy is stored as internal energy (energy elastic) or as entropy (entropy elastic). If the storage of energy is entropy elastic, a part of the temperature changes are reversible. If the free energy, or equivalently the stress model, of a viscoelastic fluid is known, it is possible to relate all thermodynamic coefficients in the temperature equation to experimental data in equilibrium, for example the thermal expansion coefficient and the heat capacity at constant pressure. The consequences for viscoelastic materials will be elucidated by means of the 'neo-Hookean' model, which is often used in the literature. On the basis of experimental data from the literature the order of magnitude of

the temperature dependences of the thermodynamic coefficients will be reviewed. Furthermore, an overview of nonisothermal rheological experiments will be included which indicate that the temperature history is important. Through dimensional analysis it will be checked which temperature effects may be important in shear flows.

It is too difficult to solve the complete, coupled system of equations analytically. When the coefficients are independent of the temperature, however, analysis of the equations is possible for steady flows. In a shear flow and a uniaxial elongation flow the behaviour of some well-known differential models will be worked out for high deformation rates. With these results the consequences will be examined for a simple model, with constant coefficients, for the anisotropy of the heat conduction tensor. The simple model does not give a qualitative agreement with the experimental data for all stress models. Only if the stress model has a second normal stress difference, the decrease of the thermal conductivity perpendicular to the flow can be described. If the coefficients are assumed to depend on the invariants the qualitative agreement is still possible for the other stress models.

The system of nonisothermal equations has been implemented in a computer program for isothermal flows of viscoelastic fluids. The equations of motion and the temperature equation have been solved by using a finite element method. The stresses have been calculated by a streamline integration method. For the numerical solution process a number of problems arise. For the temperature equation a standard upwind method (SUPG) has been used to avoid too much grid refinement for convection-dominated flows. Another problem arises when the mechanical dissipation has to be calculated. For this, the inverse of the internal deformation tensor is needed. Although theoretically the internal deformation tensors are positive definite, they may become indefinite due to numerical errors. To avoid large numerical errors in the mechanical dissipation, a positive lower bound of the determinant of the internal deformation tensor is needed then. A method has been developed to determine the theoretical lower bound of the determinant. For many models a positive lower bound can be obtained. The outflow boundary condition also requires some extra attention. In convection-dominated flows it is often necessary to prescribe an approximation of the normal stress due to the normal stress differences of viscoelastic fluids. A Dirichlet boundary condition or a constant pressure at the outflow does not work then.

For the numerical calculations two different polymer melts will be taken: a polyethylene (LDPE) and a polystyrene (PS 678E) melt. These fluids show a different behaviour for the same type of flow. The viscosity of the polystyrene melt is a much stronger function of the temperature than for the polyethylene melt. On the other hand the anisotropy of the heat conduction tensor of polystyrene is much smaller than for polyethylene. For the numerical calculations the influence of the mechanical dissipation, the anisotropy of the heat conduction tensor, the cooling due to the thermal expansion and the temperature dependence of the shear modulus will be examined in more detail. Firstly the simple case of a fully developed axisymmetrical pipe flow will be discussed. Except the mechanical dissipation, the cooling due to the thermal expansion and the anisotropy of the heat conduction tensor, may be important, particularly for high flow rates (Brinkman numbers). For LDPE the decrease of the thermal conductivity perpendicular to the flow may cause a considerable increase of the temperature. Next a Graetz–Nusselt problem, with a temperature jump on the wall, will be examined. Due to the dominance of the convection, the mechanical dissipation and the cooling due to the

thermal expansion are less important. The solution is mainly determined by convection and diffusion. For LDPE the anisotropy of the heat conduction tensor may become very large. This is mainly caused by the large values of the thermal conductivity parallel to the flow. Finally the flow through a 4:1 contraction will be considered. For this problem a vortex may arise in the entry corner. For LDPE the internal production of heat is not very important (due to the dominance of the convection). For PS, however, the internal heat production may be important, particularly for the vortex intensity. If the wall is cooled from the contraction, the magnitude of the vortex also changes, particularly for PS. Although the difference between the mechanical dissipation and the stress work are large near the contraction, the influence on the temperature distribution is relatively small due to the dominance of the convection. For LDPE the anisotropy of the heat conduction tensor also appears to be important. Besides a decrease in the direction to the flow, the thermal conductivity perpendicular to the flow may become very large.

Samenvatting

De niet-isotherme stroming van visco-elastische vloeistoffen:
Thermodynamica, analyse en numerieke simulatie.

Peter Wapperom

Visco-elastische materialen vertonen, afhankelijk van de tijdschaal van de stroming, voornamelijk viskeus of elastisch gedrag. De laatste jaren is er veel vooruitgang geboekt op het gebied van de numerieke simulatie van stromingen van deze materialen. Zo is het mogelijk geworden stationaire stromingen voor hoge Deborah getallen te berekenen. Dit beperkte zich veelal tot isotherme stromingen. In de praktijk zijn veel stromingen echter niet isotherm. Enerzijds vanwege koeling of verwarming van buitenaf, anderzijds vanwege interne warmteproduktie door bijvoorbeeld dissipatie van mechanische energie.

Naast de gebruikelijke balansvergelijkingen voor massa, impuls, impulsmoment en energie, zijn nog een aantal vergelijkingen nodig om het specifieke materiaalgedrag van polymeren te beschrijven. Deze zogenaamde constitutieve vergelijkingen zijn nodig voor de spanning, de warmteflux en de interne energie. Algemene vergelijkingen voor deze grootheden worden afgeleid vanuit de thermodynamica, waarbij inwendige (tensor)variabelen worden gebruikt om de relaxatieverschijnselen te beschrijven. Deze inwendige tensorvariabelen zijn een maat voor de elastische deformatie van het materiaal. De resulterende vergelijkingen omvatten de in de literatuur veel gebruikte differentiaalmodellen voor de spanning. Voor niet-isotherme stromingen is vooral de sterke temperatuurafhankelijkheid van de materiaalfuncties, zoals de viscositeit en de normaalspanningscoëfficiënten van belang. De resulterende vergelijking voor de warmteflux is een uitbreiding van de bekende wet van Fourier. De warmtegeleidingstensor kan afhangen van de (elastische) deformatie van het materiaal. Hiermee kan de experimenteel waargenomen anisotropie van de warmtegeleidingstensor worden beschreven: een toename van de warmtegeleiding in de richting van de deformatie en een afname in de richting loodrecht daarop. Tenslotte kan de interne-energiebalans met behulp van de thermodynamica worden omgeschreven in een temperatuurvergelijking. Hierbij is het van belang de irreversibele (dissipatieve) en reversibele processen te onderscheiden. Dit kan met behulp van de entropievergelijking. Vooral de temperatuurafhankelijkheid van de dichtheid en de afschuifmodulus blijken belangrijk te zijn. Hoewel deze coëfficiënten niet zo sterk van de temperatuur afhangen, hebben ze toch een grote invloed op de reversibele processen in de temperatuurvergelijking. Zo veroorzaakt de temperatuurafhankelijkheid van de dichtheid de koeling bij expansie en opwarming bij compressie. De temperatuurafhankelijkheid van de modulus bepaalt of de reversibele energie wordt opgeslagen als interne energie (energie-elastisch) of als entropie (entropie-elastisch). Indien de opslag entropie-elastisch is, is een gedeelte van de temperatuurverandering reversibel. Indien de vrije energie, dan wel het spanningsmodel, voor een visco-elastische vloeistof bekend is, kunnen alle thermodynamische coëfficiënten in de temperatuurvergelijking gerelateerd worden aan experimentele data in evenwicht, zoals de thermische-expansiecoëfficiënt en de warmtecapaciteit bij

constante druk. De consequenties worden toegelicht aan de hand van het 'neo-Hookean' model, dat vaak gebruikt wordt in de literatuur. Aan de hand van experimentele gegevens uit de literatuur wordt voor polymeren een overzicht gegeven van de orden van grootte van de temperatuurafhankelijkheden van alle coëfficiënten. Tevens is hierbij inbegrepen een overzicht van niet-isotherme reologische experimenten, welke aangeven dat de temperatuurgeschiedenis van belang is. Via dimensieanalyse wordt nagegaan welke temperatuureffecten belangrijk zijn in afschuifstromingen.

Het analytisch oplossen van het volledige, gekoppelde, stelsel niet-isotherme vergelijkingen is te moeilijk. Voor de stationaire vergelijkingen, met coëfficiënten onafhankelijk van de temperatuur, is een analyse van de vergelijkingen echter wel mogelijk. In een afschuif- en elongatiestroming wordt nagegaan hoe veelgebruikte visco-elastische modellen zich voor grote deformatiesnelheden gedragen. Hiermee zal worden onderzocht wat de consequenties voor een simpel model met constante coëfficiënten zijn voor de anisotropie van de warmtegeleidingstensor. Niet voor alle spanningsmodellen geeft dit simpele model een kwalitatieve overeenkomst met de experimentele data. Alleen indien het spanningsmodel een tweede normaalspanningsverschil bezit, wordt de afname van de warmtegeleiding in loodrechte richting voorspeld. Door de coëfficiënten van de invarianten te laten afhangen wordt dit voor de andere spannningsmodellen ook mogelijk.

Het stelsel niet-isotherme vergelijkingen is geïmplementeerd in een computerprogramma voor isotherme stromingen van visco-elastische materialen. Voor de bewegingsvergelijkingen en de temperatuurvergelijking zijn eindige elementen methoden gebruikt. De spanning wordt via stroomlijnintegratie berekend. Bij het numeriek oplossen van de vergelijkingen ontstaan een aantal problemen. Voor de temperatuurvergelijking is een standaard upwind methode (SUPG) gebruikt, om te veel roosterverfijning voor convectie-gedomineerde stromingen te voorkomen. Een ander probleem doet zich voor bij de berekening van de dissipatie, waarvoor de inverse van de interne-deformatietensor nodig is. Hoewel de interne-deformatietensoren theoretisch gezien positief definiet zijn, kunnen ze door numerieke fouten indefiniet worden. Om grote numerieke fouten in de dissipatie te voorkomen, is dan een positieve ondergrens van de determinant van de interne-deformatietensor nodig. Hiervoor is een methode ontwikkeld waarmee de theoretische ondergrens van de determinant kan worden bepaald. Voor veel modellen kan een positieve ondergrens worden gevonden. Speciale aandacht vergt ook de uitstroomrandvoorwaarde. Vanwege de normaalspanningsverschillen bij visco-elastische vloeistoffen, is het in een door convectie gedomineerde stroming vaak noodzakelijk aan de uitstroomrand een benadering van de normaalspanningen op te leggen. Een Dirichlet of randvoorwaarde of een constante druk op de uitstroomrand werken dan niet.

Voor de berekeningen worden twee verschillende polymeersmelten genomen: een polyethyleen (LDPE) en een polystyreen (PS 678E) smelt. Deze vloeistoffen vertonen namelijk een verschillend gedrag in een zelfde type stromingen. De viscositeit van polystyreen hangt veel sterker van de temperatuur af dan voor polyethyleen. Daarentegen is de anisotropie van de warmtegeleidingstensor van polystyrene veel kleiner dan die voor polyethyleen. Bij de berekeningen wordt nader onderzocht wat de invloed van de dissipatie, de anisotropie van de warmtegeleidingstensor, de koeling door de thermische-expansieterm en de temperatuur afhankelijkheid van de afschuifmodulus zijn. Allereerst wordt het eenvoudige geval van een volledig ontwikkelde axisymmetrische pijpstroming besproken. Behalve de dissipatie kunnen

ook de koeling door de thermische-expansieterm en de anisotropie van de warmtegeleiding van belang zijn, voornamelijk voor hoge debieten (Brinkman getallen). Voor LDPE kan de verlaging van de warmtegeleiding loodrecht op de stroming ook een aanzienlijke temperatuurverhoging veroorzaken. Vervolgens wordt een Graetz–Nusselt probleem, met een temperatuursprong op de wand, onderzocht. Door de dominantie van de convectie, blijken de dissipatie en de koeling door thermische expansie van minder belang. De oplossing wordt vooral bepaald door convectie en diffusie. Voor LDPE blijkt de anisotropie va de warmtegeleiding erg groot te kunnen worden. Deze wordt voornamelijk veroorzaakt door de grote warmtegeleiding parallel aan de stroming. Tenslotte wordt de stroming door een 4:1 contractie behandeld, waarbij een vortex in de hoek in de contractie kan ontstaan. Voor LDPE blijkt de interne warmteproduktie niet erg belangrijk te zijn (door de dominantie van de convectie). Voor PS kan de interne warmteproduktie wel belangrijk zijn, vooral voor de vortexintensiteit. Indien de wand vanaf de contractie gekoeld wordt, wordt naast de vortexintensiteit ook de grootte van de vortex sterk beïnvloed, vooral voor PS. Hoewel het verschil tussen de dissipatie en de spanningsarbeid groot is in de buurt van de contractie, is de invloed op de temperatuurverdeling relatief gering door de dominantie van de convectie. Voor LDPE blijkt ook de anisotropie van de warmtegeleiding van belang te zijn voor de temperatuurverdeling. Naast een afname loodrecht op de stroming, wordt vooral de warmtegeleiding in de stromingsrichting zeer groot.

List of symbols

symbol	description	definition in formula or at page
Italic symbols		
a_T	shift factor	(2.123), (2.124)
$\underline{\underline{b}}$	Finger tensor	(2.12)
$\underline{\underline{b}}_k$	internal deformation tensor	(2.19)
$\underline{\underline{b}}_k^c$	corrected internal deformation tensor	(3.83)
B_k	function of the invariants	(2.19)
Br	Brinkman number	(2.143)
c_b	heat capacity at constant Finger tensor	(2.39)
c_p	heat capacity at constant pressure	(2.34)
$c_{p,b}$	heat capacity at constant pressure and internal deformation	(2.42)
$c_{p,b}^{\text{eq}}$	heat capacity at constant pressure and $\underline{\underline{b}}_k = \underline{\underline{I}}$	p. 33
c_{p,τ_e}	heat capacity at constant pressure and elastic stress	(2.42)
c_{p,τ_e}^{eq}	heat capacity at constant pressure and constant elastic stress in $\underline{\underline{b}}_k = \underline{\underline{I}}$	(2.102)
c_v	heat capacity at constant volume	(2.34)
c_σ	heat capacity at constant stress	(2.39)
C_v	penalty matrix	(4.10)
C_1	constant in WLF and Andrade shift factor	(2.123), (2.124)
C_2	constant in WLF shift factor	(2.123)
d	integration constant for shear stress	(4.49)
$\underline{\underline{d}}$	Eulerian rate-of-deformation tensor	(2.10)
$\underline{\underline{d}}_{\text{irr},k}$	irreversible rate-of-deformation tensor	(2.21)
$\bar{D}$	averaged Eulerian rate-of-deformation tensor	(4.13)
D_{m}^{e}, D_{m}^{v}, D_{m}^{ve}	elastic, viscous and viscoelastic mechanical dissipation	(2.74), (2.69), (2.90)
De	Deborah number	(2.141), (2.146)
e	total energy	(2.9)
$\underline{e}$	unit vector	(2.134)
$\underline{f}$	body force per unit of mass	(2.4)
$\underline{\underline{F}}$	deformation gradient tensor	p. 15
F_T, F_v	right-hand-side vector in the discretised temperature equation and the equations of motion	(4.33), (4.10)
g	gravitation constant	(2.6)

g	free enthalpy per unit of mass	(2.35)
$g_{1,k},\ g_{2,k},\ g_{3,k}$	functions of the invariants of $\underline{\underline{b}}_k$	(3.1)
$\underline{g}$	acceleration due to gravity	(2.6)
$\underline{\underline{g}}_k$	isotropic tensor function of $\underline{\underline{b}}_k$	(2.22)
$G,\ G_0$	shear modulus, total shear modulus	(2.12), (2.151)
G_k	modal shear modulus	(2.19)
$\underline{\underline{G}}$	right-hand-side tensor in streamline integration	(4.38)
Gr	Grashof number	(2.144)
h	maximum size of an element	(4.28)
$\underline{\underline{I}}$	unit tensor	(2.5)
I_ψ	vortex intensity	(5.4)
$I_{1,k},\ I_{2,k},\ I_{3,k}$	first, second and third invariant of the internal deformation tensor	(2.17)
J	Number of nodal points	(4.6)
$\underline{J}_s$	entropy flux	(2.44)
k	Boltzmann constant	p. 46
K	total number of stress modes	(2.15)
L	length	p. 35
L	characteristic length	(2.134)
$\hat{\underline{\underline{L}}}$	modified $\underline{\underline{L}}$ in the mixed convected derivative	(2.23)
$\underline{\underline{L}}$	transpose of the velocity gradient	(2.10)
$M_T,\ M_v$	linearisation matrix for the convective terms in the discretised temperature equation and the equations of motion	(4.34), (4.11)
Ma	Mach number	(2.155)
$\underline{n}$	unit outward normal	(4.4)
N_1	first normal stress difference	(1.2)
N_2	second normal stress difference	(1.3)
$N_T,\ N_v$	discretisation matrix of the convective terms for the temperature equation and the equations of motion	(4.33), (4.10)
Na	Nahme–Griffith number	(2.147)
p	thermodynamic pressure	(2.5)
p_{m}	modified pressure	(2.6)
P_n	conjugate force of a mechanical state variable	(2.28)
Pe	Péclet number	(2.142)
Pe_{m}	mesh Péclet number	p. 91
Q	function of the discretised stresses	(4.10)
Q	flow rate	p. 114
r	external heat source per unit of mass	(2.10)
r	axisymmetrical coordinate	(4.46)
R	cooling rate	p. 48
R	outer radius	p. 113
$\underline{R}$	end-to-end vector of polymer chains	p. 46
$R_T,\ R_v$	residual for the temperature equation and the equations of motion	(4.36), (4.13)
Re	Reynolds number	(2.140)

s	entropy per unit of mass	(2.27)
s	streamline parameter	(4.38)
S_T, S_v	discretisation matrix with contributions of the diffusive part of the temperature equation and the equations of motion	(4.33), (4.10)
S_T^{it}	iteration diffusivity matrix	(4.34)
t	time	p. 48
T	absolute temperature	(2.7)
T_{c}	critical temperature	p. 41
T_{g}	glass transition temperature	p. 41
T^{h}	homogeneous temperature solution	(4.65)
T_{m}	melting temperature solution	p. 41
T^{p}	particular temperature solution	(4.59)
T_{ref}	reference temperature	(2.7)
u	internal energy per unit of mass	(2.10)
$\underline{v}$	velocity	(2.1)
V	characteristic velocity	(2.134)
w	axisymmetrical velocity component	(4.46)
$\underline{\underline{w}}$	vorticity tensor	(2.47)
W	averaged velocity	(5.1)
$\underline{x}$	coordinate vector	(4.6)
Y_k	function in Phan-Thien–Tanner model	(A.6)
z	streamwise direction for axisymmetrical coordinate	(4.46)
z_n	mechanical state variables	(2.28)

Greek symbols

α	thermal expansion coefficient	(2.34)
α_c	temperature coefficient for heat capacity	(2.120)
α_k	parameter in Giesekus and Modified Leonov model	(A.3), (A.5)
$\alpha_{T,b}$	thermal expansion coefficient at constant internal deformation	(2.42)
α_κ	temperature coefficient for heat conduction	(2.121)
α_ρ	linear thermal expansion coefficient	(2.7)
β	opening angle	p. 136
β_k	parameter in Larson and Modified Leonov model	(A.9), (A.5)
β_u	element Péclet number	(4.28)
$\dot{\gamma}$	shear rate	(1.1)
γ_k	non-dimensional shear or elongation rate	p. 59, p. 65
Γ	boundary	p. 99
Γ_{ax}	axis of symmetry, free slip or free streamline boundary	(4.40)
Γ_{w}	fixed wall boundary	(4.39)
Δ	increment	(4.12), (4.35)
Δs_b	(isothermal) entropy change	(2.73), (2.89)
Δc	heat capacity difference	(2.77), (2.95)
Δc^0, Δc^{eq}	heat capacity difference in the reference state or in equilibrium	(2.87), (2.103)
ϵ	elongation ratio	p. 35

$\dot{\epsilon}$	elongation rate	(1.4)
ϵ_k	parameter in Phan-Thien–Tanner model	(A.7), (A.8)
$\epsilon_{T,\mathrm{inc}}$, $\epsilon_{v,\mathrm{inc}}$	truncation criterion for the increment of the temperature and the velocity	(4.37), (4.14)
ϵ_p	penalty parameter	(4.8)
$\epsilon_{T,\mathrm{res}}$, $\epsilon_{v,\mathrm{res}}$	truncation criterion for the residual of the temperature equation and the equations of motion	(4.37), (4.14)
ζ	bead friction coefficient	p. 46
η	steady shear viscosity	(1.1)
η_k	modal viscosity	(2.19)
η_0	zero strain rate viscosity	(2.135)
η_{co}	extra viscosity	(4.13)
η_E	steady elongational viscosity	(1.5)
η_{it}	iteration viscosity	(4.11)
η_{ref}	viscosity at reference temperature	(2.123), (2.124)
η_s	extra viscosity	(2.15)
$\eta_{s,\mathrm{ref}}$	extra viscosity at reference temperature	(2.125)
η_v, $\eta_{s,v}$	bulk viscosity	(2.11), (2.15)
κ_{eq}	heat conduction coefficient in equilibrium	(2.114)
κ_{it}	iteration diffusivity or relaxation factor	(4.34), (4.60)
κ_T	isothermal compressibility	(2.34)
κ_0, κ_1, κ_2	coefficients in the model of the heat conduction tensor	(2.113)
$\kappa_\parallel$	heat conductivity parallel to the deformation	p. 37
$\kappa_\perp$	heat conductivity perpendicular to the deformation	p. 37
$\underline{\underline{\kappa}}$	heat conduction tensor	(2.112)
λ_k	modal relaxation time	(2.19)
$\lambda_{k,\mathrm{ref}}$	modal relaxation time at reference temperature	(2.123)
$\lambda_{0,\mathrm{ref}}$	mean relaxation time at reference temperature	(2.146)
$\underline{\underline{\Lambda}}$, $\underline{\underline{\Lambda}}$, $\underset{\approx}{\Lambda}$	phenomenological coefficient tensors	(2.58)
μ	integration constant for shear stress	(4.49)
ξ_k	parameter in the mixed convected derivative	(2.23)
ξ_u	nondimensional numerical diffusivity	(4.29)
Π_s	entropy production	(2.44)
Π_s^{e}, Π_s^{v}, Π_s^{ve}	elastic, viscous and viscoelastic entropy production	(2.46), (2.45), (2.53)
ρ	fluid density	(2.1)
$\underline{\underline{\sigma}}$	total stress tensor	(2.4)
σ_n	stress in normal direction	(4.41)
$\underline{\sigma}_t$	stress in tangential direction	(4.41)
τ	upwind function	(4.29)
$\underline{\underline{\tau}}$	extra stress tensor	(2.5)
$\underline{\underline{\tau}}_e$	total elastic stress tensor	(2.55)
$\underline{\underline{\tau}}_{e,k}$	elastic modal stress tensor	(2.55)
$\underline{\underline{\tau}}_{\mathrm{irr}}$	irreversible stress tensor	(2.56)
$\underline{\underline{\tau}}_k$	modal stress tensor	(2.15)

Υ	vector with discretised extra stress	p. 82
ϕ_k	function in the modified Leonov model	(A.5)
$\underline{\phi}_q$	heat flux vector	(2.10)
$\underline{\psi}$	Helmholtz free energy per unit of mass	(2.29)
ψ	stream function	(5.4)
ψ_d	test function for the mass equation	(4.1)
ψ_e	test function for the temperature equation	(4.15)
$\underline{\psi}_m$	test function for the momentum equations	(4.2)
$\underline{\psi}_p$	basis functions for the pressure	(4.6)
ψ_T	basis functions for the temperature	(4.7)
ψ_u	upwind test function for the temperature equation	(4.17)
$\underline{\psi}_v$	basis functions for the velocity	(4.6)
Ψ_d	space of test functions ψ_d	(4.1)
Ψ_m	space of test functions $\underline{\psi}_m$	(4.2)
Ψ_e	space of test functions ψ_T	(4.15)
Ψ_u	space of upwind test functions ψ_u	(4.17)
Ψ_1	first normal stress coefficient	(1.4)
Ω	integration area	(4.1)
Ω_e	integration area without element boundaries	(4.1)

Calligraphic symbols

$\mathcal{B}_k$	discretised internal deformation tensor	p. 82
$\mathcal{P}$	discretised pressure	(2.5)
$\mathcal{T}$	discretised temperature vector	p. 82
$\mathcal{V}$	discretised velocity vector	p. 82

Miscellaneous symbols

$(\ )_{\mathrm{ax}}$	subscript denoting a quantity at a symmetry axis
$(\ )^{\mathrm{e}}$	superscript denoting an elastic quantity
$(\ )_{\mathrm{eq}}$, $(\ )^{\mathrm{eq}}$	subscript denoting the equilibrium part
$(\ )^i$	superscript denoting the iteration number
$(\ )_j$, $(\ )^j$	subscript or superscript denoting the nodal point number
$(\ )_k$	subscript denoting the kth stress mode
$(\ )^{\mathrm{min}}$	superscript denoting the minimum value of a quantity
$(\ )_{\mathrm{ref}}$	subscript denoting a quantity at reference temperature
$(\ )^T$	superscript denoting the transpose of a quantity
$(\ )_T$	subscript denoting a temperature quantity
$(\ )_v$	subscript denoting a velocity or momentum quantity
$(\ )^{\mathrm{v}}$	superscript denoting a viscous quantity
$(\ )^{\mathrm{ve}}$	superscript denoting a viscoelastic quantity
$(\ )_{\mathrm{w}}$	subscript denoting a quantity at the wall
$(\ )^*$	superscript denoting a dimensionless quantity

$(\ )_0,\ (\ )^0$	subscript or superscript denoting a quantity in the reference state	
$\|.\|$	maximum norm	(4.14)
$\|.\|$	Euclidean norm	(4.26)
$\|.\|_f$	Euclidean norm over the free degrees of freedom	(4.14)
$\|.\|_t$	Euclidean norm over the total degrees of freedom	(4.14)
$(\ ,\ )$	product of two scalars on Ω	(4.5)
$(\ ,\ )_\Gamma$	product of two scalars on Γ	(4.5)
$(\ ,\ )_{\Omega_e}$	inner product of two scalars on Ω_e	(4.18)
$[\ ,\ ]$	inner product of two vectors on Ω	(4.5)
$[\ ,\ ]_\Gamma$	inner product of two scalars on Γ	(4.5)
$[\ ,\ ]_{\Omega_e}$	inner product of two scalars on Ω_e	(4.18)
$\langle\ ,\ \rangle$	contraction of two tensors on Ω	(4.5)
$\tilde{y}$	discrete approximation of y	
$\underline{y}$	vector	
$\underline{\underline{y}}$	second order tensor	
$\underline{\underline{\underline{y}}}$	third order tensor	
$\underline{\underline{\underline{\underline{y}}}}$	fourth order tensor	
∇	gradient operator	
$\dot{y}$	material derivative of y	
$\overset{\square}{\underline{\underline{y}}},\ \overset{\triangledown}{\underline{\underline{y}}}$	mixed convected derivative and upper-convected derivative of $\underline{\underline{y}}$	(2.23), (2.24)
$\langle\ \rangle$	phase-space average	p. 46
$\left.\dfrac{\partial}{\partial x}\right\|_y$	derivative at constant y	(2.31)
$\left.\dfrac{\partial}{\partial x}\right\|_{\underline{\underline{b}}}$	derivative at constant (internal) deformation	(2.38), (2.41)
$\left.\dfrac{\partial}{\partial x}\right\|_{\underline{\underline{b}}'_k}$	derivative at constant internal deformation, except $\underline{\underline{b}}_k$	(2.41)

Abbreviations

LDPE	low density polyethylene
HDPE	high density polyethylene
PCTFE	polychlorotrifluoroethylene
PMMA	polymethylmethacrylate
PP	polypropylene
PS	polystyrene
PST	polystyrol
PVC	polyvinylchloride

Chapter 1

Introduction

In virtual all products of modern industry polymers are applied as a construction material. The processing of polymers essentially consists of three steps. Firstly the polymer is heated to a temperature above its glass transition in order to facilitate its plastic deformation. Next the polymer is shaped into a product. Finally, the product is cooled back to room temperature and solidified into its final shape. Well-known examples of polymer processing are injection moulding, extrusion and fibre spinning.

In polymer processing both the temperature and the deformation are important. First a short overview will be given of the behaviour of polymeric materials during deformation. Then the extension to nonisothermal flows will be made. The introduction will be ended with the aims and the framework of this thesis.

1.1 Non-Newtonian fluid behaviour

Since macromolecules can be considered as long and thin objects they are oriented in a flowing polymer melt or solution. So deformation of a polymeric fluid causes molecular orientation and thus a degree of anisotropy of the material properties. For this reason the behaviour of these fluids can no longer be described by the simple models that are valid for low molecular weight fluids having a purely viscous behaviour. The main difference between low molecular weight viscous fluids and macromolecular fluids is that the latter possess a material time scale, i.e. a time scale necessary to relax from a deformed state into a stress-free state. Dependent on the ratio of the time scale of the deformation and the material time scale a so-called viscoelastic fluid may behave more or less like a viscous fluid (slow deformations) or on the other side of the spectrum like an elastic material (very fast deformations). The ratio between the material time scale and the time scale of the flow is indicated by a non-dimensional number: the Deborah or the Weissenberg number.

Viscoelastic fluids show unexpected behaviour if ones intuition is based on experiences with viscous fluids. Some well-known examples are rod-climbing (a polymeric fluid climbs up a rotating rod) and die swell (the diameter of a polymeric fluid that exits from a capillary into air grows). For a comprehensive overview of typical viscoelastic phenomena refer to Barnes et al. (1989) or Bird et al. (1987a). Some properties of viscoelastic fluids such as the behaviour of the shear viscosity and the normal stress differences in steady shear flows and the elongational viscosity will be discussed briefly. Of course a lot of different polymeric fluids exist, with different kinds of behaviour. In the following summary only the global trends of the material properties will be indicated. For a comprehensive overview of the viscoelastic properties of polymeric fluids and the used experimental methods refer to Ferry (1980).

- Polymeric fluids have a non-constant shear viscosity. The shear viscosity η is defined by

$$\eta = \frac{\sigma}{\dot{\gamma}}, \tag{1.1}$$

where σ is the shear stress and $\dot{\gamma}$ the shear rate. The shear viscosity may be a strong function of the shear rate and the temperature. In figure 1.1 the generic behaviour of the shear viscosity has been depicted. The shear viscosity curve, at some fixed temperature,
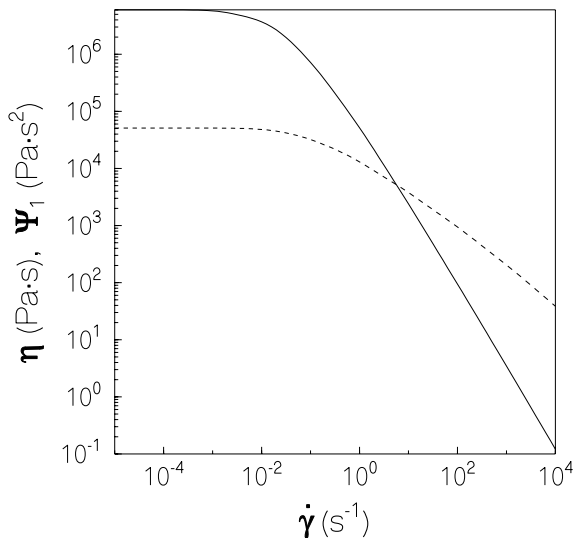

Figure 1.1: Model predictions of the shear viscosity η (dashed line) and first normal stress coefficient Ψ_1 (solid line) for an LDPE melt versus the shear rate. The model predictions are of the eight-mode Giesekus model described in chapter 5.
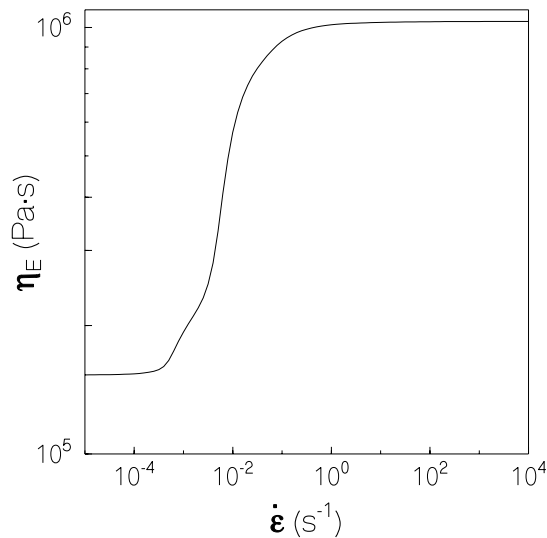
Figure 1.2: Model prediction of the elongational viscosity η_E for an LDPE melt versus elongation rate at different temperatures. The model prediction is of the eight-mode Giesekus model described in chapter 5.

of polymer melts and polymer solutions may be divided into three regions. For low shear rates, compared to the time scale of the fluid, the viscosity is approximately constant. It then equals the so-called zero-shear-rate viscosity η_0. Next, the viscosity decreases rapidly with increasing shear rate. This behaviour is called shear thinning. For high shear rates the viscosity often approximates a constant value again.

To describe shear flows of polymeric fluids it is sometimes sufficient to model the behaviour of the shear viscosity in a certain interval of the shear rate. The shear thinning can be described with a generalised Newtonian model, where the viscosity is modelled as a decreasing function of the shear rate. Examples of these viscous models are the power-law and the Carreau model. The advantage of these models is that, even for non-trivial geometries, the solution of the system of equations is relatively easy. However, the drawback of these models is that the elastic (memory) effects are not taken into account and these models have no normal stress differences (i.e. rod-climbing, die-swell and other typical viscoelastic phenomena can not be described by these models). Therefore these viscous models will not be considered in more detail in this thesis. For a more comprehensive description of the purely viscous models refer to Bird et al. (1987a).

To take the elastic effects into account more difficult models have to be considered. In the literature several integral and differential equations that relate the stress to the deformation history have been proposed. Dependent on the type of flow these models are more or less able to describe the elastic effects. However, instead of a relatively simple algebraic equation for the viscosity one or more extra equations have to be solved for the stresses then. Not only the extra computing time is a problem, but the system of equations is also much more difficult to solve.

- Polymeric fluids show normal stress differences in steady shear flows. The first normal stress difference N_1 is defined as

$$N_1 = \sigma_{11} - \sigma_{22}, \qquad (1.2)$$

where σ_{11} is the normal stress component in the streamwise direction and σ_{22} the normal stress in the gradient direction. For polymeric materials N_1 is positive. The second normal stress difference N_2 is defined as

$$N_2 = \sigma_{22} - \sigma_{33}, \qquad (1.3)$$

where σ_{33} is the normal stress component in the indifferent direction. The magnitude of N_2 is in general much smaller than N_1 and its sign is usually negative. Often not the first normal stress difference N_1 is given, but a related quantity: the first normal stress coefficient Ψ_1. This coefficient is defined by

$$\Psi_1 = \frac{N_1}{\dot{\gamma}^2} \qquad (1.4)$$

and decreases with increasing shear rate. The typical behaviour of the first normal stress coefficient has been depicted in figure 1.1.

- Polymeric fluids show a non-constant elongational viscosity in steady and unsteady elongational flow. The elongational viscosity η_E defined for a steady elongational flow is defined as

$$\eta_E = \frac{\sigma_E}{\dot{\epsilon}}, \qquad (1.5)$$

where the normal stress difference is $\sigma_E = \sigma_{11} - \sigma_{22}$ and $\dot{\epsilon}$ the elongation rate. The stress σ_{11} is in the direction of the elongation and σ_{22} in a direction perpendicular to the elongation.

In figure 1.2 the typical behaviour of the elongation viscosity has been depicted. The elongation viscosity of polymer melts and polymer solutions may be divided into three regions. For small elongation rates the elongational viscosity is approximately constant and equals $\eta_E = 3\eta_0$, just as for a Newtonian fluid. For somewhat larger elongation rates the elongational viscosity increases with increasing elongation rate until a maximum value has been reached. Dependent on the type of fluid this increase is large, as for low density polyethylene, or small, as for high density polyethylene. If the elongation rate is increased once more the elongational viscosity decreases again for polymer melts. For polymer solutions this situation is unclear, see Tirtaatmadja & Sridhar (1993).

A number of models that have been developed are able to describe (some) of the viscoelastic properties, see for example Larson (1988) or Tanner (1985). Dependent on the type of flow, some models give better results than others.

In the last fifteen years much attention has been paid to the numerical simulation of isothermal flows of viscoelastic fluids. Much attention has been paid to the flow through a contraction, die-swell and the flow past a cylinder or a sphere. For recent reviews of numerical simulation methods for the flow of viscoelastic fluids refer to Crochet (1989) or Keunings (1989). For steady flows the use of streamline integration methods made it possible to solve the equations for high Deborah numbers ($\mathcal{O}(10^2)$). For the computation of unsteady flows there are still difficulties for high Deborah (or Weissenberg) numbers. However, industrial flows are often flows with high Deborah numbers. Furthermore the influence of various aspects of the nonisothermal behaviour, such as mechanical dissipation and anisotropic heat conduction, will be small for most flows of polymeric fluids if the Deborah number is small. Therefore this thesis will be restricted to steady flows.

1.2 Nonisothermal polymer flows

In the first section of this introductory chapter a short overview has been given of the isothermal rheological behaviour of polymeric fluids. Another effect of great importance on the material properties, and thus on the flow, is the temperature of the fluid. For polymeric fluids the shear and elongation viscosity are strong decaying functions of the temperature. Especially near the phase change from the liquid to the solid state, this temperature dependence may be extremely large.

Roughly the temperature of polymeric fluids is influenced in two ways. On the one hand the temperature of a polymeric material in industrial processes is influenced by external heating (at the start of the production process) or cooling (at the end of the production process). However, during the deforming of polymeric fluids the temperature changes due to the internal energy production are also important. Due to the high viscosity and the small thermal conductivity of polymer melts and concentrated polymeric solutions the internal heat production is often not negligible. In this introduction the important effects will only be indicated to obtain an overview of the situation. They will be discussed in more detail in chapter 2.

A first cause of internal heat production is the dissipation of mechanical energy. Here an interesting problem arises: what exactly is the mechanical dissipation of a viscoelastic fluid? For viscous fluids it simply equals the stress work and in elastic materials there is no mechanical dissipation since all stress work is stored reversibly. For viscoelastic fluids, however, it depends on the flow whether the fluid behaves more viscous or more elastic and thus which part of the mechanical energy is dissipated (irreversible) and which part is stored reversibly. The next question is of course: how is the mechanical energy stored? There are two possibilities. It can be stored in the form of internal energy (energy elastic) or in the form of entropy (entropy elastic). The energy elastic storage of energy does not contribute to the temperature change, but the entropy elastic storage of energy does. The effect of energy elasticity is well-known for springs. The effect of entropy elasticity is well-known for elastic materials: a rubber band heats up during the stretching and cools down during the recoil.

The temperature may also be influenced by compression or expansion of the fluid. This

effect is well-known for gases, but also for polymeric fluids it is often not negligible. During compression the temperature of the material rises (similar to the considerable increase of the temperature of the valve during the pumping of a bicycle tyre) and it drops during expansion (similar to the decreases of the temperature of your finger when you use a spray). Especially for injection moulding, where the pressure is increased by a few hundred bars in a short time, the temperature rise due to compression effects plays an important role, see Flaman & Veltman (1988).

Another topic of interest is the anisotropy of the heat conduction when the polymeric material is deformed and the polymer chains have a preferential direction. Experiments of Hellwege et al. (1963) already showed that with increasing orientation of the polymer fluid the thermal conductivity in the direction of orientation increases and perpendicular to the orientation the thermal conductivity decreases. For some polymeric materials the thermal conductivity in the direction of orientation may become a few tens times larger, while perpendicular to the direction of orientation the conductivity may become a few times smaller than the thermal conductivity in equilibrium.

As for isothermal flows, viscous models are also frequently used to describe the nonisothermal flow of polymeric fluids. For a review refer to Pearson (1978). Except the drawbacks mentioned earlier for the isothermal flows, the separation of the reversible and the irreversible parts and the anisotropy of the heat conduction can not be described with these models. As will be shown in chapter 2 this is possible for more advanced models.

Contrary to the isothermal viscoelastic flow, however, relatively small numbers of publications have appeared on nonisothermal flows of viscoelastic fluids, especially not for high Deborah numbers. However, recently some articles have been published which include both the viscoelasticity and the influence of the temperature. Sugeng et al. (1987) and McClelland & Finlayson (1988), for example, studied the influence of the temperature on die swell. A hydrodynamically and thermally developing flow has been examined by Nikoleris & Darby (1989). The injection molding process has been simulated numerically by Goyal et al. (1988) and Baaijens (1991). However, these numerical simulations are restricted to temperature dependent relaxation times and viscosities and a relatively simple temperature equation, without paying attention to the storage and release of reversible energy, the effect of compression and extension and the anisotropy of the heat conduction. Braun & Friedrich (1989) have taken into account the storage of elastic energy for a purely energy elastic fluid, without paying attention to the other effects. They compared the entirely energy elastic and the entirely entropy elastic case for the thermal start-up due to the step-function-shear-rate experiment. A comprehensive overview of the latest developments on the nonisothermal flow of viscoelastic fluids can be found in the proceedings of the IUTAM symposium on numerical simulation of nonisothermal flow of viscoelastic liquids (Dijksman & Kuiken 1995).

1.3   Objective and outline of this thesis

The first objective of this thesis is the derivation of nonisothermal equations for isotropic viscoelastic materials with the help of the thermodynamics. Because the description of all phenomena would be too ambitious for one thesis, the area of investigation has to be restricted.

Therefore degradation of the material and phase changes, which have there own specific problems, will not be discussed. In fact the temperature range is then limited to the fluid phase below the temperature at which degradation takes place. Except the well-known stress differential equations from the literature, the temperature equation do have to include the effects mentioned in section 1.2: the anisotropy of the heat conduction, the temperature changes due to compression and expansion, and the separation of reversible and dissipative processes.

The second objective is the development of a numerical code for the simulation of the obtained equations for the nonisothermal flow of viscoelastic fluids. Of course it would be nice to have a time dependent, three-dimensional code for nonisothermal viscoelastic fluid flows. However, this would be asking too much. Not the temperature equation would be the problem, but the stress equations as has been explained in 1.1. Therefore the computer code for steady and isothermal flows described by Hulsen (1990a) will be extended. On the one hand the computations are then restricted to steady, 2D Cartesian or axisymmetrical, flows. On the other hand, however, with this code it is possible to calculate flows with high Deborah numbers. This gives the opportunity to examine the anisotropy of the heat conduction and the different contributions of the internal energy production. For too low Deborah numbers these effects are small for most of the fluids.

The objectives sketched above will be realised as follows. In chapter 2 the equations describing the nonisothermal flow of viscoelastic fluids are derived from the thermodynamics of viscoelastic fluids. The derived equations include the well-known differential stress models described in the literature. The emphasis, however, is on the derivation of the temperature equation from the balance of energy. The typical contributions of viscoelastic fluids to the temperature equation will be argued extensively. The treatment of the constitutive equation of the heat flux will be focused on the experimentally observed anisotropy of the heat conduction, and how this effect can be modelled in the thermodynamic derivation. Next the theoretical results will be related to experimental results: an overview will be given of the influence of the temperature on the coefficients appearing in the derived system of equations and the results of nonisothermal rheology. Finally the obtained system of equations will be simplified with the help of dimensional analysis.

Chapter 3 contains the analysis of the system of equations. The behaviour of the stress models for high deformation rates will be calculated for steady simple shear and uniaxial elongational flow. With these results it will be checked which stress models are able to describe the experimentally observed anisotropy for a simple model of the heat conduction tensor and how this simple model may be extended for the other stress models. Furthermore a method to calculate the lower bounds for the invariants of the internal deformation tensor will be given. This lower bound can be used in the numerical calculations for the correction of the mechanical dissipation. From the obtained results the most appropriate models for the numerical calculations will be selected.

Chapter 4 contains a description of the numerical method that has been used to solve the system of equations derived in chapter 2. In the equations of motion and the constitutive equation for the stress the emphasis will be on the implementation of the nonisothermal effects. The implementation of the temperature equation will be discussed in more detail, including the use of upwind methods for convection-dominated flows. Furthermore the outflow boundary

conditions need extra attention.

In chapter 5 some calculations will be performed for a polystyrene and a polyethylene melt to show the (possible) influence of the various terms in the temperature equation. These calculations will be restricted to relatively simple geometries. Three flow geometries will be argued. Firstly two introductory examples will be discussed: the fully developed pipe flow and a Graetz–Nusselt problem. Then the flow through a 4:1 contraction, a standard test geometry for isothermal flows, with and without cooling of the downstream boundary will be discussed.

Finally in chapter 6 the concluding remarks will be made.

Chapter 2

Governing equations

In this chapter the governing equations that can be used to describe the nonisothermal flow of a viscoelastic fluid are considered. Firstly the balance equations are given in section 2.1. In the balance equations some material dependent quantities appear, like the stress tensor. To obtain a complete set of equations, these quantities have to be specified by a constitutive equation, describing the typical behaviour of the material. The next three sections contain these constitutive equations. To gain insight, first the stress equations will be given in section 2.2. Then, in section 2.3, the temperature equation will be derived with the help of the thermodynamics from the balance of energy. From the thermodynamics also general constitutive equations for the stress and the heat flux will be derived, which include the equations that are commonly used in the literature. In section 2.4 the heat flux constitutive equation and the observed experimental results will be discussed. The obtained constitutive equations still contain coefficients (viscosity, relaxation time etc.) that may, among other things, depend on the temperature. The temperature dependence is the topic of section 2.5, which includes an overview of nonisothermal rheological measurements (a simultaneous temperature change and deformation) and the theories which have been proposed to describe these experiments. Finally, in section 2.6, the dimensionless forms of the balance equations and constitutive equations are given, which will be used to neglect the minor effects.

2.1 The balance equations

In this section a short description will be given of the four balance equations describing the nonisothermal flow of a nonpolar fluid. A more detailed derivation from continuum mechanics can for example be found in Bird et al. (1960). In a fixed bounded space Ω the balance equations for a system with a constant total mass are:

- *The conservation of mass*

$$\dot{\rho} = -\rho \nabla \cdot \underline{v}, \tag{2.1}$$

  where ρ is the fluid density and $\underline{v}$ the velocity. As usual a ∇ denotes the gradient operator and a $(\dot{\ })$ denotes the material derivative of a quantity.

  If the density is a function of the pressure and the temperature: $\rho = \rho(p, T)$, the mass balance can be written as

$$\frac{\dot{\rho}}{\rho} = \frac{1}{\rho}\frac{\partial \rho}{\partial p}\dot{p} + \frac{1}{\rho}\frac{\partial \rho}{\partial T}\dot{T} = -\nabla \cdot \underline{v}. \tag{2.2}$$

  For polymeric fluids the density is only a weak function of the pressure. The compression modulus (the inverse of the compressibility) of polymeric liquids is much higher than the

8

shear modulus, so that under normal pressures a constant density is a good approximation. Under some conditions of high pressures this may not be true. For nonisothermal flows the density may also vary due to temperature variations. For polymeric fluids the density depends only weakly on the temperature. See section 2.5.1 for more details about the pressure and temperature dependence.

In section 2.6, where the dimensionless equations are discussed, it will be shown when the incompressibility condition

$$\nabla \cdot \underline{v} = 0 \tag{2.3}$$

is a good approximation of the equation for the conservation of mass.

- *The balance of linear momentum*

$$\rho \underline{\dot{v}} = \nabla \cdot \underline{\underline{\sigma}} + \rho \underline{f}, \tag{2.4}$$

in which $\underline{\underline{\sigma}}$ is the total stress and $\underline{f}$ a body force per unit of mass. For fluids the total stress tensor can be decomposed in a pressure part $-p\underline{\underline{I}}$ and an extra-stress tensor $\underline{\underline{\tau}}$

$$\underline{\underline{\sigma}} = -p\underline{\underline{I}} + \underline{\underline{\tau}}, \tag{2.5}$$

where $\underline{\underline{I}}$ is the unit tensor. The (thermodynamic) pressure may depend on the density and the temperature. In equilibrium the pressure reduces to the hydrostatic pressure and the extra-stress tensor $\underline{\underline{\tau}}$ vanishes.

An example of a body force is gravitation $\underline{f} = \underline{g}$, with $\underline{g}$ the acceleration due to gravity. The gravity term can be split in a reference value $\rho_{\text{ref}}\underline{g}$ and a deviatoric part $(\rho - \rho_{\text{ref}})\underline{g}$. Then (2.4) becomes

$$\rho \underline{\dot{v}} = -\nabla p_{\text{m}} + \nabla \cdot \underline{\underline{\tau}} + (\rho - \rho_{\text{ref}})\underline{g}, \tag{2.6}$$

where the modified pressure is defined as $p_{\text{m}} = p - \rho_{\text{ref}}gz$, with z the coordinate in the direction of the acceleration due to gravity. The density differences in the flow result in a buoyant force $(\rho - \rho_{\text{ref}})\underline{g}$. Linearization of the density with respect to the temperature, $(\rho - \rho_{\text{ref}}) = \rho_{\text{ref}}\alpha_\rho (T - T_{\text{ref}})$ gives an approximation of the buoyant force. If furthermore the density differences in the convective term are neglected, $\rho\underline{\dot{v}} \simeq \rho_{\text{ref}}\underline{\dot{v}}$, the well-known Boussinesq approximation, which is often used for low viscous Newtonian fluids, is obtained:

$$\rho_{\text{ref}}\underline{\dot{v}} = -\nabla p_{\text{m}} + \nabla \cdot \underline{\underline{\tau}} + \rho_{\text{ref}}\alpha_\rho (T - T_{\text{ref}})\underline{g}, \tag{2.7}$$

where α_ρ is the linear expansion coefficient and T the absolute temperature. The subscript $_{\text{ref}}$ denotes a quantity at reference temperature. For polymeric liquids the linear dependence of the density on the temperature is often a good approximation, see section 2.5.1. In section 2.6 it will be shown under which circumstances this term may be important for shear flows of viscoelastic fluids.

- *The balance of angular momentum*

$$\underline{\underline{\sigma}} = \underline{\underline{\sigma}}^T, \tag{2.8}$$

due to the assumption of nonpolar fluids.

- *The balance of energy*

$$\rho \dot{e} = \nabla \cdot (\underline{\underline{\sigma}} \cdot \underline{v}) + \rho \underline{f} \cdot \underline{v} - \nabla \cdot \underline{\phi}_q + \rho r, \qquad (2.9)$$

where $\underline{\phi}_q$ is the heat flux vector and r an external heat source per unit of mass, for example due to radiation. The external heat source will be neglected henceforth. The total energy per unit of mass $e = u + \frac{1}{2}\underline{v} \cdot \underline{v}$ is the sum of the internal energy per unit of mass u and the kinetic energy. With the help of the balance of linear momentum (2.4) this equation reduces to the balance equation for the internal energy:

$$\rho \dot{u} = \underline{\underline{\sigma}} : \underline{\underline{d}} - \nabla \cdot \underline{\phi}_q, \qquad (2.10)$$

where use has been made of the symmetry of the total stress tensor $\underline{\underline{\sigma}}$. Then $\underline{\underline{\sigma}} : (\nabla \underline{v})^T = \underline{\underline{\sigma}} : \underline{\underline{d}}$, where the Euler rate-of-deformation tensor is defined as $\underline{\underline{d}} = (\underline{\underline{L}} + \underline{\underline{L}}^T)/2$, with the velocity gradient $\underline{\underline{L}}^T = \nabla \underline{v}$.

To obtain a complete set of equations, the extra-stress tensor $\underline{\underline{\tau}}$, the heat flux $\underline{\phi}_q$ and the internal energy u have to be specified by constitutive equations that describe these quantities for a specific material. In the following three sections of this chapter an overview will be given of some specific constitutive equations for polymeric liquids and how these equations can be obtained from the thermodynamics.

The discussion in the following sections is focused on the constitutive equations of isotropic viscoelastic fluids. However, the more common equations for viscous fluids and elastic materials will be given for comparison. Firstly an overview will be given of the stress models. Next the thermodynamics will be described that can be used to obtain a temperature equation from the energy equation for these models. From the thermodynamics also general equations may be obtained for the stress and the heat flux. These equations include the commonly used models for the stress and the heat flux. The equations for the heat flux will be treated in more detail after the thermodynamics.

2.2   Stress constitutive equations

In this section the constitutive equations for the stress, which are used in the literature, are summarised for isotropic viscoelastic materials. In this section only the general form of these stress models will be discussed. Some specific examples can be found in appendix A. However, first the stress equations for viscous fluids and elastic solids will be discussed shortly for comparison.

Viscous fluids

The extra stress of an isotropic viscous fluid $\underline{\underline{\tau}}$ can be described by a simple algebraic relation of the form (Bird et al. 1960)

$$\underline{\underline{\tau}} = 2\eta \underline{\underline{d}} + \left(\eta_v - \tfrac{2}{3}\eta\right) \nabla \cdot \underline{v} \, \underline{\underline{I}}, \qquad (2.11)$$

where η is the shear viscosity and η_v the bulk viscosity. For shear flows the shear viscosity is important, for compression flows the bulk viscosity. In a Newtonian fluid model the shear viscosity η is independent of the velocity gradient. For other models, such as the power-law

model and the Carreau model, the viscosity is a function of the velocity gradient. With these models the shear thinning behaviour of a fluid can be described: a decrease of the viscosity with increasing shear rate. A comprehensive overview of these models has been given by Bird et al. (1987a). In addition to the dependence on the velocity gradient, the viscosity depends on the pressure and temperature.

Elastic materials

The stress of an isotropic elastic material can be described by the Finger tensor $\underline{\underline{b}}$[1]. The Finger tensor will be given explicitly in section 2.3. In this section it is only important that the Finger tensor is a measure for the deformation. For a neo-Hookean elastic material, which is incompressible (the determinant of the Finger tensor is $\det \underline{\underline{b}} = 1$), the stress can be described by a simple algebraic relation

$$\underline{\underline{\sigma}} = -p\underline{\underline{I}} + \underline{\underline{\tau}} = -p\underline{\underline{I}} + G(\underline{\underline{b}} - \underline{\underline{I}}), \tag{2.12}$$

where G is the shear modulus of the elastic material. The extra stress $\underline{\underline{\tau}}$ has been chosen such that it vanishes for $\underline{\underline{b}} = \underline{\underline{I}}$, i.e. in the undeformed state. The pressure p is rheologically undetermined. It can only be determined by solving a complete problem including the boundary conditions. The Finger tensor satisfies a differential equation of the form[2]

$$\overset{\triangledown}{\underline{\underline{b}}} = \underline{\underline{0}}, \tag{2.13}$$

where $\overset{\triangledown}{(\,)}$ is the upper-convected derivative

$$\overset{\triangledown}{(\,)} = \overset{\cdot}{(\,)} - \underline{\underline{L}} \cdot (\,) - (\,) \cdot \underline{\underline{L}}^T. \tag{2.14}$$

The deformation of an elastic material is completely reversible. When all external forces are removed, the elastic material returns to the original state. An extensive description of elastic materials can for example be found in Treloar (1975). A recent overview of constitutive equations for compressible and incompressible elastic materials has been given by Beatty (1987).

Viscoelastic fluids

Viscoelastic fluids show both viscous and elastic behaviour when they are deformed. When all external forces are removed, the fluid relaxes to a hydrostatic stress state. In contrast with the elastic material, however, the hydrostatic stress state is not the original state. The viscous part of the deformation is irreversible.

Polymer melts and solutions consist of (macro)molecules of high molecular weights. Therefore it is often necessary to distinguish different contributions (modes) to the extra-stress tensor. In this thesis it is assumed that the extra-stress tensor $\underline{\underline{\tau}}$ consists of a Newtonian (solvent) contribution and the polymer contributions, which are determined by the deformation history of a fluid particle

$$\underline{\underline{\tau}} = 2\eta_s \underline{\underline{d}} + (\eta_{s,v} - \tfrac{2}{3}\eta_s) \, \nabla \cdot \underline{v} \, \underline{\underline{I}} + \sum_{k=1}^{K} \underline{\underline{\tau}}_k, \tag{2.15}$$

---

[1]In the literature the Finger tensor is often denoted by $\underline{\underline{c}}$. In this thesis, however, the usual notation from the continuum mechanics will be used, where $\underline{\underline{c}}$ or $\underline{\underline{C}}$ is reserved for the left Cauchy–Green tensor and $\underline{\underline{b}}$ or $\underline{\underline{B}}$ for the right Cauchy–Green (or Finger) tensor.

[2]In the literature on elastic materials this equation is unusual. However, it only expresses the observability of the Finger tensor. It has only been mentioned to stress the analogy with the constitutive equations of viscoelastic materials, which will be described next.

in which η_s is the Newtonian shear viscosity, $\eta_{s,v}$ the Newtonian bulk viscosity and K the number of modes. The Newtonian stress can be a contribution of the solvent, or an approximation of the modes with very small relaxation times for a melt. A modal stress $\underline{\underline{\tau}}_k$ can be specified by a differential or an integral model. In this thesis only differential models will be used.

The internal deformation tensor.

Most of the (sub)stress models have been derived from an internal deformation tensor[3]: $\underline{\underline{b}}_k$. The internal deformation tensor $\underline{\underline{b}}_k$ describes the elastic deformation of a viscoelastic fluid, the deformation relative to the stress state that would be obtained after relaxation from the current state[4]. Compare the elastic materials, where the Finger tensor $\underline{\underline{b}}$ describes the total (elastic) deformation of an elastic material, relative to the original state.

The internal deformation tensor $\underline{\underline{b}}_k$ has to be positive definite to guarantee well-posedness of the system of equations (van der Zanden & Hulsen 1988). The positive definiteness is a pleasant property for numerical calculations. It is then possible to correct for numerical errors, which can cause indefinite internal deformation tensors.

For multi-mode models it is customary to assume that different modes do not couple. Then the most general (isothermal) model for a modal stress $\underline{\underline{\tau}}_k$ of an isotropic viscoelastic fluid is an isotropic tensor function of the internal deformation tensor $\underline{\underline{b}}_k$

$$\underline{\underline{\tau}}_k = c_{0,k}\underline{\underline{I}} + c_{1,k}\underline{\underline{b}}_k + c_{2,k}\underline{\underline{b}}_k^2, \tag{2.16}$$

where the scalars $c_{0,k}$, $c_{1,k}$ and $c_{2,k}$ are functions of the invariants of the kth mode of the internal deformation tensor

$$
\begin{aligned}
I_{1,k} &= \ \text{tr}\,\underline{\underline{b}}_k, \\
I_{2,k} &= \ \frac{1}{2}\left(I_{1,k}^2 - \text{tr}\,\underline{\underline{b}}_k^2\right) = I_{3,k}\,\text{tr}\,\underline{\underline{b}}_k^{-1}, \\
I_{3,k} &= \ \det\underline{\underline{b}}_k.
\end{aligned} \tag{2.17}
$$

From the Cayley–Hamilton relation, which reads for $\underline{\underline{b}}_k$

$$\underline{\underline{b}}_k^3 - I_{1,k}\underline{\underline{b}}_k^2 + I_{2,k}\underline{\underline{b}}_k - I_{3,k}\underline{\underline{I}} = \underline{\underline{0}}, \tag{2.18}$$

it follows that it is sufficient to consider three different powers of $\underline{\underline{b}}_k$. All other powers of $\underline{\underline{b}}_k$ can be expressed in these three tensors and the invariants of $\underline{\underline{b}}_k$.

For all well-known differential models, described in appendix A, the viscoelastic (sub)stress can be found from the internal deformation tensor with the help of a simple algebraic relation (see Larson 1988):

$$
\begin{aligned}
\underline{\underline{\tau}}_k &= \ \frac{G_k}{1 - \xi_k}\left(B_k\underline{\underline{b}}_k - \underline{\underline{I}}\right), \\
G_k &= \ \frac{\eta_k}{\lambda_k},
\end{aligned} \tag{2.19}
$$

---

[3]$\underline{\underline{b}}_k$ is also called the conformation tensor or the configuration tensor.

[4]The recoverable or elastic strain of a one-mode model can be obtained in a thought experiment for an infinitesimal small element of the fluid that has been cut from the material. The recoverable deformation is then the difference between the deformation before and after relaxation of the material. For multi-mode models it is more complicated. Then all the modes have to be separated and the recoverable deformation can be obtained for each mode.

where G_k is the shear modulus, λ_k the relaxation time and η_k the viscosity of the kth mode. The parameter ξ_k will be explained shortly. If $B_k = 1$, as for most of the models in appendix A, and $\xi_k = 0$ the relation between the stress and the internal deformation tensor is essentially the same as the relation for the neo-Hookean elastic material (2.12). For the Larson model B_k is function of the first invariant.

In the following sections the derivatives of the invariants with respect to the symmetric tensor $\underline{\underline{b}}_k$ are also needed. For the symmetric tensor $\underline{\underline{b}}_k$ they are given by

$$
\begin{aligned}
\frac{\partial I_{1,k}}{\partial \underline{\underline{b}}_k} &= \underline{\underline{I}}, \\
\frac{\partial I_{2,k}}{\partial \underline{\underline{b}}_k} &= I_{1,k}\underline{\underline{I}} - \underline{\underline{b}}_k, \\
\frac{\partial I_{3,k}}{\partial \underline{\underline{b}}_k} &= I_{3,k}\underline{\underline{b}}_k^{-1} = I_{2,k}\underline{\underline{I}} - I_{1,k}\underline{\underline{b}}_k + \underline{\underline{b}}_k^2.
\end{aligned}
\tag{2.20}
$$

The last equality in $(2.20)_3$ follows from the Cayley–Hamilton relation (2.18). Multiplication of this equation with $\underline{\underline{b}}_k^{-1}$ gives the obtained result.

General differential model for the internal deformation tensor.

Following Leonov (1976, 1987) the internal deformation tensor is supposed to satisfy a differential equation of the form

$$
\overset{\triangledown}{\underline{\underline{b}}}_k = -\underline{\underline{b}}_k \cdot \underline{\underline{d}}_{\text{irr},k} - \underline{\underline{d}}_{\text{irr},k} \cdot \underline{\underline{b}}_k,
\tag{2.21}
$$

where $\underline{\underline{d}}_{\text{irr},k}$ is the irreversible rate-of-deformation tensor, which has to be specified by a constitutive relation. The generic equation for $\underline{\underline{d}}_{\text{irr},k}$ will be derived from the thermodynamics in section 2.3, where it will be shown how $\underline{\underline{d}}_{\text{irr},k}$ may depend on the deformation tensor $\underline{\underline{d}}$ and the internal deformation tensor $\underline{\underline{b}}_k$.

The stress models of appendix A are only a subset of equation (2.21), and have the generic form

$$
\lambda_k \overset{\square}{\underline{\underline{b}}}_k + \underline{\underline{g}}_k = \underline{\underline{0}},
\tag{2.22}
$$

in which $\underline{\underline{g}}_k$ is an isotropic tensor function (in general non-linear) of the internal deformation tensor of the kth mode, $\underline{\underline{b}}_k$. The mixed (or Gordon–Schowalter) convected derivative of a tensor $\overset{\square}{(\ )}$ is defined by

$$
\begin{aligned}
\overset{\square}{(\ )} &= \overset{\cdot}{(\ )} - \underline{\underline{\hat{L}}} \cdot (\ ) - (\ ) \cdot \underline{\underline{\hat{L}}}^T, \\
\underline{\underline{\hat{L}}} &= \underline{\underline{L}} - \xi_k \underline{\underline{d}},
\end{aligned}
\tag{2.23}
$$

in which ξ_k is a parameter for which holds $0 \le \xi_k \le 2$. The values $0 < \xi_k < 2$ represent a sort of frictionless slip of the internal microstructure with respect to the macroscopic flow. In section 2.3, where the thermodynamics of viscoelastic fluids is given, it will be shown that the slip is indeed frictionless or non-dissipative. The upper-convected derivative $\overset{\triangledown}{(\ )}$ is a special case of the mixed convected derivative:

$$
\overset{\triangledown}{(\ )} = \overset{\square}{(\ )}_{\xi_k=0}.
\tag{2.24}
$$

For a zero Newtonian viscosity $\eta_s = 0$, only the values for the upper-convected derivative, $\xi_k = 0$, and the lower convected derivative, $\xi_k = 2$, can be used. Other values may cause

unphysical instabilities, so-called Hadamard instabilities. See for example Leonov (1992). The addition of a Newtonian viscosity η_s stabilises the system of equations in that case.

The model (2.22) corresponds to an irreversible rate-of-deformation tensor

$$\underline{\underline{d}}_{\mathrm{irr},k} = \xi_k \underline{\underline{d}} + \frac{1}{2\lambda_k} \underline{\underline{b}}_k^{-1} \cdot \underline{\underline{g}}_k \tag{2.25}$$

in the equation (2.21) given by Leonov. The specific form of the tensor $\underline{\underline{g}}_k$ for some viscoelastic stress models can be found in appendix A. It is good to keep in mind that for polymeric fluids there is not one equation that is able to describe the stress under all types of flow, even isothermally. For specific types of flow, however, some models give good results. See for example Tanner (1985) or Larson (1988) for the predictions of different stress models for various flow types.

As usual for multi-mode models it has been assumed that different modes have no direct interaction with each other, so there are K decoupled equations for the modal stresses. From the Cayley–Hamilton relation it follows that it is sufficient to consider functions $\underline{\underline{g}}_k$ that only depend on three different powers of $\underline{\underline{b}}_k$, for example $\underline{\underline{I}}$, $\underline{\underline{b}}_k$ and $\underline{\underline{b}}_k^2$. With the help of (2.18) all other powers of $\underline{\underline{b}}_k$ can be expressed in these three tensors and the invariants of $\underline{\underline{b}}_k$.

In appendix A a short overview is given of some well-known isothermal differential stress equations, i.e. the specific form of $\underline{\underline{g}}_k$ in (2.22) and B_k in (2.19). A first extension to nonisothermal models are temperature dependent coefficients, such as the relaxation times and the viscosities. This temperature dependence will be the subject of section 2.5.1.

2.3   Thermodynamics of isotropic materials

In this section the nonequilibrium thermodynamics of isotropic materials[5] will be discussed extensively. The thermodynamics are necessary to calculate a temperature equation from the balance of internal energy for the stress models discussed in section 2.2. The emphasis is on the thermodynamics of viscoelastic fluids. However, all the time the more easy thermodynamics of viscous fluids and elastic materials will be discussed shortly as well for comparison. The discussion will be restricted to rheologically simple materials. This means that the principle of local action holds: the response of a material in a material point is determined by the processes found in the infinitesimal material surroundings. Practically all constitutive equations are based on the principle of local action.

The starting point of the thermodynamics is the usual Gibbs equation for a material in equilibrium. The reader, who is not familiar with thermodynamics, is referred to Callen (1960), Pippard (1966) or Kuiken (1994). The equilibrium Gibbs equation will first be extended to non-equilibrium situations. Then internal variables will be introduced to describe the relaxation phenomena. Combination of the resulting Gibbs equation with the balance of internal energy gives the balance of entropy. The balance of entropy of a viscoelastic fluid has a similarity to both viscous fluids and elastic solids. A viscous fluid can only dissipate energy and an elastic material is only able to store and release elastic energy. A viscoelastic fluid can both dissipate

---

[5] For an isotropic material all anisotropy is a consequence of the anisotropy in the deformation history. The *relation* between some quantity and the deformation history has to be an isotropic relation.

and store or release the energy. Analogously to Leonov (1976, 1987) the balance of entropy of viscoelastic fluids will be used to separate the reversible and the irreversible part of the stress and the rate-of-deformation. The resulting general constitutive equations for the irreversible stress and the irreversible rate-of-deformation tensor contain the stress models in appendix A. The details about the constitutive equation for the heat flux are postponed until section 2.4. Finally the temperature equation will be derived from the balance of entropy. The emphasis is on the usage of the heat capacity, the energy and entropy elasticity and the temperature changes due to compression and expansion. As an example the theory will be applied to the neo-Hookean stress model.

2.3.1 The Gibbs equation

For a rheologically simple material at rest, a fluid or a solid, the entropy per unit of mass s is a function of the internal energy per unit of mass u and the deformation of the material: $s = s(u, \underline{\underline{F}})$, where $\underline{\underline{F}} = \partial \underline{x}/\partial \underline{X}$ is the deformation gradient tensor which describes the deformation with respect to a reference configuration described by the position vector $\underline{X}$. For a comprehensive introduction of deformation tensors see Truesdell & Noll (1965) or Tanner (1985). If the material is isotropic the deformation is fully described by the Finger tensor $\underline{\underline{b}} = \underline{\underline{F}} \cdot \underline{\underline{F}}^T$. Then the entropy is a function of the Finger tensor and the internal energy: $s = s(u, \underline{\underline{b}}) = s(u, \operatorname{tr} \underline{\underline{b}}, \operatorname{tr} \underline{\underline{b}}^{-1}, \det \underline{\underline{b}})$. The change of the entropy can be described by the Gibbs equation

$$du = Tds + \underline{\underline{P}} : d\underline{\underline{b}}, \tag{2.26}$$

where $\underline{\underline{P}}$ is the conjugated force of the Finger tensor. An isotropic fluid does not have any preferential configuration. Then the entropy reduces to $s = s(u, \det \underline{\underline{b}}) = s(u, \rho)$. For a fluid in equilibrium the Gibbs equation reduces to

$$du = Tds - pd\rho^{-1} = Tds + \frac{p}{\rho^2}d\rho, \tag{2.27}$$

where p is the thermodynamic pressure.

For non-homogeneous systems the principle of local and instantaneous equilibrium is assumed to hold. The assumption is that, although the total system is not in equilibrium, the system consists of small volume elements for which the local entropy s is the same function as in real equilibrium. The length and time scale of such an element are infinitesimally small from a macroscopic point of view and large from a molecular point of view. This means that the thermodynamic equations are still valid if the differentials $d(\ )$ are replaced by the material derivatives $(\dot{\ })$. For a comprehensive discussion of the principle of local and instantaneous equilibrium refer to Kuiken (1994).

The relaxation phenomena of viscoelastic fluids can not be described with the Gibbs equation (2.27) together with the principle of local and instantaneous equilibrium. In the thermodynamics of irreversible processes the relaxation phenomena are characterised by internal processes. These internal processes can be described by so-called internal variables, which appear in the Gibbs equation and the equations of state. For a comprehensive description of the introduction of internal variables refer to Kuiken (1994).

With the principle of local and instantaneous equilibrium and the introduction of internal

variables the Gibbs equation then becomes

$$\dot{u} = T\dot{s} + \sum_{n=1}^{N} P_n \dot{z}_n, \tag{2.28}$$

where z_n are the mechanical state variables (the Finger tensor or the density and the internal variables) and P_n the conjugate forces. Note that s and z_n are the independent state variables.

For the thermodynamics of elastic materials and viscous or viscoelastic fluids it is sometimes more advantageous to use the Helmholtz free energy ψ, which is defined as

$$\psi = u - Ts. \tag{2.29}$$

Combination with the Gibbs equation (2.28) gives an expression for the change of the free energy per unit of mass

$$\dot{\psi} = -s\dot{T} + \sum_{n=1}^{N} P_n \dot{z}_n. \tag{2.30}$$

Note that now the independent state variables are T and z_n. The equations of state for the entropy and the conjugate forces are then

$$s = -\left.\frac{\partial \psi}{\partial T}\right|_z, \qquad P_n = \left.\frac{\partial \psi}{\partial z_n}\right|_{T,z'_n}, \tag{2.31}$$

where a $|_x$ means a quantity at constant x. In the notation in (2.31) a $|_z$ is used if all mechanical state variables are constant and a $|_{z'_n}$ if all state variables are constant except the nth mechanical state variable.

Viscous fluids

For a viscous fluid the only mechanical state variable is the density. The Gibbs equation then becomes

$$\dot{u} = T\dot{s} + \frac{p}{\rho^2}\dot{\rho}, \tag{2.32}$$

and the equations of state

$$s = -\left.\frac{\partial \psi}{\partial T}\right|_\rho, \qquad p = \rho^2 \left.\frac{\partial \psi}{\partial \rho}\right|_T, \tag{2.33}$$

where p is the thermodynamic pressure.

It will be useful to introduce the following definitions for the thermodynamic coefficients of viscous fluids

$$\begin{aligned}
c_p &= T\left.\frac{\partial s}{\partial T}\right|_p, & c_v &= T\left.\frac{\partial s}{\partial T}\right|_\rho, \\
-\frac{\alpha}{\rho} &= \left.\frac{\partial s}{\partial p}\right|_T = \frac{1}{\rho^2}\left.\frac{\partial \rho}{\partial T}\right|_p, & \kappa_T &= \frac{1}{\rho}\left.\frac{\partial \rho}{\partial p}\right|_T,
\end{aligned} \tag{2.34}$$

where c_p is the heat capacity at constant pressure, c_v the heat capacity at constant density, α the coefficient of thermal expansion and κ_T the isothermal compressibility. The second equality in $(2.34)_3$ follows from (2.32) as follows

$$\dot{g} = -s\dot{T} + \rho^{-1}\dot{p}, \tag{2.35}$$

where g is the free enthalpy $g = u - Ts - p/\rho$. From the compatibility relation

$$\frac{\partial}{\partial T}\left(\left.\frac{\partial g}{\partial p}\right|_T\right)\Bigg|_p = \frac{\partial}{\partial p}\left(\left.\frac{\partial g}{\partial T}\right|_p\right)\Bigg|_T \tag{2.36}$$

the second equality in $(2.34)_3$ can easily be derived.

Elastic materials

For an isotropic elastic material the only mechanical state variable is the Finger tensor. The Gibbs equation then becomes

$$\dot{u} = T\dot{s} + \underline{\underline{P}} : \dot{\underline{\underline{b}}}, \tag{2.37}$$

and the equations of state

$$s = -\left.\frac{\partial \psi}{\partial T}\right|_{\underline{\underline{b}}}, \qquad \underline{\underline{P}} = \left.\frac{\partial \psi}{\partial \underline{\underline{b}}}\right|_T. \tag{2.38}$$

It will be useful to introduce the following definitions for the heat capacities of elastic materials

$$c_\sigma = T\left.\frac{\partial s}{\partial T}\right|_{\underline{\underline{\sigma}}}, \qquad c_b = T\left.\frac{\partial s}{\partial T}\right|_{\underline{\underline{b}}}, \tag{2.39}$$

where c_σ is the heat capacity at constant stress $\underline{\underline{\sigma}}$ and c_b is the heat capacity at constant Finger tensor $\underline{\underline{b}}$.

Viscoelastic fluids

For an isotropic viscoelastic fluid the mechanical state variables will be taken the density and the K internal deformation tensors. So possible scalar internal variables describing the volume relaxation or internal vector variables describing the relaxation of the heat flux will not be taken into account. The Gibbs equation then becomes

$$\dot{u} = T\dot{s} + \frac{p}{\rho^2}\dot{\rho} + \sum_{k=1}^{K}\underline{\underline{P}}_k : \dot{\underline{\underline{b}}}_k, \tag{2.40}$$

and the equations of state

$$s = -\left.\frac{\partial \psi}{\partial T}\right|_{\rho,\underline{\underline{b}}}, \qquad p = \rho^2\left.\frac{\partial \psi}{\partial \rho}\right|_{T,\underline{\underline{b}}}, \qquad \underline{\underline{P}}_k = \left.\frac{\partial \psi}{\partial \underline{\underline{b}}_k}\right|_{T,\underline{\underline{b}}'_k}, \tag{2.41}$$

where p is the thermodynamic pressure and $\underline{\underline{P}}_k$ the conjugate force of the kth internal deformation tensor $\underline{\underline{b}}_k$. A $|_{\underline{\underline{b}}}$ means that all K internal deformation tensors $\underline{\underline{b}}_k$ are constant. A $|_{\underline{\underline{b}}'_k}$ will be used if all K internal deformation tensors $\underline{\underline{b}}_k$ except the kth internal deformation tensor.

Furthermore it will be useful to introduce the following definitions for the thermodynamic coefficients of viscoelastic fluids

$$c_{p,\tau_e} = T\frac{\partial s}{\partial T}\bigg|_{p,\underline{\underline{\tau}}_e}, \qquad\qquad c_{p,b} = T\frac{\partial s}{\partial T}\bigg|_{p,\underline{b}},$$

$$-\frac{\alpha_{T,b}}{\rho} = \frac{\partial s}{\partial p}\bigg|_{T,\underline{b}} = \frac{1}{\rho^2}\frac{\partial\rho}{\partial T}\bigg|_{p,\underline{b}}, \qquad \kappa_{T,b} = \frac{1}{\rho}\frac{\partial\rho}{\partial p}\bigg|_{T,\underline{b}}, \tag{2.42}$$

where c_{p,τ_e} is the heat capacity at constant pressure and elastic stress $\underline{\underline{\tau}}_e$, $c_{p,b}$ is the heat capacity at constant pressure and internal deformation tensors $\underline{b}_k$, $\alpha_{T,b}$ the coefficient of thermal expansion at constant internal deformation and $\kappa_{T,b}$ the isothermal compressibility at constant internal deformation. The second equality in $(2.42)_3$ follows from (2.40), analogously to the derivation for viscous fluids.

2.3.2   The balance of entropy

Combination of the balance of internal energy (2.10) and the Gibbs equation (2.28) gives the balance of entropy

$$\rho T\dot{s} = -\nabla\cdot\underline{\phi}_q + \underline{\underline{\sigma}} : \underline{\underline{d}} - \rho\sum_{n=1}^{N}P_n\dot{z}_n, \tag{2.43}$$

or in the local balance form

$$\begin{aligned}
\rho\dot{s} &= -\nabla\cdot\underline{J}_s + \Pi_s, \\
\underline{J}_s &= \frac{1}{T}\underline{\phi}_q, \\
T\Pi_s &= -T^{-1}\underline{\phi}_q\cdot\nabla T + \underline{\underline{\sigma}} : \underline{\underline{d}} - \rho\sum_{n=1}^{N}P_n\dot{z}_n,
\end{aligned} \tag{2.44}$$

where $\underline{J}_s$ is the entropy flux and Π_s the entropy production. The second law of thermodynamics states that the entropy production must be non-negative: $\Pi_s \geq 0$.

In the next part of this section the specific equations for the entropy production of viscous fluids, elastic materials and viscoelastic fluids will be given.

Viscous fluids

For viscous fluids the two independent state variables are the temperature T and the density ρ. Thus the viscous entropy production Π_s^v is simply

$$T\Pi_s^v = -T^{-1}\underline{\phi}_q\cdot\nabla T + \underline{\underline{\sigma}} : \underline{\underline{d}} - \frac{p}{\rho}\dot{\rho} = T^{-1}\underline{\phi}_q\cdot\nabla T + 2\eta\underline{\underline{d}} : \underline{\underline{d}} + (\eta_v - \tfrac{2}{3}\eta)(\nabla\cdot\underline{v})^2, \tag{2.45}$$

where the pressure term has been eliminated with the help of the balance of mass (2.1) and (2.11) has been used for the viscous stress. From the restriction that the entropy production has to be non-negative for independent ∇T, $\underline{\underline{d}} - (\nabla\cdot\underline{v}/3)\underline{\underline{I}}$ and $\nabla\cdot\underline{v}$ it follows that the shear viscosity η and the bulk viscosity η_v are non-negative.

Elastic materials

For an isotropic elastic material the independent state variables are the temperature T and

the Finger tensor $\underline{\underline{b}}$. Note that the density ρ is not an independent state variable for elastic materials. From the continuum mechanics it follows that $\rho_0/\rho = \det \underline{\underline{F}} = \sqrt{\det \underline{\underline{b}}}$, where ρ_0 is the density in the reference state. This result can again be found after multiplication of (2.13) scalarly with $\underline{\underline{b}}^{-1}$. Combination of the result with the mass balance (2.1) gives the following relation between the Finger tensor $\underline{\underline{b}}$ and the density: $\rho\sqrt{\det \underline{\underline{b}}} = \rho_0$.

With (2.38) the entropy production for an elastic material Π_s^{e} becomes

$$T\Pi_s^{\mathrm{e}} = -T^{-1}\underline{\phi}_q \cdot \nabla T + \underline{\underline{\sigma}} : \underline{\underline{d}} - \rho \left.\frac{\partial\psi}{\partial\underline{\underline{b}}}\right|_T : \dot{\underline{\underline{b}}}. \tag{2.46}$$

Combination with (2.13) gives

$$T\Pi_s^{\mathrm{e}} = -T^{-1}\underline{\phi}_q \cdot \nabla T + \left(\underline{\underline{\sigma}} - \rho\left(\underline{\underline{b}} \cdot \left.\frac{\partial\psi}{\partial\underline{\underline{b}}}\right|_T + \left.\frac{\partial\psi}{\partial\underline{\underline{b}}}\right|_T \cdot \underline{\underline{b}}\right)\right) : \underline{\underline{d}} +$$
$$\rho\left(-\underline{\underline{b}} \cdot \left.\frac{\partial\psi}{\partial\underline{\underline{b}}}\right|_T + \left.\frac{\partial\psi}{\partial\underline{\underline{b}}}\right|_T \cdot \underline{\underline{b}}\right) : \underline{\underline{w}}, \tag{2.47}$$

where the vorticity tensor is defined as $\underline{\underline{w}} = 1/2(\underline{\underline{L}} - \underline{\underline{L}}^T)$. From the assumption that the material is isotropic, it follows that

$$\underline{\underline{b}} \cdot \left.\frac{\partial\psi}{\partial\underline{\underline{b}}}\right|_T = \left.\frac{\partial\psi}{\partial\underline{\underline{b}}}\right|_T \cdot \underline{\underline{b}},$$

$$T\Pi_s^{\mathrm{e}} = -T^{-1}\underline{\phi}_q \cdot \nabla T + \left(\underline{\underline{\sigma}} - 2\rho\underline{\underline{b}} \cdot \left.\frac{\partial\psi}{\partial\underline{\underline{b}}}\right|_T\right) : \underline{\underline{d}}. \tag{2.48}$$

For an ideal elastic material it is assumed that no energy is dissipated due to mechanical work. Because the mechanical entropy production has to vanish for any $\underline{\underline{d}}$, (2.48) gives a relation between the stress and the free energy of an elastic material:

$$\underline{\underline{\sigma}} = 2\rho\underline{\underline{b}} \cdot \left.\frac{\partial\psi}{\partial\underline{\underline{b}}}\right|_T. \tag{2.49}$$

The elastic entropy production now becomes

$$T\Pi_s^{\mathrm{e}} = -T^{-1}\underline{\phi}_q \cdot \nabla T. \tag{2.50}$$

The constitutive equation for the heat flux will not be examined in this section. This will be postponed until section 2.4.

For an incompressible material ($\rho = \rho_0$, the density in the reference state, and $\det \underline{\underline{b}} = 1$) the isotropic part remains rheologically undetermined. The stress may then be written as

$$\underline{\underline{\sigma}} = -p\underline{\underline{I}} + \underline{\underline{\tau}} = -(p+c)\underline{\underline{I}} + 2\rho_0\underline{\underline{b}} \cdot \left.\frac{\partial\psi}{\partial\underline{\underline{b}}}\right|_T, \tag{2.51}$$

where c is chosen such that in equilibrium, i.e. $\underline{\underline{b}} = \underline{\underline{I}}$, this equation reduces to $\underline{\underline{\sigma}} = -p\underline{\underline{I}}$. The free energy for an incompressible material is then $\psi = \psi(\mathrm{tr}\,\underline{\underline{b}}, \mathrm{tr}\,\underline{\underline{b}}^{-1}, T)$. Comparison with

(2.12) and using (2.20) gives an expression for the free energy of an incompressible neo-Hookean elastic material. Then the constant c equals the shear modulus. The shear modulus G is then only a function of the temperature and the integration with respect to $\underline{\underline{b}}$ of (2.51) can easily be performed:

$$\psi = \frac{G}{2\rho_0} \left(\mathrm{tr}\, \underline{\underline{b}} - 3 \right) + \overline{\psi}(T), \tag{2.52}$$

where $\overline{\psi}$ is an arbitrary function of the temperature, which vanishes in equilibrium. The constant in the first term on the right-hand side has been added to make the free energy vanish in equilibrium[6].

Viscoelastic fluids

For an isotropic viscoelastic fluid the independent state variables are the temperature T, the density ρ and the K internal deformation tensors $\underline{\underline{b}}_k$. With (2.41) the entropy production for a viscoelastic fluid Π_s^{ve} becomes

$$T\Pi_s^{\mathrm{ve}} = -T^{-1}\underline{\phi}_q \cdot \nabla T + \underline{\underline{\sigma}} : \underline{\underline{d}} - \rho \sum_{k=1}^{K} \left. \frac{\partial \psi}{\partial \underline{\underline{b}}_k} \right|_{T,\rho,\underline{\underline{b}}_k'} : \dot{\underline{\underline{b}}}_k - \rho \left. \frac{\partial \psi}{\partial \rho} \right|_{T,\underline{\underline{b}}} \dot{\rho}. \tag{2.53}$$

For models of the form (2.21) this results in

$$T\Pi_s^{\mathrm{ve}} = -T^{-1}\underline{\phi}_q \cdot \nabla T + \left(\underline{\underline{\sigma}} - \sum_{k=1}^{K} 2\rho \underline{\underline{b}}_k \cdot \left. \frac{\partial \psi}{\partial \underline{\underline{b}}_k} \right|_{T,\rho,\underline{\underline{b}}_k'} - \rho^2 \left. \frac{\partial \psi}{\partial \rho} \right|_{T,\underline{\underline{b}}} \underline{\underline{I}} \right) : \underline{\underline{d}} +$$

$$2\rho \sum_{k=1}^{K} \left(\left. \frac{\partial \psi}{\partial \underline{\underline{b}}_k} \right|_{T,\rho,\underline{\underline{b}}_k'} : \underline{\underline{d}}_{\mathrm{irr},k} \right), \tag{2.54}$$

where the isotropy of the material has been used to eliminate the vorticity tensor, analogously to the derivation of the entropy production for elastic materials. The material derivative of the density has been eliminated with the mass balance (2.1).

Leonov (1976) assumes that the high-elasticity state is a local equilibrium state, which can be characterised by the internal deformation tensors $\underline{\underline{b}}_k$. This means that, besides the usual local state variables ρ and T, all coefficients may depend on the internal deformation tensors $\underline{\underline{b}}_k$, or invariants of them, as well. The mechanical entropy production is caused by small deviations from this equilibrium. It will be assumed that the high-elasticity state can be described by K internal deformation tensors. Analogously to the elastic case, (2.49), a mode of the equilibrium stress $\underline{\underline{\tau}}_{e,k}$ is defined by

$$\underline{\underline{\tau}}_{e,k} = 2\rho \underline{\underline{b}}_k \cdot \left. \frac{\partial \psi}{\partial \underline{\underline{b}}_k} \right|_{T,\rho,\underline{\underline{b}}_k'}. \tag{2.55}$$

The total elastic stress is the sum over the K modes, $\underline{\underline{\tau}}_e = \sum_{k=1}^{K} \underline{\underline{\tau}}_{e,k}$.

With the definitions of the elastic stresses (2.55), the entropy production of a viscoelastic fluid can be written as

$$T\Pi_s^{\mathrm{ve}} = -T^{-1}\underline{\phi}_q \cdot \nabla T + \underline{\underline{\tau}}_{\mathrm{irr}} : \underline{\underline{d}} + \sum_{k=1}^{K} \underline{\underline{d}}_{\mathrm{irr},k} : \underline{\underline{\tau}}_{e,k}, \tag{2.56}$$

---

[6]In section 3.2.1 it will be shown that for $\det \underline{\underline{b}} = 1$ holds $\mathrm{tr}\, \underline{\underline{b}} \geq 3$ and thus $\psi \geq 0$.

where the definition of the thermodynamic pressure (2.41) has been used to eliminate the free energy derivative with respect to the density. The irreversible stress is defined as

$$\underline{\underline{\tau}}_{\mathrm{irr}} = \underline{\underline{\sigma}} - \underline{\underline{\tau}}_e + p\underline{\underline{I}} = \underline{\underline{\tau}} - \underline{\underline{\tau}}_e, \tag{2.57}$$

where the last equality follows from (2.5). The terms contributing to the entropy production (2.56) consist of the product of a thermodynamic flux and its conjugate force. The fluxes are the heat flux $\underline{\phi}_q$, the irreversible stress $\underline{\underline{\tau}}_{\mathrm{irr}}$ and the irreversible deformation tensors $\underline{\underline{d}}_{\mathrm{irr},k}$. The conjugate forces are the temperature gradient $T^{-1}\nabla T$, the rate-of-deformation tensor $\underline{\underline{d}}$ and the elastic stresses $\underline{\underline{\tau}}_{e,k}$.

The irreversible stress $\underline{\underline{\tau}}_{\mathrm{irr}}$, the irreversible rate-of-deformation tensors $\underline{\underline{d}}_{\mathrm{irr},k}$ and the heat flux $\underline{\phi}_q$ still have to be specified by phenomenological relations. In the thermodynamics of irreversible processes it is assumed that the thermodynamic fluxes can be described by a linear combination of the forces. Then the general form of the phenomenological equations is

$$\underline{\phi}_q = T^{-1}\underline{\underline{\Lambda}}_{qq} \cdot \nabla T + \underline{\underline{\Lambda}}_{qd} : \underline{\underline{d}} + \sum_{l=1}^{K} \underline{\underline{\Lambda}}_{q\tau_{e,l}} : \underline{\underline{\tau}}_{e,l},$$

$$\underline{\underline{\tau}}_{\mathrm{irr}} = T^{-1}\underline{\underline{\Lambda}}_{dq} \cdot \nabla T + \underline{\underline{\Lambda}}_{dd} : \underline{\underline{d}} + \sum_{l=1}^{K} \underline{\underline{\Lambda}}_{d\tau_{e,l}} : \underline{\underline{\tau}}_{e,l},$$

$$\underline{\underline{d}}_{\mathrm{irr},k} = T^{-1}\underline{\underline{\Lambda}}_{\tau_{e,k}q} \cdot \nabla T + \underline{\underline{\Lambda}}_{\tau_{e,k}d} : \underline{\underline{d}} + \sum_{l=1}^{K} \underline{\underline{\Lambda}}_{\tau_{e,k}\tau_{e,l}} : \underline{\underline{\tau}}_{e,l}, \tag{2.58}$$

where a $(\underline{\ })$ denotes a third order tensor and a $(\underset{\approx}{\ })$ a fourth order tensor. For the linear phenomenological relations of isotropic materials two restrictions on the phenomenological coefficients can be derived, based on the symmetry properties. The first restriction is the Onsager–Casimir reciprocal relation. The reciprocal relation for a coefficient $\Lambda_{\alpha\beta}$, of certain tensorial order can be obtained by considering the time reversal of the variables α and β (i.e. a reversion of the velocity). This means that $\Lambda_{\alpha\beta} = -\Lambda_{\beta\alpha}$ if α is even and β is odd with respect to the time reversal, or vice versa. $\Lambda_{\alpha\beta} = \Lambda_{\beta\alpha}$ if α and β are both even or odd with respect to the time reversal. In equation (2.58) this gives $\underline{\underline{\Lambda}}_{\tau_{e,k}d} = -\underline{\underline{\Lambda}}_{d\tau_{e,k}}$. The second restriction is the Curie principle. In an isotropic system the coefficients do not change under an arbitrary rotation. Then thermodynamic fluxes and forces of different tensorial order are not coupled, so $\underline{\underline{\Lambda}}_{\tau_{e,k}q} = \underline{\underline{\Lambda}}_{q\tau_{e,k}} = \underline{0}$ and $\underline{\underline{\Lambda}}_{dq} = \underline{\underline{\Lambda}}_{qd} = \underline{0}$ in equation (2.58). This so-called Curie principle follows from spatial symmetry considerations. A proof of both properties can for example be found in de Groot & Mazur (1984) or Kuiken (1994).

Equation (2.58) has now been simplified considerably. The phenomenological equation for the heat flux, which has been reduced to $\underline{\phi}_q = T^{-1}\underline{\underline{\Lambda}}_{qq} \cdot \nabla T$ with application of the Curie principle, will not be examined in this section. It will be postponed until section 2.4. In the remainder of this subsection only the linear relations (2.58) for the irreversible stress and the irreversible rate-of-deformation tensor, will be treated. They become after application of the Onsager–Casimir reciprocal relations and the Curie principle

$$\underline{\underline{\tau}}_{\mathrm{irr}} = \underline{\underline{\Lambda}}_{dd} : \underline{\underline{d}} - \sum_{l=1}^{K} \underline{\underline{\Lambda}}_{d\tau_{e,l}} : \underline{\underline{\tau}}_{e,l},$$

$$\underline{\underline{d}}_{\mathrm{irr},k} = \underline{\underline{\Lambda}}_{d\tau_{e,k}} : \underline{\underline{d}} + \sum_{l=1}^{K} \underline{\underline{\Lambda}}_{\tau_{e,k}\tau_{e,l}} : \underline{\underline{\tau}}_{e,l}, \tag{2.59}$$

where the fourth order tensors $\underset{\approx}{\Lambda}$ may depend on the local state variables ρ, T and $\underline{b}_k$. In the following it will be assumed that the irreversible rate-of-deformation tensor $\underline{d}_{\text{irr},k}$ only depends on the kth internal deformation tensor $\underline{b}_k$, i.e. $\underset{\approx}{\Lambda}_{\tau_{e,k}\tau_{e,l}} = \underset{\approx}{0}$ for $k \neq l$, so that $(2.59)_2$ becomes

$$\underline{d}_{\text{irr},k} = \underset{\approx}{\Lambda}_{d\tau_{e,k}} : \underline{d} + \underset{\approx}{\Lambda}_{\tau_{e,k}\tau_{e,k}} : \underline{\tau}_{e,k}. \tag{2.60}$$

This is the same assumption as for the multi-mode models in section 2.2. Substitution of (2.60) in the viscoelastic entropy production (2.56) gives

$$T\Pi_s^{\text{ve}} = -T^{-1}\underline{\phi}_q \cdot \nabla T + \underline{d} : \underset{\approx}{\Lambda}_{dd} : \underline{d} + \sum_{k=1}^{K} \underline{\tau}_{e,k} : \underset{\approx}{\Lambda}_{\tau_{e,k}\tau_{e,k}} : \underline{\tau}_{e,k}. \tag{2.61}$$

Due to the restriction that the entropy production has to be non-negative for independent ∇T, $\underline{d}$ and $\underline{\tau}_{e,k}$ the tensors $\underset{\approx}{\Lambda}_{dd}$ and $\underset{\approx}{\Lambda}_{\tau_{e,k}\tau_{e,k}}$ have to be positive definite. The cross terms with $\underset{\approx}{\Lambda}_{d\tau_{e,k}}$ are non-dissipative, so the entropy production does not give any restriction on these tensors.

Comparing the equations for the irreversible rate-of-strain tensor (2.60) and (2.25) for the models (2.22) leads to

$$\underset{\approx}{\Lambda}_{d\tau_{e,k}} = \xi_k \underset{\approx}{I}, \qquad \underset{\approx}{\Lambda}_{\tau_{e,k}\tau_{e,k}} : \underline{\tau}_{e,k} = \frac{1}{2\lambda_k} \underline{b}_k^{-1} \cdot \underline{g}_k, \tag{2.62}$$

which shows that the frictionless slip in the mixed convected derivative, represented by the parameter ξ_k, is indeed non-dissipative. Comparing the constitutive equations for the irreversible stress $(2.59)_1$, (2.57) and (2.15) then gives

$$\underset{\approx}{\Lambda}_{dd} = 2\eta_s \underset{\approx}{I} + (\eta_{s,v} - \tfrac{2}{3}\eta_s) \underset{\approx}{II}, \quad \underline{\tau}_{e,k} = \frac{1}{1 - \xi_k} \underline{\tau}_k. \tag{2.63}$$

The entropy production (2.61) can then be written as

$$T\Pi_s^{\text{ve}} = -T^{-1}\underline{\phi}_q \cdot \nabla T + 2\eta_s \underline{d} : \underline{d} + (\eta_{s,v} - \tfrac{2}{3}\eta_s)(\nabla \cdot \underline{v})^2 +$$
$$\sum_{k=1}^{K} \frac{1}{2\lambda_k(1 - \xi_k)} \left(\underline{\tau}_k \cdot \underline{b}_k^{-1}\right) : \underline{g}_k. \tag{2.64}$$

The entropy production consists of three separate parts. The first term represents the entropy production due to heat conduction. The second and third term are the contributions of the Newtonian part, which is the same as the viscous mechanical entropy production in (2.45). From the restriction that the entropy production has to be non-negative it follows that $\eta_s \geq 0$ and $\eta_{s,v} \geq 0$. The last term is the viscoelastic contribution, which depends on the specific stress model. The expressions for the multi-mode part of the dissipation $T\Pi_s^{\text{ve}}$ and the restrictions for the coefficients of the specific stress models of appendix A are given in appendix B.

For the models of appendix A the relation between the stress and the internal deformation tensor is given by (2.19). It then follows from (2.55) and $(2.63)_2$ that the derivative of the free energy with respect to an internal deformation tensor $\underline{b}_k$ equals

$$\left.\frac{\partial \psi}{\partial \underline{b}_k}\right|_{T,\rho,\underline{b}_k'} = \frac{G_k}{2\rho(1 - \xi_k)^2} \left(B_k \underline{I} - \underline{b}_k^{-1}\right), \tag{2.65}$$

where G_k may depend on the temperature and the density. With the help of (2.20) equation (2.65) can easily be integrated for the stress models of appendix A. For the models with $B_k = 1$ it becomes[7]:

$$\psi = \sum_{k=1}^{K} \frac{G_k}{2\rho(1-\xi_k)^2} \left(I_{1,k} - \ln I_{3,k} - 3 \right) + \overline{\psi}(\rho, T), \tag{2.66}$$

and for the Larson model with $B_k = (1 + \beta_k(I_{1,k} - 3)/3)^{-1}$ the free energy is given by

$$\psi = -\sum_{k=1}^{K} \frac{G_k}{2\rho} \left(\frac{3}{\beta_k} \ln B_k + \ln I_{3,k} \right) + \overline{\psi}(\rho, T), \tag{2.67}$$

when $\beta_k \neq 0$[8]. With a Taylor expansion around $\beta_k = 0$ it is easy to show that in the limit $\beta_k \to 0$ the free energy (2.66) is obtained. The part of the free energy that is independent of the internal deformation tensor, $\overline{\psi}$, is an arbitrary function of the other independent state variables, the temperature and the density. Note that when $\overline{\psi}$ vanishes in equilibrium, both expressions for the internal energy vanish in equilibrium.

2.3.3 The temperature equation

With the help of the balance of entropy (2.44) it is now possible to obtain a temperature equation. Except the heat flux, the right-hand side of (2.44) has been elaborated. The heat flux will be the topic of section 2.4. In the following part of this section the left-hand side of (2.44), the material derivative of the entropy, will be worked out. This results in the temperature equation for viscoelastic fluids. However, for comparison the temperature equations for viscous fluids and elastic materials will be given first.

Viscous fluids

The change of the entropy, which is considered as a function of the temperature and pressure $s = s(T, p)$, can be written as

$$\dot{s} = \left. \frac{\partial s}{\partial p} \right|_T \dot{p} + \left. \frac{\partial s}{\partial T} \right|_p \dot{T} = -\frac{\alpha}{\rho} \dot{p} + \frac{c_p}{T} \dot{T}, \tag{2.68}$$

where α is the coefficient of thermal expansion and c_p the heat capacity at constant pressure. These coefficients may depend on the state variables p and T. In the derivation use has been made of the definitions of the heat capacity and the coefficient of thermal expansion $(2.34)_{1,3}$. Substitution of (2.68) in the local entropy balance (2.44) with the viscous entropy production (2.45), gives the temperature equation

$$\rho c_p \dot{T} - T\alpha \dot{p} = T\Pi_s^{\text{v}} - T\nabla \cdot \underline{J}_s = D_{\text{m}}^{\text{v}} - \nabla \cdot \underline{\phi}_q,$$
$$D_{\text{m}}^{\text{v}} = T\Pi_s^{\text{v}}|_{\nabla T=0} = \underline{\underline{\tau}} : \underline{\underline{d}} = 2\eta \underline{\underline{d}} : \underline{\underline{d}} + (\eta_v - \tfrac{2}{3}\eta)(\nabla \cdot \underline{v})^2, \tag{2.69}$$

---

[7]It is essential to take the $\ln I_{3,k}$ term into account in the neo-Hookean and Larson free energies. This term results in the isotropic term in (2.19). The $\ln I_{3,k}$ term represents the free energy of noninteracting macromolecules (Carreau & Grmela 1991). Other free energies of some micro-rheological models, such as the FENE free energy and the free energy in an entangled network, have been discussed by Carreau & Grmela (1991).

[8]Note that $\psi - \overline{\psi}$ is non-negative for both the neo-Hookean and the Larson free energy. This result simply follows after a decomposition on the principal axes. The resulting functions $x - \ln x - 1$ for the neo-Hookean free energy and $1/\beta_k \ln(1 + \beta_k(x-1)) - \ln x$ for the Larson free energy are both non-negative for $x > 0$.

where $D_{\mathrm{m}}^{\mathrm{v}}$ is the viscous mechanical dissipation which equals the total amount of work, or stress power, $\underline{\underline{\tau}} : \underline{\underline{d}}$. In the remaining part the thermal expansion coefficient α and the heat capacity c_p will shortly be discussed.

The thermal expansion coefficient α.

In computations the thermal expansion is often not taken into account. For the mass balance it is sufficient that $|\alpha \Delta T| \ll 1$ to neglect the thermal expansion term. This will be clarified in section 2.6. However, this condition is not sufficient to neglect the thermal expansion term in the temperature equation. For shear flows the pressure gradient scales the same as the mechanical dissipation, see also section 2.6. When the mechanical dissipation term in the temperature equation is important $T\alpha \ll 1$ must hold to neglect the influence of thermal expansion in the temperature equation. For normal processing temperatures this condition is much more severe then the condition for the mass balance.

The heat capacity c_p.

The heat capacity at constant pressure is related to the heat capacity at constant volume $(2.34)_2$ by

$$c_p = T \left.\frac{\partial s}{\partial T}\right|_p = T\left.\frac{\partial s}{\partial T}\right|_\rho + T\left.\frac{\partial s}{\partial \rho^{-1}}\right|_T \left.\frac{\partial \rho^{-1}}{\partial T}\right|_p = c_v + \frac{T\alpha^2}{\rho \kappa_T}. \tag{2.70}$$

The last equality follows from (2.34), the compatibility relation

$$\left.\frac{\partial s}{\partial \rho^{-1}}\right|_T = \frac{\partial}{\partial \rho^{-1}}\left(\left.\frac{\partial \psi}{\partial T}\right|_\rho\right)\bigg|_T = \frac{\partial}{\partial T}\left(\left.\frac{\partial \psi}{\partial \rho^{-1}}\right|_T\right)\bigg|_\rho = \left.\frac{\partial p}{\partial T}\right|_\rho \tag{2.71}$$

and

$$0 = \left.\frac{\partial p}{\partial T}\right|_p = \left.\frac{\partial p}{\partial T}\right|_\rho + \left.\frac{\partial p}{\partial \rho^{-1}}\right|_T \left.\frac{\partial \rho^{-1}}{\partial T}\right|_p. \tag{2.72}$$

Thus only for incompressible viscous fluids the heat capacity at constant pressure would equal the heat capacity at constant volume, otherwise c_p is larger than c_v.

Elastic materials

For isotropic elastic materials the change of the entropy, which is considered as a function of the temperature and the Finger tensor $s = s(T, \underline{\underline{b}})$, can be written as

$$\dot{s} = \left.\frac{\partial s}{\partial T}\right|_{\underline{\underline{b}}} \dot{T} + \left.\frac{\partial s}{\partial \underline{\underline{b}}}\right|_T : \dot{\underline{\underline{b}}} = \frac{c_b}{T}\dot{T} + \Delta \dot{s}_b^{\mathrm{e}}, \tag{2.73}$$

which defines the isothermal entropy change Δs_b^{e} for an elastic material. For the heat capacity c_b the definition $(2.39)_2$ has been used. Substitution in the local entropy balance (2.44), with the elastic entropy production (2.50), gives a temperature equation without mechanical dissipation:

$$\rho c_b \dot{T} + \rho T \Delta \dot{s}_b^{\mathrm{e}} = -\nabla \cdot \underline{\phi}_q,$$
$$D_{\mathrm{m}}^{\mathrm{e}} = T\Pi_s^{\mathrm{e}}|_{\nabla T=\underline{0}} = 0. \tag{2.74}$$

Note that when the free energy is known as a function of $\underline{\underline{b}}$ and T, it is possible to calculate c_b and the entropy derivative in Δs_b^{e}. These two quantities will be elaborated in the remaining

part.

The entropy difference Δs_b^{e}.

If the free energy function ψ is known, the entropy can be calculated with the help of the equation of state $(2.38)_1$. Differentiation with respect to the Finger tensor $\underline{\underline{b}}$ then gives the entropy difference Δs_b^{e}. Next, this entropy difference will be calculated for various forms of the free energy function.

If the free energy can be written as $\psi = \psi_T(T) + \psi_b(\underline{\underline{b}})$ the entropy does not depend on $\underline{\underline{b}}$ and the derivative of the entropy in Δs_b^{e}, and thus Δs_b^{e} itself, vanishes. In this case the entropy is a function of the temperature only $(u(\underline{\underline{b}}, T) = \psi(\underline{\underline{b}}, T) + Ts(T))$ and the reversible part of the energy will be stored as internal energy. Then the material is called energy elastic and the polymer chains act like springs. An example is the neo-Hookean free energy (2.52) where the shear modulus G does not depend on the temperature.

If the free energy consists of products of functions of the temperature and functions of the invariants of the Finger tensor the derivative of the entropy does not vanish. For the example that the free energy can be written $\psi = \psi_T(T) + T\psi_b(\underline{\underline{b}})$ the derivative of the entropy becomes with $(2.38)_1$

$$\rho_0 T \Delta s_b^{\mathrm{e}} = \rho_0 T \left. \frac{\partial s}{\partial \underline{\underline{b}}} \right|_T : \dot{\underline{\underline{b}}} = -\rho_0 \left. \frac{\partial \psi}{\partial \underline{\underline{b}}} \right|_T : \dot{\underline{\underline{b}}}, \tag{2.75}$$

which equals exactly minus the stress work for elastic materials (see the derivation of the mechanical dissipation for elastic materials in section 2.3.2). In this case the internal energy is a function of the temperature only $(u(T) = \psi(\underline{\underline{b}}, T) + Ts(\underline{\underline{b}}, T))$ and the reversible part of the energy will then be stored as entropy. Then the material is called entropy elastic and the polymer chains act like rods which can not be stretched, but are oriented in a preferential direction when they are deformed. An example is the neo-Hookean model ($\det \underline{\underline{b}} = 1$ thus $\rho = \rho_0$), with a linear dependence on the temperature of $G = TG_{\mathrm{ref}}/T_{\mathrm{ref}}$. Thus for a constant shear modulus the work of the fluid is stored as internal energy (without a temperature change) and when the modulus scales linearly with the temperature all the work of the elastic material is stored as entropy which is attended with a (reversible) temperature rise as can be seen from (2.74).

If the free energy is not known $\partial s/\partial \underline{\underline{b}}|_T$ may be obtained from experimental results of the temperature dependence of the stress $\underline{\underline{\tau}}$. From the equation of state for the entropy (2.38) and the relation (2.51) between the stress $\underline{\underline{\tau}}$ and the free energy of an incompressible fluid, it follows that

$$\left. \frac{\partial s}{\partial \underline{\underline{b}}} \right|_T = -\left. \frac{\partial}{\partial \underline{\underline{b}}} \left(\left. \frac{\partial \psi}{\partial T} \right|_{\underline{\underline{b}}} \right) \right|_T = -\left. \frac{\partial}{\partial T} \left(\left. \frac{\partial \psi}{\partial \underline{\underline{b}}} \right|_T \right) \right|_{\underline{\underline{b}}} = -\frac{1}{2\rho_0} \underline{\underline{b}}^{-1} \cdot \left. \frac{\partial \underline{\underline{\tau}}}{\partial T} \right|_{\underline{\underline{b}}}. \tag{2.76}$$

Thus when some measurements of the temperature dependence of the stress are available, $\partial s/\partial \underline{\underline{b}}|_T$ may be calculated from them.

The heat capacity c_b.

In principle, the heat capacity can be calculated from the free energy. However, the free energy is in general not completely known for a material, especially $\overline{\psi}$ in (2.52) and the temperature and density dependence of the shear modulus are generally not known. Therefore the heat capacity at constant deformation c_b has to be related to a measurable quantity: the heat capacity at

constant stress c_σ or the value of the latter in equilibrium, denoted by c_σ^0. The heat capacity at constant stress c_σ is related to c_b by

$$c_\sigma = T \left. \frac{\partial s}{\partial T} \right|_{\underline{\underline{\sigma}}} = c_b + \Delta c = T \left. \frac{\partial s}{\partial T} \right|_{\underline{\underline{b}}} + T \left. \frac{\partial s}{\partial \underline{\underline{b}}} \right|_T : \left. \frac{\partial \underline{\underline{b}}}{\partial T} \right|_{\underline{\underline{\sigma}}}, \tag{2.77}$$

where the definitions of the heat capacities in (2.39) have been used. If the free energy $\psi(\underline{\underline{b}}, T)$ is known Δc, the difference between c_σ and c_b can be calculated. In the remaining part c_b will be related to c_σ and c_σ^0 for the example of a neo-Hookean material.

For the neo-Hookean free energy (2.52), where the shear modulus G depends only on the temperature, Δc can be calculated analytically. With the thermodynamic relation between the entropy and the free energy (2.38) and the expression for the free energy of neo-Hookean elastic materials (2.52) the entropy can be calculated:

$$s = - \left. \frac{\partial \psi}{\partial T} \right|_{\underline{\underline{b}}} = -\frac{1}{2\rho_0} \frac{dG}{dT} (\mathrm{tr}\, \underline{\underline{b}} - 3) + \frac{d\bar{\psi}}{dT}. \tag{2.78}$$

Differentiation of this equation with respect to the Finger tensor at constant temperature gives

$$\left. \frac{\partial s}{\partial \underline{\underline{b}}} \right|_T = -\frac{1}{2\rho_0} \frac{dG}{dT} \underline{\underline{I}}. \tag{2.79}$$

The last term on the right-hand side of (2.77) follows after differentiation of (2.12) with respect to the temperature at constant stress:

$$\underline{\underline{0}} = \left. \frac{\partial \underline{\underline{\sigma}}}{\partial T} \right|_{\underline{\underline{\sigma}}} = - \left. \frac{\partial p + G}{\partial T} \right|_{\underline{\underline{\sigma}}} \underline{\underline{I}} + \left. \frac{\partial G \underline{\underline{b}}}{\partial T} \right|_{\underline{\underline{\sigma}}}. \tag{2.80}$$

The derivative of the pressure may be calculated as follows. From (2.12) it follows that the determinant of the stress tensor equals

$$\det \underline{\underline{\sigma}} = -(p + G) + G \det \underline{\underline{b}} = -p. \tag{2.81}$$

Differentiation with respect to the temperature at constant stress then gives

$$- \left. \frac{\partial p}{\partial T} \right|_{\underline{\underline{\sigma}}} = 0, \tag{2.82}$$

for an incompressible material. Combination with (2.80) then gives[9]

$$\left. \frac{\partial \underline{\underline{b}}}{\partial T} \right|_{\underline{\underline{\sigma}}} = -\frac{1}{G} \frac{dG}{dT} (\underline{\underline{b}} - \underline{\underline{I}}). \tag{2.83}$$

---

[9] A non-vanishing derivative of G in (2.83) also implicates that the thermal expansion is anisotropic. This topic will be discussed in more detail in section 2.5.1 about the temperature dependence of the shear modulus.

Combination of (2.77), (2.79) and (2.83) gives an expression for Δc, the difference between the heat capacity at constant stress and the heat capacity at constant deformation

$$\Delta c = c_\sigma - c_b = \frac{T}{2G\rho_0}\left(\frac{dG}{dT}\right)^2 (\mathrm{tr}\,\underline{\underline{b}} - 3). \tag{2.84}$$

Note that if the shear modulus G does not depend on the temperature, the heat capacity at constant stress equals the heat capacity at constant deformation. If G does depend on the temperature a distinction has to be made between c_σ and c_b. For an incompressible elastic material, $\det \underline{\underline{b}} = 1$, it is possible to prove that $\mathrm{tr}\,\underline{\underline{b}} \geq 3$. The proof will be given in section 3.2.1. Thus except when $\mathrm{tr}\,\underline{\underline{b}} = 3$, the heat capacity at constant stress is larger then the heat capacity at constant volume $c_\sigma > c_b$ (compare the result of viscous fluids $c_p > c_v$).

When c_σ is measured (as function of the stress and temperature) the heat capacity that is needed in (2.74) may be calculated from $c_b = c_\sigma - \Delta c$. However, it is also possible to relate c_b to the heat capacity c_σ in equilibrium. For a neo-Hookean material from (2.78):

$$\frac{c_b}{T} = \left.\frac{\partial s}{\partial T}\right|_{\underline{\underline{b}}} = -\frac{1}{2\rho_0}\frac{d^2G}{dT^2}(\mathrm{tr}\,\underline{\underline{b}} - 3) + \frac{d^2\overline{\psi}}{dT^2}. \tag{2.85}$$

From this equation it follows that the arbitrary function of the temperature $\overline{\psi}$ in the neo-Hookean free energy (2.52) can be related to the heat capacity c_b^0, which is the heat capacity c_b in the reference state $\underline{\underline{b}} = \underline{\underline{I}}$. If the shear modulus is constant or scales linearly with the temperature the second derivative of G vanishes, so then holds $c_b = c_b^0$ for all $\underline{\underline{b}}$. The heat capacity c_b only depends on the temperature then. Otherwise, the dependence on the Finger tensor is completely determined by the dependence on the Finger tensor of the neo-Hookean free energy (2.52). It also follows from (2.85) and (2.84) that in equilibrium the heat capacity at constant stress is equal to the heat capacity at constant deformation

$$c_\sigma^0 = c_\sigma|_{\underline{\underline{b}}=\underline{\underline{I}}} = c_b|_{\underline{\underline{b}}=\underline{\underline{I}}} = c_b^0, \tag{2.86}$$

where $c_\sigma^0 = d^2\overline{\psi}/dT^2$ is only a function of the temperature. The heat capacity at constant deformation c_b, which is needed in (2.74), may then also be written as

$$c_b = c_\sigma^0 - \Delta c^0 = c_\sigma^0 - \frac{1}{2\rho_0}\frac{d^2G}{dT^2}(\mathrm{tr}\,\underline{\underline{b}} - 3). \tag{2.87}$$

If the temperature dependence of the shear modulus is known, it only remains to determine the heat capacity $c_\sigma^0 = c_b^0$ as a function of the temperature. With the help of some measurements of c_σ it is then possible to check whether the model for the free energy is appropriate. Note that when the shear modulus G scales linearly with the temperature the second term on the right-hand side of (2.87) cancels and $c_b = c_\sigma^0$ for all possible deformations.

In terms of c_σ^0 the temperature equation for an incompressible neo-Hookean material finally becomes

$$\rho_0(c_\sigma^0 - \Delta c^0)\dot{T} + \rho_0 T \Delta s_b^e = -\nabla \cdot \underline{\phi}_q,$$
$$\Delta s_b^e = \left.\frac{\partial s}{\partial \underline{\underline{b}}}\right|_T : \dot{\underline{\underline{b}}},$$
$$\Delta c^0 = \frac{1}{2\rho_0}\frac{d^2G}{dT^2}(\mathrm{tr}\,\underline{\underline{b}} - 3), \tag{2.88}$$

which follows from (2.74) and (2.87).

Viscoelastic fluids

For a viscoelastic fluid the change of the entropy, which is considered as a function of the temperature, the thermodynamic pressure and the internal deformation tensors $s = s(T, p, \underline{\underline{b}}_k)$, can be written as

$$\dot{s} = \left.\frac{\partial s}{\partial T}\right|_{p,\underline{\underline{b}}} \dot{T} + \left.\frac{\partial s}{\partial p}\right|_{T,\underline{\underline{b}}} \dot{p} + \sum_{k=1}^{K} \left.\frac{\partial s}{\partial \underline{\underline{b}}_k}\right|_{p,T,\underline{\underline{b}}_k'} : \dot{\underline{\underline{b}}}_k = \frac{c_{p,b}}{T}\dot{T} - \frac{\alpha_{T,b}}{\rho}\dot{p} + \Delta s_b^{\mathrm{ve}}, \tag{2.89}$$

which defines the entropy difference Δs_b^{ve} for a viscoelastic fluid. For the last equality the definitions of the heat capacity and the thermal expansion coefficient $(2.42)_{2,3}$ have been used. The coefficients in (2.89) may still depend on the state variables p, T and the invariants of $\underline{\underline{b}}_k$. More details about the entropy difference and typical values for polymers of the thermal expansion coefficient and the heat capacity in equilibrium can be found in section 2.5.1.

Substitution of the entropy change (2.89) in the local entropy balance (2.44) with the viscoelastic entropy production (2.53), gives a temperature equation for viscoelastic fluids[10]

$$\rho c_{p,b}\dot{T} - T\alpha_{T,b}\dot{p} + \rho T\Delta s_b^{\mathrm{ve}} = T\Pi_s^{\mathrm{ve}} - T\nabla \cdot \underline{J}_s = D_{\mathrm{m}}^{\mathrm{ve}} - \nabla \cdot \underline{\phi}_q,$$

$$D_{\mathrm{m}}^{\mathrm{ve}} = T\Pi_s^{\mathrm{ve}}|_{\nabla T=\underline{0}} = \underline{\underline{\tau}} : \underline{\underline{d}} - \rho \sum_{k=1}^{K} \left.\frac{\partial \psi}{\partial \underline{\underline{b}}_k}\right|_{T,\rho,\underline{\underline{b}}_k'} : \dot{\underline{\underline{b}}}_k. \tag{2.90}$$

The viscoelastic mechanical dissipation, the production of irreversible heat, equals the stress work minus the isothermal change of the free energy. If the product of the derivatives in the second term on the right-hand side of $(2.90)_2$ is positive the mechanical dissipation is smaller than the stress work and (elastic) energy is stored. If it is negative the stored (elastic) energy is dissipated and the mechanical dissipation is larger than the stress work. With the help of (2.55) the derivatives of the free energy in the mechanical dissipation may be eliminated (compare section 2.3.2). The material derivatives of $\underline{\underline{b}}_k$ may be eliminated with the constitutive differential equations of appendix A. The resulting expressions for the various stress models are summarised in appendix B. Note that for steady homogeneous flows and fully developed channel or pipe flows the material derivatives of $\underline{\underline{b}}_k$ in $(2.90)_2$ vanish and that the viscoelastic mechanical dissipation $D_{\mathrm{m}}^{\mathrm{ve}}$ then equals the stress work $\underline{\underline{\tau}} : \underline{\underline{d}}$.

If the free energy $\psi(T, \rho, \underline{\underline{b}}_k)$ is known completely, the stress, the mechanical dissipation and the entropy derivatives in (2.90) may be calculated. Figure 2.1 gives an overview through which derivatives these quantities are related to the free energy ψ. The entropy can be calculated from the free energy with the equation of state $(2.41)_1$. Differentiation of the entropy, with respect to the concerned quantity, then gives the heat capacity $c_{p,b}$, the thermal expansion

---

[10]In a similar way a temperature equation has been derived by Flaman (1990), Akkerman (1993) and Peters (1995). By analogy with the theory for elastic materials the free energy (or entropy) has been split into two parts in the first two articles. The first part only depends on a reduced internal deformation tensor (Flaman uses $\underline{\underline{b}}_k^r = I_{3,k}^{1/3}\underline{\underline{b}}$ and Akkerman $\underline{\underline{b}}_k^r = \underline{\underline{b}} - I_{3,k}^{1/3}\underline{\underline{I}}$) and the second part only depends on the density and the temperature. For viscoelastic materials this is rather strange, because the density and the internal deformation tensors are independent variables. Peters only considers incompressible viscoelastic materials, where the free energy may depend on both the temperature and the internal deformation tensors: $\psi = \psi(\underline{\underline{b}}_k, T)$. For the models with an upper-convected derivative his results for the mechanical dissipation are in error.
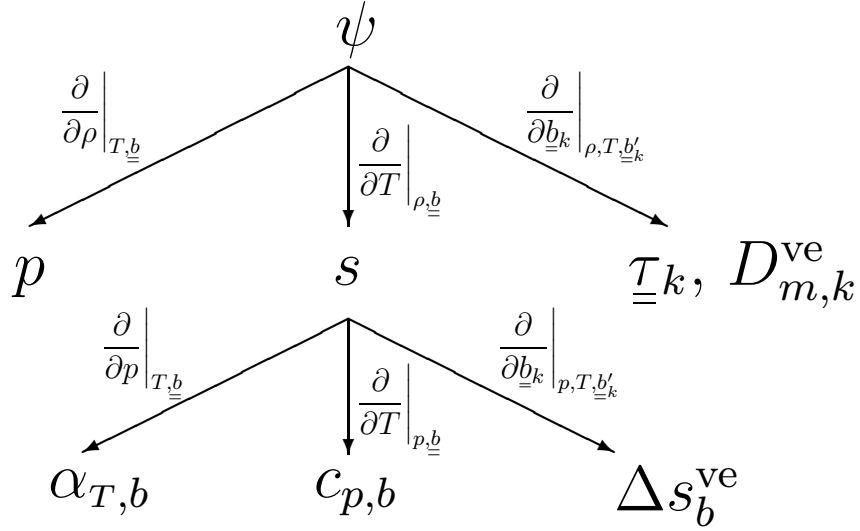
$$\psi$$

$$\frac{\partial}{\partial \rho}\Big|_{T,\underline{b}} \qquad \frac{\partial}{\partial T}\Big|_{\rho,\underline{\underline{b}}} \qquad \frac{\partial}{\partial \underline{\underline{b}}_k}\Big|_{\rho,T,\underline{\underline{b}}'_k}$$

$$p \qquad\qquad s \qquad\qquad \underline{\underline{\tau}}_k,\ D^{\mathrm{ve}}_{m,k}$$

$$\frac{\partial}{\partial p}\Big|_{T,\underline{b}} \qquad \frac{\partial}{\partial T}\Big|_{p,\underline{\underline{b}}} \qquad \frac{\partial}{\partial \underline{\underline{b}}_k}\Big|_{p,T,\underline{\underline{b}}'_k}$$

$$\alpha_{T,b} \qquad\qquad c_{p,b} \qquad\qquad \Delta s^{\mathrm{ve}}_b$$

Figure 2.1: Overview of the derivatives through which the thermodynamic quantities are related to the free energy ψ and the entropy s.

coefficient $\alpha_{T,b}$ and the entropy change Δs^{ve}_b. Unfortunately there are no measurements of the free energy, so that ψ is often specified by a theoretical model. Therefore it is necessary to express the coefficients in (2.90) in measurable quantities. In the remaining part of this section the entropy difference Δs^{ve}_b, the heat capacity $c_{p,b}$ and the thermal expansion coefficient $\alpha_{T,b}$ will be related to quantities which have been measured or are more easily to measure. As an example the coefficients will be elaborated for the neo-Hookean model. In the literature review in section 2.5.1 the scaling of the moduli with the temperature and the density will be discussed, which mainly determines the resulting coefficients. For these dependences all coefficients will be calculated explicitly.

The entropy difference Δs^{ve}_b.

If the free energy is not known $\partial s/\partial \underline{\underline{b}}_k|_{p,T,\underline{\underline{b}}'_k}$ may be related to the temperature dependence of the corresponding mode of the elastic stress $\underline{\underline{\tau}}_{e,k}$. From the equation of state for the entropy (2.41) and the relation (2.55) between the elastic modal stress $\underline{\underline{\tau}}_{e,k}$ and the free energy, it follows that

$$\frac{\partial s}{\partial \underline{\underline{b}}_k}\Big|_{T,p,\underline{\underline{b}}'_k} = -\frac{\partial}{\partial \underline{\underline{b}}_k}\left(\frac{\partial \psi}{\partial T}\Big|_{\rho,\underline{\underline{b}}_k}\right)\Big|_{T,p,\underline{\underline{b}}'_k} = -\frac{\partial}{\partial T}\left(\frac{\partial \psi}{\partial \underline{\underline{b}}_k}\Big|_{T,p,\underline{\underline{b}}'_k}\right)\Big|_{\rho,\underline{\underline{b}}_k} = -\frac{1}{2\rho}\underline{\underline{b}}_k^{-1}\cdot\frac{\partial \underline{\underline{\tau}}_k + \underline{\underline{\Delta}}_\psi}{\partial T}\Big|_{\rho,\underline{\underline{b}}},$$

$$\underline{\underline{\Delta}}_\psi = \frac{\partial \psi}{\partial \rho^{-1}}\Big|_{T,\underline{\underline{b}}}\ \frac{\partial \rho^{-1}}{\partial \underline{\underline{b}}_k}\Big|_{p,T,\underline{\underline{b}}'_k}. \tag{2.91}$$

The $\underline{\underline{\Delta}}_\psi$ term vanishes if $\rho = \rho(p,T)$. Then the entropy derivative $\partial s/\partial \underline{\underline{b}}_k|_{p,T,\underline{\underline{b}}'_k}$ is directly related to the stress derivative, as for the relation for elastic materials (2.76). Thus then the entropy derivative $\partial s/\partial \underline{\underline{b}}_k|_{p,T,\underline{\underline{b}}'_k}$ may be calculated from experimental data, when some measurements of the temperature dependence of the stress are available.

If the free energy is known, the entropy may be calculated from the equation of state for the entropy (2.41). Differentiation of the entropy with respect to the internal deformation

tensor $\underline{b}_k$ then gives the entropy derivative in Δs_b^{ve}. The calculation will be performed for the neo-Hookean and the Larson free energies, with various choices of the shear modulus $G(\rho, T)$.

Examples: Δs_b^{ve} for the neo-Hookean and Larson free energies.

Successively the entropy difference will be calculated explicitly for the free energies with constant moduli, moduli that depend linearly on the temperature and moduli that depend linearly on the temperature and the density.

- If the free energy can be written as $\psi(\rho, \underline{b}_k, T) = \psi_\rho(\rho, T) + \psi_{b_k}(\underline{b}_k)$, and if it is assumed that $\rho = \rho(p, T)$, the entropy does not depend on $\underline{b}_k$ and in Δs_b^{ve} the derivatives of the entropy with respect to the internal deformation tensor in (2.90) vanish. In this case the entropy is a function of the temperature and the density or pressure only $(u(\rho, \underline{b}_k, T) = \psi(\rho, \underline{b}_k, T) + Ts(\rho, T))$ and the reversible part of the energy is stored as internal energy. The fluid is then called entirely energy elastic and the polymer chains act like springs. The temperature equation (2.90) becomes

$$\rho c_{p,b} \dot{T} - T\alpha_{T,b}\dot{p} = D_{\text{m}}^{\text{ve}} - \nabla \cdot \underline{\phi}_q,$$

$$D_{\text{m}}^{\text{ve}} = 2\eta_s \underline{d} : \underline{d} + (\eta_{s,v} - \tfrac{2}{3}\eta_s)(\nabla \cdot \underline{v})^2 + \sum_{k=1}^{K} \frac{1}{2\lambda_k(1 - \xi_k)} \left(\underline{\tau}_k \cdot \underline{b}_k^{-1}\right) : \underline{g}_k, \qquad (2.92)$$

where the expression (2.64) has been used for the viscoelastic entropy production[11]. Examples of the energy elasticity are the viscoelastic neo-Hookean free energy (2.66) and the Larson free energy (2.67) where the shear moduli G_k, and the parameters β_k for the Larson free energy, do not depend on the temperature.

- If the free energy consists of products of functions of the temperature and functions of the invariants of the internal deformation tensor, $\psi(\rho, \underline{b}_k, T) = \psi_\rho(\rho, T) + \psi_{b_k}(\underline{b}_k, T)$, the derivatives of the entropy in Δs_b^{ve} do not vanish. If, for example, the free energy can be written as $\psi(\rho, \underline{b}_k, T) = \psi_\rho(\rho, T) + T\psi_{b_k}(\underline{b}_k)$, the entropy difference Δs_b^{ve} becomes

$$\Delta s_b^{\text{ve}} = \sum_{k=1}^{K} \left.\frac{\partial s}{\partial \underline{b}_k}\right|_{p,T,\underline{b}_k'} : \dot{\underline{b}}_k = -\sum_{k=1}^{K} \frac{1}{T}\left.\frac{\partial \psi}{\partial \underline{b}_k}\right|_{p,T,\underline{b}_k'} : \dot{\underline{b}}_k = -\sum_{k=1}^{K} \frac{1}{T}\left.\frac{\partial \psi}{\partial \underline{b}_k}\right|_{\rho,T,\underline{b}_k'} : \dot{\underline{b}}_k, \qquad (2.93)$$

where the equation of state for the entropy $(2.41)_1$ has been used for the first and $\rho = \rho(p, T)$ for the last equality. In this case the internal energy is a function of the temperature and density or pressure only $(u(\rho, T) = \psi(\rho, \underline{b}_k, T) + Ts(\rho, \underline{b}_k, T))$ and the reversible part of the energy is stored as entropy. Then the material is called entropy elastic and the polymer chains act like rods, which are not stretched, but oriented in a preferential direction when they are deformed. Examples of the entropy elasticity are the neo-Hookean free energy (2.66) and the Larson free energy (2.67) where the shear moduli depend linearly on the temperature $G_k = TG_{k,\text{ref}}/T_{\text{ref}}$ and $\rho = \rho(p, T)$. For the Larson model β_k has to be independent of the temperature as well.

Substitution of Δs_b^{ve} in $(2.90)_1$ and comparison with the right-hand side of the mechanical dissipation $(2.90)_2$ shows that both terms cancel out. The temperature equation for viscoelastic fluids then reduces to

$$\rho c_{p,b}\dot{T} - T\alpha_{T,b}\dot{p} = \underline{\tau} : \underline{d} - \nabla \cdot \underline{\phi}_q. \qquad (2.94)$$

---

[11]Due to the condition $\rho = \rho(p, T)$ the derivative of the ψ_ρ-term with respect to $\underline{b}_k$ vanishes.

Thus for a linear temperature dependence of the moduli G_k and $\rho = \rho(p, T)$ the stress work contributes completely to the temperature change of the fluid. Contrary to the case where G_k does not depend on the temperature, no elastic energy will be stored now. However, a part of the heat, viz. $\underline{\underline{\tau}} : \underline{\underline{d}} - D_{\mathrm{m}}^{\mathrm{ve}}$, is reversible heat. This result is analogous to the elastic case (2.75), except that then the whole stress work was converted into reversible heat.

- If the free energy can be written as $\psi(\rho, \underline{\underline{b}}_k, T) = \psi_\rho(\rho, T) + \rho T \psi_{b_k}(\underline{\underline{b}}_k)$, the equality (2.93) still holds. Thus the temperature equation is given by (2.94) as well. Examples are the neo-Hookean and Larson free energies where the moduli are given by $G_k = \rho T G_{k,\mathrm{ref}}/\rho_{\mathrm{ref}} T_{\mathrm{ref}}$ and $\rho = \rho(p, T)$. For the Larson model β_k has to be independent of the density and the temperature as well.

Experiments indicating whether a viscoelastic fluid is entropy, energy elastic or something in between, will be discussed in the section about the temperature dependence of the shear modulus in 2.5.1.

The heat capacity $c_{p,b}$.

In principle, the heat capacity $c_{p,b}$ can be calculated from the free energy. However, the elastic energy is in general not completely known for viscoelastic fluids, especially the $\overline{\psi}$ and the temperature and density dependence of the shear moduli in the free energies (2.66) or (2.67) is not known. Furthermore it is doubtful whether both free energies are still good approximations for large deformation rates. Therefore the heat capacity at constant pressure and internal deformation $c_{p,b}$ has to be related to a measurable quantity. This could be the heat capacity at constant pressure and constant elastic stress or the value of the latter in equilibrium. The heat capacity at a constant pressure and elastic stress c_{p,τ_e} is related to $c_{p,b}$ by

$$c_{p,\tau_e} = T \left.\frac{\partial s}{\partial T}\right|_{p,\underline{\underline{\tau}}_e} = c_{p,b} + \Delta c = T \left.\frac{\partial s}{\partial T}\right|_{p,\underline{\underline{b}}} + T \sum_{k=1}^{K} \left.\frac{\partial s}{\partial \underline{\underline{b}}_k}\right|_{T,p,\underline{\underline{b}}_k'} : \left.\frac{\partial \underline{\underline{b}}_k}{\partial T}\right|_{p,\underline{\underline{b}}_k',\underline{\underline{\tau}}_{e,k}}, \tag{2.95}$$

where the definitions of the heat capacities (2.42) have been used. If the free energy $\psi(\underline{\underline{b}}_k, \rho, T)$ is known Δc, the difference between c_{p,τ_e} and $c_{p,b}$, can be calculated. For the neo-Hookean model, with the free energy (2.66), this can be done analytically. For the Larson model it is also possible to calculate the difference analytically. However, the $\partial \underline{\underline{b}}_k/\partial T|_{p,\underline{\underline{b}}_k',\underline{\underline{\tau}}_{e,k}}$ is more difficult to elaborate due to the nonlinear relation between the extra-stress and the internal deformation. Therefore, only the expressions for the neo-Hookean model will be given.

Example: $c_{p,b}$ for the neo-Hookean free energy.

For the neo-Hookean model, with the free energy (2.66), the moduli are given by $G_k = G_k(\rho, T)$. With the help of the thermodynamic relation between the entropy and the free energy (2.41) the entropy may then be calculated by differentiation of ψ

$$s = -\left.\frac{\partial \psi}{\partial T}\right|_{\rho,\underline{\underline{b}}} = -\sum_{k=1}^{K} \frac{1}{2\rho(1-\xi_k)^2} \left.\frac{\partial G_k}{\partial T}\right|_{\rho} (I_{1,k} - \ln I_{3,k} - 3) + \left.\frac{\partial \overline{\psi}}{\partial T}\right|_{\rho}. \tag{2.96}$$

Differentiation of this equation with respect to the kth internal deformation tensor at constant

temperature, pressure and $\underline{b}_l$ for all l except $l = k$ gives

$$
\left.\frac{\partial s}{\partial \underline{\underline{b}}_k}\right|_{T,p,\underline{b}'_k} = -\frac{1}{2\rho(1-\xi_k)^2}\left.\frac{\partial G_k}{\partial T}\right|_{\rho}(\underline{I} - \underline{b}_k^{-1}),
\tag{2.97}
$$

where the assumption that $\rho = \rho(p,T)$ has been used. The last term on the right-hand side of (2.95) may be calculated from (2.19) and (2.63). Differentiation of the elastic modal stress $\underline{\tau}_{e,k}$ with respect to the temperature gives

$$
\underline{\underline{0}} = \left.\frac{\partial \underline{\tau}_{e,k}}{\partial T}\right|_{p,\underline{b}'_k,\underline{\tau}_{e,k}} = \frac{G_k}{(1-\xi_k)^2}\left.\frac{\partial \underline{b}_k}{\partial T}\right|_{p,\underline{b}'_k,\underline{\tau}_{e,k}} + \frac{1}{(1-\xi_k)^2}(\underline{b}_k - \underline{I})\left.\frac{\partial G_k}{\partial T}\right|_{p,\underline{b}'_k,\underline{\tau}_{e,k}}.
\tag{2.98}
$$

After rearrangement of this equation the expression for the last term on the right-hand side of (2.95) becomes[12]

$$
\left.\frac{\partial \underline{b}_k}{\partial T}\right|_{p,\underline{b}'_k,\underline{\tau}_{e,k}} = -\frac{1}{G_k}\left.\frac{\partial G_k}{\partial T}\right|_p(\underline{b}_k - \underline{I}).
\tag{2.99}
$$

Combination of (2.95), (2.97) and (2.99) gives an expression for the heat capacity difference Δc

$$
\Delta c = c_{p,\tau_e} - c_{p,b} = \sum_{k=1}^{K}\frac{T}{2(1-\xi_k)^2\rho G_k}\left.\frac{\partial G_k}{\partial T}\right|_p\left.\frac{\partial G_k}{\partial T}\right|_{\rho}(I_{1,k} + \mathrm{tr}\,\underline{b}_k^{-1} - 6).
\tag{2.100}
$$

Thus when c_{p,τ_e} is measured the heat capacity $c_{p,b}$ that is needed in (2.90) may be calculated from $c_{p,b} = c_{p,\tau_e} - \Delta c$, where Δc is obtained from a viscoelastic model.

The term with the invariants in (2.100) vanishes in equilibrium and is always positive out of equilibrium. A decomposition on the principle axes immediately proves this result, because the function $x + 1/x - 2$ has a local minimum at $x = 1$. So dependent on the signs of the temperature derivatives of the moduli Δc is positive or negative. It is illustrative to distinguish the following examples.

- If G_k does not depend on the temperature, the heat capacity at constant pressure and elastic stress equals the heat capacity at constant pressure and internal deformation.
- If $G_k = G_{k,\mathrm{ref}}T/T_{\mathrm{ref}}$ is taken Δc is positive. This is analogous to the viscous example, where $c_p > c_v$, and the elastic example, where $c_\sigma > c_b$.
- If $G_k = G_{k,\mathrm{ref}}\rho T/\rho_{\mathrm{ref}}T_{\mathrm{ref}}$ is taken, and $\rho = \rho(p,T)$, Δc will still be positive, because the temperature dependence of the density is weak. Then $\partial G_k/\partial T|_p = (1-\alpha T)G_k/T$, which is positive (the thermal expansion coefficient in equilibrium is $\alpha T_\mathrm{g} \simeq 0.16$ for polymers, see section 2.5.1) in the temperature region where the scaling of the moduli is valid.

For the neo-Hookean model it is also possible to relate $c_{p,b}$ to the heat capacity in equilibrium. Differentiation of the entropy (2.96) gives an expression for $c_{p,b}$

$$
\frac{c_{p,b}}{T} = \left.\frac{\partial s}{\partial T}\right|_{p,\underline{\underline{b}}} = -\sum_{k=1}^{K}\frac{1}{2(1-\xi_k)^2}\left.\frac{\partial}{\partial T}\left(\frac{1}{\rho}\left.\frac{\partial G_k}{\partial T}\right|_{\rho}\right)\right|_p(I_{1,k} - \ln I_{3,k} - 3) + \left.\frac{\partial}{\partial T}\left(\left.\frac{\partial \overline{\psi}}{\partial T}\right|_{\rho}\right)\right|_p.
\tag{2.101}
$$

---

[12]A non-vanishing derivative of G_k in (2.99) also implicates that the thermal expansion is anisotropic. This topic will be discussed in more detail in section 2.5.1 about the temperature dependence of the moduli G_k.

From (2.101) it follows that the arbitrary function of the temperature and density $\overline{\psi}$ can be related to the heat capacity in equilibrium $c_{p,b}^{\text{eq}} = c_{p,b}(\underline{\underline{b}}_k = \underline{\underline{I}})$. The heat capacity $c_{p,b}^{\text{eq}}$ only depends on the pressure and the temperature.

In equilibrium, where $\underline{\underline{b}}_k = \underline{\underline{I}}$ for all modes $k = 1, ..., K$, the heat capacity at constant pressure and elastic stress equals $c_{p,b}^{\text{eq}}$:

$$c_{p,\tau_e}^{\text{eq}} = c_{p,\tau_e}|_{\underline{\underline{b}}_k = \underline{\underline{I}}} = c_{p,b}|_{\underline{\underline{b}}_k = \underline{\underline{I}}} = c_{p,b}^{\text{eq}}. \qquad (2.102)$$

Thus c_{p,τ_e}^{eq} also corresponds to the derivative of $\overline{\psi}$ in (2.101), which is only a function of the pressure and the temperature. The heat capacity at constant pressure and internal deformation is then

$$c_{p,b} = c_{p,\tau_e}^{\text{eq}} - \Delta c^{\text{eq}} = c_{p,\tau_e}^{\text{eq}} - \sum_{k=1}^{K} \frac{T}{2(1-\xi_k)^2} \frac{\partial}{\partial T}\left(\rho^{-1} \left.\frac{\partial G_k}{\partial T}\right|_\rho\right)\Bigg|_p (I_{1,k} - \ln I_{3,k} - 3). \quad (2.103)$$

If the temperature dependence of the shear modulus and the density are known, it only remains to determine (measure) the heat capacity $c_{p,\tau_e}^{\text{eq}} = c_{p,b}^{\text{eq}}$ as a function of the pressure and the temperature. The heat capacity difference Δc^{eq} is given by the (viscoelastic) model.

The term with the invariants in (2.103) vanishes in equilibrium and is positive out of equilibrium. A decomposition on the principle axes immediately proves this result, because the function $x + \ln x - 1$ has a local minimum at $x = 1$. So, dependent on the sign of the temperature derivative in (2.103), Δc^{eq} is positive or negative. It is illustrative to distinguish the following examples.

- If G_k does not depend on the temperature the temperature derivative vanishes and $c_{p,b} = c_{p,\tau_e}^{\text{eq}}$ then. So $c_{p,b}$ can directly be obtained from published experimental data of the heat capacity at constant pressure.
- If $G_k = G_{k,\text{ref}}T/T_{\text{ref}}$, the heat capacity difference Δc^{eq} becomes

$$\Delta c^{\text{eq}} = \sum_{k=1}^{K} \frac{\alpha_{T,b} G_k}{2\rho(1-\xi_k)^2}\left((I_{1,k} - \ln I_{3,k} - 3)\right), \qquad (2.104)$$

  where the definition for the thermal expansion (2.42) has been used. Then the difference Δc^{eq} is positive, thus $c_{p,b}$ decreases when the material is deformed.
- If the shear modulus scales with $G_k = G_{k,\text{ref}}\rho T/\rho_{\text{ref}}T_{\text{ref}}$ the temperature derivative in (2.103) vanishes. Then holds again that $c_{p,b} = c_{p,\tau_e}^{\text{eq}}$ for all types of deformations. So again $c_{p,b}$ can directly be obtained from published experimental data of the heat capacity at constant pressure.

The thermal expansion coefficient $\alpha_{T,b}$.

In nonisothermal computations of viscoelastic fluids the thermal expansion is often not taken into account, due to the assumption of incompressible fluids. Even in shear flows this is not always justified, as will be shown with a non-dimensional analysis in section 2.6: when the mechanical dissipation term in the temperature equation is important $\alpha_{T,b}T \ll 1$ should hold to neglect the influence of thermal expansion term in the temperature equation. Although the thermal expansion coefficient is relatively small, for normal processing temperatures this

condition is not fulfilled for polymers. Refer to section 2.5.1 for the order of magnitude of the thermal expansion coefficient.

When the free energy, or the entropy, is known the thermal expansion coefficient may be calculated. For a neo-Hookean material the entropy is given by (2.96) and $\alpha_{T,b}$ can simply be found by differentiation of the entropy.

Example: $\alpha_{T,b}$ for the neo-Hookean free energy.

For the neo-Hookean model, with the free energy (2.66), the moduli are given by $G_k = G_k(\rho, T)$. It is illustrative to distinguish the following examples.

- If the density is constant and $G_k = G_k(T)$ only $\overline{\psi}$ may depend on the pressure and the thermal expansion coefficient becomes

$$\left.\frac{\partial s}{\partial p}\right|_{T,\underline{\underline{b}}} = \left.\frac{\partial}{\partial p}\left(\left.\frac{\partial \overline{\psi}}{\partial T}\right|_{\rho}\right)\right|_{T} = \alpha, \tag{2.105}$$

  where α equals the thermal expansion coefficient in equilibrium, which may still depend on the temperature and the pressure.

- If $\rho = \rho(p,T)$ and $G_k = G_k(T)$ the thermal expansion coefficient becomes

$$\left.\frac{\partial s}{\partial p}\right|_{T,\underline{\underline{b}}} = \alpha - \sum_{k=1}^{K} \frac{1}{2(1-\xi_k)^2} \left.\frac{\partial \rho^{-1}}{\partial p}\right|_{T,\underline{\underline{b}}} \frac{dG_k}{dT}\left(I_{1,k} - \ln I_{3,k} - 3\right), \tag{2.106}$$

  which is approximately equal to α, because the isothermal compressibility κ_T, defined by (2.42), is small for polymeric fluids.

- If $\rho = \rho(p,T)$ and $G_k = \rho G_k(T)/\rho_{\mathrm{ref}}$ the thermal expansion coefficient becomes

$$\left.\frac{\partial s}{\partial p}\right|_{T,\underline{\underline{b}}} = \alpha. \tag{2.107}$$

For these examples the thermal expansion coefficient in equilibrium α seems to be a good approximation of $\alpha_{T,b}$.

In terms of $c_{p,\tau_e}^{\mathrm{eq}}$ and α the temperature equation for a viscoelastic fluid finally becomes

$$\rho\left(c_{p,\tau_e}^{\mathrm{eq}} - \Delta c^{\mathrm{eq}}\right)\dot{T} - T\alpha\dot{p} + \rho T\Delta s_b^{\mathrm{ve}} = D_{\mathrm{m}}^{\mathrm{ve}} - \nabla\cdot\underline{\phi}_q,$$

$$D_{\mathrm{m}}^{\mathrm{ve}} = 2\eta_s\underline{\underline{d}}:\underline{\underline{d}} + \left(\eta_{s,v} - \tfrac{2}{3}\eta_s\right)(\nabla\cdot\underline{v})^2 + \sum_{k=1}^{K}\frac{1}{2\lambda_k(1-\xi_k)}\left(\underline{\underline{\tau}}_k\cdot\underline{\underline{b}}_k^{-1}\right):\underline{\underline{g}}_k, \tag{2.108}$$

where (2.64) has been used for the viscoelastic mechanical dissipation. For neo-Hookean models the difference between the heat capacities Δc^{eq} is given by (2.103).

2.4 Heat flux constitutive equations

In this section the constitutive equation for the heat flux, which is still needed in the temperature equation (2.90) or (2.108) will be discussed. Firstly a brief description will be given for viscous

fluids and elastic materials. Then the heat flux constitutive equation for viscoelastic fluids will be discussed more extensively. The discussion will be focused on a general form of the well-known Fourier law, where the anisotropy caused by orientation of the polymer chains can be taken into account.

Viscous fluids

For viscous fluids a widely used constitutive equation is Fourier's law with an isotropic heat conduction:

$$\underline{\phi}_q = -\kappa \nabla T, \tag{2.109}$$

where κ is the heat conduction coefficient. It may be a function of the state variables T and p.

In the literature of thermodynamics, another equation for the heat flux is proposed. It is obtained when an internal vector process is introduced, similar to the internal tensor process for the description of viscoelastic fluids (see Kuiken 1994). For one internal process and constant coefficients the internal variable can be eliminated. With the upper-convected derivative as the frame invariant derivative the following equation is obtained

$$\lambda_\phi \overset{\triangledown}{\underline{\phi}_q} + \underline{\phi}_q = -\kappa \left(\nabla T + \lambda_T \overset{\triangledown}{\underline{\nabla T}} \right),$$

$$\overset{\triangledown}{\underline{\phi}_q} = \dot{\underline{\phi}}_q - \underline{\underline{L}} \cdot \underline{\phi}_q, \tag{2.110}$$

where $\overset{\triangledown}{(\;)}$ is the upper-convected derivative for a vector. A line below the convected derivative denotes that the derivative works on the complete overlined quantity. If $\lambda_T = 0$ (2.110) reduces to the Vernotte–Cattaneo equation. Then the term with the derivative of the heat flux avoids that the heat propagates with an infinite velocity through the fluid. For a small relaxation time λ_ϕ compared to the time scale of the flow, Fourier's law is a good approximation of this equation.

Elastic materials

For an isotropic elastic material the Fourier law for the heat flux can be described by

$$\underline{\phi}_q = -\underline{\underline{\kappa}} \cdot \nabla T, \tag{2.111}$$

where the heat conduction tensor $\underline{\underline{\kappa}}$ may depend on the state variables, the temperature and the Finger tensor $\underline{\underline{b}}$. For isotropic elastic materials $\underline{\underline{\kappa}}$ is an isotropic tensor function of the Finger tensor. Therefore the heat conduction tensor is symmetric, just as the Finger tensor.

The effect of orientation on the thermal conductivity of elastic rubbers has, among others, been measured by Hands (1980). In his experiments thin sheets have been elongated biaxially to a certain elongation ratio. Then the thermal conductivity perpendicular to the stretching direction has been measured. The measurements show that the perpendicular conductivity decreases when the elongation ratio is increased. The effect is considerable. The conductivity perpendicular to the elongation at an elongation ratio $\epsilon = L/L_{\text{eq}} = 1.8$, where L is the length of the sample in the direction of elongation, is only 25 % of the thermal conductivity at rest. Van den Brule & O'Brien (1990) were able to fit the data of Hands (1980) with the model $\underline{\underline{\kappa}} = (1-c)\underline{\underline{I}} + c\underline{\underline{b}}$, with $c = 0.25$

.

Viscoelastic fluids

For an isotropic viscoelastic fluid the Fourier law for the heat flux has the general form

$$\underline{\phi}_q = -\underline{\underline{\kappa}} \cdot \nabla T, \tag{2.112}$$

where the heat conduction tensor $\underline{\underline{\kappa}}$ corresponds to the tensor $T^{-1}\underline{\underline{\Lambda}}_{qq}$ in the phenomenological equation (2.58). In section 2.3 it has been shown that this was the most general expression if the internal deformation tensors were the only internal variables. The heat conduction tensor may still depend on the state variables: the internal deformation tensors $\underline{\underline{b}}_k$, the density or pressure, and the temperature. Mostly the thermal conductivity is a weak function of the temperature, see section 2.5.1. For polymeric fluids no data could be found in the literature about the pressure dependence. For an isotropic material the heat conduction tensor has to be an isotropic tensor function of the internal deformation tensors. Due to the symmetry of $\underline{\underline{b}}_k$ the heat conduction tensor will be symmetric as well.

Possible internal vector variables, as used by Kuiken (1994), have not be taken into account in (2.112). For a viscous fluid the introduction of an internal vector variable led to (2.110). Both equation (2.110) and (2.112) describe the relaxation of the heat flux. The internal vector variables describe the relaxation of the heat flux due to the change of the temperature gradient. The dependence of the heat conduction tensor on the internal deformation tensor describes the relaxation due to the change of the velocity gradient. When the relaxation of the heat flux due to the change of the temperature gradient is significant, internal vector variables, which fulfil a certain frame invariant differential equation, may be added to the heat flux equation (2.112). Then extra equations for the internal vector variables have to be solved and extra parameters, such as relaxation times, have to be determined. Due to lack of experimental evidence the internal vector variables will not be taken into account.

For nonisothermal simulations of viscoelastic fluids, following the standard practice of viscous fluids, it is generally assumed that the heat conduction tensor is isotropic. Measurements show however that this is not always correct. For most of the polymeric materials for which the anisotropy has been measured the thermal conductivity parallel to the orientation increases monotonically with increasing orientation. The thermal conductivity perpendicular to the orientation decreases until a minimum value has been reached. Then it remains constant.

Before discussing the model for the anisotropic heat conduction, a short overview will be given of some measurements of the anisotropy of the heat conduction tensor for various polymers.

The effect of orientation on the thermal conductivity for the amorphous polymers polymethylmethacrylate (PMMA) and polystyrene (PS) has been measured by Washo & Hansen (1969). The samples have first been stretched uniaxially to a certain elongation ratio. Next they were cooled to room temperature and the thermal conductivities parallel and perpendicular to the stretching direction have been measured. The elongation rate and the cooling rate have not been reported, although this may be important in connection with the ratio of the reversible and irreversible deformation and the possible relaxation after the elongation.

They found an increase of the heat conduction in the direction of orientation and a decrease in the directions perpendicular to it, see figure 2.2. The effect is smaller than for

the rubber experiments of Hands (1980). For an elongation ratio of $\epsilon = 4$, $\kappa_\perp/\kappa_{eq} \simeq 0.85$ and $\kappa_\parallel/\kappa_{eq} \simeq 1.4$ for the most isotropic fluid. However, no asymptotic value for $\kappa_\perp$ has been reached then. There is also a temperature effect in the experiments of Washo & Hansen (1969). The polymers are stretched at a temperature in the range of $373 - 433$ K and then cooled to a temperature of 313 K at which the thermal conductivities are measured. The increasing stretching temperature causes a decrease of the orientation and consequently a decrease of the anisotropy.

Hellwege et al. (1963) have measured the anisotropy in a uniaxial elongation of PMMA, polyvinylchloride (PVC), polycarbonate (PC) and polystyrol (PST). The stretching has been performed in the liquid state. Then the samples were cooled down below the glass transition temperature after which the anisotropy was measured. The deformations of the polymer fluids could be considered as completely elastic, because compared to a reference sample no dimensional changes were observed after relaxation in the liquid state. For PST the anisotropy was relatively small, changes of less than 10 % for $\kappa_\perp$ and $\kappa_\parallel$ for $\epsilon = 5$. For PC the anisotropy was the largest, changes of about 25 % for $\kappa_\perp$ and 40 % for $\kappa_\parallel$ for an elongation ratio smaller than one. For the PVC melt the influence on $\kappa_\perp$ and $\kappa_\parallel$ of the temperature has been measured. For the equilibrium and the perpendicular thermal conductivity no measurable changes could be found. For the parallel thermal conductivity, however, a week linear increase with the temperature was observed. With increasing elongation the slope $\partial\kappa_\parallel/\partial T$ becomes larger.

Picot et al. (1982) measured the perpendicular thermal conductivity for a polyethylene melt. For shear rates of about 50 s^{-1} they found a small increase of the thermal conductivity of about 2 %. Then $\kappa_\perp$ decreased until the highest shear rate of 400 s^{-1}. At the highest shear rate the decrease of the perpendicular thermal conductivity was about 10 %. An asymptotic value has not been reached then.

Wallace et al. (1985) measured the perpendicular thermal conductivity for two high density polyethylene melts (HDPE) with different molecular weights in a Couette flow, between two concentric cylinders. The measurements were done at a temperature of 433 K and a shear rate up to 400 s^{-1}. For the lower molecular weight polyethylene, $\kappa_\perp$ decreased until it was 40 % of the equilibrium conductivity at 150 s^{-1}. Then it remained constant up to the highest shear rate. After shearing at 400 s^{-1}, approximately 90 minutes were required to recover the equilibrium thermal conductivity. For the higher molecular weight polyethylene $\kappa_\perp$ decreased, until it was 30 % of the equilibrium conductivity at 50 s^{-1}. Then it increased again until 10 % above κ_{eq} at a shear rate of 300 s^{-1}. They gave a rather speculative explanation, without paying attention to degradation and heat production due to dissipation.

Choy et al. (1978, 1981) measured the parallel and perpendicular conductivity for semicrystalline polymers with a different amount of crystallinity, one of it was HDPE. The temperature was between the glass transition temperature and the melting temperature. They found that for the amorphous polymer the effect of the stretching is relatively small compared to semicrystalline polymers. For amorphous polymers the ratio of the thermal conductivities parallel and perpendicular to the direction of elongation can be $\kappa_\parallel/\kappa_\perp \simeq 2$ for an elonga-

tion ratio of $\epsilon = 4$ (Godovsky 1992). For semicrystalline polymers it can be much more: $\kappa_\parallel/\kappa_\perp \simeq 10$ for HDPE. See figure 2.3.
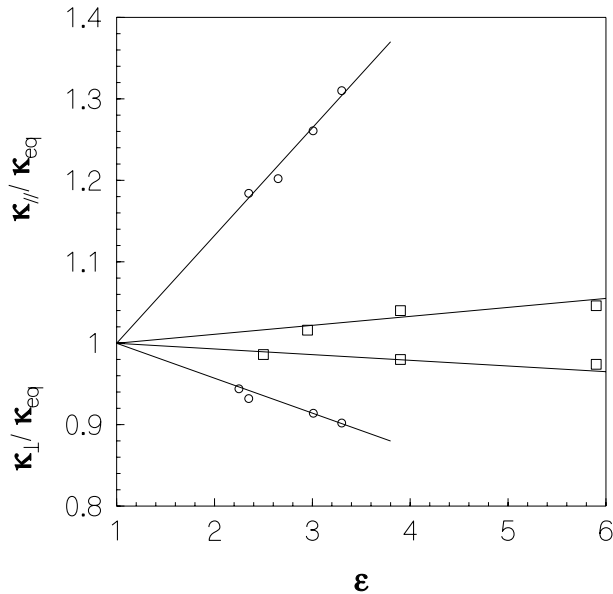

Figure 2.2: Thermal conductivities in the direction of orientation and perpendicular to the orientation for various amorphous polymers. A $\square$ denotes data of polystyrene and a $\circ$ data of plexiglas PMMA. From Washo & Hansen (1969).
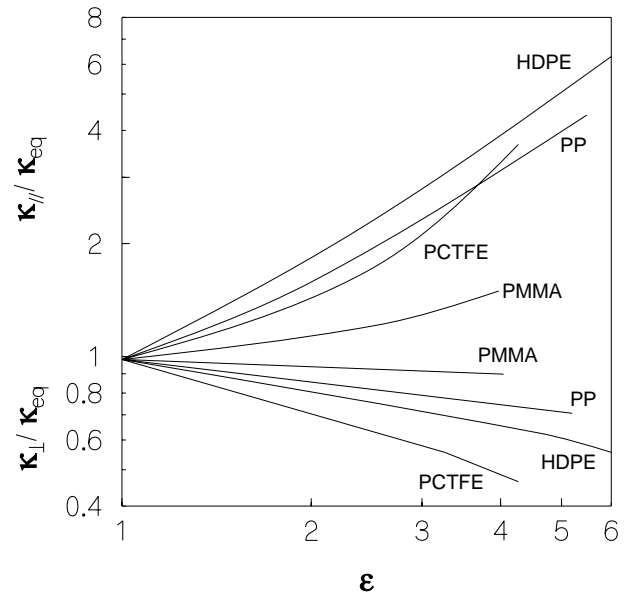
Figure 2.3: Thermal conductivities in the direction of orientation and perpendicular to the orientation for various polymer melts as function of the elongation. The anisotropy increases with the amount of crystallinity of the polymer. From Choy et al. (1981).

The physical idea behind the anisotropy of the heat conduction is that energy can be transported more easily along the backbone of polymer chains than from one chain to another. The interaction between two neighbouring molecules is determined by relatively weak van der Waals interactions, while the interactions between two adjacent segments in a molecule are determined by relatively strong chemical bonds. Due to their short range the van der Waals interactions are about the same in all directions and can be modelled with an isotropic term. In equilibrium there is no preferential direction for the polymer chains, thus the heat conduction is isotropic then. A deformation causes preferential directions in a viscoelastic fluid. The orientation is stronger if the deformation is larger. This energy transport through the polymer chains can be modelled with the internal deformation tensor, which is a measure for the elastic deformation.

In the remaining part of this section only the dependence on the internal deformation tensor will be considered. The dependence on the temperature of the heat conduction tensor will be given in section 2.5.1.

Dependence on the internal deformation tensor.

Analogously to the multi-mode stress constitutive equations in section 2.2, the usual assumption to handle multi-mode models, will be made for the heat conduction tensor as well. This means that the anisotropic contribution can be written as a sum over K isotropic tensor functions, where the kth function only depends on the kth internal deformation tensor. Then it follows

from the Cayley–Hamilton relation (2.18) that the most general model that can be obtained for the heat conduction tensor for the multi-mode models described in section 2.2, is

$$\underline{\underline{\kappa}} = \kappa_0 \underline{\underline{I}} + \sum_{k=1}^{K} \left(\kappa_{1,k} \underline{\underline{b}}_k + \kappa_{2,k} \underline{\underline{b}}_k^2 \right), \tag{2.113}$$

where the scalars κ_0, $\kappa_{1,k}$ and $\kappa_{2,k}$ may be functions of the density, the temperature and the invariants of $\underline{\underline{b}}_k$. For incompressible stress models such as the Leonov models (A.4) and (A.5) the third invariant equals $I_{3,k} = 1$, so the scalars κ_0, $\kappa_{1,k}$ and $\kappa_{2,k}$ 'only' depend on the density, the temperature and the first and second invariants. In chapter 3 it will be examined which stress models are capable of describing the increase of the thermal conductivity in the parallel direction and the decrease in the perpendicular direction.

In the equilibrium state the internal deformation tensor equals $\underline{\underline{b}}_k = \underline{\underline{I}}$ and the heat conduction tensor reduces to

$$\underline{\underline{\kappa}} = \kappa_{\text{eq}} \underline{\underline{I}},$$
$$\kappa_{\text{eq}} = \kappa_0 + \sum_{k=1}^{K} \left(\kappa_{1,k} + \kappa_{2,k} \right), \tag{2.114}$$

where κ_{eq} is the heat conduction coefficient that would be measured in the equilibrium state. For a one-mode model where $\kappa_{2,k} = 0$ is taken in (2.113), the heat conduction tensor reduces to the one derived from microrheological considerations for a Hookean dumbbell by van den Brule (1990). The stress of a Hookean dumbbell can be described by the Maxwell model, which corresponds the Johnson–Segalman model (A.2) with $\xi_k = 0$.

Note that the temperature effect in the measurements of Washo & Hansen (1969), mentioned in the literature review earlier in this section, are in qualitative agreement with (2.113). Elongation at a higher temperature gives a smaller relaxation time λ_k. A smaller relaxation time implies a smaller deviation from equilibrium of the internal deformation tensor $\underline{\underline{b}}_k$ and thus a smaller deviation from the equilibrium heat conduction.

Restrictions for the heat conduction tensor.

From the restriction that the entropy production Π_s has to be positive for all possible processes, it follows that each term in equation (2.44) has to be positive. For the heat flux term this gives the restriction

$$\nabla T \cdot \underline{\underline{\kappa}} \cdot \nabla T \geq 0, \tag{2.115}$$

which implies that $\underline{\underline{\kappa}}$ has to be a positive definite tensor. Due to the positive definiteness of the internal deformation tensors it follows that to fulfil the entropy inequality it is sufficient to require that

$$\left.\begin{array}{rcl} \kappa_0 & \geq & 0, \\ \kappa_{1,k} & \geq & 0, \\ \kappa_{2,k} & \geq & 0, \end{array}\right\} \qquad k = 1, \ldots, K, \tag{2.116}$$

for the intervals of the internal deformation tensor, the temperature and the pressure where the approximation is valid. Mathematically these conditions are too severe. Consider the example

of constant coefficients κ_0, $\kappa_{1,k}$ and $\kappa_{2,k}$ for all modes k and denote by b_k a component of the positive definite tensor $\underline{\underline{b}}_k$ in a principal direction. It is straightforward to show that the minimum contribution of a mode k to the heat conduction tensor $\kappa_{1,k}b_k + \kappa_{2,k}b_k^2$ is then achieved at

$$b_k^{\min} = -\frac{\kappa_{1,k}}{2\kappa_{2,k}}, \tag{2.117}$$

for $\kappa_{2,k} > 0$. The positive definiteness of the internal deformation tensor, $0 < b_k < \infty$, gives that a local minimum only exists if $\kappa_{1,k} < 0$. Furthermore the minimum value at the boundary $b_k \to 0$ is the isotropic part of the heat conduction tensor, so that $\kappa_0 \geq 0$. The values of $\kappa_{1,k}$ may then be negative. For the example that $\kappa_{1,k} = \kappa_1$ and $\kappa_{2,k} = \kappa_2$ for all modes k, the heat conduction tensor is positive definite when the coefficient κ_1 fulfils

$$\kappa_1 \geq -2\sqrt{\frac{\kappa_0 \kappa_2}{K}}. \tag{2.118}$$

On the other hand, if $\kappa_2 = 0$ there is no local minimum. To obtain a positive definite heat conduction tensor, the coefficients have to fulfil

$$\kappa_0 \geq 0, \qquad \kappa_1 \geq 0, \tag{2.119}$$

which simply follows from inspection of the boundary extrema at $b_k \to 0$ and $b_k \to \infty$.

If the temperature dependence is the same for the coefficients κ_0, κ_1 and κ_2 and if they do not depend on the invariants of the internal deformation tensors, relation (2.118) still holds. Of course the temperature dependence of the coefficients must then be such that the coefficients remain positive. Otherwise, if the coefficients κ_0, $\kappa_{1,k}$ and $\kappa_{2,k}$ depend on the invariants of the internal deformation tensors or if they depend differently on the temperature, it may become very difficult to calculate the minimum value of κ_1. However, if they fulfil equation (2.116) the entropy condition is automatically fulfilled.

2.5 Temperature dependent behaviour

In this section the temperature dependent behaviour of viscoelastic fluids will be summarised. In the first part the temperature dependence of the coefficients in the balance equations and the constitutive equations will be discussed. These coefficients are measured in mechanical equilibrium. In mechanical equilibrium the fluid is at rest. This state is reached after waiting long enough so that all possible internal processes have relaxed. The second part contains an overview of the small number of measurements with a varying temperature when the body is deformed. It seems that the results can not be predicted with the normal temperature dependence of the coefficients. Some theories to fit these data will be reviewed as well.

2.5.1 Temperature dependent coefficients

In general all the coefficients in the balance equations and the constitutive equations depend on the temperature. For some coefficients such as the heat capacity, the thermal conductivity, the density and the shear modulus this temperature dependence is relatively weak. Often the effect of the temperature on these quantities are, and can be, neglected. The relaxation time and related material properties like the viscosity, normal stress coefficients etc. strongly

depend on the temperature, so in general this effect can not be neglected. Specific values of the temperature dependencies for various polymers are given by van Krevelen & Hoftyzer (1976). They also present some general rules that may be convenient to check whether a temperature effect is negligible or not. These generalisations will be summarised below.

A characteristic temperature for the behaviour of polymeric materials is the glass transition temperature T_g: the temperature at which the transition of the glassy state into a rubbery state takes place. For temperatures above the glass transition the polymer behaviour is rubberlike, viscoelastic or liquidlike, depending on temperature and molecular weight of the polymer. For polymers this temperature can vary from less than 200 K to more than 400 K. In experiments it turns out that the precise value of T_g depends on the cooling rate of the sample. Usually, it is assumed that the sample is cooled slowly enough to ignore this effect. Matsumoto & Bogue (1977) reported an increase of T_g by 10 K for cooling rates of the order of 1 K·s^{-1}. A generic picture of the influence of the temperature on the behaviour of amorphous polymeric systems is presented in figure 2.4.
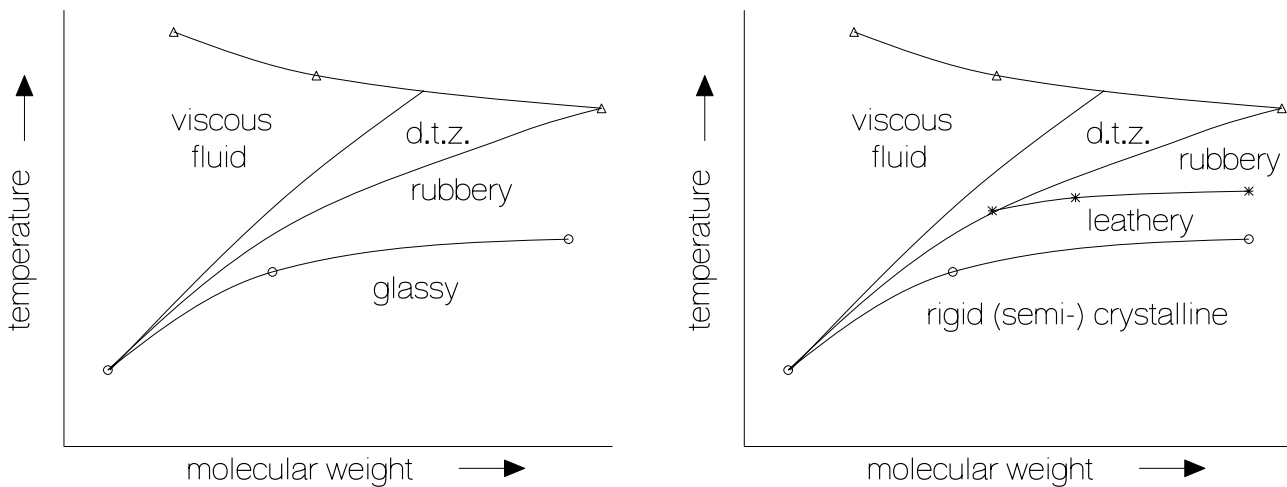
Figure 2.4: Temperature-molecular weight diagram with different phases for amorphous and semi-crystalline polymers. The abbreviation d.t.z. denotes the diffuse transition zone. The line with a ∘ denotes the glass transition, the line with a △ the thermal decomposition and the line with a ∗ the melting point. From van Krevelen & Hoftyzer (1976).

For semicrystalline polymers the melting temperature $T_m > T_g$ is important as well. The melting temperature is the highest temperature at which polymer crystallites can exist. Above the melting point the material behaves as an amorphous material. Above the melting point the semi-crystalline polymer is rubbery (elastic effects dominant), viscous or viscoelastic (the diffuse transition zone where elastic and viscous effects are important), as for the amorphous polymers. A generic picture of the influence of the temperature on the behaviour of semi-crystalline polymeric systems is also presented in figure 2.4.

In this thesis polymer fluids will be considered only in the temperature region $T_g < T < T_c$, where T_c is the temperature at which degrading of the polymer takes place. For this temperature region the temperature dependences of the various coefficients will be given.

Temperature dependence of the heat capacity.

For polymeric liquids above T_g the temperature dependence of the heat capacity can be described by a linear relation, with a small positive slope

$$
\begin{aligned}
c_{p,\tau_e}^{\mathrm{eq}}(T) &= c_{p,\tau_e}^{\mathrm{eq}}(T_{\mathrm{ref}})\left(1 + \alpha_c(T - T_{\mathrm{ref}})\right), \\
\alpha_c &= \frac{1}{c_{p,\tau_e}^{\mathrm{eq}}(T_{\mathrm{ref}})}\frac{dc_{p,\tau_e}^{\mathrm{eq}}}{dT} \simeq 1.2 \cdot 10^{-3}\ \mathrm{K}^{-1},
\end{aligned}
\tag{2.120}
$$

with a reference temperature of $T_{\mathrm{ref}} = 298$ K. The mean deviation of α_c for different polymers is 30 % (van Krevelen & Hoftyzer 1976). For a temperature difference of 100 K the difference in heat capacity is then of the order of 12 %.

Temperature dependence of the thermal conductivity.

For amorphous polymers the temperature dependence of the thermal conductivity is weak. Above T_g it is a linear relation with a small negative slope:

$$
\begin{aligned}
\kappa(T) &= \kappa(T_\mathrm{g})\left(1 - \alpha_\kappa(T - T_\mathrm{g})\right), \\
\alpha_\kappa &= \frac{1}{\kappa(T_\mathrm{g})}\frac{d\kappa}{dT} \simeq \frac{0.2}{T_\mathrm{g}},
\end{aligned}
\tag{2.121}
$$

with small deviations for different polymers. For a temperature difference of 100 K the difference in heat conduction is smaller than about 10 % (van Krevelen & Hoftyzer 1976). For the anisotropic heat conduction from section 2.4 one may take the same temperature dependence for each heat conduction constant in (2.113), so that $(2.114)_2$ is automatically fulfilled in mechanical equilibrium.

Temperature dependence of the density.

The temperature dependence of the density is relatively small for polymeric liquids. Van Krevelen & Hoftyzer give an empirical rule from Boyer & Spencer (1944) for polymeric liquids above T_g

$$
\begin{aligned}
\rho(T) &= \rho(T_\mathrm{g})\left(1 - \alpha_\rho(T - T_\mathrm{g})\right), \\
\alpha_\rho &= -\frac{1}{\rho(T_\mathrm{g})}\frac{d\rho}{dT} \simeq \frac{0.16}{T_\mathrm{g}},
\end{aligned}
\tag{2.122}
$$

where α_ρ is the linear coefficient of thermal expansion. The deviation of α_ρ for different polymers is about 25 %. For a temperature difference of 100 K this means a difference in density of less than 10 %.

The pressure dependence of the density is also weak for polymeric liquids. Usually the compressibility κ_T is about $10^{-9} - 10^{-10}$ Pa^{-1} for polymers.

Temperature dependence of the relaxation time and viscosity.

For polymeric liquids the dependence of the relaxation time and the viscosity on the temperature is relatively strong, in particular near the glass transition temperature. It can be described with a shift factor a_T, which is an exponential function of the temperature. Isothermal measurements

at different temperatures of the viscosity or the relaxation time as a function of the shear rate may be shifted onto a single 'master curve'. This means that the viscosity and the relaxation time are known at all temperatures as soon as the they are known at a reference temperature, provided the shift factor a_T is known. Figure 2.5 shows the viscosity at different temperatures and the master curve that can be obtained when the axes are scaled with the shift factor a_T. This method is also known as time-temperature superposition. For a more detailed discussion
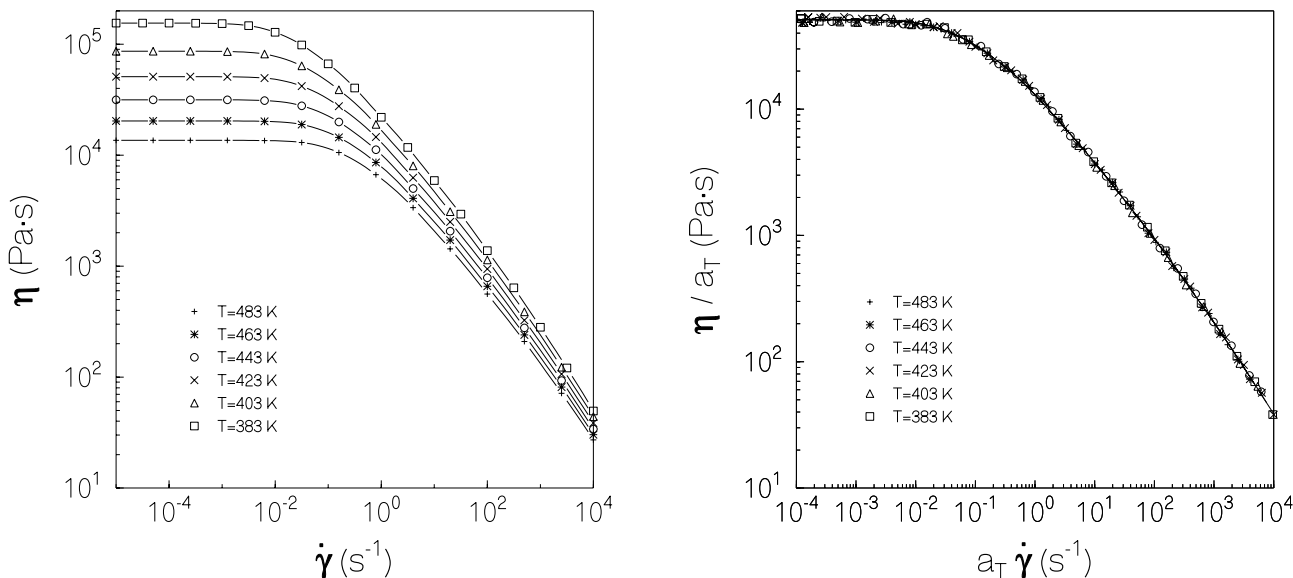
Figure 2.5: Steady shear viscosity of LDPE as function of the shear rate at different temperatures and the master curve obtained after the time-temperature superposition. From Bird et al. (1987a).

about this subject see for example Ferry (1981) or Tanner (1985).

The temperature dependence of the viscosity and the relaxation time are almost equal. The viscosity only contains a small extra temperature dependence. This dependence will be discussed in the section about the temperature dependence of the shear modulus, which equals the ratio of the viscosity and relaxation time. The temperature dependence will only be given for the relaxation time, because the viscoelastic models in section 2.2 and appendix A are posed in terms of the moduli G_k and the relaxation times λ_k.

Two commonly used shift factors for polymeric liquids are the Williams–Landel–Ferry (WLF) and the Andrade or Arrhenius shift factor.

The WLF shift factor.

The WLF shift factor can be used for a lot of amorphous polymers in the range $T_\mathrm{g} < T < T_\mathrm{g} + 100$ K, where the temperature dependence is extremely strong. The WLF shift factor a_T is defined as

$$^{10}\log\left(\frac{\lambda_k}{\lambda_{k,\mathrm{ref}}}\right) = {}^{10}\log a_T = \frac{-C_{1,k}(T - T_\mathrm{ref})}{C_{2,k} + (T - T_\mathrm{ref})}, \tag{2.123}$$

where $\lambda_{k,\mathrm{ref}}$ is the relaxation time at a reference temperature T_ref. The parameters T_ref, $C_{1,k}$ and $C_{2,k}$ have to be determined by fitting of the experimental data. Usually it is assumed that the shifts are the same for all modes, $C_{1,k} = C_1$ and $C_{2,k} = C_2$ for all k. If no experimental

data are available, the 'universal values' $C_1 = 17.44$, $C_2 = 51.6$ K and $T_{\text{ref}} = T_{\text{g}}$ can be used to give a first approximation. If some data are available one can take $C_1 = 8.86$, $C_2 = 101.6$ K and choose T_{ref} to give a best fit (Tanner 1985). For a temperature rise of 100 K from T_{g}, the 'universal values' predict a relaxation time that is $3 \cdot 10^{11}$ times as small as the relaxation time at T_{g}. However, because of the extremely large relaxation times near T_{g}, the relaxation times may still be substantial then.

The Andrade shift factor.

For values of T larger than $T_{\text{g}} + 100$ K or where T_{g} is irrelevant the Andrade shift factor can be used. The temperature dependence is smaller than below $T_{\text{g}} + 100$ K. The Andrade shift factor is defined as

$$^{10}\log\left(\frac{\lambda_k}{\lambda_{k,\text{ref}}}\right) = {}^{10}\log a_T = C_{1,k}\left(\frac{1}{T} - \frac{1}{T_{\text{ref}}}\right), \tag{2.124}$$

where the shift constant $C_{1,k}$ and the reference temperature T_{ref} have to be determined by fitting of the experimental data. Usually it is assumed that the shifts are the same for all modes, $C_{1,k} = C_1$ for all k. For most of the polymers C_1 is in the range $1.0 \cdot 10^3$ to $5.0 \cdot 10^3$ K. Taking a reference temperature of 500 K and $C_1 = 3 \cdot 10^3$ K the relaxation time at 600 K is only 10 % of the relaxation time at 500 K.

For polymer solutions the temperature dependence of the Newtonian viscosity has to be specified as well. The viscosity of a Newtonian fluid can also be described by an Andrade shift factor

$$^{10}\log\left(\frac{\eta_s}{\eta_{s,\text{ref}}}\right) = {}^{10}\log a_T = C_1\left(\frac{1}{T} - \frac{1}{T_{\text{ref}}}\right), \tag{2.125}$$

where for water $C_1 \simeq 8.2 \cdot 10^2$ K.

For the Newtonian solvent the temperature dependence of the viscosity has an instantaneous effect on the stress, just like the deformation. For viscoelastic models described in appendix A, which are of the form (2.22), the 'right-hand side' g_k does not depend on the temperature. The temperature dependence is only due to the λ_k in front of the convected derivative. Besides the dependence on the deformation history (via 'the right-hand side'), the internal deformation tensor depends on the temperature history (via the temperature dependence of λ_k).

The viscosities and relaxation times depend on the pressure as well. Compared to the temperature dependence this dependence is often negligible. A doubling of the viscosity needs a change of the pressure of the order of $10^7 - 10^8$ Pa, depending on the temperature. Refer to Ferry (1981) or Kadijk & van den Brule (1994) for more detailed information.

Temperature dependence of the shear modulus.

The viscosity and the relaxation time show almost the same behaviour for different temperatures. Therefore the moduli $G_k = \eta_k/\lambda_k$ are only a weak function of the temperature. From the kinetic theory of elastic dumbbells (see Bird et al. 1987b), in which a polymer is described on micro level as a bead-spring system, it follows that for a linear system the shear modulus

has to be scaled by[13]

$$G_k(T) = \frac{\rho T}{\rho_{\text{ref}} T_{\text{ref}}} G_{k,\text{ref}}. \tag{2.126}$$

Compared with the exponential shift of the relaxation time this is not a very important factor for the viscosity and stresses. For a temperature increase of 100 K above $T_{\text{ref}} = 500$ K the difference in T/T_{ref} is of the order of 20 %. Furthermore the effect of increasing temperature is partly compensated by the density, which decreases with increasing temperature. Taking a decrease of 10 % of the density, which has been found in an earlier part of this section, $G_k/G_{k,\text{ref}}$ is about 10 %.

For elastic materials a temperature dependence of the shear modulus G corresponds to the Gough–Joule effect, as explained by Treloar (1975). This effect consists of the following two observations: a rubber held in a stretched state, under a constant load, contracts on heating and a rubber gives out heat when stretched. If the heat is not emitted but is retained, as in an adiabatic extension, the energy supplied by the stretching causes a temperature rise. Both effects are reversible. For a neo-Hookean material $\underline{\underline{\sigma}} = -p\underline{\underline{I}} + G(\underline{\underline{b}} - \underline{\underline{I}})$ the Gough–Joule effect corresponds to a temperature dependent shear modulus with $dG/dT > 0$. The corresponding 'Gough–Joule effect of viscoelastic fluids' is that at constant elastic stress $\underline{\underline{\tau}}_{e,k}$ the 'internal deformation tensor becomes smaller' when the fluid is heated. This effect is obtained when $dG/dT > 0$, which is fulfilled for (2.126). An indication whether the linear temperature scaling is good or not may be obtained by measuring the entropy or energy elasticity (see section 2.3.3).

Experiments of Astarita & Sarti (1976) and Sarti & Esposito (1977/1978) indicate that some polymers show purely entropic elasticity in shear and elongation. In the case of entirely entropy elasticity the temperature rise under adiabatic conditions must equal the stress work, when pressure effects may be neglected. Thus when the change in free energy due to changes in the elastic deformation, the $\partial \psi / \partial \underline{\underline{b}}_k$ terms in (2.90), is large compared to the mechanical dissipation, measurement of the temperature rise and the stress work gives an indication of the entropy or energy elasticity of the fluid. This condition should be ensured by the fact that the total force on the sample is a strong increasing function of time. Astarita & Sarti (1976) performed the experiment for polyisobutylene at room temperature, which is above the glass transition. They obtained values of the heat capacity that are in good agreement with the literature. However, it is not completely clear whether the obtained values of the heat capacity are in contradiction with the purely energy elasticity, or something in between. Sarti & Esposito (1977/1978) performed adiabatic shear and elongational experiments, at various temperatures above T_g, on polyisobutylene and polyvinylacetate with different molecular weights. The materials were deformed from equilibrium at a constant rate until a maximum deformation. Then the deformation was stopped and the material relaxed adiabatically towards a stress-free state. For a purely entropic elasticity the temperature has to remain constant during the relaxation process ($\underline{\underline{d}} = \underline{\underline{0}}$). For the polyisobutylene melts they found a vanishing temperature rise during the adiabatic stress relaxation process. The heat capacity remained constant during deformation and relaxation. However, for the polyvinylacetate at 333 K, more than 20 K above T_g, the temperature was not constant during the relaxation (it even decreased) and the heat capacity was not constant during the elongation and relaxation. During elongation the heat capacity

---

[13]As stated by Bird (1979) the extrapolation of the results of an infinite-dilution theory, in particular the scaling with the density in (2.126), to a melt is risky.

decreased and during relaxation it increased.

   Another method to obtain the temperature dependence of G_k is via the anisotropy of the thermal expansion. For PMMA, PVC, PC and PST these measurements have been performed by Hellwege et al. (1963) for uniaxially stretched samples. After cooling below the glass transition temperature they found that $\beta_\perp$, the expansion perpendicular to the elongation, increased compared to α and $\beta_\parallel$, the expansion parallel to the elongation, decreased compared to α. For a neo-Hookean material this effect corresponds to $dG/dT > 0$. This can be shown easily by inspection of the equation for the temperature dependence of $\underline{\underline{b}}$ at constant elastic stress (2.83). For a uniaxial elongation then holds

$$\left.\frac{\partial b_\parallel}{\partial T}\right|_{\underline{\underline{\sigma}}} = -\frac{1}{G}\frac{\partial G}{\partial T}\left(b_\parallel - 1\right) < 0,$$

$$\left.\frac{\partial b_\perp}{\partial T}\right|_{\underline{\underline{\sigma}}} = -\frac{1}{G}\frac{\partial G}{\partial T}\left(b_\perp - 1\right) = -\frac{1}{G}\frac{\partial G}{\partial T}\left(\frac{1}{\sqrt{b_\parallel}} - 1\right) > 0, \tag{2.127}$$

where $b_\parallel$ and $b_\perp$ are the components of $\underline{\underline{b}}$ parallel and perpendicular to the elongation. This means that compared to the thermal expansion coefficient α, $\beta_\parallel$ decreases and $\beta_\perp$ increases in a uniaxial elongation. Furthermore, the deviations in the parallel direction will be larger than in the perpendicular direction. This has also been observed in the experiments.

With the help of equation (2.126) an equation for the stress can be derived which depends on the temperature history. This has been done by Bird (1979) for the Maxwell model and by Wiest (1989) for the Giesekus model[14]. Substitution of (2.126) and (2.19) in the stress equation for the one-mode Maxwell model, (A.2) with $\xi_k = 0$, gives a stress equation that depends on the temperature history

$$\lambda\overset{\triangledown}{\underline{\underline{\tau}}} + \underline{\underline{\tau}}(1 + \lambda\dot{z}_1) = 2\lambda G\underline{\underline{d}},$$

$$z_1 = \ln\left(\frac{G_{\text{ref}}}{G}\right), \tag{2.128}$$

where the subscript $_1$ for the mode number has been suppressed. Because the material derivative of the temperature does not appear in the differential equation for the internal deformation tensor, it is of course much easier to solve that equation instead of the stress equation. The contribution of the temperature history to the stress is only due to the temperature dependence of the shear modulus, which can then be accounted for in the simple algebraic relation (2.19). Often the dependence of the shear modulus on the temperature is neglected, because the temperature dependence of the modulus is small compared to the exponential temperature dependence of the relaxation times. However, although this may be justified for the calculation of the stress from (2.19), the term may be important in the calculation of the heat production (see section 2.3.3).

---

[14]For convenience the derivation has been performed in the internal deformation tensor and the relaxation time. The notation is equivalent with the notation for the dumbbell models used by Bird and Wiest with $\lambda = \zeta\,\text{tr}\langle\underline{R}\underline{R}\rangle_{\text{eq}}/12kT$, $G = 3nkT/\text{tr}\langle\underline{R}\underline{R}\rangle_{\text{eq}}$, and $\underline{\underline{b}} = \langle\underline{R}\underline{R}\rangle/(\text{tr}\langle\underline{R}\underline{R}\rangle_{\text{eq}}/3)$. ζ is the bead friction coefficient, k the Boltzmann constant and $\text{tr}\langle\underline{R}\underline{R}\rangle$ the mean square end-to-end distance of the chains. The bead friction coefficient may strongly depend on the temperature, although this has not explicitly been taken into account in the derivations of Bird and Wiest.

Temperature dependence of nonlinear parameters.

The nonlinear viscoelastic differential models described in appendix A contain some extra parameters. With these nonlinear parameters the viscoelastic behaviour of a fluid can be fitted to experimental data of the shear and elongational viscosity. For nonisothermal flows these quantities may be a function of the temperature. However, the temperature dependence of these parameters has not been studied so far, experimentally or theoretically. Therefore it will be assumed in this thesis that the nonlinear parameters do not depend on the temperature.

2.5.2 Nonisothermal rheology

In the previous subsection the influence of the temperature has been examined under isothermal conditions at different temperatures. Another possibility is to vary the temperature while the material is being deformed. This is called nonisothermal rheology. In this section firstly a short overview will be given of nonisothermal rheological measurements. Then some theories that have been developed to fit the rheological behaviour when the material is simultaneously deformed and heated or cooled will be reviewed.

Nonisothermal rheological experiments.

Very little data are available on nonisothermal rheological experiments. Sridhar (1988) measured the shear stress of a dilute polyacrylamide solution in a rheogoniometer, while the sample was heated. Matsui & Bogue (1977), Matsumoto & Bogue (1977) and Joshi & Bogue (1990) tried to measure elongational stresses with a varying temperature in time. The polystyrene samples used by Bogue et al. are oblong cylindrical rods with a diameter of about 1 mm. Although the diameter of the samples is small, it is still problematic to attain a homogeneous, i.e. spatially constant, temperature distribution. For comparison with theoretical models, however, they assumed a homogeneous temperature. The stress model, which described the isothermal data, was made temperature dependent by the introduction of a shift factor for the viscosity and relaxation time. The shift factor was taken to be the same for all relaxation times.

Matsui & Bogue (1977) performed two nonisothermal experiments with a temperature jump (cooling and heating) during retardation and elongation. The initial temperature was 25 K above T_{g} for the heating experiments and more than 40 K above T_{g} for the cooling experiments. The time needed to realise the temperature change was about 6 seconds for the heating and 15 seconds for the cooling experiments.

In the first set of experiments, a polystyrene sample was stretched to an elongation ratio between 1.45 and 2. The elongation ratio is defined as the ratio between the final length and the initial length of the sample, $\epsilon = L/L_{\mathrm{eq}}$. At various points during the retardation process (once per sample), a temperature jump of $16-18$ K was imposed. The agreement of the measurements of the elongational stress and their theoretical model is reasonable.

In the second set of experiments, the temperature jump was performed during the elongation process with constant pulling rate $\dot{L}$. The pulling rates were about 2 mm·s^{-1} and 8 mm·s^{-1}. In both cases the accommodation of the nonisothermal elongational stress to the isothermal elongational stress at the new temperature is more quickly than time-temperature superposition predicts, see figure 2.5.2 for the results of the heating experiment. The cooling experiment also showed the quicker adjustment to the new temperature. For
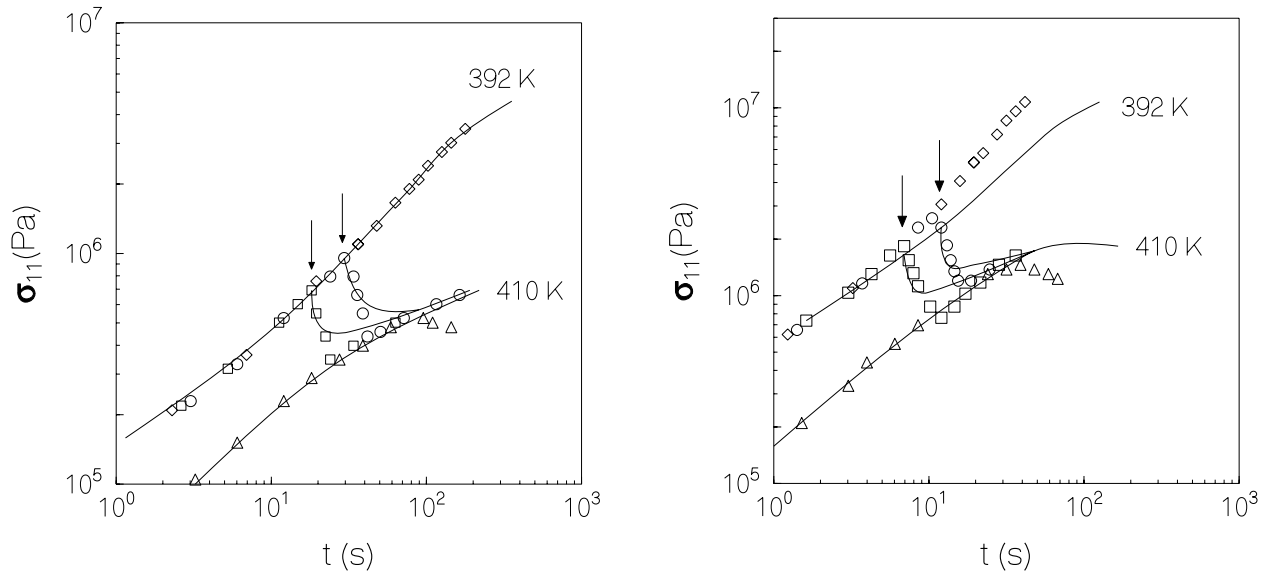
Figure 2.6: Isothermal and nonisothermal heating data for tensile pulling at a low rate $\dot{L} = 2.1$ mm·s^{-1} and a high rate $\dot{L} = 8.5$ mm·s^{-1} (TC 3-30). The arrows show the points where a temperature jump has been imposed. The lines are predictions from the theoretical model. The $\diamond$ and the $\triangle$ denote the isothermal data at 392 K and 410 K. The $\circ$ and the $\square$ denote the nonisothermal data. The material seems to accommodate itself more quickly to the new temperature than the time-temperature shifting predicts. Figure from Matsui & Bogue (1977).

the high rate, however, the differences between the isothermal model predictions and the measured isothermal data are relatively large as well.

Matsumoto & Bogue (1977) examined the influence of the cooling rate. The samples are pulled at a constant elongation rate and are simultaneously cooled at a constant cooling rate R. For the test runs at different constant temperatures and with different elongation rates, they found that the agreement between the model predictions and the measurements of the elongational stress was good. For the nonisothermal experiments the constant elongation rate was about $\dot{\epsilon} = \dot{L}/L = 5 \cdot 10^{-2}$ s^{-1}. The initial temperature of the sample was 433 K, somewhat more than 60 K above T_{g}. The temperature at the end of the experiments was about $10-20$ K above T_{g}. For their nonisothermal model the temperature of the sample is supposed to be given by $T(t) = T_0 - Rt$, with T_0 the initial temperature of the sample and t the time. In their experiments the cooling rate varied from 0 to more than 2 K·s^{-1}. In the experiments the temperature distribution was not homogeneous. The difference in temperature between the axis of symmetry and the outside of the sample was relatively large, about 4 K after a cooling of 30 K at a cooling rate of 1.9 K·s^{-1}.

The stress model with shift factors for the temperature dependence seems to underpredict the elongational stresses. In other words: the experimental curves cross the isothermal curves earlier than expected. This effect was also present in the experiments of Matsui & Bogue (1977). The higher the cooling rates are, the larger the deviation between the elongational stress from the time-temperature superposition theory and the measured elongational stress. This is illustrated in figure 2.5.2, where the elongational viscosity, defined by (1.5)

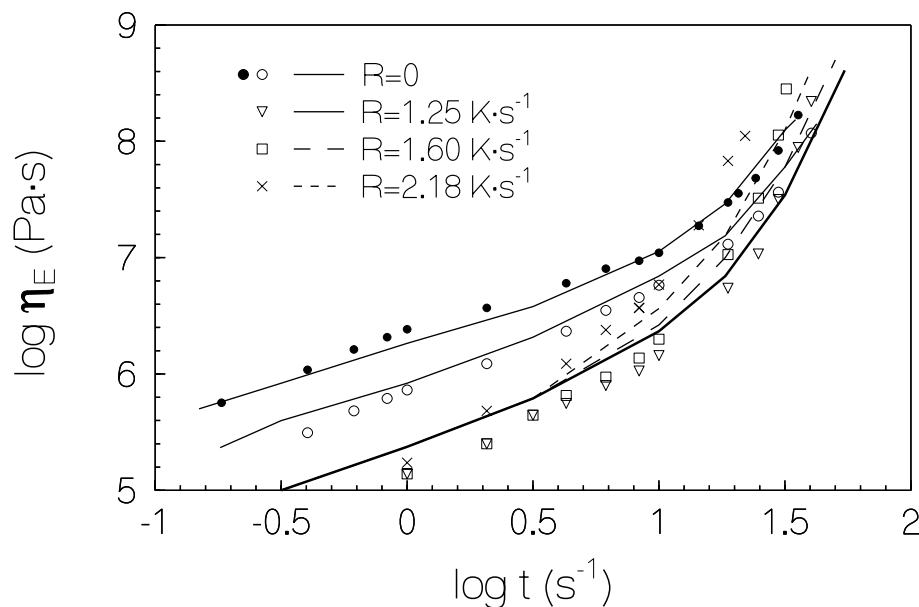and proportional to the elongational stress, has been depicted.

Figure 2.7: Comparison of theory with experiment for isothermal and nonisothermal stress development at a constant elongation rate of about $\dot{\epsilon} = 5 \cdot 10^{-2}$ s^{-1}. The thin lines and the $\bullet$ and the $\circ$ are isothermal model predictions and isothermal data at 393 K and 403 K. The model (with shift factors for the viscosity and the relaxation time) seems to underpredict the elongational viscosity (and the elongational stress). As the cooling rate increases the deviations between the model and the data seem to increase. Figure from Matsumoto & Bogue (1977).

Joshi & Bogue (1990) have also done some nonisothermal experiments on polymers in the neighbourhood of the glass transition temperature ($T_g - 20$ K $< T < T_g + 20$ K). The maximum cooling rate in their experiments was 4.0 K·s^{-1}. The experiment consists of a sample of constrained length in which the stress build-up due to density changes was measured. As for the experiment of Matsumoto and Bogue (1977), the elongational stresses are again underpredicted.

Sridhar (1988) presented a technique for measurements in a nonisothermal shear flow and reported some preliminary data. A Weissenberg rheogoniometer has been put in a microwave cavity to control the temperature of the sample. A sample thickness of $5 \cdot 10^{-5}$ m should ensure a constant temperature across the sample. The heating rates are up to 1.86 K · s^{-1} and the shear rates up to 8.9 s^{-1}. Opposite to the experiments of Bogue et al. the measured shear stresses are higher than their model predictions (the Maxwell model with a temperature dependent relaxation time). The differences increase at a higher heating rate or shear rate.

Fitting models for the nonisothermal experiments.

A few attempts have been made to fit the nonisothermal experiments of Bogue et al. and Sridhar, described in the first part of section 2.5.2. These fitting models will be summarised in the remaining part of this section.

As already noted in section 2.5.1 the glass transition temperature may vary with the cooling rate. Although the experiments are above T_g it is assumed that the molecular properties that determine the glass transition also determine part of the mechanical response above T_g. Both Matsumoto & Bogue (1977) and Upadhyay & Isayev (1984) tried to incorporate this effect by fitting the experiments of Matsumoto & Bogue (1977) with a glass transition temperature that was about 10 K higher than the glass transition temperature determined at a very low cooling rate. This increase of T_g results in a shift factor that is 10^3 times larger than the shift factor used previously.

For cooling rates in the range of 0.5–4.5 K·s^{-1} the glass transition temperature increases $12-16$ K. Upadhyay & Isayev took for all cooling rates a glass transition temperature, that is 14 K higher than T_g at a zero cooling rate. They showed that the elongational stress data can be fit better when the cooling rate dependent shift factor is used.

Joshi & Bogue (1990) showed that a cooling rate dependent WLF shift factor still under-predicts the stress at high cooling rates. They tried an empirical formula where the shear modulus depends on the cooling rate. The moduli were supposed to fulfil a linear differential equation of the form

$$\lambda_{G,k} \frac{dG_k}{dt} = -G_k + G_{k,\text{eq}} + P, \tag{2.129}$$

where $\lambda_{G,k}$ is the relaxation time of the shear modulus and P is an exponential function of the cooling rate that goes to zero when the cooling rate approaches zero. The relaxation times of the moduli were supposed to equal the relaxation times of the stress. With the differential equation for the moduli they could obtain a better fit of the data of Matsumoto & Bogue (1977) and Joshi & Bogue (1990).

From the dumbbell theory for Hookean dumbbells Bird (1979) derived a nonisothermal constitutive equation when the spring force H is a function of the temperature. A Hookean dumbbell consists of two spherical beads joined by a linear spring. The stress $\underline{\underline{\tau}}$ of elastic dumbbells may be described by the Kramers expression and an equation of change for the dyadic product $\underline{\underline{b}}_H = \langle \underline{R}\underline{R} \rangle$, where $\underline{R}$ is the vector connecting the two beads of the dumbbell:

$$
\begin{aligned}
\underline{\underline{\tau}} &= G\left(B\underline{\underline{b}}_H - \underline{\underline{I}}\right), \\
\overset{\triangledown}{\underline{\underline{b}}_H} &= -\frac{1}{\lambda_H}\left(\underline{\underline{b}}_H - B^{-1}\underline{\underline{I}}\right),
\end{aligned}
\tag{2.130}
$$

where the parameters correspond to $B = H/kT$, $G = nkT$ and $\lambda_H = \zeta/4H$ in the usual notation for Hookean dumbbells. The spring constant H may be a function of the temperature and the scaling of the shear modulus G corresponds to by (2.126). The internal deformation tensor $\underline{\underline{b}} = \langle \underline{R}\underline{R} \rangle/(\text{tr}\langle \underline{R}\underline{R} \rangle_{\text{eq}}/3)$ is related to $\underline{\underline{b}}_H$ by the simple algebraic relation: $\underline{\underline{b}} = H\underline{\underline{b}}_H/kT$. Combining the two equations in (2.130), a stress equation that depends on the temperature history can be obtained:

$$
\begin{aligned}
\lambda_H \overset{\triangledown}{\underline{\underline{\tau}}} + \underline{\underline{\tau}}(1 + \lambda_H \dot{z}_1) + B^{-1}\lambda_H G \dot{z}_2 \underline{\underline{I}} &= 2B^{-1}\lambda_H G \underline{\underline{d}}, \\
z_1 &= \ln\left(\frac{G_{\text{ref}} B_{\text{ref}}}{GB}\right), \\
z_2 &= \ln\left(\frac{B_{\text{ref}}}{B}\right).
\end{aligned}
\tag{2.131}
$$

Usually it is assumed that H is proportional to kT, i.e. $B = B_{\mathrm{ref}}$. Then $z_2 = 0$ and (2.131) reduces to (2.128). When $B \neq B_{\mathrm{ref}}$ it is not advantageous to solve (2.131). However, contrary to the case where $B = B_{\mathrm{ref}}$ and $G = G(\rho, T)$, it is also inconvenient to solve an equation for the internal deformation tensor. To avoid temperature derivatives the equation (2.130) for $\underline{\underline{b}}_H$ has to solved. The stress $\underline{\underline{\tau}}$ and the internal deformation tensor $\underline{\underline{b}}$ can easily be calculated when $\underline{\underline{b}}_H$ is known.

Gupta & Metzner (1982) proposed a stronger dependence of B on the temperature. They argued that B decreases with temperature, because it depends on the inverse of the mean square end-to-end distance $\mathrm{tr}\langle \underline{R}\underline{R} \rangle$. When the temperature increases the mean square end-to-end distance increases. Besides the exponential temperature dependence of ζ, they introduced the following temperature dependence of B:

$$B(T) = \alpha_h \left(\frac{T_{\mathrm{ref}}}{T} \right)^{\beta_h} B_{\mathrm{ref}}, \tag{2.132}$$

where α_h and β_h are fit parameters. To obtain a qualitative agreement with the experiments of Matsui & Bogue (1977) $\alpha_h > 0$ and $\beta_h > 0$ have to be chosen. Only with very strong dependences of B on the temperature, of the order of $\beta_h = 10$, a better fit could be obtained of the nonisothermal experiments.

The fitting parameters α_h and β_h were only matched to the nonisothermal data and not to some measurements at isothermal conditions. Such a strong temperature dependence must have a large effect on the time-temperature shift. A strong temperature dependence of B causes a large extra vertical shift in a plot of the master curve (figure 2.5, where the viscosity is plotted against the reduced shear rate $a_T \dot{\gamma}$). The correctness of this model seems therefore doubtful.

Sridhar (1988) also used the model described by Gupta & Metzner, equations (2.130) and (2.132), to fit his experimental data in a shear flow. Even with $\beta_h = 10$ no reasonable fit could be obtained with the experimental data.

The equations for the stress (2.19) and (2.22), with a temperature dependent shift factor and shear modulus, cannot predict the quicker adjustment to the new temperature equation when it is assumed that the temperature of the material can be described by $T = T_0 - Rt$. However, when a certain amount of heat is supplied to the material, and the temperature is measured at a sample in equilibrium as Joshi & Bogue (1990) did, the temperature equation (2.108) may predict a faster adjustment to the new temperature. For example, if the shear modulus depends linearly on the temperature, $G_k = G_{k,\mathrm{ref}} T/T_{\mathrm{ref}}$, the following temperature equation is obtained for a neo-Hookean material

$$\rho \left(c_{p,\tau_e}^{\mathrm{eq}} - \sum_{k=1}^{K} \frac{\alpha G_k}{2\rho(1-\xi_k)^2}(I_{1,k} - \ln I_{3,k} - 3) \right) \dot{T} = \underline{\underline{\tau}} : \underline{\underline{d}} - \nabla \cdot \underline{\phi}_q + \rho r, \tag{2.133}$$

where the last term represents the amount of radiation heat that is supplied in the experiments of Matsui & Bogue (1977) to cool or to heat the material. When the material is stretched the temperature of the material changes more rapidly than in equilibrium, because the term between the brackets is smaller than $c_{p,\tau_e}^{\mathrm{eq}}$ for a uniaxial extension. Thus qualitatively the effect

can then be predicted with the help of the thermodynamic model. It seems that the term with $I_{1,k}$ is not negligible. Although α/ρ is small, the sum over k of $G_k I_{1,k}$ may be large. However it remains the question whether the effect is large enough. When the material relaxes the effect diminishes, because the internal deformation tensors go to unity then. This is also in agreement with the results of Matsui & Bogue (1977).

2.6 Non-dimensional equations for shear flows

In this section the dimensionless forms of the conservation laws and the constitutive equations, described in sections 2.1, 2.2, 2.3.3 and 2.4 of this chapter, are considered. From these dimensionless formulations follow the characteristic numbers of a nonisothermal viscoelastic fluid flow. Two different non-dimensional forms for steady shear flows will be considered. One is useful for low, the other for high Deborah numbers. As an example for the stress constitutive equation the Giesekus model will be taken, see appendix A. Furthermore the moduli G_k are assumed to be constant, so that the fluid is energy elastic. Then the heat capacity difference Δc^{eq} and the entropy difference Δs_b^{ve} vanish in (2.108).

2.6.1 Low Deborah numbers

For low Deborah numbers the dimensionless quantities, denoted by a *, can be introduced as follows

$$\underline{v} = V \underline{v}^*, \qquad\qquad p = \frac{\eta_{0,\mathrm{ref}} V}{L} p^*, \qquad p_{\mathrm{m}} = \frac{\eta_{0,\mathrm{ref}} V}{L} p_m^*,$$

$$\underline{\underline{\tau}}_k = \frac{\eta_{k,\mathrm{ref}} V}{L} \underline{\underline{\tau}}_k^*, \qquad \underline{\underline{\kappa}} = \kappa_{\mathrm{eq}} \underline{\underline{\kappa}}^*, \qquad\qquad D_{\mathrm{m},k}^{\mathrm{ve}} = \frac{\eta_{k,\mathrm{ref}} V^2}{L^2} D_{\mathrm{m},k}^{\mathrm{ve},*}, \qquad (2.134)$$

$$\underline{\underline{L}} = \frac{V}{L} \underline{\underline{L}}^*, \qquad\qquad \underline{\underline{d}} = \frac{V}{L} \underline{\underline{d}}^*, \qquad\qquad \nabla = \frac{1}{L} \nabla^*,$$

and $T = \Delta T\, T^* + T_0$ for the scaling of the temperature differences and $T = T_0 T^*$ for the scaling of the absolute temperature. For the characteristic velocity V the downstream mean velocity can be taken and for the characteristic length L the downstream channel width. ΔT is a characteristic temperature difference, for example between the two downstream boundaries. The temperature T_0 is a reference temperature, for example the temperature at one of the downstream boundaries. The shear viscosity for zero strain rate at reference temperature T_{ref}, used for the scaling of the pressure, is

$$\eta_{0,\mathrm{ref}} = \eta_{s,\mathrm{ref}} + \sum_{k=1}^{K} \eta_{k,\mathrm{ref}}. \qquad (2.135)$$

Note that the stress as well as the mechanical dissipation are scaled as if they were the Newtonian stress and the Newtonian mechanical dissipation.

The mass balance (2.2), the balance of linear momentum with the Boussinesq approximation (2.7), the constitutive equations for the Giesekus stress model (2.15) and (A.3), and the temperature equation (2.92) with the constitutive equation for the heat flux (2.112), can now

be written in dimensionless form as follows[15]

$$-\frac{\kappa_T \eta_{0,\text{ref}} V}{L} \underline{v}^* \cdot \nabla^* p^* + \alpha_\rho \Delta T \underline{v}^* \cdot \nabla^* T^* = \nabla^* \cdot \underline{v}^*, \tag{2.136}$$

$$Re\ \underline{v}^* \cdot \nabla^* \underline{v}^* + \nabla^* p_{\text{m}}^* = 2\frac{\eta_{s,\text{ref}}}{\eta_{0,\text{ref}}} \nabla^* \cdot (a_T \underline{\underline{d}}^*) + \sum_{k=1}^{K} \frac{\eta_{k,\text{ref}}}{\eta_{0,\text{ref}}} \nabla^* \cdot \underline{\underline{\tau}}_k^* + \frac{Gr}{Re} T^* \underline{e}_g, \tag{2.137}$$

$$De_k \left(\underline{v}^* \cdot \nabla^* \underline{\underline{\tau}}_k^* - \underline{\underline{L}}^* \cdot \underline{\underline{\tau}}_k^* - \underline{\underline{\tau}}_k^* \cdot \underline{\underline{L}}^{*T} \right) + \underline{\underline{\tau}}_k^* + \alpha_k De_k \underline{\underline{\tau}}_k^{*2} = 2a_T \underline{\underline{d}}^*, \quad k = 1, \ldots, K, \tag{2.138}$$

$$Pe\ \underline{v}^* \cdot \nabla^* T^* - Br T_0 \alpha_\rho T^* \underline{v}^* \cdot \nabla^* p^* = \nabla^* \cdot (\underline{\underline{\kappa}}^* \cdot \nabla^* T^*) +$$
$$Br \left(2a_T \frac{\eta_{s,\text{ref}}}{\eta_{0,\text{ref}}} \underline{\underline{d}}^* : \underline{\underline{d}}^* + \sum_{k=1}^{K} \frac{\eta_{k,\text{ref}}}{\eta_{0,\text{ref}}} D_{m,k}^{\text{ve},*} \right), \tag{2.139}$$

where $\underline{e}_g$ is the unit vector in the direction of the force of gravity. The density is supposed to be given by (2.122) and the moduli are assumed to be constant.

The above equations contain $K + 4$ dimensionless numbers:

- The well-known Reynolds number denoting the ratio of the inertia force and the viscous force

$$Re = \frac{\rho_{\text{ref}} V L}{\eta_{0,\text{ref}}}. \tag{2.140}$$

- K Deborah numbers denoting the ratio of the characteristic time scale of a specific stress mode of the fluid and a characteristic time scale of the flow

$$De_k = \frac{\lambda_{k,\text{ref}} V}{L}. \tag{2.141}$$

- The Péclet number denoting the ratio of the convective transport of heat and the transport of heat by conduction

$$Pe = \frac{\rho_{\text{ref}} c_{p,\tau_e,\text{ref}}^{\text{eq}} V L}{\kappa_{\text{eq}}}. \tag{2.142}$$

- The Brinkman number denoting the ratio of the heat production by mechanical dissipation and the heat loss due to conduction

$$Br = \frac{\eta_{0,\text{ref}} V^2}{\kappa_{\text{eq}} \Delta T}. \tag{2.143}$$

- The Grashof number which is the Reynolds number times the ratio of the force due to differences in density and the viscous force

$$Gr = \frac{\rho_{\text{ref}}^2 L^3 g \alpha_\rho \Delta T}{\eta_{0,\text{ref}}^2}. \tag{2.144}$$

---

[15]For normal fluids the bulk viscosity is of the same order as the shear viscosity, see Kuiken (1994). For shear flows $(\nabla^* \cdot \underline{v}^*)^2 \ll \underline{\underline{d}}^* : \underline{\underline{d}}^*$ and the Newtonian part of the stress and the mechanical dissipation is dominated by the shear viscosity term.

Furthermore the balance of linear momentum and the temperature equation contain $K + 1$ ratios of viscosities,

$$\frac{\eta_{k,\text{ref}}}{\eta_{0,\text{ref}}}, \quad k = 1, \dots, K,$$

$$\frac{\eta_{s,\text{ref}}}{\eta_{0,\text{ref}}}. \tag{2.145}$$

From (2.136) it follows that the flow can be considered as divergence free when $|\alpha_\rho \Delta T| \ll 1$ and $\kappa_T \eta_{0,\text{ref}} V/L \ll 1$. For normal temperature differences the first condition is fulfilled, because α_ρ is small for polymers (see equation (2.122)). Furthermore $\underline{v}^* \cdot \nabla^* T^*$ can be small if they are almost perpendicular, as for fully developed flows. For normal flow conditions the second condition is also fulfilled due to the small value of κ_T, which is normally between 10^{-9} and 10^{-10}.

Due to the large viscosity and the small expansion coefficient the ratio between the buoyant force and the viscous force is in general small, $Gr/Re \ll 1$. Under extreme conditions such as a small viscosity, due to shear thinning and a high temperature, and large temperature differences in the flow the buoyant term may become important.

In the temperature equation the pressure term is relatively small compared to the mechanical dissipation term, due to the factor $T_0\alpha_\rho$. If $T_0 = T_{\text{ref}}$ this factor equals $T_{\text{ref}}\alpha_\rho \simeq 0.16$, see equation (2.122). However, for a pipe flow this term is large in the centre of the flow and small near the wall, whereas the mechanical dissipation is large at the wall and small in the centre of the flow. Therefore it may be more important than follows from the non-dimensional analysis.

Instead of specifying K Deborah numbers for each mode, it is common to define a mean Deborah number for the fluid

$$De = \frac{\lambda_{0,\text{ref}} V}{L},$$

$$\lambda_{0,\text{ref}} = \sum_{k=1}^{K} \frac{\lambda_{k,\text{ref}} \eta_{k,\text{ref}}}{\eta_{0,\text{ref}}}, \tag{2.146}$$

where $\lambda_{0,\text{ref}}$ is a mean relaxation time at reference temperature.

Finally a dimensionless number denoting the strength of coupling between the balance of linear momentum and the temperature equation can be introduced, the Nahme–Griffith number

$$Na = \frac{\eta_{0,\text{ref}} V^2}{\kappa_{\text{eq}} \Delta T^{\text{shift}}}, \tag{2.147}$$

where $\Delta T^{\text{shift}} = a_T/da_T/dT$ is a temperature measure based on the shift factor. For the WLF shift factor

$$\Delta T^{\text{shift}} = \frac{-(C_2 + T - T_{\text{ref}})^2}{C_1 C_2} \tag{2.148}$$

and for the Andrade shift factor

$$\Delta T^{\text{shift}} = \frac{-T^2}{C_1}. \tag{2.149}$$

For the temperature T the mean temperature, the reference temperature or the maximum temperature can be taken.

2.6.2 High Deborah numbers

For high Deborah numbers the following dimensionless quantities, again denoted by a *, are introduced

$$\underline{v} = V\underline{v}^*, \qquad p = G_{0,\text{ref}}p^*, \qquad p_{\text{m}} = G_{0,\text{ref}}p_{\text{m}}^*,$$

$$\underline{\underline{\tau}}_k = G_{k,\text{ref}}\underline{\underline{\tau}}_k^*, \qquad \underline{\underline{\kappa}} = \kappa_{\text{eq}}\underline{\underline{\kappa}}^*, \qquad D_{\text{m},k}^{\text{ve}} = \frac{G_{k,\text{ref}}}{\lambda_{k,\text{ref}}}D_{\text{m},k}^{\text{ve},*}, \qquad (2.150)$$

$$\underline{\underline{L}} = \frac{V}{L}\underline{\underline{L}}^*, \qquad \underline{\underline{d}} = \frac{V}{L}\underline{\underline{d}}^*, \qquad \nabla = \frac{1}{L}\nabla^*,$$

and $T = \Delta T\, T^* + T_0$ for the scaling of the temperature differences and $T = T_0 T^*$ for the scaling of the absolute temperature. The total shear modulus at reference temperature, used for the scaling of the pressure, is defined as

$$G_{0,\text{ref}} = \sum_{k=1}^{K} G_{k,\text{ref}}. \qquad (2.151)$$

Note that the stress and mechanical dissipation are scaled as if they were the elastic stress and the mechanical dissipation defined in appendix B.

For high Deborah numbers the scaling with the total shear modulus $G_{0,\text{ref}}$ results in useful dimensionless equations for the balance of linear momentum, the stress equations and the temperature equation:

$$Ma^2\underline{v}^* \cdot \nabla^*\underline{v}^* + \nabla^*p_m^* = \frac{Ma^2}{Re}2\frac{\eta_{s,\text{ref}}}{\eta_{0,\text{ref}}}\nabla^* \cdot (a_T\underline{\underline{d}}^*) + \sum_{k=1}^{K}\frac{G_{k,\text{ref}}}{G_{0,\text{ref}}}\nabla^* \cdot \underline{\underline{\tau}}_k^* + \frac{Ma^2\,Gr}{Re^2}T^*\underline{e}_g, \quad (2.152)$$

$$De_k\left(\underline{v}^* \cdot \nabla^*\underline{\underline{\tau}}_k^* - \underline{\underline{L}}^* \cdot \underline{\underline{\tau}}_k^* - \underline{\underline{\tau}}_k^* \cdot \underline{\underline{L}}^{*T}\right) + \underline{\underline{\tau}}_k^* + \alpha_k\underline{\underline{\tau}}_k^{*2} = 2De_k a_T\underline{\underline{d}}^*, \quad k = 1,\ldots,K, \qquad (2.153)$$

$$Pe\underline{v}^* \cdot \nabla^*T^* - \frac{Br}{De}T_0\alpha_\rho T^*\underline{v}^* \cdot \nabla^*p^* = \nabla^* \cdot (\underline{\underline{\kappa}}^* \cdot \nabla^*T^*) +$$

$$Br\left(2a_T\frac{\eta_{s,\text{ref}}}{\eta_{0,\text{ref}}}\underline{\underline{d}}^* : \underline{\underline{d}}^* + \sum_{k=1}^{K}\frac{\eta_{k,\text{ref}}}{\eta_{0,\text{ref}}}\frac{1}{De_k^2}D_{\text{m},k}^{\text{ve},*}\right), \qquad (2.154)$$

where the small terms with the bulk viscosity, due to the same argument as for the low Deborah number flows, have been neglected. The dimensionless numbers Re, De_k, Pe and Br have already been defined in equation (2.140-2.143). The Mach number denoting the ratio of the velocity and the shear wave speed of the fluid is defined as

$$Ma = \frac{V}{\sqrt{G_{0,\text{ref}}/\rho_{\text{ref}}}}, \qquad (2.155)$$

where the bulk viscosity has again been neglected. Again a mean Deborah number can be specified, analogously to (2.146) and a Nahme–Griffith number analogously to (2.147).

2.7   Conclusions

In the balance equations the stress, the heat flux and the internal energy of the material still have to be specified by a constitutive equation. From the thermodynamics of irreversible processes these constitutive equations have been derived for isotropic viscoelastic materials. The derived stress equation contains the well-known stress differential models from the literature. The obtained equation for the heat flux is a generalisation of the Fourier law, where the heat conduction may depend on the (elastic) deformation of the fluid. Then it is possible to take into account the experimentally observed anisotropy of the heat conduction tensor (an increasing thermal conductivity in the direction of orientation and a decreasing thermal conductivity in the direction perpendicular to the orientation). With the help of the thermodynamics also the temperature equation has been derived from the equation of energy. Due to the high viscosity of polymers the internal heat production is also important. A first cause of the internal heat production is the (irreversible) heat production due to mechanical dissipation D_m^{ve}. The mechanical dissipation has been calculated for the well-known differential stress models, including the models with a mixed convective derivative. The reversible part of the heat production consists of two contributions. Firstly pressure changes may cool (during expansion) or heat (during compression) the fluid. The second reversible contribution, the Δs_b^{ve} term, has to do with the storage of the reversible energy and is determined by the temperature dependence of the shear modulus. For a constant shear modulus the reversible energy is completely stored as elastic energy (energy elastic). However, if the shear modulus depends linearly on the temperature the reversible energy completely contributes to the temperature rise. The sum of the reversible elastic energy and the mechanical dissipation exactly equal the stress work then.

After elimination of the small terms in the obtained system of equations, with the help of dimensional analysis, the resulting equations are:

balance of mass :
$$\nabla \cdot \underline{v} = 0,$$

balance of linear momentum :
$$\rho \dot{\underline{v}} + \nabla p = 2 \nabla \cdot (\eta_s \underline{\underline{d}}) + \sum_{k=1}^{K} \nabla \cdot \underline{\underline{\tau}}_k,$$

temperature equation :
$$\rho \left(c_{p,\tau_e}^{eq} - \Delta c^{eq} \right) \dot{T} - T \alpha \dot{p} + \rho T \Delta s_b^{ve} = D_m^{ve} - \nabla \cdot \underline{\phi}_q,$$

stress constitutive equation :
$$\underline{\underline{\tau}}_k = \frac{G_k}{1 - \xi_k} \left(B_k \underline{\underline{b}}_k - \underline{\underline{I}} \right),$$

$$\lambda_k \overset{\square}{\underline{\underline{b}}}_k + \underline{\underline{g}}_k(\underline{\underline{b}}_k) = \underline{\underline{0}},$$

heat flux constitutive equation :
$$\underline{\phi}_q = -\underline{\underline{\kappa}}(\underline{\underline{b}}_k, T) \cdot \nabla T,$$

$$\underline{\underline{\kappa}}(\underline{\underline{b}}_k, T) = \kappa_0 \underline{\underline{I}} + \sum_{k=1}^{K} \left(\kappa_{1,k} \underline{\underline{b}}_k + \kappa_{2,k} \underline{\underline{b}}_k^2 \right), \qquad (2.156)$$

where the heat capacity difference Δc^{eq}, the entropy difference Δs_b^{ve} and the mechanical dissi-

pation D_{m}^{ve} are given by

$$\Delta c^{\text{eq}} = \sum_{k=1}^{K} \frac{T}{2(1 - \xi_k)^2} \left(\frac{\partial}{\partial T} \left(\rho^{-1} \frac{\partial G_k}{\partial T} \Big|_\rho \right) \Big|_p (I_{1,k} - \ln I_{3,k} - 3) \right),$$

$$\Delta s_b^{\text{ve}} = \sum_{k=1}^{K} \frac{\partial s}{\partial \underline{\underline{b}}_k} \Big|_{p,T,\underline{\underline{b}}_k'} : \dot{\underline{\underline{b}}}_k,$$

$$D_{\text{m}}^{\text{ve}} = 2\eta_s \underline{\underline{d}} : \underline{\underline{d}} + \sum_{k=1}^{K} \frac{1}{2(1 - \xi_k)\lambda_k} \left(\underline{\underline{\tau}}_k \cdot \underline{\underline{b}}_k^{-1} \right) : \underline{\underline{g}}_k. \tag{2.157}$$

Dependent on the density and temperature dependence of the shear modulus the heat capacity difference Δc^{eq} may vanish or not. For a neo-Hookean viscoelastic fluid the entropy difference and the heat capacity have been calculated from the free energy.

Except the importance, in the temperature equation, of the temperature scaling of the shear modulus the (exponential) temperature dependence of the relaxation time and the material functions is important. Especially near the glass transition temperature this temperature dependence is extremely strong. The (linear) temperature dependences of the other coefficients are less important.

Chapter 3

Analysis of the equations

In this chapter the equations describing the nonisothermal flow of a viscoelastic fluid will be analysed analytically. In the first part, section 3.1, the limit behaviour for large deformation rates will be discussed for the stress models of appendix A. For steady elongation and steady simple shear the limit values of the internal deformation tensor will be given and with the obtained results the behaviour of the heat conduction and the mechanical dissipation will be calculated. The emphasis is on the behaviour of the heat conduction for the different stress models. It will be checked which stress models are able to describe the experimentally observed anisotropy of section 2.4. In the second part, section 3.2, attention is paid to the calculation of the inverse of an internal deformation tensor. Normally this should not give any problem, because $\underline{b}_k$ is positive definite. However, due to numerical errors an internal deformation tensor may become indefinite. A method will be developed to find the theoretical lower bound for the invariants of the internal deformation tensor. The method will be applied to the models of appendix A. Also two possibilities to correct an indefinite internal deformation tensor will be given. Finally, in section 3.3, the advantages and drawbacks of the specific models for describing nonisothermal viscoelastic flows are summarised.

3.1   Limit behaviour in simple flows

The system of equations (2.156), that has been obtained in chapter 2, is in general too difficult to solve analytically. For simple flows as a steady uniaxial elongation or a steady simple shear flow, however, it is possible to obtain some limit solutions. It is important that both types of flow can be described by the viscoelastic model. For the calculations in chapter 5 a simple shear flow occurs at the wall and a uniaxial elongation at the axis of symmetry of a contraction.

Experimentally it is found that for increasing orientation the thermal conductivity perpendicular to the orientation of the polymer chains decreases until a lower bound has been reached, then it remains constant. Further on this will be called restriction I. The thermal conductivity parallel to the orientation increases with increasing orientation and does not approach a maximum for the highest deformations in the experiments. Further on this will be called restriction II.

For the fitting of the model to experimental data from the literature a few problems arise. Firstly the anisotropy of the heat conduction tensor has not been measured for a lot of polymeric fluids. Secondly, for the polymeric fluids for which the anisotropy has been measured, only few data points are available. These two reasons cause that it does not make much sense to use a very complicated model for the heat conduction. An obvious choice is to take constant coefficients in the equation for the heat conduction tensor (2.113), or even $\kappa_{1,k} = \kappa_1$ and $\kappa_{2,k} = \kappa_2$ for all modes k. Besides the thermal conductivity in equilibrium, only two coefficients

have to be determined then. A third problem is that the experimental data are expressed as relations between the elongation ratio or shear rate and the heat conduction tensor. The model (2.113), however, gives a relation between the internal deformation tensor and the heat conduction tensor. For large shear or elongation rates the internal deformation tensor can be written as an explicit function of the shear or elongation rate. This gives a possibility to compare the limit behaviour with experimental results. Also some coefficients in (2.113) may be determined in this way. With constant coefficients in the equation for the heat conduction tensor (2.113) these restrictions can only be fulfilled for some of the stress models of appendix A. For steady uniaxial elongation and steady simple shear it will be checked which stress models are able to fulfil the restrictions I and II then.

For the analysis in this chapter the starting point is the general equation for the internal deformation tensor (2.22). For an isotropic tensor function $\underset{=}{g}_k$ it can be written as

$$\lambda_k \overset{\square}{\underline{\underline{b}}}_k = g_{1,k}\left(\underline{\underline{b}}_k\right)\underline{\underline{I}} + g_{2,k}\left(\underline{\underline{b}}_k\right)\underline{\underline{b}}_k + g_{3,k}\left(\underline{\underline{b}}_k\right)\underline{\underline{b}}_k^2,\tag{3.1}$$

where the scalars $g_{i,k}$ are functions of the invariants of the internal deformation tensor.

3.1.1 Steady uniaxial elongation

For a uniaxial elongation, in the 11-direction, the modified velocity gradient $\hat{\underline{\underline{L}}}$ and the internal deformation tensor $\underline{\underline{b}}_k$ are

$$\hat{\underline{\underline{L}}} = \begin{bmatrix} (1-\xi_k)\dot{\epsilon} & 0 & 0 \\ 0 & -\frac{1-\xi_k}{2}\dot{\epsilon} & 0 \\ 0 & 0 & -\frac{1-\xi_k}{2}\dot{\epsilon} \end{bmatrix}, \quad \underline{\underline{b}}_k = \begin{bmatrix} b_{11,k} & 0 & 0 \\ 0 & b_{22,k} & 0 \\ 0 & 0 & b_{33,k} \end{bmatrix},\tag{3.2}$$

where $b_{33,k} = b_{22,k}$. The invariants of $\underline{\underline{b}}_k$ are then

$$I_{1,k} = b_{11,k} + 2b_{22,k}, \qquad I_{2,k} = b_{22,k}(2b_{11,k} + b_{22,k}), \qquad I_{3,k} = b_{11,k}b_{22,k}^2.\tag{3.3}$$

For convenience the non-dimensional elongation rate $\gamma_k = \lambda_k\dot{\epsilon}$ is introduced. For a uniaxial elongation (3.1) then reduces to

$$2(1-\xi_k)\gamma_k b_{11,k} + g_{1,k} + g_{2,k}b_{11,k} + g_{3,k}b_{11,k}^2 = 0,$$
$$-(1-\xi_k)\gamma_k b_{22,k} + g_{1,k} + g_{2,k}b_{22,k} + g_{3,k}b_{22,k}^2 = 0.\tag{3.4}$$

For given γ_k this is a nonlinear equation in the internal deformation tensor. Dependent on the scalars $g_{i,k}$ it is possible to obtain an analytic solution or only a limit solution for small and large values of the non-dimensional elongation rate γ_k.

The mechanical dissipation of a steady uniaxial elongation equals the stress work. With $\tau_{22,k} = \tau_{33,k}$ the mechanical dissipation of mode k becomes

$$D_{\mathrm{m},k}^{\mathrm{ve}} = (\tau_{11,k} - \tau_{22,k})\dot{\epsilon} = \eta_E(\dot{\epsilon})\dot{\epsilon}^2 = \frac{G_k B_k}{\lambda_k(1-\xi_k)}(b_{11,k} - b_{22,k})\gamma_k,\tag{3.5}$$

where definition of the elongational viscosity (1.5) and the relation between the extra-stress and the internal deformation tensor (2.19) have been used.

With the model (2.113) the parallel and perpendicular thermal conductivities in a uniaxial elongation become

$$\kappa_{\parallel} = \kappa_0 + \sum_{k=1}^{K} (\kappa_{1,k} b_{11,k} + \kappa_{2,k} b_{11,k}^2),$$

$$\kappa_{\perp} = \kappa_0 + \sum_{k=1}^{K} (\kappa_{1,k} b_{22,k} + \kappa_{2,k} b_{22,k}^2). \tag{3.6}$$

Note that for constant coefficients the parallel and perpendicular thermal conductivities only depend on the components of the internal deformation tensors in that direction.

In the remaining part of this subsection the internal deformation tensor, the corresponding mechanical dissipation, and the parallel and perpendicular thermal conductivity will be calculated for various stress models in a steady elongational flow. As far as possible an analytic expression will be given, otherwise only the approximations for large elongation rates will be presented.

The Johnson–Segalman model

The Johnson–Segalman model is given by (A.2). The scalars $g_{i,k}$ are $g_{1,k} = 1$, $g_{2,k} = -1$ and $g_{3,k} = 0$. Furthermore the coefficients in (2.19) are $B_k = 1$ and $0 \leq \xi_k \leq 2$.

Limit of the internal deformation tensor.

For given γ_k the equation for the internal deformation tensor of the Johnson–Segalman model reduces to a linear algebraic equation. It is straightforward to solve this equation analytically:

$$b_{11,k} = 1 + \frac{2(1 - \xi_k)\gamma_k}{1 - 2(1 - \xi_k)\gamma_k}, \qquad b_{22,k} = 1 - \frac{(1 - \xi_k)\gamma_k}{1 + (1 - \xi_k)\gamma_k}. \tag{3.7}$$

There is no limit $\gamma_k \gg 1$, because the solution of $b_{11,k}$ has a singularity at $2(1 - \xi_k)\gamma_k = 1$.

The Giesekus model

The Giesekus model is given by (A.3). The scalars $g_{i,k}$ are $g_{1,k} = (1 - \alpha_k)$, $g_{2,k} = -(1 - 2\alpha_k)$ and $g_{3,k} = -\alpha_k$. The coefficients in (2.19) are $B_k = 1$ and $\xi_k = 0$.

Limit of the internal deformation tensor.

The equation for the internal deformation tensor of the Giesekus model can be solved analytically for given γ_k. This equation has been solved by Giesekus (1982). For $\alpha_k = 0$ it reduces to the Johnson–Segalman model with $\xi_k = 0$. For $0 < \alpha_k < 1$ the solution is

$$b_{11,k} = \frac{1}{2\alpha_k} \left(2\gamma_k - (1 - 2\alpha_k) + \sqrt{1 - 4(1 - 2\alpha_k)\gamma_k + 4\gamma_k^2} \right),$$

$$b_{22,k} = \frac{1}{2\alpha_k} \left(-\gamma_k - (1 - 2\alpha_k) + \sqrt{1 + 2(1 - 2\alpha_k)\gamma_k + \gamma_k^2} \right). \tag{3.8}$$

The limit for $\gamma_k \gg 1$ for these values can be found by a standard Taylor expansion of the root:

$$b_{11,k} \simeq \frac{2\gamma_k}{\alpha_k}, \qquad b_{22,k} \to \frac{1 - \alpha_k}{\gamma_k}. \tag{3.9}$$

The invariants then become

$$I_{1,k} \simeq \frac{2\gamma_k}{\alpha_k}, \qquad I_{2,k} \to 4\frac{1 - \alpha_k}{\alpha_k}, \qquad I_{3,k} \to 2\frac{(1 - \alpha_k)^2}{\alpha_k \gamma_k}. \tag{3.10}$$

Limit of the mechanical dissipation.

Substitution of the limit values of the internal deformation tensor (3.9) in the mechanical dissipation expression for steady uniaxial elongation (3.5) gives

$$D_{\mathrm{m},k}^{\mathrm{ve}} \simeq \frac{2G_k}{\lambda_k \alpha_k} \gamma_k^2, \tag{3.11}$$

which increases quadratically with the elongation rate.

Limit of the heat conduction tensor.

Substitution of the limit values of the internal deformation tensor (3.9) in the expression for the parallel and perpendicular thermal conductivities for uniaxial elongation (3.6) gives

$$\kappa_{\parallel} \simeq \kappa_0 + \sum_{k=1}^{K} \left(\kappa_{1,k} \frac{2\gamma_k}{\alpha_k} + \kappa_{2,k} \frac{4\gamma_k^2}{\alpha_k^2} \right),$$

$$\kappa_{\perp} \to \kappa_0 + \sum_{k=1}^{K} \left(\kappa_{1,k} \frac{1 - \alpha_k}{\gamma_k} + \kappa_{2,k} \frac{(1 - \alpha_k)^2}{\gamma_k^2} \right). \tag{3.12}$$

For constant heat conduction coefficients the limit value for the perpendicular thermal conductivity is $\kappa_{\perp} = \kappa_0$. For $\kappa_{2,k} = 0$ the parallel thermal conductivity increases linearly with γ_k, otherwise it increases quadratically. Thus with the Giesekus model and the anisotropic heat conduction model with constant coefficients it is possible to describe the experimentally observed behaviour in elongation for large values of γ_k.

The (modified) Leonov model

The modified Leonov model is given by (A.5). The scalars $g_{i,k}$ are $g_{1,k} = \phi_k/2$, $g_{2,k} = -\phi_k(I_{1,k} - I_{2,k})/6$ and $g_{3,k} = -\phi_k/2$. The coefficients in (2.19) are $B_k = 1$ and $\xi_k = 0$. The Leonov model is the modified Leonov model with $\phi_k = 1$. In contrast with the modified Leonov model, the Leonov model can be solved analytically. The Leonov model will not be treated separately, because in this section only the limit values will be examined. The limit values of the Leonov model can be found by substitution of $\alpha_k = 0$ in the results for the modified Leonov model.

Limit of the internal deformation tensor.

For the modified Leonov model a nonlinear equation for $b_{11,k}$ has to be solved

$$4\gamma_k b_{11,k} + \phi_k(1 + \frac{1}{3}(I_{1,k} - I_{2,k})b_{11,k} - b_{11,k}^2) = 0,$$

$$b_{22,k} = b_{11,k}^{-1/2}, \tag{3.13}$$

where $I_{3,k} = 1$ has been used for the second equation. For $\gamma_k \gg 1$ it follows that

$$b_{11,k} \simeq 6\gamma_k(1 + \alpha_k), \qquad b_{22,k} \to \frac{1}{\sqrt{6\gamma_k(1 + \alpha_k)}}. \tag{3.14}$$

The invariants become

$$I_{1,k} \simeq 6\gamma_k(1 + \alpha_k), \qquad I_{2,k} \simeq 2\sqrt{6\gamma_k(1 + \alpha_k)}, \qquad I_{3,k} = 1. \tag{3.15}$$

Limit of the mechanical dissipation.

Substitution of the limit values of the internal deformation tensor (3.14) in the mechanical dissipation expression for steady uniaxial elongation (3.5) gives

$$D^{\text{ve}}_{\text{m},k} \simeq 6\frac{G_k}{\lambda_k}(1 + \alpha_k)\gamma_k^2, \tag{3.16}$$

which increases quadratically with the elongation rate.

Limit of the heat conduction tensor.

Substitution of the values of the internal deformation tensor for large γ_k (3.14) in the expression for the parallel and perpendicular thermal conductivities for uniaxial elongation (3.6) gives

$$\kappa_\| \simeq \kappa_0 + \sum_{k=1}^K \left(\kappa_{1,k}6(1 + \alpha_k)\gamma_k + \kappa_{2,k}36(1 + \alpha_k)^2\gamma_k^2 \right),$$

$$\kappa_\perp \rightarrow \kappa_0 + \sum_{k=1}^K \left(\kappa_{1,k}\frac{1}{6\sqrt{(1 + \alpha_k)\gamma_k}} + \kappa_{2,k}\frac{1}{6(1 + \alpha_k)\gamma_k} \right). \tag{3.17}$$

For constant heat conduction coefficients the limit value for the perpendicular thermal conductivities is $\kappa_\perp = \kappa_0$. For $\kappa_{2,k} = 0$ the parallel thermal conductivity increases linearly with γ_k, otherwise it increases quadratically. Thus with the (modified) Leonov model and the anisotropic heat conduction model with constant coefficients it is possible to describe the behaviour for large values of γ_k.

The Phan-Thien–Tanner model

The Phan-Thien–Tanner model is given by (A.6). The scalars $g_{i,k}$ are $g_{1,k} = Y_k$, $g_{2,k} = -Y_k$ and $g_{3,k} = 0$. The coefficients in (2.19) are $B_k = 1$ and $0 \leq \xi_k \leq 2$.

Limit of the internal deformation tensor.

For the Phan-Thien–Tanner model the equations

$$2(1 - \xi_k)\gamma_k b_{11,k} + Y_k(1 - b_{11,k}) = 0,$$
$$-(1 - \xi_k)\gamma_k b_{22,k} + Y_k(1 - b_{22,k}) = 0 \tag{3.18}$$

have to be solved. Two different parameters will be considered: a linear Y_k and an exponential Y_k. It is not possible to solve these equations analytically. For large values of γ_k however a limit solution can be calculated.

The linear Phan-Thien–Tanner model

The nonlinear parameter in the linear PTT model is $Y_k = 1 + \epsilon_k(b_{11,k} + 2b_{22,k} - 3)$. For $\gamma_k \gg 1$ and $\xi_k \neq 1$ it follows from (3.18) that

$$b_{11,k} \simeq \frac{2(1 - \xi_k)\gamma_k}{\epsilon_k}, \qquad b_{22,k} \rightarrow \frac{2}{3}. \tag{3.19}$$

The invariants become

$$I_{1,k} \simeq \frac{2(1 - \xi_k)\gamma_k}{\epsilon_k}, \qquad I_{2,k} \simeq \frac{8(1 - \xi_k)\gamma_k}{3\epsilon_k}, \qquad I_{3,k} \simeq \frac{8}{9}\frac{(1 - \xi_k)\gamma_k}{\epsilon_k}. \tag{3.20}$$

Limit of the mechanical dissipation.

Substitution of the limit values of the internal deformation tensor (3.19) in the mechanical dissipation expression for steady uniaxial elongation (3.5) gives

$$D_{\text{m},k}^{\text{ve}} \simeq \frac{2G_k}{\lambda_k \epsilon_k} \gamma_k^2, \tag{3.21}$$

which increases quadratically with the elongation rate.

Limit of the heat conduction tensor.

Substitution of the values of the internal deformation tensor for $\gamma_k \gg 1$ (3.19) in the expression for the parallel and perpendicular thermal conductivities for uniaxial elongation (3.6) gives

$$\kappa_{\parallel} \simeq \kappa_0 + \sum_{k=1}^{K} \left(\kappa_{1,k} \frac{2(1 - \xi_k)\gamma_k}{\epsilon_k} + \kappa_{2,k} \frac{4(1 - \xi_k)^2 \gamma_k^2}{\epsilon_k^2} \right),$$

$$\kappa_{\perp} \to \kappa_0 + \sum_{k=1}^{K} \left(\frac{2}{3}\kappa_{1,k} + \frac{4}{9}\kappa_{2,k} \right). \tag{3.22}$$

For constant heat conduction coefficients the limit value for the perpendicular thermal conductivity $\kappa_{\perp}$ is smaller than the equilibrium thermal conductivity κ_{eq}. For $\kappa_{2,k} = 0$ the perpendicular thermal conductivity is always larger than $2\kappa_{\text{eq}}/3$. When the coefficients are assumed to depend on a small negative power of one of the invariants, the perpendicular thermal conductivity may be decreased further. For $\kappa_{2,k} = 0$ the parallel thermal conductivity increases linearly with γ_k, otherwise it increases quadratically. Thus with the linear PTT model and the anisotropic heat conduction model with constant coefficients it is possible to describe the behaviour for large values of γ_k.

The exponential Phan-Thien–Tanner model

The nonlinear parameter in the exponential PTT model is $Y_k = \exp[\epsilon_k(b_{11,k} + 2b_{22,k} - 3)]$. For $\gamma_k \gg 1$ and $\xi_k \neq 1$ it follows from (3.18) that

$$b_{11,k} \simeq \frac{1}{\epsilon_k} \ln(2(1 - \xi_k)\gamma_k), \qquad b_{22,k} \to \frac{2}{3}. \tag{3.23}$$

The invariants become

$$I_{1,k} \simeq \frac{1}{\epsilon_k} \ln(2(1 - \xi_k)\gamma_k), \qquad I_{2,k} \simeq \frac{4}{3\epsilon_k} \ln(2(1 - \xi_k)\gamma_k),$$

$$I_{3,k} \simeq \frac{4}{9} \frac{1}{\epsilon_k} \ln(2(1 - \xi_k)\gamma_k). \tag{3.24}$$

Limit of the mechanical dissipation.

Substitution of the limit values of the internal deformation tensor (3.23) in the mechanical dissipation expression for steady uniaxial elongation (3.5) gives

$$D_{\text{m},k}^{\text{ve}} \simeq \frac{G_k}{(1 - \xi_k)\lambda_k \epsilon_k} \ln(2(1 - \xi_k)\gamma_k)\gamma_k, \tag{3.25}$$

which increases less then quadratically with the elongation rate.

Limit of the heat conduction tensor.

Substitution of the limit values of the internal deformation tensor (3.23) in the expression for the parallel and perpendicular thermal conductivities for uniaxial elongation (3.6) gives

$$\kappa_\| \simeq \kappa_0 + \sum_{k=1}^{K}\left(\kappa_{1,k}\frac{1}{\epsilon_k}\ln(2(1-\xi_k)\gamma_k) + \kappa_{2,k}\frac{1}{\epsilon_k^2}\ln^2(2(1-\xi_k)\gamma_k)\right),$$

$$\kappa_\perp \to \kappa_0 + \sum_{k=1}^{K}\left(\frac{2}{3}\kappa_{1,k} + \frac{4}{9}\kappa_{2,k}\right). \tag{3.26}$$

For constant heat conduction coefficients the limit value for the perpendicular thermal conductivity is the same as for the linear model. The parallel thermal conductivity increases logarithmically with the elongation rate, with $\ln^2\gamma_k$ when $\kappa_{2,k}\neq 0$ or with $\ln\gamma_k$ when $\kappa_{2,k}=0$.

The Larson model

The Larson model is given by (A.9). The scalars $g_{i,k}$ are $g_{1,k}=1/B_k$, $g_{2,k}=-1/B_k$ and $g_{3,k}=0$. The coefficients in (2.19) are $B_k=(1+\beta_k(I_{1,k}-3)/3)^{-1}$ and $\xi_k=0$.

Limit of the internal deformation tensor.

The differential equation for the internal deformation tensor equals the differential equation for the linear Phan-Thien–Tanner model with $\xi_k=0$ and $\epsilon_k=\beta_k/3$. Thus the resulting internal deformation tensors and thermal conductivities are also equal. However, the relation between the stress and the internal deformation tensor is different, so the mechanical dissipation is different as well.

Limit of the mechanical dissipation.

Substitution of the limit values of the internal deformation tensor (3.19) in the mechanical dissipation expression for steady uniaxial elongation (3.5) gives

$$D_{m,k}^{ve} \simeq \frac{3G_k}{\lambda_k\beta_k}\gamma_k, \tag{3.27}$$

which increases only linearly with the elongation rate.

3.1.2   Steady simple shear

For a simple shear flow the modified velocity gradient $\hat{\underline{\underline{L}}}$ and the internal deformation tensor $\underline{\underline{b}}_k$ are

$$\hat{\underline{\underline{L}}} = \begin{bmatrix} 0 & (1-\frac{\xi_k}{2})\dot{\gamma} & 0 \\ -\frac{\xi_k}{2}\dot{\gamma} & 0 & 0 \\ 0 & 0 & 0 \end{bmatrix}, \quad \underline{\underline{b}}_k = \begin{bmatrix} b_{11,k} & b_{12,k} & 0 \\ b_{12,k} & b_{22,k} & 0 \\ 0 & 0 & b_{33,k} \end{bmatrix}. \tag{3.28}$$

The invariants of $\underline{\underline{b}}_k$ are then

$$I_{1,k} = b_{11,k} + b_{22,k} + b_{33,k}, \qquad I_{2,k} = b_{11,k}b_{22,k} + b_{11,k}b_{33,k} + b_{22,k}b_{33,k} - b_{12,k}^2,$$

$$I_{3,k} = b_{33,k}(b_{11,k}b_{22,k} - b_{12,k}^2). \tag{3.29}$$

For convenience the non-dimensional shear rate $\gamma_k = \lambda_k \dot{\gamma}$ is introduced. For a simple shear flow (3.1) then reduces to

$$(2 - \xi_k)\gamma_k b_{12,k} + g_{1,k} + g_{2,k} b_{11,k} + g_{3,k}(b_{11,k}^2 + b_{12,k}^2) = 0,$$

$$(1 - \frac{\xi_k}{2})\gamma_k b_{22,k} - \frac{\xi_k}{2}\gamma_k b_{11,k} + g_{2,k} b_{12,k} + g_{3,k} b_{12,k}(b_{11,k} + b_{22,k}) = 0,$$

$$-\xi_k \gamma_k b_{12,k} + g_{1,k} + g_{2,k} b_{22,k} + g_{3,k}(b_{22,k}^2 + b_{12,k}^2) = 0,$$

$$g_{1,k} + g_{2,k} b_{33,k} + g_{3,k} b_{33,k}^2 = 0. \tag{3.30}$$

The values of $g_{i,k}$ for the specific models have already been given in section 3.1.1 and will not be repeated in this section.

For a steady simple shear flow the material derivative of the internal deformation tensor cancels out, so the mechanical dissipation equals the stress work. With (2.19) the mechanical dissipation can be written as

$$D_{\mathrm{m},k}^{\mathrm{ve}} = \tau_{12,k}\dot{\gamma} = \eta(\dot{\gamma})\dot{\gamma}^2 = \frac{G_k B_k}{(1 - \xi_k)\lambda_k} b_{12,k}\gamma_k, \tag{3.31}$$

where definition of the shear viscosity (1.1) and the relation between the extra-stress and the internal deformation tensor (2.19) have been used.

The thermal conductivities parallel and perpendicular to the flow direction in a simple shear flow are

$$\kappa_{\parallel} = \kappa_0 + \sum_{k=1}^{K} \left(\kappa_{1,k} b_{11,k} + \kappa_{2,k}(b_{11,k}^2 + b_{12,k}^2) \right),$$

$$\kappa_{\perp} = \kappa_0 + \sum_{k=1}^{K} \left(\kappa_{1,k} b_{22,k} + \kappa_{2,k}(b_{22,k}^2 + b_{12,k}^2) \right). \tag{3.32}$$

Note that if $\kappa_{2,k} = 0$ the parallel and perpendicular thermal conductivities only depend on the components of the internal deformation tensors in that direction, just as for the steady elongational flow. However, if $\kappa_{2,k} \neq 0$ both conductivities also depend on the shear components of the internal deformation tensors.

In the remaining part of this subsection the internal deformation tensor, the corresponding mechanical dissipation and the parallel and perpendicular thermal conductivity will be calculated for various stress models in a steady simple shear flow. If possible an analytic expression will be given for these quantities, otherwise only the approximations for large shear rates will be presented.

The Johnson–Segalman model

For the values of $g_{i,k}$, B_k and ξ_k refer to section 3.1.1. For given γ_k the equation (3.30) is a linear algebraic equation, which can easily be solved analytically. The solution for the components of the internal deformation tensor is

$$b_{11,k} = 1 + (2 - \xi_k)\gamma_k b_{12,k}, \qquad b_{12,k} = \frac{(1 - \xi_k)\gamma_k}{1 + \xi_k(2 - \xi_k)\gamma_k^2},$$

$$b_{22,k} = 1 - \xi_k \gamma_k b_{12,k}, \qquad\qquad b_{33,k} = 1. \tag{3.33}$$

For the limit $\gamma_k \gg 1$ three cases have to be considered for the parameter ξ in the mixed convected derivative: $\xi_k = 0$, $\xi_k = 2$ and $0 < \xi_k < 2$.

- $\xi_k = 0$

  Limit of the internal deformation tensor.

  Substitution of $\xi_k = 0$ in (3.33) gives

  $$b_{11,k} \simeq 2\gamma_k^2, \qquad b_{12,k} = \gamma_k, \qquad b_{22,k} = 1, \tag{3.34}$$

  for large values of γ_k. The invariants become

  $$I_{1,k} \simeq 2\gamma_k^2, \qquad I_{2,k} \simeq 3\gamma_k^2, \qquad I_{3,k} \simeq \gamma_k^2. \tag{3.35}$$

  Limit of the mechanical dissipation.

  Substitution of the values of the internal deformation tensor (3.34) in the mechanical dissipation expression for steady simple shear (3.31) gives

  $$D_{\mathrm{m},k}^{\mathrm{ve}} = \frac{G_k}{\lambda_k}\gamma_k^2, \tag{3.36}$$

  which equals exactly the Newtonian mechanical dissipation $\eta_k\dot{\gamma}^2$, for all possible values of the shear rate.

  Limit of the heat conduction tensor.

  Substitution of the components of the internal deformation tensor (3.34) in (3.32) gives

  $$\kappa_{\parallel} \simeq \kappa_0 + \sum_{k=1}^{K}\left(\kappa_{1,k}2\gamma_k^2 + \kappa_{2,k}4\gamma_k^4\right),$$
  $$\kappa_{\perp} \simeq \kappa_0 + \sum_{k=1}^{K}\left(\kappa_{1,k} + \kappa_{2,k}\gamma_k^2\right). \tag{3.37}$$

  For constant heat conduction coefficients this model predicts an increase of the parallel thermal conductivity. For the model with constant coefficients the perpendicular thermal conductivity is at least equal to the equilibrium conductivity or even increases when $\kappa_{2,k}$ are positive. When the scalars are supposed to depend on the invariants it is possible to fulfil restrictions I and II. If $\kappa_{2,k} = 0$, a dependence of the scalars on a small negative power of one of the invariants is sufficient.

- $\xi_k = 2$

  Limit of the internal deformation tensor.

  Substitution of $\xi_k = 2$ in (3.33) gives

  $$b_{11,k} = 1, \qquad b_{12,k} = -\gamma_k, \qquad b_{22,k} \simeq 2\gamma_k^2. \tag{3.38}$$

  The invariants are the same as for $\xi_k = 0$: (3.35).

Limit of the mechanical dissipation.

The mechanical dissipation is the same as for $\xi_k = 0$: (3.36).

Limit of the heat conduction tensor.

Substitution of the limit values of the internal deformation tensors (3.38) in (3.32) gives

$$\kappa_\| \simeq \kappa_0 + \sum_{k=1}^{K} \left(\kappa_{1,k} + \kappa_{2,k} \gamma_k^2 \right),$$

$$\kappa_\perp \simeq \kappa_0 + \sum_{k=1}^{K} \left(\kappa_{1,k} 2\gamma_k^2 + \kappa_{2,k} 4\gamma_k^4 \right). \tag{3.39}$$

It is clear that this model with constant coefficients is completely in contradiction with the experiments.

- $0 < \xi_k < 2$

Limit of the internal deformation tensor.

For $0 < \xi_k < 2$ the components of the internal deformation tensor (3.33) become for large γ_k

$$b_{11,k} \to 1 + \frac{1 - \xi_k}{\xi_k}, \qquad b_{12,k} \to \frac{(1 - \xi_k)}{\xi_k(2 - \xi_k)\gamma_k} = \frac{C_k}{\gamma_k}, \qquad b_{22,k} \to 1 - \frac{1 - \xi_k}{2 - \xi_k}. \tag{3.40}$$

The invariants become

$$I_{1,k} \to 1 + \frac{2}{(2 - \xi_k)\xi_k}, \qquad I_{2,k} \to \frac{3}{(2 - \xi_k)\xi_k}, \qquad I_{3,k} \to \frac{1}{(2 - \xi_k)\xi_k}. \tag{3.41}$$

Limit of the mechanical dissipation.

Substitution of the limit values of the internal deformation tensor (3.40) in the mechanical dissipation expression for a steady simple shear flow (3.31) gives

$$D_{\mathrm{m},k}^{\mathrm{ve}} \to \frac{G_k}{\lambda_k(1 - \xi_k)} C_k, \tag{3.42}$$

which is independent of the shear rate.

Limit of the heat conduction tensor.

Substitution of the values of the internal deformation tensor for large γ_k (3.40) in the expression (3.32) for the parallel and perpendicular thermal conductivities for a steady shear flow gives

$$\kappa_\| \to \kappa_0 + \sum_{k=1}^{K} \left(\kappa_{1,k} \frac{1}{\xi_k} + \kappa_{2,k} \frac{1}{\xi_k^2} \right),$$

$$\kappa_\perp \to \kappa_0 + \sum_{k=1}^{K} \left(\kappa_{1,k} \frac{1}{2 - \xi_k} + \kappa_{2,k} \frac{1}{(2 - \xi_k)^2} \right). \tag{3.43}$$

For constant $\kappa_{1,k}$ and $\kappa_{2,k}$, and even when they depend on the invariants, the thermal conductivities only depend on the values of ξ_k. The perpendicular thermal conductivity decreases and the parallel thermal conductivity increases when $\xi_k < 1$. When $\xi_k > 1$ the perpendicular thermal conductivity increases and the parallel thermal conductivity decreases.

The Giesekus model

For the values of $g_{i,k}$, B_k and ξ_k refer to section 3.1.1.

Limit of the internal deformation tensor.

For $0 < \alpha_k < 1$ the equations for a simple shear flow of the internal deformation tensors (3.30) have been solved analytically by Giesekus (1982). For $\alpha_k = 0$ the Giesekus equation reduces to the Johnson–Segalman with $\xi_k = 0$. The resulting solution is a complicated function of the non-dimensional shear rate and the parameter α_k. It will not be repeated. The limit value for $\gamma_k \gg 1$ can be found by a Taylor expansion of the solution given by Giesekus. This results in

$$b_{11,k} \simeq \frac{1}{\alpha_k}\sqrt[4]{\alpha_k(1-\alpha_k)}\sqrt{2\gamma_k}, \qquad b_{12,k} \to \sqrt{\frac{1-\alpha_k}{\alpha_k}},$$

$$b_{22,k} \to \frac{2(1-\alpha_k)}{\sqrt[4]{\alpha_k(1-\alpha_k)}\sqrt{2\gamma_k}}, \qquad b_{33,k} = 1. \tag{3.44}$$

The invariants become

$$I_{1,k} \simeq \frac{1}{\alpha_k}\sqrt[4]{\alpha_k(1-\alpha_k)}\sqrt{2\gamma_k}, \qquad I_{2,k} \simeq \frac{1}{\alpha_k}\sqrt[4]{\alpha_k(1-\alpha_k)}\sqrt{2\gamma_k},$$

$$I_{3,k} \to \frac{1-\alpha_k}{\alpha_k}. \tag{3.45}$$

Limit of the mechanical dissipation.

Substitution of the limit values of the internal deformation tensor (3.44) in the mechanical dissipation expression for a steady shear (3.31) gives

$$D_{\mathrm{m},k}^{\mathrm{ve}} \simeq \frac{G_k}{\lambda_k}\sqrt{\frac{1-\alpha_k}{\alpha_k}}\gamma_k, \tag{3.46}$$

which increases linearly with the shear rate.

Limit of the heat conduction tensor.

Substitution of the limit values of the internal deformation tensor (3.44) in the expression for the parallel and perpendicular thermal conductivities for a steady shear flow (3.32) gives

$$\kappa_{\parallel} \simeq \kappa_0 + \sum_{k=1}^{K}\left(\kappa_{1,k}\frac{\sqrt[4]{\alpha_k(1-\alpha_k)}}{\alpha_k}\sqrt{2\gamma_k} + \kappa_{2,k}\frac{\sqrt{\alpha_k(1-\alpha_k)}}{\alpha_k^2}2\gamma_k\right),$$

$$\kappa_{\perp} \to \kappa_0 + \sum_{k=1}^{K}\left(\kappa_{1,k}\frac{2(1-\alpha_k)}{\sqrt[4]{\alpha_k(1-\alpha_k)}\sqrt{2\gamma_k}} + \kappa_{2,k}\frac{1-\alpha_k}{\alpha_k}\right). \tag{3.47}$$

For constant heat conduction coefficients the limit value for the perpendicular thermal conductivity is $\kappa_\perp = \kappa_0 + \sum_{k=1}^{K} \kappa_{2,k}(1 - \alpha_k)/\alpha_k$. For $\kappa_{2,k} = 0$ this limit is always smaller than κ_{eq}. For $\kappa_{2,k} > 0$ it depends on the values of α_k whether the perpendicular thermal conductivity decreases. For $\kappa_{2,k} = 0$ the parallel thermal conductivity increases with the root of γ_k, otherwise it increases linearly. Thus with the Giesekus model and the anisotropic heat conduction model it is possible to describe the behaviour for large values of γ_k. It is interesting to note that the anisotropy is smaller than for a uniaxial elongation with the same γ_k. For the elongation the $\kappa_{1,k}$ term in the parallel thermal conductivity increased with the elongation rate and the $\kappa_{2,k}$ term with the square of the elongation rate.

The (modified) Leonov model

For the values of $g_{i,k}$, B_k and ξ_k refer to section 3.1.1. The results for the Leonov model may be obtained by substitution of $\phi_k = 1$ or $\alpha_k = 0$ in the results for the modified Leonov model.

Limit of the internal deformation tensor.

For the modified Leonov model the following equations have to be solved:

$$
\begin{aligned}
&\gamma_k b_{12,k}^2 + \phi_k b_{12,k} = \gamma_k, \\
&\gamma_k b_{22,k}^2 = \phi_k b_{12,k}, \\
&4\gamma_k b_{12,k} + \phi_k(1 - b_{11,k}^2 - b_{12,k}^2) = 0, \\
&b_{33,k} = 1.
\end{aligned}
\tag{3.48}
$$

For $\gamma_k \gg 1$ follows

$$
b_{11,k} \simeq 2\sqrt{(1 + \alpha_k)\gamma_k}, \qquad b_{12,k} \to 1, \qquad b_{22,k} \to \sqrt{\frac{1}{(1 + \alpha_k)\gamma_k}}.
\tag{3.49}
$$

The invariants become

$$
I_{1,k} \simeq 2\sqrt{(1 + \alpha_k)\gamma_k}, \qquad I_{2,k} \simeq 2\sqrt{(1 + \alpha_k)\gamma_k}, \qquad I_{3,k} = 1.
\tag{3.50}
$$

Limit of the mechanical dissipation.

Substitution of the limit values of the internal deformation tensor (3.49) in the mechanical dissipation expression for a steady simple shear flow (3.31) gives

$$
D_{m,k}^{ve} \simeq \frac{G_k}{\lambda_k} \gamma_k,
\tag{3.51}
$$

which increases linearly with the shear rate.

Limit of the heat conduction tensor.

Substitution of the values of the internal deformation tensor for large γ_k (3.49) in the expression for the parallel and perpendicular thermal conductivities for a steady simple shear flow (3.32) gives

$$
\begin{aligned}
\kappa_\parallel &\simeq \kappa_0 + \sum_{k=1}^{K} \left(\kappa_{1,k} 2\sqrt{(1 + \alpha_k)\gamma_k} + \kappa_{2,k} 4(1 + \alpha_k)\gamma_k \right), \\
\kappa_\perp &\to \kappa_0 + \sum_{k=1}^{K} \left(\kappa_{1,k} \frac{1}{\sqrt{(1 + \alpha_k)\gamma_k}} + \kappa_{2,k} \right).
\end{aligned}
\tag{3.52}
$$

For constant heat conduction coefficients the limit value for the perpendicular thermal conductivity is $\kappa_\perp = \kappa_0 + \sum_{k=1}^{K} \kappa_{2,k}$. For positive $\kappa_{1,k}$ this is smaller than the equilibrium thermal conductivity. For $\kappa_{2,k} = 0$ the parallel thermal conductivity increases with the root of γ_k, otherwise it increases linearly. Thus with the (modified) Leonov model and the anisotropic heat conduction model with constant coefficients it is possible to describe the behaviour for large values of γ_k. It is interesting to note that the anisotropy is smaller than for a uniaxial elongation with the same γ_k. For the elongation the $\kappa_{1,k}$ term increased linearly and the $\kappa_{2,k}$ term quadratically with the elongation rate.

The Phan-Thien–Tanner model

For the values of $g_{i,k}$, B_k and ξ_k refer to section 3.1.1. For the PTT model the following equations have to be solved for the internal deformation tensor

$$
(2 - \xi_k)\gamma_k b_{12,k} + Y_k(1 - b_{11,k}) = 0,
$$
$$
(1 - \frac{\xi_k}{2})\gamma_k b_{22,k} - \frac{\xi_k}{2}\gamma_k b_{11,k} - Y_k b_{12,k} = 0,
$$
$$
-\xi_k \gamma_k b_{12,k} + Y_k(1 - b_{22,k}) = 0,
$$
$$
b_{33,k} = 1. \tag{3.53}
$$

Two different parameters will be considered: a linear Y_k and an exponential Y_k.

The linear Phan-Thien–Tanner model

The nonlinear parameter in the linear PTT model is $Y_k = 1 + \epsilon_k(b_{11,k} + b_{22,k} - 2)$. For the limit $\gamma_k \gg 1$ three cases have to be considered: $\xi_k = 0$, $\xi_k = 2$ and $0 < \xi_k < 2$.

- $\xi_k = 0$

  Limit of the internal deformation tensor.

  For $\xi_k = 0$ the limit solutions of (3.53) are

  $$
  b_{11,k} \simeq \sqrt[3]{\frac{2\gamma_k^2}{\epsilon_k^2}}, \qquad b_{12,k} \simeq \sqrt[3]{\frac{\gamma_k}{2\epsilon_k}}, \qquad b_{22,k} \to 1. \tag{3.54}
  $$

  The invariants become

  $$
  I_{1,k} \simeq \sqrt[3]{\frac{2\gamma_k^2}{\epsilon_k^2}}, \qquad I_{2,k} \simeq (2\sqrt[3]{2} - \frac{1}{\sqrt[3]{4}})\sqrt[3]{\frac{\gamma_k^2}{\epsilon_k^2}}, \qquad I_{3,k} \simeq (\sqrt[3]{2} - \frac{1}{\sqrt[3]{4}})\sqrt[3]{\frac{\gamma_k^2}{\epsilon_k^2}}. \tag{3.55}
  $$

  Limit of the mechanical dissipation.

  Substitution of the limit values of the internal deformation tensor (3.54) in the mechanical dissipation expression for steady simple shear (3.31) gives

  $$
  D_{\mathrm{m},k}^{\mathrm{ve}} \simeq \frac{G_k}{\lambda_k}\sqrt{\frac{\gamma_k}{2\epsilon_k}}\gamma_k, \tag{3.56}
  $$

  which increases with a 3/2 power of the shear rate.

Limit of the heat conduction tensor.

Substitution of the values of the internal deformation tensor for $\gamma_k \gg 1$ (3.54) in the expression for the parallel and perpendicular thermal conductivities for a steady simple shear flow (3.32) gives

$$\kappa_\| \simeq \kappa_0 + \sum_{k=1}^{K} \left(\kappa_{1,k} \sqrt[3]{\frac{2\gamma_k^2}{\epsilon_k^2}} + \kappa_{2,k} \sqrt[3]{\frac{4\gamma_k^4}{\epsilon_k^4}} \right),$$

$$\kappa_\perp \simeq \kappa_0 + \sum_{k=1}^{K} \left(\kappa_{1,k} + \kappa_{2,k} \sqrt[3]{\frac{\gamma_k^2}{4\epsilon_k^2}} \right). \tag{3.57}$$

For constant heat conduction coefficients it follows from restriction I that $\kappa_{2,k} = 0$. But even then the limit value for the perpendicular thermal conductivity equals the equilibrium thermal conductivity $\kappa_\perp = \kappa_{\rm eq}$. Thus in contrast with the elongational flow, restriction I cannot be fulfilled in a simple shear flow. For $\kappa_{2,k} = 0$ the parallel thermal conductivity increases less than linearly with the shear rate: $\gamma_k^{2/3}$. This is less than for the elongational flow which increased linearly with the elongation rate. It is possible to fulfil restriction I when the coefficients $\kappa_{1,k}$ and $\kappa_{2,k}$ depend on a small negative power of one of the invariants.

- $\xi_k = 2$

Limit of the internal deformation tensor.

For $\xi_k = 2$ the limits of the components of the internal deformation tensors in (3.53) become

$$b_{11,k} \to 1, \qquad b_{12,k} \simeq -\sqrt[3]{\frac{\gamma_k}{2\epsilon_k}}, \qquad b_{22,k} \simeq \sqrt[3]{\frac{2\gamma_k^2}{\epsilon_k^2}}. \tag{3.58}$$

The limits of the invariants are the same as for $\xi_k = 0$: (3.55).

Limit of the mechanical dissipation.

The mechanical dissipation is the same as for $\xi_k = 0$: (3.56).

Limit of the heat conduction tensor.

Substitution of the limit values of the internal deformation tensor (3.58) in the expression for the parallel and perpendicular thermal conductivities for steady shear (3.32) gives

$$\kappa_\| \simeq \kappa_0 + \sum_{k=1}^{K} \left(\kappa_{1,k} + \kappa_{2,k} \sqrt[3]{\frac{\gamma_k^2}{4\epsilon_k^2}} \right),$$

$$\kappa_\perp \simeq \kappa_0 + \sum_{k=1}^{K} \left(\kappa_{1,k} \sqrt[3]{\frac{2\gamma_k^2}{\epsilon_k^2}} + \kappa_{2,k} \sqrt[3]{\frac{4\gamma_k^4}{\epsilon_k^4}} \right). \tag{3.59}$$

For constant heat conduction coefficients $\kappa_{1,k} = \kappa_{2,k} = 0$ due to restriction I. Thus only the isotropic thermal conductivity remains. Even the dependence of $\kappa_{1,k}$ and $\kappa_{2,k}$ on the

invariants does not help. It is then possible to obtain a limit value for the perpendicular thermal conductivity which is smaller than the equilibrium conductivity. However, then the parallel thermal conductivity is also smaller than the equilibrium conductivity.

- $0 < \xi_k < 2$

Limit of the internal deformation tensor.

For large γ_k the limit of an internal deformation tensor is

$$b_{11,k} \to \frac{1}{\xi_k}, \qquad b_{12,k} \to \frac{(1-\xi_k)Y_k}{\xi_k(2-\xi_k)\gamma_k} = \frac{C_k}{\gamma_k},$$

$$b_{22,k} \to \frac{1}{2-\xi_k}, \qquad Y_k \to 1 + \frac{2\epsilon_k(1-\xi_k)^2}{\xi_k(2-\xi_k)}. \tag{3.60}$$

The invariants become

$$I_{1,k} \to \frac{1}{\xi_k} + \frac{1}{2-\xi_k} + 1, \qquad I_{2,k} \to \frac{3}{\xi_k(2-\xi_k)}, \qquad I_{3,k} \to \frac{1}{\xi_k(2-\xi_k)}. \tag{3.61}$$

Note that the limits of the invariants are equal to the limits of the invariants of the Johnson–Segalman model (3.41).

Limit of the mechanical dissipation.

Substitution of the limit values of the internal deformation tensor (3.60) in the mechanical dissipation expression for a steady simple shear flow (3.31) gives

$$D_{\mathrm{m},k}^{\mathrm{ve}} \to \frac{G_k}{\lambda_k}(1-\xi_k)C_k, \tag{3.62}$$

which is independent of the shear rate.

Limit of the heat conduction tensor.

Substitution of the values of the internal deformation tensor for large γ_k (3.60) in the expression for the parallel and perpendicular thermal conductivities for simple shear (3.32) gives

$$\kappa_\parallel \to \kappa_0 + \sum_{k=1}^{K}\left(\kappa_{1,k}\frac{1}{\xi_k} + \kappa_{2,k}\frac{1}{\xi_k^2}\right),$$

$$\kappa_\perp \to \kappa_0 + \sum_{k=1}^{K}\left(\kappa_{1,k}\frac{1}{2-\xi_k} + \kappa_{2,k}\frac{1}{(2-\xi_k)^2}\right). \tag{3.63}$$

For constant heat conduction coefficients $\kappa_\perp$ and $\kappa_\parallel$ are limited. It depends on ξ_k whether these limits are larger or smaller than the thermal conductivity in equilibrium κ_{eq}. For $0 < \xi_k < 1$ the limit of the perpendicular conductivity is smaller and the parallel conductivity larger than the equilibrium conductivity. For $1 < \xi_k < 2$ the behaviour is opposite. A dependence on the invariants does not help to fulfil restriction II. The invariants are also independent of the shear rate and only dependent on ξ_k. The behaviour of the parallel thermal conductivity is completely different from the steady elongation, where $\kappa_\parallel$ increased with increasing elongation rate.

The exponential Phan-Thien–Tanner model

In a steady shear flow the nonlinear parameter in the exponential Phan-Thien–Tanner model equals $Y_k = \exp[\epsilon_k(b_{11,k} + 2b_{22,k} - 3)]$. For the limit solution $\gamma_k \gg 1$ for (3.53) three cases have to be considered: $\xi_k = 0$, $\xi_k = 2$ and $0 < \xi_k < 2$.

- $\xi_k = 0$

Limit of the internal deformation tensor.

For large γ_k the limit of an internal deformation tensor is

$$b_{11,k} \simeq \frac{1}{\epsilon_k} \ln \gamma_k, \qquad b_{12,k} \simeq \sqrt{\frac{\ln \gamma_k}{2\epsilon_k}}, \qquad b_{22,k} \to 1. \tag{3.64}$$

The invariants then become

$$I_{1,k} \simeq \frac{1}{\epsilon_k} \ln \gamma_k, \qquad I_{2,k} \simeq \frac{3}{2\epsilon_k} \ln \gamma_k, \qquad I_{3,k} \simeq \frac{1}{2\epsilon_k} \ln \gamma_k. \tag{3.65}$$

Limit of the mechanical dissipation.

Substitution of the limit values of the internal deformation tensor (3.64) in the mechanical dissipation expression for a steady simple shear flow (3.31) gives

$$D^{\text{ve}}_{\text{m},k} \simeq \frac{G_k}{\lambda_k} \gamma_k \sqrt{\frac{\ln \gamma_k}{2\epsilon_k}}, \tag{3.66}$$

which increases more than linearly with the shear rate.

Limit of the heat conduction tensor.

Substitution of the limit values of the internal deformation tensor in (3.32) gives

$$\kappa_{\parallel} \simeq \kappa_0 + \sum_{k=1}^{K} \left(\kappa_{1,k} \frac{1}{\epsilon_k} \ln \gamma_k + \kappa_{2,k} \frac{1}{\epsilon_k^2} \ln^2 \gamma_k \right),$$

$$\kappa_{\perp} \simeq \kappa_0 + \sum_{k=1}^{K} \left(\kappa_{1,k} + \kappa_{2,k} \frac{1}{2\epsilon_k} \ln \gamma_k \right). \tag{3.67}$$

When the coefficients $\kappa_{1,k}$ and $\kappa_{2,k}$ are constants, the parallel conductivity increases logarithmically with the deformation rate. This behaviour is equal to the steady elongation. However, in contrast with the elongational flow, the perpendicular conductivity does not decrease. When $\kappa_{2,k}$ is positive it even increases logarithmically with the shear rate. Restriction I and II can be fulfilled when $\kappa_{1,k}$ or $\kappa_{2,k}$ depend on a small negative power of one of the invariants.

- $\xi_k = 2$

Limit of the internal deformation tensor.

For $\gamma_k \gg 1$ the components of an internal deformation tensor become

$$b_{11,k} \to 1, \qquad b_{12,k} \simeq -\sqrt{\frac{\ln \gamma_k}{2\epsilon_k}}, \qquad b_{22,k} \simeq \frac{1}{\epsilon_k} \ln \gamma_k. \tag{3.68}$$

The invariants are the same as for $\xi_k = 0$: (3.65).

Limit of the mechanical dissipation.

The mechanical dissipation is the same as for $\xi_k = 0$: (3.66).

Limit of the heat conduction tensor.

Substitution of the limit values of the internal deformation tensor in (3.32) gives

$$\kappa_\| \simeq \kappa_0 + \sum_{k=1}^{K} \left(\kappa_{1,k} + \kappa_{2,k} \sqrt{\frac{\ln \gamma_k}{2\epsilon_k}} \right),$$

$$\kappa_\perp \simeq \kappa_0 + \sum_{k=1}^{K} \left(\kappa_{1,k} \frac{1}{\epsilon_k} \ln \gamma_k + \kappa_{2,k} \frac{1}{\epsilon_k^2} \ln^2 \gamma_k \right). \tag{3.69}$$

It is clear that this model with constant coefficients is completely in contradiction with the experiments. A dependence on the invariants does not help, because then only restriction I or restriction II can be fulfilled.

- $0 < \xi_k < 2$

  The results are the same as for the linear Phan-Thien–Tanner model, except that the limit of Y_k, which is independent of the shear rate, is different:

$$Y_k \rightarrow \exp \left[2\epsilon_k (1 - \xi_k)^2 \xi_k (2 - \xi_k) \right]. \tag{3.70}$$

The Larson model

For the values of $g_{i,k}$, B_k and ξ_k refer to section 3.1.1.

Limit of the internal deformation tensor.

The differential equation for the internal deformation tensor of the Larson model is the same as for the linear Phan-Thien–Tanner model with $\beta_k/3 = \epsilon_k$. Only the stress is different. Therefore only the expression for the mechanical dissipation will be given.

Limit of the mechanical dissipation.

Substitution of the limit values of the internal deformation tensor of the linear Phan-Thien–Tanner model (3.54) in the mechanical dissipation expression for steady simple shear (3.31) gives

$$D_{\mathrm{m},k}^{\mathrm{ve}} \simeq \frac{G_k}{\lambda_k} \sqrt[3]{\frac{9\gamma_k^2}{4\beta_k^2}}, \tag{3.71}$$

which increases with a 2/3 power of the shear rate.

3.2   A lower bound for the invariants of the internal deformation tensor

Hulsen (1990b) has shown that it is possible to identify a positive definite configuration tensor (the internal deformation tensor $\underline{b}_k$) for the differential stress models of appendix A. Due to numerical errors an internal deformation tensor may become indefinite. This indefiniteness causes large non-linear instabilities, Hulsen (1988b). The positive definiteness of an internal

deformation tensor gives the opportunity to correct $\underline{\underline{b}}_k$ to a semi-positive definite tensor, with vanishing determinant. When the inverse of $\underline{\underline{b}}_k$ is needed, for example for the mechanical dissipation in the temperature equation (2.92), it is not sufficient to have a semi-positive definite $\underline{\underline{b}}_k$. In this subsection a method will be developed to determine the lower bound of the invariants of $\underline{\underline{b}}_k$. With the results also the positiveness of the term with the invariants in Δc and Δc^ϑ, equation (2.100) and 2.103), can be demonstrated. The method will be applied to the models of appendix A. Finally two possibilities to correct an indefinite internal deformation tensor in an axisymmetrical flow are discussed.

Starting point is the general equation for the internal deformation tensor (3.1). Combining this relation with

$$\dot{I}_{3,k} = \frac{\partial I_{3,k}}{\partial \underline{\underline{b}}_k} : \dot{\underline{\underline{b}}}_k = I_{3,k} \underline{\underline{b}}_k^{-1} : \dot{\underline{\underline{b}}}_k, \tag{3.72}$$

which follows from (2.20), the following expression for the material derivative of the third invariant is obtained:

$$\lambda_k \dot{I}_{3,k} = 2\lambda_k (1 - \xi_k) I_{3,k} \nabla \cdot \underline{v} + g_{1,k} I_{2,k} + (3 g_{2,k} + g_{3,k} I_{1,k}) I_{3,k}. \tag{3.73}$$

In the following a divergence free flow will be assumed. Then the first term on the right-hand side vanishes[1].

3.2.1 A lower bound for $I_{2,k}$ and $I_{1,k}$ on a surface of constant $I_{3,k}$

In this subsection it will be shown that the invariants $I_{1,k}$ and $I_{2,k}$ are positive if the internal deformation tensors are positive definite.

For a surface with constant determinant $I_{3,k} = C > 0$ the second invariant equals

$$I_{2,k}(b_{1,k}, b_{2,k}) = b_{1,k} b_{2,k} + \frac{C}{b_{1,k}} + \frac{C}{b_{2,k}}, \tag{3.74}$$

where $b_{1,k}$ and $b_{2,k}$ are the values of $\underline{\underline{b}}_k$ on two principal axes. The third value $b_{3,k}$ has been eliminated with $I_{3,k} = C$. The local extrema can be found from:

$$\frac{\partial I_{2,k}}{\partial b_{1,k}} = b_{2,k} - \frac{C}{b_{1,k}^2} = 0,$$

$$\frac{\partial I_{2,k}}{\partial b_{2,k}} = b_{1,k} - \frac{C}{b_{2,k}^2} = 0,$$

which gives one real extremum $b_{1,k} = b_{2,k} = b_{3,k} = \sqrt[3]{C}$. The second derivatives of $I_{2,k}$ in this extremum are

$$\frac{\partial^2 I_{2,k}}{\partial b_{1,k}^2} = 2, \qquad \frac{\partial^2 I_{2,k}}{\partial b_{2,k}^2} = 2, \qquad \frac{\partial^2 I_{2,k}}{\partial b_{1,k} \partial b_{2,k}} = 1.$$

The conditions for a minimum are

$$\frac{\partial^2 I_{2,k}}{\partial b_{1,k}^2} > 0, \qquad \frac{\partial^2 I_{2,k}}{\partial b_{1,k}^2} \frac{\partial^2 I_{2,k}}{\partial b_{2,k}^2} > \left(\frac{\partial^2 I_{2,k}}{\partial b_{1,k} \partial b_{2,k}} \right)^2,$$

[1]For compressible flows no positive lower bound can be obtained, because $\nabla \cdot \underline{v}$ term may be negative. However, the $I_{3,k}$ in that term avoids the indefiniteness of the internal deformation tensor.

which are fulfilled in the local extremum.

Substitution of $b_{1,k} = b_{2,k} = \sqrt[3]{C}$ in (3.74) gives the value for the second invariant in the local minimum: $I_{2,k}^{\min} = 3C^{2/3}$.

For a surface with constant determinant $I_{3,k} = C$ the first invariant equals

$$I_{1,k}(b_{1,k}, b_{2,k}) = b_{1,k} + b_{2,k} + \frac{C}{b_{1,k}b_{2,k}}. \tag{3.75}$$

The local extrema can be found from:

$$\frac{\partial I_{1,k}}{\partial b_{1,k}} = 1 - \frac{C}{b_{1,k}^2 b_{2,k}} = 0,$$

$$\frac{\partial I_{1,k}}{\partial b_{2,k}} = 1 - \frac{C}{b_{2,k}^2 b_{1,k}} = 0,$$

which is essentially the same condition as for the equation of the second invariant. Substitution of $b_{1,k} = b_{2,k} = \sqrt[3]{C}$ in (3.75) then gives the value for the first invariant in the local minimum: $I_{1,k}^{\min} = 3\sqrt[3]{C}$.

3.2.2   Lower bounds of the determinant for viscoelastic models

With the results of section 3.2.1 a lower bound will given for the determinant $I_{3,k}$ of the differential models of appendix A. It will be shown that in 3D flows it is not possible for all models to obtain a positive lower bound for the invariants.

The Johnson–Segalman model

The Johnson–Segalman model is given by (A.2). For the scalars $g_{i,k}$ refer to section 3.1.1. Substitution of these scalars in equation (3.73) gives

$$\dot{I}_{3,k} = \frac{1}{\lambda_k} I_{2,k} - \frac{3}{\lambda_k} I_{3,k}. \tag{3.76}$$

With the result of section 3.2.1 for the minimum of the second invariant, equation (3.76) leads to

$$\dot{I}_{3,k} \geq \frac{3C^{2/3}}{\lambda_k} \left(1 - C^{1/3}\right), \tag{3.77}$$

on the surface $I_{3,k} = C$. For $C = 1$ it follows that $\dot{I}_{3,k} \geq 0$. Thus the lower bound for the Johnson–Segalman model is $I_{3,k}^{\min} = 1$, if it is assumed that any path starts from $\underline{b}_k = \underline{I}$. From the results in section 3.2.1 it also follows that the minima of the first and second invariant are $I_{1,k}^{\min} = \sqrt[3]{C} = 3$ and $I_{2,k}^{\min} = 3C^{2/3} = 3$, which corresponds to the values of the invariants in equilibrium.

From (3.77) it also follows that for $0 < C < 1$ the material derivative of the determinant is positive. So, if for some reason the determinant has become smaller than its lower bound $I_{3,k} < 1$, it will increase again.

The Phan-Thien–Tanner model

The linear and exponential Phan-Thien–Tanner model can be described by (A.6). For the

scalars $g_{i,k}$ refer to section 3.1.1. Substitution of these scalars in equation (3.73) gives

$$\dot{I}_{3,k} = \frac{Y_k}{\lambda_k} I_{2,k} - \frac{3Y_k}{\lambda_k} I_{3,k}. \tag{3.78}$$

With the result of section 3.2.1 for the minimum of the second invariant, equation (3.78) leads to

$$\dot{I}_{3,k} \geq \frac{3Y_k C^{2/3}}{\lambda_k} \left(1 - C^{1/3}\right), \tag{3.79}$$

on the surface $I_{3,k} = C$. For $C = 1$ it follows that $\dot{I}_{3,k} \geq 0$. If it is assumed that any path starts from $\underline{b}_k = \underline{I}$, the lower bound for the Phan-Thien–Tanner model is $I_{3,k}^{\min} = 1$, which is the same as for the Johnson–Segalman model. The minima of the first and second invariant also equal the minima of the Johnson–Segalman model: $I_{1,k}^{\min} = \sqrt[3]{C} = 3$ and $I_{2,k}^{\min} = 3C^{2/3} = 3$, which corresponds to the values of the invariants in equilibrium.

From (3.79) it also follows that for $0 < C < 1$ the material derivative of the determinant is positive. So, if for some reason the determinant has become smaller than its lower bound $I_{3,k} < 1$, it will increase again.

The Larson model

The Larson model is given by (A.9). This is exactly the differential equation for the internal deformation tensor of the linear Phan-Thien–Tanner model, when $\beta_k = 3\epsilon_k$. So $I_{1,k}^{\min} = 3$, $I_{2,k}^{\min} = 3$ and $I_{3,k}^{\min} = 1$ are also lower bounds for the Larson model.

The Leonov model

The Leonov model can be described by (A.4). For the scalars $g_{i,k}$ refer to section 3.1.1. Substitution of these scalars in equation (3.73) gives

$$\dot{I}_{3,k} = \frac{1}{2\lambda_k} I_{2,k} \left(1 - I_{3,k}\right). \tag{3.80}$$

If $I_{3,k} = 1$ initially, then it always equals $I_{3,k} = 1$. From the results in section 3.2.1 it also follows that the minima of the first and second invariant are $I_{1,k}^{\min} = \sqrt[3]{C} = 3$ and $I_{2,k}^{\min} = 3C^{2/3} = 3$, which are equal to the values of the invariants in equilibrium.

Otherwise, if for some reason the determinant has become smaller or larger than $I_{3,k} = 1$, it will tend to $I_{3,k} = 1$ for $t \to \infty$.

The modified Leonov model

The modified Leonov model can be described by (A.5). For the scalars $g_{i,k}$ refer to section 3.1.1. Substitution of these scalars in equation (3.73) gives

$$\dot{I}_{3,k} = \frac{\phi_k}{2\lambda_k} I_{2,k} \left(1 - I_{3,k}\right). \tag{3.81}$$

As for the Leonov model $I_{3,k} = 1$, if it equals $I_{3,k} = 1$ initially. Then the minima of the first and second invariant are also $I_{1,k}^{\min} = \sqrt[3]{C} = 3$ and $I_{2,k}^{\min} = 3C^{2/3} = 3$, which are equal to the values of the invariants in equilibrium.

Otherwise, if for some reason the determinant is positive but does not equal 1 at the starting point of the path, it will tend to $I_{3,k} = 1$ for $t \to \infty$.

The Giesekus model

The Giesekus model can be described by (A.3). For the scalars $g_{i,k}$ refer to section 3.1.1.

Substitution of these scalars in equation (3.73) gives

$$\dot{I}_{3,k} = \frac{1-\alpha_k}{\lambda_k} I_{2,k} - I_{3,k}\left(\frac{3(1-2\alpha_k)}{\lambda_k} + \frac{\alpha_k}{\lambda_k}I_{1,k}\right). \tag{3.82}$$

Hulsen (1988b) has shown that a positive lower bound exists for a 2D flow. However, for a 3D flow of the Giesekus model it is not possible to find a positive lower bound for the determinant. This will be demonstrated with a counter example: the steady uniaxial elongation described in section 3.1.1. The limit solution of the determinant for large γ_k is given by (3.10):

$$\lim_{\gamma_k \to \infty} I_{3,k} = \lim_{\gamma_k \to \infty} \frac{2(1-\alpha_k)^2}{\alpha_k \gamma_k} = 0,$$

which shows that no general positive lower bound can be given for the 3D Giesekus model. Together with the positive definiteness of the internal deformation tensor this gives that the lower bound for the determinant equals $I_{3,k}^{\min} = 0$.

Whether positive lower bounds for $I_{1,k}$ and $I_{2,k}$ exist remains inconclusive from our analysis in section 3.2.1 (only $I_{1,k}^{\min} = I_{2,k}^{\min} > 0$).

3.2.3   Correction of indefinite internal deformation tensors in 3D flows

In the previous subsection it has been shown that for a 3D flow the value of the determinant is always positive for a finite velocity gradient $\underline{\underline{L}}^T$. Except for the Giesekus model, it is possible to obtain a positive lower bound for the determinant of an internal deformation tensor. The question remains how an internal deformation tensor has to be corrected. Two possibilities will be discussed for an axisymmetrical flow: a 2D and a 3D correction method.

Isotropic 2D correction.

The 2D correction is based on the idea that the indefiniteness of $\underline{b}_k$ is caused by the velocity derivatives. For axisymmetrical flows the $\phi\phi$-component does not depend on velocity derivatives, only on the radial velocity. When it is assumed that the error in the $\phi\phi$-component is small compared to the other components, the internal deformation tensor may be corrected with a 2D isotropic term

$$b_{rr,k}^c = b_{rr,k} + c, \qquad b_{zz,k}^c = b_{zz,k} + c, \qquad b_{\phi\phi,k}^c = b_{\phi\phi,k}. \tag{3.83}$$

The positive correction parameter c is calculated from the condition that the determinant of the corrected internal deformation tensor $\underline{\underline{b}}_k^c$ equals the minimum value for the specific stress model: $I_{3,k}^c = I_{3,k}^{\min}$. This requires the solution of a quadratic equation. The correction method is illustrated in figure 3.1.

Isotropic 3D correction.

When all the terms are affected due to numerical errors a 3D isotropic correction is an obvious choice. The corrected internal deformation tensor then becomes

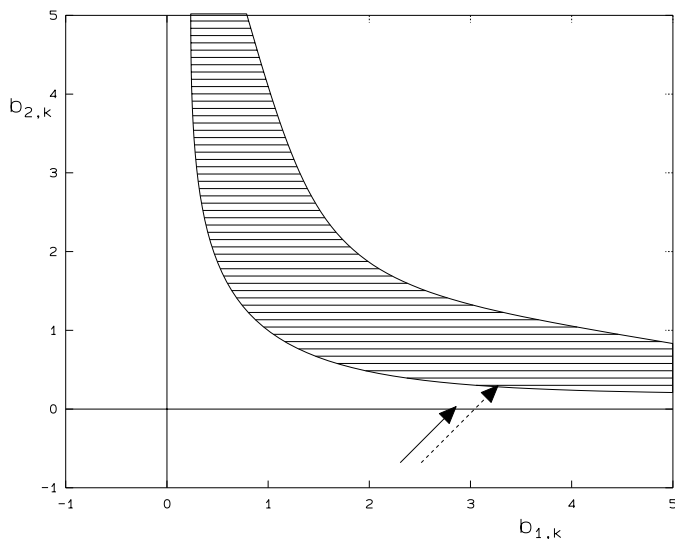$$\underline{\underline{b}}_k^c = \underline{\underline{b}}_k + c\underline{\underline{I}}. \tag{3.84}$$

Figure 3.1: Correction of the internal deformation tensor in 2D. $b_{1,k}$ and $b_{2,k}$ are the principal values of $\underline{b}_k$. The solution of the model lies in the dashed area, which is bounded by two lines with constant $I_{3,k}$. The solid arrow is the projection on the first quadrant used by Hulsen (1990a) and Hulsen & van der Zanden (1991). The dashed arrow is a projection on the lower bound $I_{3,k}^{\min}$.

When the indefiniteness is caused by the tangential component $\underline{b}_{\phi\phi} \leq 0$, the 2D method is not sufficient. Then the 3D correction has to be made. This requires the solution of a cubic equation, which has in general three different solutions. From the three possible values of c that one must be chosen for which all three invariants of $\underline{b}_k^c$ are positive ($I_{1,k}^c > 0$, $I_{2,k}^c > 0$ and $I_{3,k}^c > 0$).

3.3 Conclusions

In this chapter the behaviour of the internal deformation tensor for the stress models of appendix A has been examined for large deformations in a steady elongational flow and a steady simple shear flow. For these two cases the anisotropy of the heat conduction tensor has been calculated as well. Because of the small amount of experimental data a simple model with constant coefficients has been taken. It has been checked whether a qualitative agreement can be obtained between the simple model and the experiments discussed in section 2.4. The results have been summarised in table 3.1. For the stress models which are not in qualitative agreement an extra dependence of the heat conduction coefficients on the invariants of $\underline{b}_k$ has to be introduced to correspond to the experimental results. With the help of the limit values of the internal deformation tensor the behaviour of the mechanical dissipation has been calculated as well.

Finally, a method has been developed to calculate the lower bound of the invariants of an internal deformation tensor for 3D flows. A positive lower bound for the determinant gives the opportunity to correct the internal deformation tensor to a positive definite tensor. The method has been applied to the stress models of appendix A, to indicate which models may cause problems with the calculation of the inverse of the internal deformation tensors. The results are summarised in table 3.1. From this table it follows that, for the anisotropy model with constant coefficients, all models, except the Johnson–Segalman model, are able to describe the

Table 3.1: Summary of the behaviour of the perpendicular and parallel thermal conductivities in steady shear and steady uniaxial elongation for the various stress models with $\xi_k = 0$. The coefficients $\kappa_{1,k}$ and $\kappa_{2,k}$ are assumed to be constant. For the perpendicular conductivity it is indicated whether it may be smaller or equal to the equilibrium conductivity. For the parallel conductivity the proportionality with the shear and elongation rate is indicated for large deformations. When two values are given, the first value is for $\kappa_{2,k} = 0$ and the second value for $\kappa_{2,k} > 0$. When a positive value of $\kappa_{2,k}$ gives an infinite perpendicular thermal conductivity only the behaviour for $\kappa_{2,k} = 0$ is indicated. The fifth column, R_I, R_{II}, indicates whether the restrictions I and II are both satisfied (+) or not (−). The last column contains the lower bound for the determinant $I_{3,k}^{\min}$ of an internal deformation tensor.

model	$\kappa_\perp^{\text{sh}}$	$\kappa_\parallel^{\text{sh}}$	$\kappa_\perp^{\text{el}}$	$\kappa_\parallel^{\text{el}}$	R_I, R_{II}	$I_{3,k}^{\min}$
Johnson–Segalman	κ_{eq}	$\dot\gamma^2$	−	−	−	1
Giesekus	$< \kappa_{\text{eq}}$	$\dot\gamma^{1/2}; \dot\gamma$	$< \kappa_{\text{eq}}$	$\dot\epsilon; \dot\epsilon^2$	+	0
(modified) Leonov	$< \kappa_{\text{eq}}$	$\dot\gamma^{1/2}; \dot\gamma$	$< \kappa_{\text{eq}}$	$\dot\epsilon; \dot\epsilon^2$	+	1
linear PTT	κ_{eq}	$\dot\gamma^{2/3}$	$< \kappa_{\text{eq}}$	$\dot\epsilon; \dot\epsilon^2$	−	1
exponential PTT	κ_{eq}	$\ln\dot\gamma$	$< \kappa_{\text{eq}}$	$\ln\dot\epsilon; \ln^2\dot\epsilon$	−	1
Larson	κ_{eq}	$\dot\gamma^{2/3}$	$< \kappa_{\text{eq}}$	$\dot\epsilon; \dot\epsilon^2$	−	1

anisotropy in uniaxial elongation. However, in steady simple shear only the Giesekus model and the Leonov models are able to fulfil both restriction I and II (a decreasing perpendicular thermal conductivity until a certain lower limit and an increasing parallel thermal conductivity). The Giesekus model, however, may cause problems with the calculation of the inverse of the internal deformation tensors. Thus the (modified) Leonov model appears to have the best properties for simulation purposes of nonisothermal flows of viscoelastic fluids with the anisotropic heat conduction with constant coefficients[2].

---

[2]Although the modified Leonov model seems to be well suited for nonisothermal calculations with anisotropic heat conduction, it has some other disadvantages as will be shown in chapter 5 and appendix C.

Chapter 4

Numerical method for the balance equations and the constitutive equations

This chapter consists of a description of the numerical method that has been used to solve the system of partial differential equations (2.156), which has been obtained in chapter 2. First the outline of the iterative method will given. In the next three sections the solution method of the three different parts of the iterative method will be discussed. The details about the discretisation method and the solution method of the equations of motion and the temperature equation can be found in sections 4.2 and 4.3. The streamline integration will be discussed in section 4.4. Finally the boundary conditions that can be imposed on the equations of motion and the temperature equation will be given in section 4.5, including the fully developed flow boundary condition at the inflow and outflow. The numerical implementation of the fully developed boundary conditions will be described as well.

The numerical code is an extension to nonisothermal equations of the isothermal code described by Hulsen & van der Zanden (1991). In this thesis the emphasis will be on the changes in the numerical implementation due to the nonisothermal effects.

4.1 Introduction

In general, the system of partial differential equations (2.156) is too difficult to solve it analytically. For this, a numerical method that is able to solve the system of partial differential equations for various types of flows will be discussed in this chapter. The discretisation method that will be used for the equations of motion, the temperature equation and the stress constitutive equation will be described in the next three sections. In these sections also the numerical solution method will be described. To use different solution methods for the elliptic part of the equations, the balance equations, and the hyperbolic part, the differential equations for the internal deformation tensors, the system of equations will be decoupled. The decoupled equations will be solved with the help of an iterative method. An additional advantage over solving the whole system at once is that less memory is needed and very large computation times are avoided. Particularly for multi-mode models, which are often needed to obtain a good description of the fluid behaviour, the matrix in the resulting matrix-vector equation may become very large when the coupled system is solved. On the other hand, however, the rate of convergence may be low due to the splitting. Therefore a large number of relatively cheap iterations has to be performed. Dependent on the problem the number of iterations is $\mathcal{O}(10^1)$ or $\mathcal{O}(10^2)$.

The outline of the iteration process, which will be described in more detail in the next sections, is as follows:

1. Start with an initial field for the velocity, the K internal deformation tensors and the

temperature. This may be a result of a previous calculation. If there is no starting field of a previous simulation available, a zero velocity and zero stress ($\underline{\underline{b}}_k = \underline{\underline{I}}$) may be taken as the initial field. However, to avoid problems with shift factors a reasonable initial field for the temperature has to be specified, for example the temperature of a Dirichlet boundary or the reference temperature.

2. Calculate an iteration step. An iteration step $(i + 1)$ of the iteration process consists of the following four or five substeps, which are performed after each other

   - Calculate the updated velocity field, by solving a matrix-vector equation for the equations of motion $(2.156)_{1,2}$: $A_v \mathcal{V}^{i+1} = f(\mathcal{V}^i, \mathcal{T}^i, \Upsilon^i, \mathcal{P}^i)$. Dependent on the solution method the pressure may be written as a function of $\mathcal{V}^i$ only (penalty method) or not (Uzawa's method). These methods, the discretisation method and the implementation in the iterative scheme will be specified in section 4.2.
   - Update the pressure field, if necessary (Uzawa's method): $\mathcal{P}^{i+1} = f(\mathcal{V}^{i+1}, \mathcal{P}^i)$.
   - Calculate the updated temperature field, by solving a matrix-vector equation for the temperature equation $(2.156)_3$: $A_T \mathcal{T}^{i+1} = f(\mathcal{V}^{i+1}, \mathcal{P}^{i+1}, \mathcal{T}^i, \mathcal{B}^i)$. The discretisation method and the implementation in the iterative scheme will be specified in section 4.3.
   - Calculate the updated internal deformation tensor field, by solving the K uncoupled equations $(2.156)_5$: $\mathcal{B}_k^{i+1} = f(\mathcal{V}^{i+1}, \mathcal{T}^{i+1}, \mathcal{B}_k^i)$ and calculate the sum of the modal stresses Υ^{i+1}. The discretisation method and the implementation in the iterative scheme will be specified in section 4.4.
   - Calculate an approximation of the outflow boundary conditions. This step will be explained further on in section 4.5.

   $\mathcal{V}$, $\mathcal{T}$, Υ and $\mathcal{P}$ are vectors with the nodal point values of the discretised velocity, the temperature, the sum of the modal stresses and the pressure. $\mathcal{B}$ represents all modes of the internal deformation tensors, while $\mathcal{B}_k$ represents only the kth mode of the internal deformation tensors.

3. Repeat step 2 until the solution has converged.

4.2   The equations of motion

For the equations of motion the finite element method has been used. This method will only be introduced briefly. A comprehensive description about finite element methods can be found in Cuvelier et al. (1986). To derive the finite element formulation for the mass balance (2.1) and the balance of linear momentum (2.4) these equations are multiplied with test functions and integrated over the domain Ω:

$$\int_{\Omega} (\dot{\rho} + \rho \nabla \cdot \underline{v}) \; \psi_d \; d\Omega = 0, \qquad \forall \psi_d \in \Psi_d, \tag{4.1}$$

$$\int_{\Omega} \left(\rho \dot{\underline{v}} + \nabla p - \rho \underline{f} - \nabla \cdot \underline{\underline{\tau}} \right) \cdot \underline{\psi}_m d\Omega = 0, \qquad \forall \underline{\psi}_m \in \Psi_m, \tag{4.2}$$

where the decomposition of the total stress (2.5) has been used. The test functions for the mass balance ψ_d and the balance of linear momentum $\underline{\psi}_m$ belong to suitable spaces Ψ_d and Ψ_m on Ω.

Before the discretisation method of (4.1) and (4.2) will be discussed, first the restrictions on the numerical implementation will be given.

Restrictions on the numerical implementation

For the equations of motion the following restrictions have been made for the numerical implementation:

- The flow is assumed to be steady.

- The type of the coordinate system is either Cartesian or axisymmetrical.

- The density of the fluid is assumed to be constant in the equations of motion. In section 2.6 it has been shown that for the mass balance a constant density is often a good approximation in shear flows with relatively small temperature differences. Then the balance of mass reduces to the incompressibility condition. In the balance of linear momentum the density appears in the convective term and in the buoyant force. The convective term is small, so small density variations can be neglected in this term. In section 2.6 it has been shown that in general the buoyant force is small either. Only for extreme conditions this term may become important. However, if the buoyant force is taken into account the flow is no longer axisymmetric for a horizontal pipe flow. Then a 3D implementation would be required. Therefore the buoyant force will be neglected as well.

- The extra-stress tensor $\underline{\underline{\tau}}$ is specified by a Newtonian (solvent) stress and K modal stresses: $\underline{\underline{\tau}} = 2\eta_s\underline{\underline{d}} + \sum_{k=1}^{K} \underline{\underline{\tau}}_k$, equation (2.15).

- The Newtonian (solvent) viscosity η_s is independent of the pressure.

- The temperature dependence of the Newtonian (solvent) viscosity η_s is given by[1] the WLF shift factor (2.123), the Andrade shift factor (2.124) or a combination of these two, the WLF shift factor below a certain separating temperature $T < T_\mathrm{s}$ and the Andrade shift factor above the separating temperature $T > T_\mathrm{s}$.

4.2.1   Discretisation method

Substitution of the restrictions on the numerical implementation, discussed in the first part of this section, in the integrated balance of mass (4.1) and the integrated balance of linear momentum (4.2) gives the following equations of motion

$$(\nabla \cdot \underline{v}, \psi_d) = 0, \quad \forall \psi_d \in \Psi_d, \tag{4.3}$$

---

[1]For test purposes also an exponential factor $\ln a_{T,k} = C_{1,k}(T - T_\mathrm{ref})$ has been implemented. With this type of shift factors an analytical solution can be computed for steady flows of a Maxwell fluid in a Cartesian coordinates. This is not possible for the Andrade and WLF shift factor.

$$[\rho_{\text{ref}} \underline{v} \cdot \nabla \underline{v}, \underline{\psi}_m] + (p, \nabla \cdot \underline{\psi}_m) + \langle 2\eta_s \underline{\underline{d}}, \nabla \underline{\psi}_m \rangle =$$

$$-\langle \sum_{k=1}^{K} \underline{\underline{\tau}}_k, \nabla \underline{\psi}_m \rangle + [\underline{n} \cdot \underline{\underline{\sigma}}, \underline{\psi}_m]_\Gamma, \qquad \forall \underline{\psi}_m \in \Psi_m, \tag{4.4}$$

where $\underline{n}$ is the outward unit normal to the boundary Γ. The order of equation (4.4) has been reduced, by applying the Gauss theorem to the stress and the pressure terms. The elliptic part of the stress (the viscous stress) has been separated from the hyperbolic part (the modal stresses). The numerical solution method for the modal stresses will be discussed in section 4.4. The Dirichlet or natural boundary conditions which have to be prescribed on Γ will be discussed in section 4.5. In the equations (4.3) and (4.4) the following notation has been used for the various surface and boundary integrals

$$(a, b) = \int_\Omega ab \, d\Omega, \qquad [\underline{a}, \underline{b}] = \int_\Omega \underline{a} \cdot \underline{b} \, d\Omega,$$

$$\langle \underline{\underline{a}}, \underline{\underline{b}} \rangle = \int_\Omega \underline{\underline{a}} : \underline{\underline{b}} \, d\Omega, \qquad (a, b)_\Gamma = \int_\Gamma ab \, d\Gamma,$$

$$[\underline{a}, \underline{b}]_\Gamma = \int_\Gamma \underline{a} \cdot \underline{b} \, d\Gamma. \tag{4.5}$$

In the finite element method the approximation of the unknown velocity $\underline{v}$ and the pressure p consists of an interpolation of the nodal point values of the concerned quantity:

$$\tilde{\underline{v}}(\underline{x}) = \sum_{j=1}^{J_v} \underline{v}^j \psi_{v,j}(\underline{x}), \quad \tilde{p}(\underline{x}) = \sum_{j=1}^{J_p} p^j \psi_{p,j}(\underline{x}), \tag{4.6}$$

where J_v is the number of velocity nodes and J_p the number of pressure unknowns. ψ_v are the velocity basis functions and ψ_p the pressure basis functions. A tilde $\tilde{}$ above a quantity denotes the discrete approximation of that quantity. The modal stress tensors and the temperature are approximated by

$$\tilde{\underline{\underline{\tau}}}_k(\underline{x}) = \sum_{j=1}^{J_\tau} \underline{\underline{\tau}}_k^j \psi_{\tau,j}(\underline{x}), \quad \tilde{T}(\underline{x}) = \sum_{j=1}^{J_T} T^j \psi_{T,j}(\underline{x}), \tag{4.7}$$

where J_τ is the number of stress nodes and J_T the number of temperature nodes. ψ_τ are the basis functions of the modal stresses and ψ_T the basis functions of the temperature.

In the standard Galerkin approximation the test functions of the incompressibility condition are taken $\psi_d = \psi_p$ and for the test functions of the balance of linear momentum $\underline{\psi}_m = \underline{e}\psi_v$, where $\underline{e}$ are unit basis vectors. In the finite element method the basis functions for the pressure and the velocity consist of piecewise polynomials.

For the pressure and the velocity the modified Crouzeix–Raviart element (P_2^+-P_1) has been used. For this element the standard 6-point quadratic triangular element for the velocity has been extended with its centre point. The discrete approximation of the pressure consists of the pressure and two derivatives in the centre point, see figure 4.1. The pressure derivatives and the velocities in the centre point can be eliminated on element level, thus there remain twelve unknown velocities and one unknown pressure at the element level. With the elimination the total number of velocity and pressure unknowns are both reduced by two times the number of elements. The remaining number of pressure unknowns, which equals the number of pressure nodes, will be denoted by J_p^r.
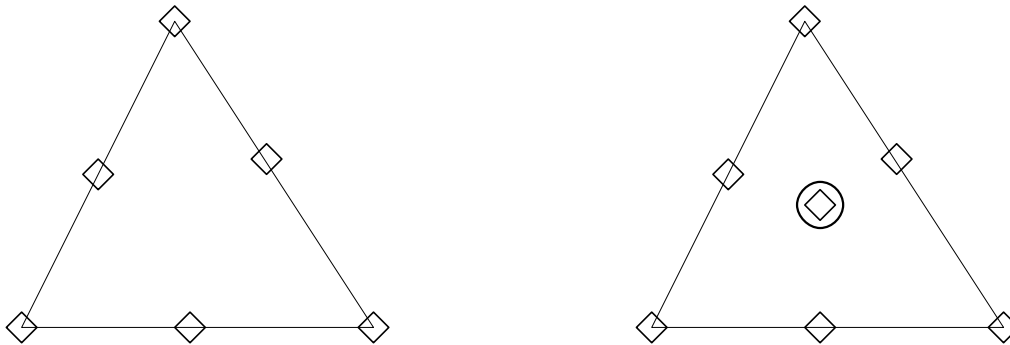
Figure 4.1: Standard quadratic element with six nodal points (denoted by a ◇) and the Crouzeix–Raviart element with seven velocity points (denoted by a ◇) and a centre point with the pressure and its derivatives (denoted by a ◯).

For the approximation (4.7) of the modal stresses and the temperature the standard quadratic triangular element basis functions has been used for ψ_τ and ψ_T. The quadratic element has also been depicted in figure 4.1.

Elimination of the pressure

Two methods will be discussed to eliminate the pressure in the centre point of an element: the penalty method and the Uzawa method.

- *The penalty method.*
  A widely used method to eliminate the J_p^r pressure unknowns p^j, is the (discrete) penalty method may be used. Instead of the divergence equation (4.3) now

  $$(\epsilon_p p^j + \nabla \cdot \underline{\tilde{v}}, \psi_{p,i}) = 0, \qquad i = 1, \ldots, J_p^r \qquad (4.8)$$

  is used. The penalty parameter ϵ_p is a small parameter. Usually $\epsilon_p p^j$ is $\mathcal{O}(10^{-5} - 10^{-7})$, so that the divergence freedom is fulfilled approximately. Through the elimination of the centre point pressures on element level, the number of unknowns is further reduced with J_p^r. Afterwards, when the solution has converged, the pressure may be reconstructed from the velocities. A drawback of this method is that the condition of the system becomes worse when the penalty parameter becomes smaller. For too small ϵ_p the iteration matrix A_v for the equations of motion becomes ill-conditioned.

- *The Uzawa method.*
  Another possibility to eliminate the remaining J_p^r pressure unknowns is the Uzawa method, which has been described by Fortin & Fortin (1985) and Fortin et al. (1991). This method can be used to obtain a better approximation of the incompressibility condition (4.3), with the same ϵ_p (or an approximation as good as the penalty method with a larger ϵ_p). A better approximation of the divergence may also give a better approximation of the pressure and the pressure gradient, which are needed in the temperature equation. For the Uzawa method the divergence of the velocity is equated to a pressure difference instead of the pressure:

  $$\left(\epsilon_p \left(p^j - p^{j,\text{ref}}\right) + \nabla \cdot \underline{\tilde{v}}, \psi_{p,i}\right) = 0, \qquad i = 1, \ldots, J_p^r , \qquad (4.9)$$

where $p^{j,\mathrm{ref}}$ is a reference pressure in the jth centre point. For the reference pressure the pressure at the previous iteration will be taken. This means that at every iteration step the pressure has to be updated and an extra array with length J_p^r has to be stored. Another drawback with regard to the penalty method is that the convergence of the iteration scheme is slower (Cuvelier et al. 1986).

Matrix-vector formulation

After elimination of the pressure by the penalty or the Uzawa method and substitution of the finite element approximations of the various quantities in the integrated balance of linear momentum (4.4), a matrix-vector equation of the following form is obtained:

$$N_v(\mathcal{V}) + (\eta_s(\mathcal{T})S_v + C_v)\,\mathcal{V} + Q(\Upsilon) + L^T\mathcal{P}^{\mathrm{ref}} = F_v, \tag{4.10}$$

where N_v is a nonlinear operator due to the convective acceleration, S_v a linear operator due to the viscous stresses, C_v the penalty matrix, Q a function of the viscoelastic stresses and F_v contains the contributions of the natural boundary conditions. The pressure term $L^T\mathcal{P}^{\mathrm{ref}}$, with L^T the gradient operator, is a contribution for the Uzawa method. For the penalty method this term vanishes. To obtain a good accuracy, the surface integrals have been evaluated numerically with a seven-point Gauss rule and the line integrals with a three-point Gauss rule.

4.2.2   Implementation in the iterative scheme

To solve the discretised equations of motion (4.10), an incremental formulation for the resulting matrix-vector equation has been used:

$$A_v^i\Delta\mathcal{V}^{i+1} = \left(\eta_{\mathrm{it}}(\mathcal{T}^i)S_v + M_v(\mathcal{V}^i) + C_v\right)\Delta\mathcal{V}^{i+1} = -R_v(\mathcal{V}^i, \Upsilon^i, \mathcal{T}^i, \mathcal{P}^i), \tag{4.11}$$

where the Picard iteration matrix contains contributions of a proper linearization of the convective terms M_v, the penalty matrix C_v and a viscous matrix $\eta_{\mathrm{it}}S_v$. The iteration viscosity η_{it} only slows down the iteration process, but is necessary to obtain a convergent solution method[2]. The increment of the velocities $\Delta\mathcal{V}^{i+1}$ is defined by

$$\Delta\mathcal{V}^{i+1} = \mathcal{V}^{i+1} - \mathcal{V}^i. \tag{4.12}$$

The residual of the equations of motion $R_v(\mathcal{V}^i, \Upsilon^i, \mathcal{T}^i, \mathcal{P}^i)$ may depend on the discrete velocities $\mathcal{V}^i$, the stress Υ^i, the temperatures $\mathcal{T}^i$ and the pressure $\mathcal{P}^i$ of a former iteration step:

$$\begin{aligned}
R_v(\mathcal{V}^i, \Upsilon^i, \mathcal{T}^i, \mathcal{P}^i) &= \left(\eta_s(\mathcal{T}^i) + \eta_{\mathrm{co}}(\mathcal{T}^i)\right)S_v\mathcal{V}^i + N_v(\mathcal{V}^i) + \\
&\quad C_v\mathcal{V}^i + Q(\Upsilon^i - 2\eta_{\mathrm{co}}(\mathcal{T}^i)\bar{D}^i) + L^T\mathcal{P}^i - F_v.
\end{aligned} \tag{4.13}$$

From the vector Q with the contributions of the modal stresses, an extra diffusive term, based on the nodal point averages of the rate-of-deformation tensor $\bar{D}^i$, has been subtracted. An

---

[2]For isothermal calculations $\eta_{\mathrm{it}} = \eta_0$ or $\eta_{\mathrm{it}} = 2\eta_0$, where η_0 is the zero-shear-rate viscosity, is often a good choice. For nonisothermal calculations the spatial temperature distribution may be strongly non-homogeneous. This results in large differences of the viscosity in the flow. To take into account this temperature effect for the iteration viscosity, a temperature dependent η_{it} has been implemented as well. The temperature dependence is assumed to be the same as for the relaxation times and viscosities in the stress model.

analogous term based on the non-averaged velocity gradients has been added to the contribution of the solvent. The extra viscosity η_{co} is necessary to avoid almost zero effective viscosities[3], which may arise due to the use of averaged velocity gradients for the streamline integration. The introduction of a correction term with the extra viscosity η_{co} improves the condition of the system but increases the viscosity of 'short wavelength' velocity modes (Hulsen & van der Zanden 1991).

For detecting convergence of the equations of motion two conditions have to be satisfied. The first condition is related to the increment of the velocity and the second to the residual of the equations of motion:

$$\frac{\max_j |\Delta \mathcal{V}_j^{i+1}|}{\max_j |\mathcal{V}_j^{i+1}|} \leq \epsilon_{v,\mathrm{inc}},$$

$$\frac{||R_v(\mathcal{V}^i, \Upsilon^i, \mathcal{T}^i, \mathcal{P}^i)||_f}{||R_v(\mathcal{V}^i, \Upsilon^i, \mathcal{T}^i, \mathcal{P}^i)||_t} \leq \epsilon_{v,\mathrm{res}}, \tag{4.14}$$

where the maximum norm $|.|$ has been taken over all nodal points j. The norm $|| \cdot ||_f$ denotes the Euclidean norm over the free degrees of freedom, without the essential boundary conditions. The norm $|| \cdot ||_t$ denotes the Euclidean norm over the total degrees of freedom, including the essential boundary conditions. $\epsilon_{v,\mathrm{inc}}$ and $\epsilon_{v,\mathrm{res}}$ are small parameters. For the calculations in chapter 5 $\epsilon_{v,\mathrm{inc}} = \epsilon_{v,\mathrm{res}} = \mathcal{O}(10^{-3})$ will be taken.

4.3 The temperature equation

As for the equations of motion, a finite element method has been used for the temperature equation. To derive the finite element formulation of the temperature equation, $(2.156)_3$ is multiplied by a test functions and integrated over the domain Ω:

$$\int_\Omega \left(\rho(c_{p,\tau_e}^{\mathrm{eq}} - \Delta c^{\mathrm{eq}})\dot{T} - \nabla \cdot (\underline{\underline{\kappa}} \cdot \nabla T) - T\alpha_{T,b}\dot{p} - D_{\mathrm{m}}^{\mathrm{ve}} + \rho T \Delta s_b^{\mathrm{ve}} \right) \psi_e d\Omega = 0, \qquad \forall \psi_e \in \Psi_e, \tag{4.15}$$

where ψ_e is the test function, which belongs to a suitable space Ψ_e on Ω.

Before the discretisation method of (4.15) will be discussed, first the restrictions on the numerical implementation will be given.

Restrictions on the numerical implementation

The following restrictions have been made for the numerical implementation of the temperature equation:

- The flow is assumed to be steady.

- The type of the coordinate system is either Cartesian or axisymmetrical.

---

[3]For isothermal calculations a value of $\eta_{\mathrm{co}} = \eta_0 - \eta_s$ is often a good choice. As for the iteration viscosity, the extra viscosity may be taken temperature dependent for nonisothermal problems. The temperature dependence is again the same as the temperature dependence of the relaxation times and viscosities of the stress model.

- The density of the fluid is assumed to be a linear function of the temperature as in (2.122). Density variations appear in three terms of $(2.156)_3$: the pressure gradient term, the convective term and the entropy term Δs_b^{ve}. The latter will be discussed together with the temperature and density dependence of the moduli. In section 2.6 it has been shown that the pressure gradient term may be important, so the variations of the density will be taken into account for this term. For the linear temperature dependence (2.122) the thermal expansion coefficient equals $\alpha_{T,b} = \alpha_\rho$. In the convective term the density variations may be important as well. Due to large values of the heat capacity and the density the convective term is often the dominant term in the temperature equation. A spatially weak non-homogeneous density field may still influence the temperature field then.

- The heat capacity in mechanical equilibrium c_{p,τ_e}^{eq}, which is usually measured, may depend linearly on the temperature as given by (2.120). As for the density this temperature dependence may be important for convection-dominated flows.

- The heat capacity c_{p,τ_e}^{eq} and the density are independent of the pressure.

- The moduli may depend on the temperature and the density as in (2.126). These dependences determine the terms Δc^{eq} and Δs_b^{ve}. Three possibilities, discussed in section 2.3.3 have been implemented. Firstly the moduli may be constant. Then the convective term is simplified, because $\Delta c^{\text{eq}} = 0$ (or $c_{p,b} = c_{p,\tau_e}^{\text{eq}}$). Also the entropy term Δs_b^{ve} cancels out then. Secondly the moduli may depend linearly on the temperature $G_k = G_{k,\text{ref}} T/T_{\text{ref}}$. On the one hand the temperature equation simplifies then, because the sum of the mechanical dissipation and the entropy term equals the stress work $D_m^{\text{ve}} + \Delta s_b^{\text{ve}} = \underline{\underline{\tau}} : \underline{\underline{d}}$. On the other hand the temperature equation becomes more complicated, because Δc^{eq} does not vanish anymore, but it depends on the internal deformation tensors as in (2.104). Thirdly the moduli may depend linearly on the temperature and the density $G_k = G_{k,\text{ref}} \rho T/\rho_{\text{ref}} T_{\text{ref}}$. Again, the sum of the mechanical dissipation and the entropy term equals the stress work $D_m^{\text{ve}} + \Delta s_b^{\text{ve}} = \underline{\underline{\tau}} : \underline{\underline{d}}$. Furthermore the convective term is simplified then, because Δc^{eq} vanishes (or $c_{p,b} = c_{p,\tau_e}^{\text{eq}}$).

- The heat flux can be specified by Fourier's law (2.112). The heat conduction tensor $\underline{\underline{\kappa}}$ is of the form (2.113). The heat conduction coefficients in (2.113) may depend linearly on the temperature as given by (2.121).

4.3.1   Discretisation method

Substitution of the restrictions of the first part of this section into the integrated temperature equation (4.15) and applying the Galerkin method ($\psi_e = \psi_T$, the basis functions of the temperature) gives the following equation for the temperature

$$(\rho(c_{p,\tau_e}^{\text{eq}} - \Delta c^{\text{eq}})\underline{v} \cdot \nabla T, \psi_T) + [\underline{\underline{\kappa}} \cdot \nabla T, \nabla \psi_T] = (D_m^{\text{ve}} + \rho T \Delta s_b^{\text{ve}} - \alpha_\rho p \underline{v} \cdot \nabla T, \psi_T) -$$
$$[T\alpha_\rho p \underline{v}, \nabla \psi_T] + (\underline{n} \cdot \underline{\underline{\kappa}} \cdot \nabla T + \alpha_\rho T p \underline{n} \cdot \underline{v}, \psi_T)_\Gamma, \qquad \forall \psi_T \in \Psi_T, \quad (4.16)$$

where the bracket notation (4.5) has again been used for the integrals. Besides the heat conduction term, also the thermal expansion term has to be integrated partially, because the pressure

is discontinuous over the element boundaries. During the partial integration use has been made of the assumptions that the flow is divergence free ($\nabla \cdot \underline{v} = 0$) and that α_ρ is constant. The normal component of the heat flux on a natural boundary, $\underline{n} \cdot \underline{\underline{\kappa}} \cdot \nabla T$ has to be specified by a boundary condition. The possible choices will be discussed in section 4.5.

The finite element approximation of the various quantities have already been given in section 4.2.1 about the discretisation of the equations of motion: equations (4.6) and (4.7). The discretisation of the internal deformation tensors is analogous to the modal stress tensors. For the temperature a standard 6-point quadratic triangular element has been used with the vertices and the mid-side nodes of the element as the nodal points (see figure 4.1). Thus the approximation of the temperature is piecewise quadratic.

In the remainder of this section the details of the calculation of the finite element integrals over the domain Ω will be given. The detailed description of the boundary integrals will be postponed until section 4.5.

Calculation of the mechanical dissipation

For many stress models the expression for the mechanical dissipation contains a term with $\operatorname{tr} \underline{\underline{b}}_k^{-1} = I_{2,k}/I_{3,k}$, the trace of the inverse of the internal deformation tensor (see appendix B). Theoretically this should not give any problems, because the internal deformation tensors are positive definite. However, due to numerical approximation errors the positive definiteness may be lost. Particularly near $I_{3,k} = 0$ this may lead to very large numerical errors or even arithmetic overflows. The causes and the ways to solve these problems will be discussed next.

A first cause of the indefiniteness of an internal deformation tensor is the (quadratic) interpolation of (positive definite) internal deformation tensors from the nodal points to the integration points[4]. Due to the (quadratic) interpolation the positive definiteness of the internal deformation tensor may be lost. Particularly, large gradients in an element may cause indefinite internal deformation tensors in the integration points. This occurs for example at the start-up from a zero-velocity initial field with fully developed boundary conditions at the inflow. These large errors can be avoided when the mechanical dissipation is firstly calculated in the nodal points and then interpolated to the integration points. However, this procedure reduces the accuracy of the calculation of the finite element integrals and will therefore be restricted to the integration points where $\underline{\underline{b}}_k$ is indefinite.

A second cause is that during the streamline integration the internal deformation tensor in some nodal point has become indefinite. Although theoretically the tensors $\underline{\underline{b}}_k$ are positive definite, they may become indefinite due to numerical approximation errors. Especially in regions where large gradients are present, for example near sharp corners. Due to the long residence time of a fluid particle near the wall, negative determinants may blow up the quadratic term in the nonlinear stress equations in appendix A. To avoid these nonlinear instabilities the internal deformation tensor is then corrected with an isotropic term to a semi-positive definite tensor. In section 3.2 the correction method with an isotropic term has been explained. To save computing time the 2D method with a lower bound of $I_{3,k}^{\min} = 0$ will be taken during

---

[4]From the streamline integration semi-positive definite internal deformation tensors are obtained in the nodal points. The calculation in the nodal points saves computing time, because the total number of nodal points is much smaller than the total number of integration points. However, to obtain a good accuracy the integrals in the finite element formulation of the temperature equation are evaluated in the integration points.

the streamline integration. The internal deformation tensor in a nodal point may therefore be semi-positive definite. This is sufficient to avoid the nonlinear instabilities during the streamline integration. However, for the calculation of the inverse of an internal deformation tensor this is not sufficient. In section 3.2 it has been shown that for most of the models it is possible to find a sharper lower bound for the determinant $I_{3,k}^{\min}$, see table 3.1. For all the stress models, except the Giesekus model, the lower bound is $I_{3,k}^{\min} = 1$. For the 2D Giesekus model it is also possible to find a lower bound which depends on the parameter α_k of that model, see Hulsen (1988b). However for the 3D axisymmetrical Giesekus model it is not possible to find such a lower bound and one has to proceed differently[5]. An obvious and cheap way is then to take the stress work of the specific mode $\underline{\underline{\tau}}_k : \underline{\underline{d}}$ instead of its mechanical dissipation $D_{\mathrm{m},k}^{\mathrm{ve}}$.

Summarising the procedure is as follows when an internal deformation tensor in a certain integration point is indefinite.

1. Check whether the indefiniteness of $\underline{\underline{b}}_k$ is caused by the interpolation to the integration points. When the internal deformation tensor is positive definite in all nodal points the mechanical dissipation $D_{\mathrm{m},k}^{\mathrm{ve}}$ is calculated in the nodal points of that element. The mechanical dissipation in the integration point is found by a quadratic interpolation of the nodal point mechanical dissipations.

2. The indefiniteness is caused by the streamline integration and a positive lower bound of the determinant exists. The deformation tensor is then corrected with a 2D isotropic term so that its determinant equals the theoretical lower bound of the determinant $I_{3,k}^{\min}$. This is possible for all the stress models of appendix A, except the 3D Giesekus model.

3. Take the stress work $\underline{\underline{\tau}}_k : \underline{\underline{d}}$ of mode k as an approximation of the mechanical dissipation $D_{\mathrm{m},k}^{\mathrm{ve}}$ of mode k. A very small positive value of the determinant may also cause large numerical errors in the mechanical dissipation. Therefore the stress work of the specific mode will be taken instead of the mechanical dissipation when the determinant of the internal deformation tensor is small, say less than 10^{-8}. For the models of appendix A this is only necessary for the 3D Giesekus model.

Calculation of the pressure

The pressure is piecewise linear per element and discontinuous over the element boundaries. In the equations of motion the pressure gradient in the centre point of an element has been eliminated with the help of the centre point velocities of that element. It can be recomputed on element level with the inverse operation used in the equations of motion. The pressure in the centre point has been eliminated on element level with the help of the penalty method or the Uzawa method. It can be recomputed with the inverse operation used to eliminate the pressure in the equations of motion (4.8) or (4.9). The pressures in the integration points of an element are then obtained from a linear interpolation of the pressure and its derivatives in the centre

---

[5]Solving a separate equation for the determinant $I_{3,k}$ of $\underline{\underline{b}}_k$, equation (3.73), did not solve this problem. The determinant was also negative when $\underline{\underline{b}}_k$ was indefinite. A possible way to avoid the problem could be to solve the differential equation for the inverse of the internal deformation tensor $\underline{\underline{b}}_k^{-1}$ as well. Then the trace of the inverse of the internal deformation tensor may be calculated directly from $\underline{\underline{b}}_k^{-1}$ instead of $\underline{\underline{b}}_k$. This has not been tried, because it will cost much extra computing time and it may only be useful for the 3D Giesekus model.

point of that element.

Upwind methods for the temperature equation

For convection-dominated problems the standard Galerkin method may give rise to unphysical solutions, i.e. solutions with a globally oscillating character. For a lot of problems the temperature equation is dominated by convection due to the small value of the diffusivity of polymeric fluids. The order of magnitude is $\kappa/\rho c_{p,b} = \mathcal{O}(10^{-7})$ m$^2 \cdot$s^{-1}. To avoid the unphysical wiggles for convection-dominated problems, the value of the mesh Péclet number must fulfil the severe condition $Pe_{\mathrm{m}} = \rho c_{p,b} v \Delta x / \kappa_v \leq 2$ in all elements. Here v, Δx and κ_v are the velocity, the size of the element and the thermal conductivity in the streamwise direction. To fulfil this restriction the size of the elements of the mesh must be extremely small. This limits of course the practical use of the Galerkin method. However, it is possible to avoid the extreme mesh refinement for high values of the mesh Péclet number by using an upwind technique. The wiggles can be suppressed with the help of such methods, but they may cause inaccurate solutions through the introduction of false (extra) diffusion, especially for coarse grids. The amount of false diffusion reduces when the element size becomes smaller.

Consistent and non-consistent upwind methods.

The non-consistent upwind methods consist of the multiplication with an extra test function in the streamwise direction of the convective term only. The finite element formulation of the temperature equation (4.16) then becomes

$$(\rho(c_{p,\tau_e}^{\mathrm{eq}} - \Delta c^{\mathrm{eq}})\underline{v} \cdot \nabla T, \psi_T) + (\rho(c_{p,\tau_e}^{\mathrm{eq}} - \Delta c^{\mathrm{eq}})\underline{v} \cdot \nabla T, \psi_u)_{\Omega_e} + [\underline{\underline{\kappa}} \cdot \nabla T, \nabla \psi_T] =$$
$$(D_{\mathrm{m}}^{\mathrm{ve}} + \rho T \Delta s_b^{\mathrm{ve}} - \alpha_\rho p \underline{v} \cdot \nabla T, \psi_T) - [T\alpha_\rho p \underline{v}, \nabla \psi_T] + (\underline{n} \cdot \underline{\underline{\kappa}} \cdot \nabla T + T\alpha_\rho p \underline{n} \cdot \underline{v}, \psi_T)_\Gamma,$$
$$\forall \psi_T \in \Psi_T, \quad \forall \psi_u \in \Psi_u, \quad (4.17)$$

where ψ_u is the upwind test function, which belongs to a suitable space Ψ_u on Ω. For the contribution of upwind terms the following notation for the finite element integrals will be used

$$(a, b)_{\Omega_e} = \sum_{e=1}^{N} \int_{\Omega_e} ab \; d\Omega_e, \qquad [\underline{a}, \underline{b}]_{\Omega_e} = \sum_{e=1}^{N} \int_{\Omega_e} \underline{a} \cdot \underline{b} \; d\Omega_e, \qquad (4.18)$$

where Ω_e is the domain of an element and N the number of elements. When the streamlines are taken as the upwind direction, the crosswind diffusion may be eliminated. However, the non-consistent method results in excessively diffusive solutions when source terms are present (Brooks & Hughes 1982). For polymeric fluids the source terms, viz. the mechanical dissipation and the thermal expansion cooling term, may be large. This makes an inconsistent upwind method inefficient for the numerical calculations in chapter 5.

For the consistent upwind methods all the terms in the temperature equation are multiplied with an upwind test function ψ_u and added to the integrated temperature equation (4.16). The total finite element formulation of the temperature equation then becomes

$$\left(\rho(c_{p,\tau_e}^{\mathrm{eq}} - \Delta c^{\mathrm{eq}})\underline{v} \cdot \nabla T, \psi_T\right) + [\underline{\underline{\kappa}} \cdot \nabla T, \nabla \psi_T] + \left(\rho(c_{p,\tau_e}^{\mathrm{eq}} - \Delta c^{\mathrm{eq}})\underline{v} \cdot \nabla T - \nabla \cdot (\underline{\underline{\kappa}} \cdot \nabla T), \psi_u\right)_{\Omega_e} =$$
$$(D_{\mathrm{m}}^{\mathrm{ve}} + \rho T \Delta s_b^{\mathrm{ve}}, \psi_T) + (D_{\mathrm{m}}^{\mathrm{ve}} + \rho T \Delta s_b^{\mathrm{ve}} + T\alpha_\rho \underline{v} \cdot \nabla p, \psi_u)_{\Omega_e} - [T\alpha_\rho p \underline{v}, \nabla \psi_T] +$$
$$(\underline{n} \cdot \underline{\underline{\kappa}} \cdot \nabla T + T\alpha_\rho p \underline{n} \cdot \underline{v}, \psi_T)_\Gamma, \qquad \forall \psi_T \in \Psi_T, \quad \forall \psi_u \in \Psi_u. \qquad (4.19)$$

Note that the sum of the integrals over element interiors cannot be written as a global integral over Ω due to the presence of the second order term $\nabla \cdot (\underline{\underline{\kappa}} \cdot \nabla T)$. Therefore the diffusion term with the upwind test function may not be integrated by parts as for the standard Galerkin term. This is not allowed because the upwind test functions are discontinuous across the element sides.

As for the inconsistent upwind method, the crosswind diffusion can be eliminated by taking the streamlines as the upwind direction. Additionally the consistent upwinding solves the problem of the diffuse solutions when source terms are present. Brooks & Hughes (1982) have shown that a consistent method eliminates the artificial diffusion that bothers many classical upwind schemes.

Firstly the implementation of the second derivative term in (4.19) will be discussed. Then some choices for the upwind test function ψ_u, which have been proposed in the literature, will be reviewed.

Implementation of the second order terms.

In the standard Galerkin approach the Gauss theorem can be used to reduce the order of the derivatives of the integrands. The test functions ψ_T are piecewise polynomials and continuous over the element boundaries. The upwind test functions ψ_u depend on the gradient of the temperature test function and are therefore discontinuous across the element boundaries. Therefore the Gauss theorem cannot be applied to the second order term in (4.19) and this term has to be treated differently. An extra difficulty is that the heat conduction tensor is not constant over an element.

The evaluation of the integral over the surface of a finite element e

$$-\int_{\Omega_e} \nabla \cdot (\underline{\underline{\kappa}} \cdot \nabla T)\, \psi_u d\Omega_e \tag{4.20}$$

can be done as follows. Firstly a finite element approximation of the heat flux $\underline{\underline{\kappa}} \cdot \nabla T$ has to be evaluated in the nodal points, because the discrete approximation of the temperature (4.7) is in the nodal points. This gives for axisymmetrical or 2D Cartesian coordinates

$$\underline{\underline{\kappa}} \cdot \nabla T = \sum_{r=1}^{2} \kappa_{pr}(\underline{x}) \sum_{j=1}^{n} T^j \frac{\partial \psi^j(\underline{x})}{\partial x_r} = \sum_{j=1}^{n} T^j q_p^j(\underline{x}), \tag{4.21}$$

where n is the number of temperature nodes. Secondly the integral (4.20), with the approximation in the nodal points of the heat flux (4.21) has to be calculated in the integration points for accuracy reasons. Therefore the values of $\nabla \cdot (\underline{\underline{\kappa}} \cdot \nabla T)$ must be known in the integration points. This can be obtained by approximating the variable q_p^j in the standard finite element way:

$$q_p^j(\underline{x}) = \sum_{l=1}^{n} q_p^{j,l} \psi^l(\underline{x}). \tag{4.22}$$

Taking the divergence of (4.21) with the approximation (4.22) gives

$$\nabla \cdot (\underline{\underline{\kappa}} \cdot \nabla T) = \sum_{j=1}^{n} T^j \sum_{l=1}^{n} \sum_{p=1}^{2} q_p^{j,l} \frac{\partial \psi^l(\underline{x})}{\partial x_p}, \tag{4.23}$$

which must be evaluated in the integration points.

With this approximation the contribution of the second order upwind term to the element matrix S_ψ^{ij} for the unknowns T^j becomes

$$S_\psi^{ij} = -\sum_{k=1}^{m} \psi_u^i(\underline{x}_k) \sum_{l=1}^{n} \sum_{p=1}^{2} q_p^{j,l} \frac{\partial \psi^l(\underline{x}_k)}{\partial x_p}, \quad i,j = 1,\dots,n, \tag{4.24}$$

where m is the number of integration points $\underline{x}_k$.

The upwind test function.

Below an overview will be given of the upwind test functions which can be used for steady flows. The upwind test functions consist of an upwind direction and an upwind function and are discontinuous across the element boundaries, because the upwind direction is multiplied scalarly by the gradient of the test functions ψ_T. This inner product will still be multiplied by an upwind function τ to take care that no (or less) upwinding is applied if it is not necessary. Successively the choice for the upwind direction and the amount of upwinding that must be applied will be discussed separately.

Determination of the upwind direction

Two different choices of the upwind direction, that can be used for quadratic elements, will be summarised: the standard upwind Petrov–Galerkin method and a method with discontinuity capturing.

- *Standard upwind Petrov–Galerkin.*

  Hughes & Brooks (1982) have described an upwind method for finite element methods. This method, which is known as the Standard Upwind Petrov–Galerkin method (SUPG), is widely used for convection-dominated problems. For the SUPG method the streamlines are taken as the upwind direction, which gives for the upwind test function

$$\psi_u = \tau \underline{v} \cdot \nabla \psi. \tag{4.25}$$

  Hughes & Brooks (1982) have shown that with this choice of ψ_u sufficiently smooth exact solutions can be approximated very well. The presence of sharp layers may create local oscillations, in contrast with the standard Galerkin method which creates globally-propagating oscillations.

- *Upwinding with discontinuity capturing.*

  Hughes, Mallet & Mizukami (1986) have developed an upwind scheme (HMM), similar to SUPG, in which they add an additional discontinuity capturing term which controls the derivatives in the direction of the temperature gradient. The wiggles in the neighbourhood of sharp layers, which arise with the SUPG method, can then be suppressed. They take for the upwind test function ψ_u

$$\psi_u = \begin{cases} \tau \underline{v} \cdot \nabla \psi + \tau_p \underline{v}_p \cdot \nabla \psi, & ||\nabla T|| \neq 0, \\ \tau \underline{v} \cdot \nabla \psi, & ||\nabla T|| = 0, \end{cases} \tag{4.26}$$

  where τ_p is the parallel upwind function and $\underline{v}_p$, the upwind direction parallel to the gradient of the temperature, defined as

$$\underline{v}_p = \begin{cases} \underline{v} \cdot \nabla T \dfrac{\nabla T}{||\nabla T||^2}, & ||\nabla T|| \neq 0, \\ \underline{0}, & ||\nabla T|| = 0. \end{cases} \tag{4.27}$$

Preliminary calculations in a contraction flow showed that for isotropic heat conduction this method gave somewhat smoother temperature profiles near the sharp corner. For anisotropic heat conduction however the iterative method did not converge, possibly because the direction of the discontinuity capturing, the direction of the temperature gradient ∇T does not equal the direction of the heat flux $\underline{\underline{\kappa}} \cdot \nabla T$ then.

Determination of the upwind function

The upwind function τ indicates the amount of upwinding that must be applied. It is based on the element Péclet number β_u, which is defined as

$$\begin{aligned}
\beta_u &= \frac{||\underline{v}||h\rho c_{p,b}}{2\kappa_v}, \\
\kappa_v &= \frac{\underline{v} \cdot \underline{\underline{\kappa}} \cdot \underline{v}}{||\underline{v}||^2},
\end{aligned} \tag{4.28}$$

where h is the maximum distance in the element in the direction of the velocity $\underline{v}$ and κ_v is a measure for the thermal conductivity in the streamwise direction. When the element Péclet number $\beta_u < 1$ the upwind function can be chosen small, because the standard Galerkin approach still gives accurate solutions. For $\beta_u > 1$ however, upwinding has to be applied to avoid unphysical wiggles. For a one-dimensional steady state problem, without mechanical dissipation and source terms Christie et al. (1976) have shown that the optimal choice for the upwind function is

$$\begin{aligned}
\tau &= \frac{h\xi_u}{2||\underline{v}||}, \\
\xi_u &= \coth \beta_u - \frac{1}{\beta_u},
\end{aligned} \tag{4.29}$$

where ξ_u is a non-dimensional numerical diffusivity. In the simple one-dimensional example of Christie et al. this choice of τ leads to nodally exact solutions.

To minimize the computing time the 'doubly asymptotic' approximation of the non-dimensional numerical diffusivity ξ_u

$$\xi_u = \begin{cases} \dfrac{\beta_u}{3} & , \quad -3 \leq \beta_u \leq 3, \\ \mathrm{sgn}\,\beta_u & , \quad |\beta_u| > 3, \end{cases} \tag{4.30}$$

or the critical approximation

$$\xi_u = \begin{cases} 1 - \dfrac{1}{\beta_u} & , \quad \beta_u > 1, \\ 0 & , \quad |\beta_u| \leq 1, \\ -1 - \dfrac{1}{\beta_u} & , \quad \beta_u < -1, \end{cases} \tag{4.31}$$

can be employed (Hughes et al. 1986). For the results the choice of the upwind function does not seem very important. In test calculations of a flow through a 4:1 contraction the

different choices of the upwind function did not give significant differences.

The parallel upwind function τ_p in the HMM upwinding (4.26) is based on $\underline{v}_p$, the velocity parallel to the temperature gradient, and h_p, the maximum distance in the direction of the parallel velocity, instead of the velocity $\underline{v}$ and h, the maximum distance in the streamwise direction. For the 'optimal' choice the parallel element Péclet number (4.28) and the parallel upwind function (4.29) become[6]

$$
\begin{aligned}
\beta_{u,p} &= \frac{||\underline{v}_p||h_p\rho c_{p,b}}{2\kappa_{v,p}}, \\
\kappa_{v,p} &= \frac{\underline{v}_p \cdot \underline{\underline{\kappa}} \cdot \underline{v}_p}{||\underline{v}_p||^2}, \\
\tau_p &= \frac{h_p\xi_{u,p}}{2||\underline{v}_p||}, \\
\xi_{u,p} &= \coth\beta_{u,p} - \frac{1}{\beta_{u,p}}.
\end{aligned}
\tag{4.32}
$$

To minimize the computing time the doubly asymptotic approximation or the critical approximation may be used for the parallel numerical diffusivity as well.

Matrix-vector formulation

Substitution of the finite element approximation (4.7) in the temperature equation (4.19) results in the matrix-vector equation

$$
N_T(\mathcal{V},\mathcal{T}) + S_T(\mathcal{B},\mathcal{T})\mathcal{T} = F_T(\mathcal{V},\mathcal{T},\mathcal{B},\mathcal{P}),
\tag{4.33}
$$

with N_T a nonlinear operator due to the convective term and S_T an operator due to heat conduction. S_T may depend on the internal deformation tensors and linearly on the temperature, via the heat conduction tensor. S_T may also contain the contributions of the natural boundary conditions. The right-hand-side vector F_T consists of contributions of the natural boundary conditions, the mechanical dissipation, the thermal expansion terms and the reversible entropy production term Δs_b^{ve}. To obtain a good accuracy, the surface integrals have been evaluated numerically with a seven-point Gauss rule and the line integrals with a three-point Gauss rule.

4.3.2 Implementation in the iterative scheme

As for the discretised equations of motion, an incremental formulation has been used to solve the discretised temperature equation (4.33) as well:

$$
\left(\kappa_{\text{it}}S_T^{\text{it}} + S_T(\mathcal{B}^i,\mathcal{T}^i) + M_T(\mathcal{V}^{i+1},\mathcal{T}^i)\right)\Delta\mathcal{T}^{i+1} = -R_T(\mathcal{V}^{i+1},\mathcal{B}^i,\mathcal{T}^i,\mathcal{P}^{i+1}),
\tag{4.34}
$$

where all of the matrices and vectors may contain contributions of the upwind scheme. The Picard iteration matrix contains contributions of the convective terms M_T, the diffusive terms S_T and an extra diffusive term $\kappa_{\text{it}}S_T^{\text{it}}$. The iteration diffusivity κ_{it} slows down the iteration

---

[6]To avoid the doubling effect when $\underline{v}_p$ is almost parallel to $\underline{v}$, they propose to take $\max(0,\tau_p-\tau)$ instead of τ_p in the upwind test function (4.26).

process, but is sometimes necessary to obtain a convergent solution method[7]. A constant and isotropic iteration diffusivity gave good results for the calculations in chapter 5. The increment of the temperature $\Delta \mathcal{T}^{i+1}$ is defined by

$$\Delta \mathcal{T}^{i+1} = \mathcal{T}^{i+1} - \mathcal{T}^i, \tag{4.35}$$

and the residual $R_T(\mathcal{V}^{i+1}, \mathcal{B}^i, \mathcal{T}^i, \mathcal{P}^{i+1})$ of the temperature equation equals

$$R_T(\mathcal{V}^{i+1}, \mathcal{B}^i, \mathcal{T}^i, \mathcal{P}^{i+1}) = S_T(\mathcal{B}^i, \mathcal{T}^i)\mathcal{T}^i + N_T(\mathcal{V}^{i+1}, \mathcal{T}^i) - F_T(\mathcal{V}^{i+1}, \mathcal{B}^i, \mathcal{T}^i, \mathcal{P}^{i+1}), \tag{4.36}$$

where the diffusive matrix $S_T(\mathcal{B}^i, \mathcal{T}^i)$ may depend on the internal deformation tensors due to the anisotropic heat conduction. N_T contains the contributions of the convective terms. The mechanical dissipation, the thermal expansion terms, the reversible entropy production term and the boundary integrals of the natural boundary conditions contribute to F_T.

For detecting convergence of the temperature equation two conditions, which are analogous to the conditions of the equations of motion, have to be satisfied. The first condition is related to the increment of the temperature and the second to the residual of the temperature equation:

$$\frac{\max_j |\Delta \mathcal{T}_j^{i+1}|}{\max_j |\mathcal{T}_j^{i+1}|} \leq \epsilon_{T,\text{inc}},$$

$$\frac{||R_T(\mathcal{V}^i, \mathcal{B}^i, \mathcal{T}^i)||_f}{||R_T(\mathcal{V}^i, \mathcal{B}^i, \mathcal{T}^i)||_t} \leq \epsilon_{T,\text{res}}, \tag{4.37}$$

where the maximum norm $|.|$ has been taken over all nodal points j. The norms $|| \cdot ||_f$ and $|| \cdot ||_t$ again denote the Euclidean norm over the free and total degrees of freedom. $\epsilon_{T,\text{inc}}$ and $\epsilon_{T,\text{res}}$ are small parameters. For the calculations in chapter 5 $\epsilon_{T,\text{inc}} = \epsilon_{T,\text{res}} = \mathcal{O}(10^{-3})$ will be taken.

4.4   The stress constitutive equation

In this section a short overview will be given of the streamline integration method that will be used to solve the differential equations for the internal deformation tensors in $(2.156)_5$. The stress models in appendix A can be written as a set of ordinary differential equations for the internal deformation tensor, by applying the method of characteristics. For a steady flow the characteristics are equal to the streamlines. Equation $(2.156)_5$ can then be written as

$$\frac{d\underline{\underline{b}}_k}{ds} \frac{ds}{dt} = \underline{\underline{G}}_k(\underline{v}, \underline{\underline{L}}^T, \underline{\underline{b}}_k, T), \tag{4.38}$$

where s is a streamline parameter and $\underline{\underline{G}}_k$ a tensor function that depends on the constitutive model. The stress that is needed in the balance equations can then be then found by (2.19).

For a detailed description of the computation of the streamlines and the integration along it for isothermal problems see Hulsen (1990a). Below only a summary of some important aspects of the streamline integration will be given, supplemented by the specific problems for the nonisothermal equation. First, however, the restrictions on the numerical implementation of

---

[7]An iteration diffusivity $\kappa_{\text{it}} = \kappa_{\text{eq}}$ is often sufficient.

the stress constitutive equation will be summarized.

Restrictions on the numerical implementation

The following restrictions have been made for the numerical implementation of the stress constitutive equation:

- The flow is assumed to be steady.

- The type of the coordinate system is either Cartesian or axisymmetrical.

- The relations between the modal stresses and the internal deformation tensors are given by (2.19).

- The moduli G_k may depend on the temperature and the density as in (2.126), where the density may be a linear function of the temperature.

- Other coefficients in (2.19) do not depend on the temperature and the pressure or density.

- The internal deformation tensors are specified by one of the differential equations discussed in appendix A.

- The temperature dependence of the relaxation times λ_k may be given by[8] the WLF shift factor (2.123), the Andrade shift factor (2.124) or a combination of these two (the WLF shift factor below a certain separating temperature $T < T_\mathrm{s}$ and the Andrade shift factor above the separating temperature $T > T_\mathrm{s}$).

- Except the relaxation times, the other coefficients in the equations for the internal deformation tensors are assumed to be independent of the temperature.

- In the differential equation for the internal deformation tensor all coefficients are independent of the pressure or density.

The isothermal streamline integration method

A detailed description of the isothermal streamline integration has been given by Hulsen (1990a). Below some important aspects of this method have been summarized.

- *Computation of the streamlines.*
  From the piecewise quadratic velocities of the first step of an iteration a quadratic stream function is calculated per element. With this stream function a piecewise quadratic streamline can then be calculated.

- *Initial conditions.*
  For the integration of (4.38) an initial condition for the internal deformation tensor $\underline{b}_k$ has to be specified. There are three possibilities. Firstly the streamline may cross an inflow boundary. Then the initial value is taken from the specified boundary value. In case a fully developed flow is prescribed, the inflow conditions have to be calculated separately.

---

[8]For test purposes also an exponential factor $\ln a_{T,k} = C_{1,k}(T - T_\mathrm{ref})$ has been implemented. With this type of shift factors an analytical solution can be computed for steady flows of a Maxwell fluid in Cartesian coordinates. This is not possible for the Andrade and WLF shift factor.

These fully developed flow boundary conditions will be examined in section 4.5. Secondly the streamline may cross an element where the internal deformation tensor has already been computed. Then the initial value is obtained from a quadratic interpolation of the nodal point values of that element. Finally, to reduce the computing time, the integration is stopped if the travel time is longer than $3\lambda_k$. The initial values are then found by a quadratic interpolation of the nodal point values of the previous iteration.

- *Integration accuracy.*
  The integration along the streamlines of the right-hand side of (4.38) has been computed numerically with a fourth order Runge–Kutta scheme. Quantities that must be computed outside the nodal points of an element are obtained by a quadratic interpolation of the nodal point values (internal deformation tensor and velocity gradient) or an extended quadratic interpolation (velocity).

- *Stepsize limitations.*
  The limitation of the stepsize of the streamline integration is based on the stability region of the linearized form of equation (4.38). Furthermore it is possible to limit the stepsize further when the change of a quantity during a step is too large. For example, it is necessary to limit the change in velocity gradient at start-up for high values of the Deborah number.

- *Shear flow correction.*
  On the wall numerical approximation errors may cause large false elongational stresses for high Deborah numbers, due to the infinite residence time on the wall. This can be avoided by imposing an exact simple shear flow on the wall.

- *Correction of the internal deformation tensors.*
  Due to numerical approximation errors the internal deformation tensor can become indefinite in regions where large gradients are present, for example near sharp corners. Negative determinants may blow up the nonlinear terms of the internal deformation tensor in (4.38). To avoid these nonlinear instabilities the internal deformation tensor will be corrected with an isotropic term. In section 3.2 the correction method has been explained. During the streamline integration the 2D method with a lower bound of $I_{3,k}^{\min} = 0$ will be taken. The internal deformation tensor $\underline{\underline{b}}_k^c$ is therefore semi-positive definite. This is sufficient to avoid the nonlinear instabilities and saves computing time.

Additions for the nonisothermal streamline integration method

On the whole the nonisothermal streamline integration method is similar to the isothermal streamline integration method described by Hulsen (1990a). It only differs in the following aspects.

- *Temperature dependence of the right-hand-side tensor $\underline{\underline{G}}_k$.*
  The tensor function $\underline{\underline{G}}_k$ in (4.38) is also a function of the temperature, due to the temperature dependence of the time constant λ_k. Therefore the temperature along the streamline has to be known. These temperatures are obtained by quadratic interpolation of the nodal point values of the element in which the part of the streamline is.

- *Stepsize limitations.*
  The computation of the step size for the numerical integration of mode k of (4.38) in a certain point along the streamline is based on the stability region of the linearized form, with respect to the internal deformation tensor $\underline{\underline{b}}_k$, of (4.38). The temperature dependence is due to the temperature dependent relaxation time λ_k in $\underline{\underline{G}}_k$. When the temperature rises, for example due to dissipation, the relaxation time decreases and the step size becomes smaller. When the temperature decreases, for example due to wall cooling, the relaxation time increases and the step size becomes larger.

- *Maximum travel time.*
  The magnitude of the particle trajectory is limited by the nonisothermal travel time of a particle $3 \max_k \lambda_{k,\mathrm{ref}} \max_k a_{T,k}$ evaluated at the end point of the streamline (the nodal point where the internal deformation tensor has to be calculated) instead of $3 \max_k \lambda_{k,\mathrm{ref}}$ for the isothermal calculations. For the nonisothermal travel time the maxima over λ_k and $a_{T,k}$ have been taken to avoid problems when different modes are described by different shift factors.

- *Maximum integration length.*
  The maximum integration length for mode k, which must of course be smaller than the travel time, is $3\lambda_k(T)$ instead of the $3\lambda_{k,\mathrm{ref}}$ for the isothermal calculations. $\lambda_k(T)$ is evaluated at the end point of the streamline. The temperature dependence of the maximum integration length avoids the calculation of many small integration steps for regions where a number of the relaxation times λ_k have become small due to the temperature rise in the fluid. On the other hand a larger particle length may be necessary when the temperature decreases. Because the relaxation time strongly depends on the temperature the isothermal value $3 \max_k \lambda_{k,\mathrm{ref}}$ may not be large enough.

- *Calculation of the modal stresses.*
  After solving the differential equation for the internal deformation tensors $\underline{\underline{b}}_k$ the sum of the modal stresses $\underline{\underline{\tau}}_k$, which is needed in the equations of motion, is calculated with the help of (2.19). For the nonisothermal calculations the nodal point values of the temperature are needed additionally, because the moduli G_k may depend on the temperature and the density $(\rho = \rho(T))$.

4.5   Boundary conditions

To obtain a complete set of equations, boundary conditions at the boundary Γ of the domain Ω have to be specified for the equations of motion, the temperature equation and the K equations for the internal deformation tensor. The equations of motion and the temperature equation are elliptic. Therefore boundary conditions have to be specified on the complete boundary. The constitutive equations for the internal deformation tensor are hyperbolic, which implies that a boundary condition may only be imposed at an inflow boundary. Firstly the boundary conditions at fixed walls and axes of symmetry will be given. Then the inflow and outflow boundary conditions will be discussed extensively.

4.5.1   Boundary conditions at a fixed wall and an axis of symmetry

Some different types of boundary conditions for the equations of motion and the temperature equation, which can be imposed on a fixed wall or an axis of symmetry, are summarized in this section.

Boundary conditions for the equations of motion.
At a fixed wall Γ_{w} the no-slip boundary condition is supposed to hold for the velocity:

$$\underline{v} = \underline{0}, \qquad \text{at} \quad \Gamma = \Gamma_{\mathrm{w}}. \tag{4.39}$$

At an axis of symmetry Γ_{ax} the boundary condition for the equations of motion is given by

$$\underline{n} \cdot \underline{v} = 0, \qquad \underline{\sigma}_t = \underline{0}, \qquad \text{at} \quad \Gamma = \Gamma_{\mathrm{ax}}, \tag{4.40}$$

where $\underline{n}$ is the outward unit normal and

$$\begin{aligned} \underline{\sigma}_t &= \underline{n} \cdot \underline{\underline{\sigma}} - \underline{n}\sigma_n, \\ \sigma_n &= \underline{n} \cdot \underline{\underline{\sigma}} \cdot \underline{n}. \end{aligned} \tag{4.41}$$

σ_n is the component of the total stress tensor in the direction normal to the boundary Γ_{ax} and $\underline{\sigma}_t$ the total stress in the direction tangential to Γ_{ax}.

Boundary conditions for the temperature equation.
At a fixed wall Γ_{w} the temperature may be prescribed by the Dirichlet boundary condition

$$T = T_0, \qquad \text{at} \quad \Gamma = \Gamma_{\mathrm{w}}, \tag{4.42}$$

or the heat flux may be prescribed by the Neumann boundary condition

$$\underline{n} \cdot (\underline{\underline{\kappa}} \cdot \nabla T) = Q_0, \qquad \text{at} \quad \Gamma = \Gamma_{\mathrm{w}}, \tag{4.43}$$

or a linear combination of the temperature and the heat flux may be prescribed by the Robin boundary condition

$$\underline{n} \cdot (\underline{\underline{\kappa}} \cdot \nabla T) + \beta_1 T = Q_1, \qquad \text{at} \quad \Gamma = \Gamma_{\mathrm{w}}. \tag{4.44}$$

The temperature T_0, the fluxes Q_0 and Q_1 and the parameter β_1 may be functions of the coordinates of the boundary.
At an axis of symmetry Γ_{ax} the temperature boundary condition is given by the symmetry condition, a vanishing normal component of the heat flux:

$$\underline{n} \cdot (\underline{\underline{\kappa}} \cdot \nabla T) = 0, \qquad \text{at} \quad \Gamma = \Gamma_{\mathrm{ax}}. \tag{4.45}$$

4.5.2   Inflow and outflow boundary conditions

At an inflow or outflow boundary the boundary conditions are based on the fully developed profiles of the equations of motion, the temperature equation and the differential equations for the K internal deformation tensors. The restrictions mentioned in the sections 4.2, 4.3 and 4.4 for the finite element implementation are also valid for the implementation of the fully

developed boundary conditions. Through the assumption of a fully developed flow the balance equations and the constitutive equations are simplified considerably. For example all material derivatives, except $\dot{p}$, vanish. From equation (2.90) then follows that the mechanical dissipation always equals the stress work $D_m^{ve} = \underset{\approx}{\tau} : \underset{\approx}{d}$. For a fully developed shear flow the mechanical dissipation reduces to the product of the shear stress and the shear rate, i.e. $D_m^{ve} = \tau_{12}\dot{\gamma}$.

The equations for a fully developed flow have been implemented for 2D Cartesian and axisymmetrical flows. In view of the axisymmetrical examples for the calculations in chapter 5 the derivation and implementation of the equations will only be discussed for axisymmetrical problems. For Cartesian coordinates, however, the derivation is completely analogous.

At an inflow boundary the obtained solutions of the fully developed velocity, temperature and internal deformation tensors may be prescribed as Dirichlet boundary conditions. At an outflow boundary natural boundary conditions are prescribed for the equations of motion and the temperature equation. These natural boundary conditions are based on the fully developed profile. Firstly the equations and boundary conditions for fully developed flows and its numerical implementation will be discussed. At the end of this section the natural boundary conditions at the outflow will be explained.

Equations for fully developed axisymmetrical flows.

For axisymmetrical flows the following solution of the fully developed flow problem in figure 4.2 is assumed

$$
\begin{aligned}
\underline{v} &= w(r)\underline{e}_z, \\
\underset{\approx}{\tau} &= \tau_{ij}(r)\underline{e}_i\underline{e}_j, \qquad i,j = r,z, \\
T &= T(r).
\end{aligned}
\tag{4.46}
$$

If the density depends on the temperature, this velocity profile still fulfils the mass balance. Only when the density also depends on the pressure the mass balance is not fulfilled anymore.
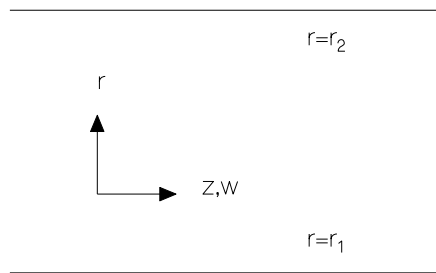
Figure 4.2: Geometry of the fully developed axisymmetrical flow. The inner wall or axis of symmetry corresponds to $r = r_1$ and the outer wall to $r = r_2$.

Substitution of the velocity and stress (4.46) in the balance of linear momentum (2.156)$_2$ yields

$$
\begin{aligned}
\frac{\partial p}{\partial r} &= \frac{1}{r}\frac{d(r\tau_{rr})}{dr}, \\
\frac{\partial p}{\partial z} &= \frac{1}{r}\frac{d(r\tau_{rz})}{dr}.
\end{aligned}
\tag{4.47}
$$

The pressure p can only be solved if the equations (4.47) are compatible, which means that

$$\frac{\partial}{\partial z}\frac{\partial p}{\partial r} - \frac{\partial}{\partial r}\frac{\partial p}{\partial z} = \frac{\partial}{\partial z}\left(\frac{1}{r}\frac{d(r\tau_{rr})}{dr}\right) - \frac{\partial}{\partial r}\left(\frac{1}{r}\frac{d(r\tau_{rz})}{dr}\right) = -\frac{d}{dr}\left(\frac{1}{r}\frac{d(r\tau_{rz})}{dr}\right) = 0. \qquad (4.48)$$

Integration of the compatibility relation (4.48) gives

$$\tau_{rz} = -\mu r + \frac{d}{r}, \qquad (4.49)$$

where μ and d are constants which have to be determined from the boundary conditions. Combination with (4.47) yields

$$p = -2\mu z + \tau_{rr} - \int_r^{r_2} \frac{\tau_{rr}(s)}{s}ds + p_0, \qquad (4.50)$$

where p_0 is an integration constant, which remains undetermined for incompressible flows.

The resulting equations for the equations of motion (4.49) and (4.50) have to be supplemented by a constitutive equation for the stress (one of the models discussed in appendix A, possibly supplemented by a solvent viscosity), which has the form

$$\tau_{ij} = \tau_{ij}(\dot\gamma, T), \qquad i, j = r, z,$$
$$\dot\gamma = \frac{dw}{dr}. \qquad (4.51)$$

Note that the differential equation for the internal deformation tensor reduces to an algebraic equation for fully developed flows. This simplifies the equations considerably.

The last equation that has to be solved is the temperature equation. After substitution of (4.46) in the temperature equation $(2.156)_3$ an ordinary differential equation results

$$-2T\alpha_\rho w\mu + \dot\gamma\tau_{rz} + \frac{1}{r}\frac{d}{dr}\left(\kappa_{rr}r\frac{dT}{dr}\right) = 0. \qquad (4.52)$$

Boundary conditions for fully developed flows.

To compute the integration constants μ and d in the equation for the shear stress (4.49) and the velocity constant resulting from the integration of $(4.51)_2$ some boundary conditions have to be specified for the velocity. One constant can be found from the prescribed pressure gradient or averaged velocity. The other two have to be found from the boundary conditions at a fixed wall or an axis of symmetry.

At a fixed wall having coordinate r_w the no-slip boundary condition is supposed to hold for the velocity:

$$w = 0, \qquad \text{at} \quad r = r_w. \qquad (4.53)$$

At an axis of symmetry having coordinate $r = 0$, the velocity boundary condition is given by

$$\frac{dw}{dr} = 0, \qquad \text{at} \quad r = 0. \qquad (4.54)$$

To solve the elliptic temperature equation (4.52) two temperature conditions are needed in the boundary points. At a fixed wall the temperature boundary condition may be prescribed by a Dirichlet condition

$$T = T_0, \qquad \text{at} \quad r = r_{\text{w}}, \tag{4.55}$$

a Neumann boundary condition

$$\kappa_{rr} \frac{dT}{dr} = Q_0, \qquad \text{at} \quad r = r_{\text{w}}, \tag{4.56}$$

or a Robin boundary condition

$$\kappa_{rr} \frac{dT}{dr} + \beta_1 T = Q_1, \qquad \text{at} \quad r = r_{\text{w}}. \tag{4.57}$$

At an axis of symmetry having coordinate $r = 0$ the temperature boundary condition is given by a vanishing normal heat flux, which reduces to

$$\frac{dT}{dr} = 0, \qquad \text{at} \quad r = 0, \tag{4.58}$$

because $\kappa_{rr} > 0$ due to the positive definiteness of the heat conduction tensor. To obtain a well-posed problem it is of course not allowed to impose two conditions of the Neumann type. Thus if there is an axis of symmetry, (4.56) cannot be imposed on the wall.

Numerical solution of the fully developed flow problem.

To solve the fully developed flow equations (4.49-4.52), each part between two finite element boundary points on an inflow or outflow boundary is divided into N subparts of equal distance. Usually $N = 4$ is sufficient. The system of equations, an algebraic equation for the shear rate and a differential equation for the temperature, is solved iteratively. The iteration process is as follows:

1. Start with a zero initial field for the shear rate and the temperature.

2. Calculate an iteration step. An iteration step $(i + 1)$ of the iteration process consists of the following two substeps, which are performed after each other:

   - Solve the temperature equation: $T^{i+1} = f(\dot{\gamma}^i, T^i, w^i, \mu^i)$.
     - Determine the particular solution of the temperature equation T^{p}.
     - Calculate the (total) temperature T by matching of the homogeneous solution T^{h} of the temperature equation to the boundary conditions.
   - Solve the nonlinear equations for the shear rate: $\dot{\gamma}^{i+1} = f(\dot{\gamma}^i, T^{i+1})$.

   If, at a certain point, the shear rate γ^i and the temperature T^i are known, the stress can be obtained by solving the nonlinear algebraic equation for the stress $(4.51)_1$, the velocity by integrating $(4.51)_2$ and the pressure from (4.50).

3. Repeat step (2) until the solution has converged: the difference between two subsequent shear rates and two subsequent particular solutions of the temperature in the iteration process must be small. For the equation for the shear rate $\max_j |\dot{\gamma}_j^{i+1} - \dot{\gamma}_j^i| < \epsilon \max_j |\dot{\gamma}_j^{i+1}|$ has to be fulfilled and for the temperature equation $\max_j |T_j^{\mathrm{p},i+1} - T_j^{\mathrm{p},i}| < \epsilon \max_j |T_j^{\mathrm{p},i+1}|$, where ϵ is a small parameter, usually $\mathcal{O}(10^{-4})$ or $\mathcal{O}(10^{-5})$, and j denotes the evaluation points.

During an iteration the temperature equation will be solved before the equation for the shear rate. After the first step of the first iteration the temperature then equals the homogeneous solution. This avoids problems with the shift factors due to a bad initial guess of the temperature. For the convergence criterion of the temperature equation the particular temperature T^{p} has been used instead of the (total) temperature T, because T^{p} vanishes in mechanical equilibrium. In the remaining part of this section a short description of the solution method of one iteration step is given. Again only axisymmetrical coordinates will be considered. However when Cartesian coordinates are used, the derivation is completely analogous.

The first part of the iteration step for the temperature consists of solving the axisymmetrical temperature equation (4.52) for any particular solution T^{p} that fulfils

$$\frac{d}{dr}\left(r\kappa_{rr}\frac{dT^{\mathrm{p}}}{dr}\right) = -r\dot{\gamma}\tau_{rz} + rT\alpha_\rho w\mu, \tag{4.59}$$

where the shear rate $\dot{\gamma}$, the shear stress τ_{rz}, the velocity w and the integration constant μ are obtained from the previous iteration step. To avoid convergence problems for strongly coupled problems, i.e. high Nahme–Griffith numbers, a relaxation factor is introduced as follows

$$(\kappa_{\mathrm{it}} + 1)\frac{d}{dr}\left(r\kappa_{rr}\frac{dT^{\mathrm{p},i+1}}{dr}\right) = -r\dot{\gamma}\tau_{rz} + rT^i\alpha_\rho w\mu + \kappa_{\mathrm{it}}\frac{d}{dr}\left(r\kappa_{rr}\frac{dT^{\mathrm{p},i}}{dr}\right), \tag{4.60}$$

where κ_{it} is a constant relaxation factor and the superscript i again denotes a quantity at the ith iteration. The iteration diffusivity equals now $\kappa_{\mathrm{it}}\kappa_{rr}$, which is only constant when the thermal conductivity κ_{rr} is independent of the temperature and the internal deformation tensor. For strongly coupled problems the iteration process must be slowed down to obtain a convergent solution method. Mostly a relaxation factor of $\kappa_{\mathrm{it}} = \mathcal{O}(10^{-1})$ or $\mathcal{O}(1)$ is sufficient. This means that the difference between two iteration steps may be small, even when the iteration process has not converged. Therefore an extra convergence criterion has been introduced, which takes into account the relaxation due to the iteration diffusivity. For a Picard iteration scheme van der Zanden (1989) has shown that the right truncation criterion is

$$\max_j |T_j^{\mathrm{p},i+1} - T_j^{\mathrm{p},i}| < \frac{1-L}{L}\epsilon \max_j |T_j^{\mathrm{p},i+1}|,$$
$$L \simeq \frac{\max_j |T_j^{\mathrm{p},i+1} - T_j^{\mathrm{p},i}|}{\max_j |T_j^{\mathrm{p},i} - T_j^{\mathrm{p},i-1}|}, \tag{4.61}$$

where ϵ is the same small parameter as for the case without an iteration diffusivity. For $L \simeq 1$ this criterion is much severe then the original truncation criterion for the temperature equation.

Integration of (4.60) yields

$$r\kappa_{rr}\frac{dT^{\mathrm{p},i+1}}{dr} = \frac{1}{\kappa_{\mathrm{it}}+1}\int_{r_1}^{r}\left(-r\dot{\gamma}\tau_{rz} + rT^i\alpha_\rho w\mu + \kappa_{\mathrm{it}}r\kappa_{rr}\frac{dT^{\mathrm{p},i}}{dr}\right)dr = f(r), \qquad (4.62)$$

which defines the function $f(r)$. Note that the integral on the right-hand side is $\mathcal{O}(r^2)$ at $r = r_1 = 0$, so that r^{-1} times the integral vanishes at $r = 0$. Integrating once more, gives the particular part of the temperature

$$-T^{\mathrm{p},i+1}(r) = \int_{r}^{r_2} f(r)dr = g(r), \qquad (4.63)$$

which defines the function $g(r)$. The integrations on the right-hand sides of equations (4.62) and (4.63) are computed numerically with the Simpson rule.

The second part of the iteration step for the temperature consists of the calculation of T^{h}, the solution of the homogeneous differential equation (equation (4.52) without source terms):

$$\frac{d}{dr}\left(\kappa_{rr}r\frac{dT}{dr}\right) = 0. \qquad (4.64)$$

After integration it follows

$$T^{\mathrm{h}}(r) = C_1\int_{r_1}^{r}(r\kappa_{rr})^{-1}dr + C_2. \qquad (4.65)$$

In case the perpendicular thermal conductivity κ_{rr} does not depend on the temperature or the internal deformation tensor, this reduces to the usual homogeneous temperature distribution $T^{\mathrm{h}}(r) = C_1\ln r + C_2$, or a constant temperature when a symmetry condition at $r = 0$ is imposed. Otherwise the integral in (4.65) has to be calculated numerically. The constants C_1 and C_2 have to be determined from the boundary conditions for the temperature.

For the example of a constant temperature at the inner wall, $T = T_1$ at $r = r_1 > 0$, and a Robin boundary condition at the outer wall, $\kappa_{rr}dT/dr + \beta_2 T = Q_2$ at $r = r_2$, the 2x2 system

$$\begin{aligned} T_1 &= T^{\mathrm{h}}(r_1) + T^{\mathrm{p}}(r_1) = C_2 - g(r_1), \\ Q_2 &= \left(\kappa_{rr}\frac{dT^{\mathrm{h}}}{dr} + \kappa_{rr}\frac{dT^{\mathrm{p}}}{dr}\right)_{r=r_2} + \beta_2\left(T^{\mathrm{h}}(r_2) + T^{\mathrm{p}}(r_2)\right) = \\ &\quad \frac{C_1}{r_2} + \frac{f(r_2)}{r_2} + \beta_2\left(C_1\int_{r_1}^{r_2}(r\kappa_{rr})^{-1}dr + C_2\right) \end{aligned} \qquad (4.66)$$

must be solved for C_1 and C_2. Substitution of these constants in the equation for the homogeneous temperature solution (4.65) and addition of the obtained particular solution (4.63) finally gives the total temperature field at iteration $(i+1)$.

In the second part of an iteration the equations of motion are solved together with the constitutive equations for the stress. The latter is simplified considerably, because for fully developed flows the differential equations for the internal deformation tensors reduce to algebraic relations. Details about the solution method for isothermal problems can be found in Hulsen (1988a). For

nonisothermal problems the solution method for the equations of motion and the stress constitutive equation remains the same, due to the decoupling of the system of equations. Only the relaxation times λ_k, the solvent viscosity η_s and the shear moduli G_k may depend on the temperature. They are calculated with the temperature T^{i+1} obtained in the first part of the iteration step.

Inflow boundary conditions.

At an inflow boundary the velocity, the temperature and the K internal deformation tensors have to be specified. For the velocity and the temperature the values in the nodal points are needed. For an internal deformation tensor the value is needed at arbitrary points on the boundary. Then the shear rate and the temperature are obtained from a linear interpolation of the surrounding boundary points. Next the initial value of the internal deformation tensor is calculated, with the help of this shear rate and temperature.

Outflow boundary conditions.

In principle it is possible to impose the Dirichlet boundary conditions of a fully developed flow at the outflow of a nonisothermal flow, as can be done for the isothermal calculations. However, if the Dirichlet boundary conditions at the outflow do not match with the flow, large wiggles may arise near the outflow. For nonisothermal flows with high Péclet numbers, very long exit lengths would be required, before the flow is fully developed. On its turn this would lead to long computation times and would require a large memory capacity. To avoid these problems fully developed natural boundary conditions, instead of fully developed Dirichlet boundary conditions, are imposed at the outflow for the equations of motion and the temperature equation. Natural boundary conditions are not explicitly satisfied by the solution, so there is more freedom to adapt to a boundary condition that does not correspond to the flow in the neighbourhood of the boundary.

For viscoelastic fluids, however, the fully developed natural boundary conditions are not as straightforward as for viscous fluids. For the equations of motion of viscous fluids a constant pressure and a vanishing tangential velocity correspond to the fully developed flow boundary condition. For the temperature equation a vanishing normal heat flux $\phi_{q,n} = \underline{n} \cdot \underline{\phi}_q = 0$, which equals $\underline{n} \cdot \nabla T = 0$, corresponds to the fully developed Dirichlet boundary condition. For viscoelastic fluids, however, these natural boundary conditions would still lead to large wiggles. A constant pressure does not correspond to a fully developed flow, because viscoelastic fluids have normal stresses in a fully developed simple shear flow. Thus for viscoelastic fluids an approximation of the normal stress $\sigma_n = \underline{n} \cdot \underline{\underline{\sigma}} \cdot \underline{n}$ along the outflow boundary is needed.

The idea is now that the velocity is already close to its fully developed profile, or at least develops much quicker than the temperature, while the temperature might be far from its fully developed profile. Because the stress is a strong function of the temperature, the normal stress at the outflow is then not close to the fully developed normal stress. For this, the approximation of the normal stress at the outflow is calculated with the help of the temperature obtained from solving the temperature equation (4.34), with the natural temperature boundary condition, and the fully developed shear rate which corresponds to this temperature distribution. For a viscoelastic fluid with anisotropic heat conduction a vanishing normal heat flux $\underline{\phi}_{q,n} = 0$ does not correspond to the fully developed Dirichlet boundary condition as well. For convenience it

will be assumed now that the normal direction corresponds to the z-direction and the tangential direction to the r-direction. For a fully developed flow, $T = T(r)$ and thus $\partial T/\partial z = 0$, the shear component of the heat conduction tensor then gives a contribution to the heat flux in the normal direction: $\underline{\phi}_{q,n} = \kappa_{rz}\partial T/\partial r$. For isotropic heat conduction this term vanishes. For anisotropic heat conduction an approximation of this term on the outflow boundary is needed.

If the cooling due to thermal expansion is taken into account the boundary integral for the temperature equation also contains a contribution of the pressure term given in (4.16). Then also an approximation of the pressure at the outflow is needed. Therefore the same approximation as for the pressure in the normal stress will be taken.

To include the fully developed natural boundary conditions in the numerical process step 2 of the iteration process outlined in the beginning of this chapter is modified as follows:

1. Solve the fully developed flow equation for the shear rate at the outflow (4.49-4.51) with the temperature in (4.51) obtained from a former iteration of step 4. Because the number of evaluation points is larger than the number of nodal points on the boundary of a finite element the nodal point temperatures have to be interpolated. The temperature in the evaluation points are obtained by a linear interpolation of the temperatures at the two neighbouring nodal points on the outflow boundary. From the obtained shear rate and the temperature from step 4 the approximation of the normal stress $\sigma_n = -p + \sum_{k=1}^{K} \tau_{k,n}$ is calculated in the nodal points at the outflow. A mode of the normal component of a modal stress is defined as $\tau_{k,n} = \underline{n} \cdot \underline{\underline{\tau}}_k \cdot \underline{n}$, which equals $\tau_{k,n} = \tau_{k,zz}$ for an axisymmetrical flow. For a fluid with anisotropic heat conduction also an approximation of the normal heat flux $\underline{\phi}_{q,n}$ is calculated from the obtained shear rate and the temperature from step 4. For a fully developed axisymmetrical flow the normal heat flux is $\underline{\phi}_{q,n} = \kappa_{rz}dT/dr$. Unfortunately it is not possible to give a good approximation of dT/dr, independent of the interior values. Therefore the temperature derivative at the interior will be taken as an approximation. If the cooling due to thermal expansion is taken into account the integrand $T\alpha_{\rho}p\underline{n} \cdot \underline{v}$ has to be evaluated. The pressure is obtained in the same way as for the normal stress for the equations of motion. The normal velocity and the temperature are obtained from step 2 and 4 respectively.

2. Calculate the updated velocity, by solving the equations of motion with the normal stress σ_n obtained from step 1 and a vanishing tangential velocity as the outflow boundary conditions.

3. Update the pressure, if necessary.

4. Calculate the updated temperature, by solving the temperature equation with a vanishing heat flux in the normal direction as the outflow boundary condition (isotropic heat conduction) or with the obtained $\underline{\phi}_{q,n}$ from step 1 (anisotropic heat conduction).

5. Calculate the updated internal deformation tensors.

4.6   Conclusions

In this chapter a numerical method has been described to solve the system of equations, derived in chapter 2 for steady 2D Cartesian or axisymmetrical flows. The system of nonisothermal equations for viscoelastic fluid flows has been decoupled into three parts: the equations of motion, the temperature equation and the constitutive equations for the modal stresses. The decoupled system of equations has been solve iteratively. For the elliptic part a finite element method has been used, for the hyperbolic part a streamline integration method.

In fact, the implementation of the equations of motion and the stress constitutive equations is analogous to the numerical implementation described by Hulsen & van der Zanden (1991), with some small modifications for the temperature dependent coefficients. For the equations of motion the standard Galerkin method has been used. The pressure has been eliminated with the help of the balance of mass for incompressible flows. The differential equations for the internal deformation tensors are solved by a streamline integration method.

For the temperature equation the attention has been focused on two subjects. Firstly, the implementation of an upwind method has been discussed. This is necessary to avoid extreme mesh refinement for flows with high Péclet numbers. Secondly, a special procedure has been developed to calculate the mechanical dissipation of viscoelastic fluids. Due to numerical errors, the internal deformation tensor may be indefinite. A straightforward calculation of the mechanical dissipation may then result in an unbounded mechanical dissipation.

Finally the boundary conditions have been given, with the emphasis on the fully developed Dirichlet boundary conditions at the inflow and the special Neumann boundary conditions at the outflow. Because nonisothermal flows are rarely fully developed at the outflow, Neumann boundary conditions are necessary to avoid large wiggles there. Due to the normal stresses of the viscoelastic fluids in simple shear flows, the usual Newtonian fully developed Neumann conditions are also not sufficient to avoid the wiggles. Therefore the normal stress at the outflow has been approximated by a special procedure based on the fully developed flow.

Chapter 5

Numerical calculations

The algorithm described in chapter 4 to solve the equations of motion, the temperature equation and the constitutive equation for the stress (2.156), has been implemented in the computer program for isothermal viscoelastic flows described by Hulsen (1990a). In the future the code will be available in the Sepran package (Segal 1984) as part of the Viscel extension described by van der Zanden (1990).

Section 5.1 contains an overview of the fluid parameters that will be used for the computations. The computations have been performed for two viscoelastic fluids. For one of them, low density polyethylene, the influence of the temperature on the viscosities and relaxation times is relatively small and for the other one, polystyrene, the influence is large. For these fluids three different types of flows will be studied. Firstly a fully developed shear flow will be examined in section 5.2, to gain insight into the behaviour of the system of equations. For a fully developed shear flow the equations simplify considerably, because almost all material derivatives vanish. Next a more difficult problem will be discussed in section 5.3: a straight pipe flow with a sudden temperature jump on the wall, a problem similar to the classical Graetz–Nusselt problem. Finally the flow through a 4:1 contraction, which has a sudden jump of the radius of the pipe, will be examined in section 5.4, with and without cooling of the outflow. For both fluids the influence of the following issues will be examined numerically: the cooling due to the thermal expansion term, the anisotropy of the heat conduction tensor, the temperature dependence of the shear modulus, and the use of the stress work or the mechanical dissipation. All computations have been performed on a HP9000-735 computer with a Linpack speed of 40 Mflops.

5.1 Fluid parameters

For the calculations in this chapter two polymer melts will be used: low density polyethylene (LDPE) and polystyrene (PS). It is attractive to use these fluids because a lot of experimental data are available for them and they behave quite differently for nonisothermal flows. The only thing missing is a set of experimental data of the anisotropy of the heat conduction tensor. Only for a few fluids there are some reliable experimental data available in the literature. However, for these fluids no viscoelastic data were available.

For the polyethylene melt the LDPE melt I of the IUPAC workshop will be taken. An overview of experimental data, such as the shear viscosity and the first normal stress difference, has been given by Bird et al. (1987a). They also show that the data may be fitted with an eight-mode Giesekus model. Bush (1989) showed that the LDPE melt may also be described by a seven-mode modified Leonov model. To obtain a reasonable fit of the elongational viscosity Bush gives $\alpha_k = 3$ and $\beta_k = 4$ for all modes $k = 1, \ldots, K$. The differential equations describing

these models can be found in appendix A.

In chapter 3 it has been shown that the Leonov models are more convenient than the Giesekus model, because the latter has no positive lower bound for the determinant of the internal deformation tensor. This suggests that the modified Leonov model will be the best choice for the simulations. However, the parameters $\alpha_k = 3$ and $\beta_k = 4$, as determined by Bush, give large wiggles in the shear viscosity, the first normal stress coefficient and the elongational viscosity, see appendix C. For this reason the Giesekus model will be taken.

The modal viscosities and the modal relaxation times of the eight-mode Giesekus model for the LDPE melt are presented in table 5.1. The temperature dependence of the relaxation time can be described by an Andrade shift factor (2.124). The shift constants and the other temperature dependences of the parameters are given by Bird et al. (1987a) and have been summarised in table 5.2. The zero-shear-rate viscosity at a reference temperature of $T_{\mathrm{ref}} = 423$ K is $\eta_{0,\mathrm{ref}} = 5.105 \cdot 10^4$ Pa·s. The mean relaxation time at the reference temperature is $\lambda_{0,\mathrm{ref}} = 5.875 \cdot 10^1$ s. Figures 5.1, 5.2 and 5.3 show the model predictions of the shear viscosity η, the first normal stress coefficient Ψ_1 and the elongation viscosity η_E as function of the shear and elongation rate for different temperatures. These quantities have been calculated with the viscoelastic parameters given in table 5.1 and the Andrade shift parameters in table 5.2. Note that the slope of the shear viscosity equals $\partial\eta/\partial\dot\gamma = -1$ for large shear rates, because $\tau_{rz,k}$ approaches a constant value for the Giesekus model. The constant value depends on the dimensional parameter α_k as given by (3.44).

Table 5.1: Viscoelastic properties of LDPE at $T = 423$ K. Successively the mode number, the modal viscosity, the modal relaxation time and the non-dimensional parameter α_k are given. The data are from Bird et al. (1987a).

k	$\eta_k(\mathrm{Pa\cdot s})$	$\lambda_k(\mathrm{s})$	α_k
1	$1.00 \cdot 10^3$	10^3	0.03
2	$1.80 \cdot 10^4$	10^2	0.05
3	$1.89 \cdot 10^4$	10^1	0.2
4	$9.80 \cdot 10^3$	10^0	0.5
5	$2.67 \cdot 10^3$	10^{-1}	0.4
6	$5.86 \cdot 10^2$	10^{-2}	0.3
7	$9.48 \cdot 10^1$	10^{-3}	0.2
8	$1.29 \cdot 10^1$	10^{-4}	0.1

Table 5.2: Thermal properties of LDPE at $T = 423$ K. Successively the density, the linear thermal expansion coefficient, the heat capacity and its temperature dependence, the thermal conductivity in equilibrium and the shift constant for the Andrade shift factor are given. The data have been obtained from Bird et al. (1987a).

ρ_{ref}	$7.80 \cdot 10^2$	kg·m^{-3}
α_ρ	$7.02 \cdot 10^{-4}$	K^{-1}
$c_{p,\tau_e,\mathrm{ref}}^{\mathrm{eq}}$	$2.54 \cdot 10^3$	J·kg^{-1}·K^{-1}
α_c	$1.00 \cdot 10^{-3}$	K^{-1}
$\kappa_{\mathrm{eq,ref}}$	$2.41 \cdot 10^{-1}$	W·m^{-1}·K^{-1}
T_{ref}	$4.23 \cdot 10^2$	K
C_1	$1.95 \cdot 10^3$	K

Table 5.3: Heat conduction constants of LDPE in (W·m^{-1}·K^{-1}) for all modes k.

κ_0	$8.92 \cdot 10^{-2}$
$\kappa_{1,k}$	$2.17 \cdot 10^{-2}$
$\kappa_{2,k}$	0

Above the melting temperature T_{m} no detailed measurements of the anisotropy of the heat conduction tensor for LDPE are available in the literature. Measurements of Wallace et al. (1985) at $T_{\mathrm{ref}} = 433$ K showed that the perpendicular thermal conductivity of some HDPE melt
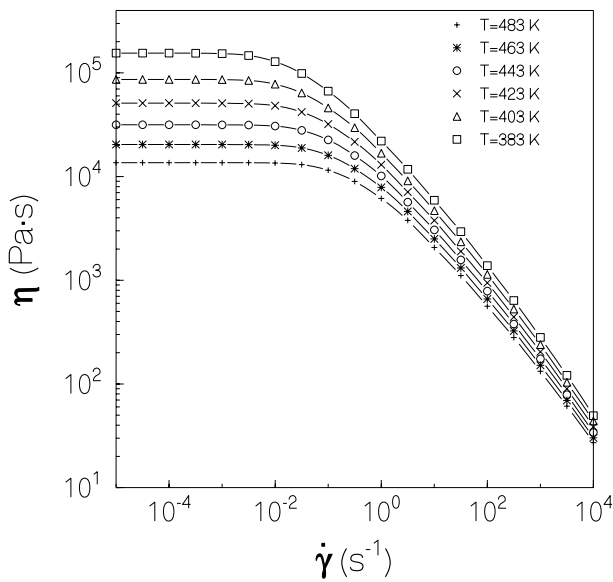
Figure 5.1: Model predictions of the Giesekus model, with parameters described in the tables 5.1 and 5.2, for the shear viscosity η of LDPE as a function of the shear rate for different temperatures.
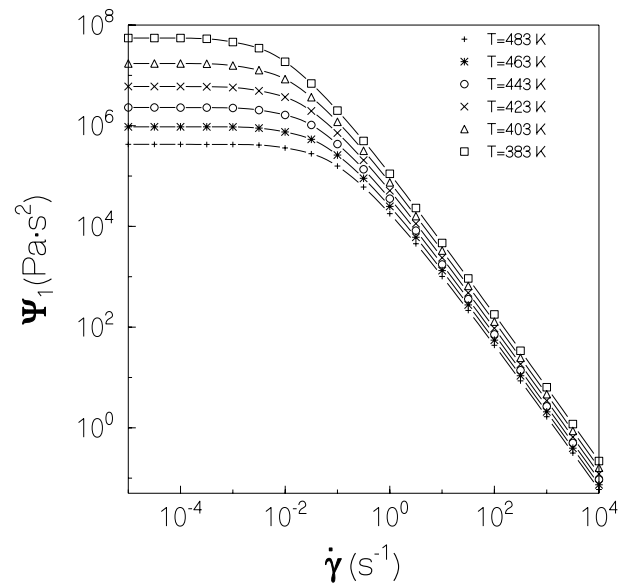

Figure 5.2: Model predictions of the Giesekus model, with parameters described in the tables 5.1 and 5.2, for the first normal stress coefficient Ψ_1 of LDPE as a function of the shear rate for different temperatures.
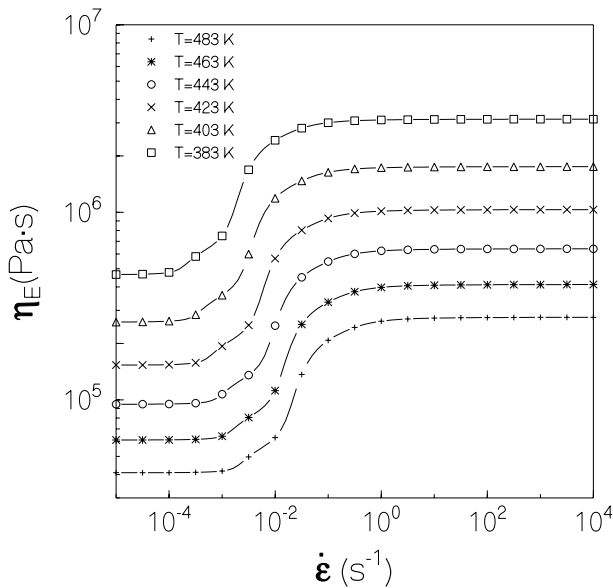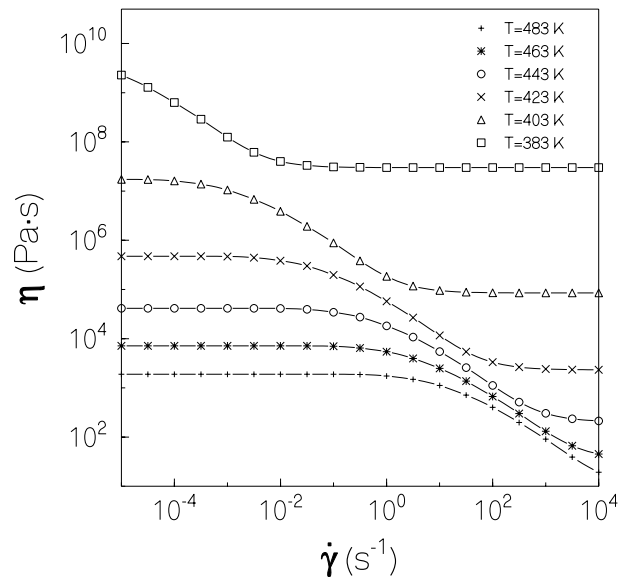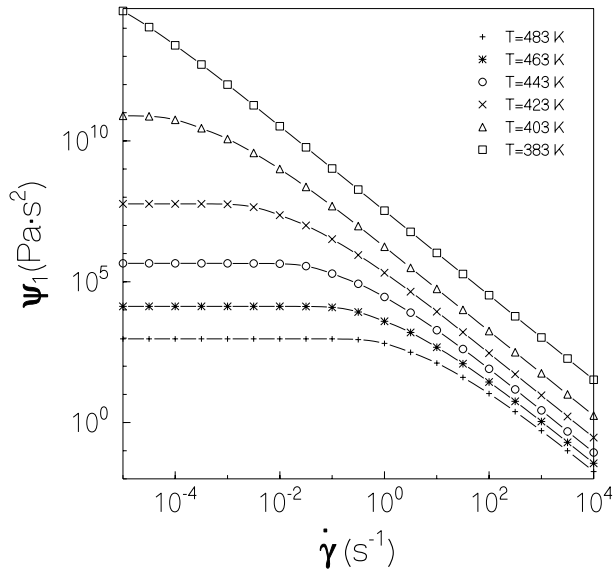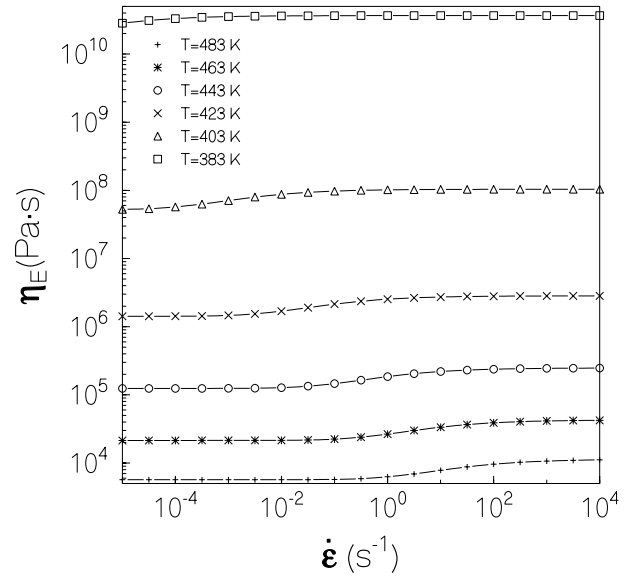

Figure 5.3: Model predictions of the Giesekus model, with parameters described in the tables 5.1 and 5.2, for the elongation viscosity η_E of LDPE as a function of the elongation rate for different temperatures.

Figure 5.4: Model predictions of the Leonov model, with parameters described in the tables 5.4 and 5.5, for the shear viscosity η of PS as a function of the shear rate for different temperatures.

decreases asymptotically until about $40\,\%$ of the equilibrium thermal conductivity. Measurements of Choy & Luk (1978) below the melting temperature T_{m} showed that the perpendicular thermal conductivity of some HDPE melt is about $30-40\,\%$ of the thermal conductivity in equilibrium. For some LDPE melt the decrease of the $\kappa_\perp$ is of the same order. It will be

Figure 5.5: Model predictions of the Leonov model, with parameters described in the tables 5.4 and 5.5, for the first normal stress coefficient Ψ_1 of PS as a function of the shear rate for different temperatures.

Figure 5.6: Model predictions of the Leonov model, with parameters described in the tables 5.4 and 5.5, for the elongation viscosity η_E of PS as a function of the elongation rate for different temperatures.

assumed that above T_{m} this decrease is of the same order. For the heat conduction constants $\kappa_{1,k} = 0.09 \cdot \kappa_{\mathrm{eq}}$ will be taken for all modes. The minimum perpendicular thermal conductivity is then $\kappa_0 = 0.28 \cdot \kappa_{\mathrm{eq}}$. The constants have been given in table 5.3.

For the polystyrene material Polystyrene 678E will be taken. The material parameters for PS 678E have been measured by Flaman (1990). The shear measurements could be fitted with a four-mode Leonov model, for which the viscoelastic properties have been summarised in table 5.4. The thermal properties have been given in table 5.5. The relaxation times and viscosities highly depend on the temperature, particularly in the region $T_{\mathrm{g}} < T < T_{\mathrm{g}} + 50$ K. The temperature dependence can be described by the WLF shift factor (2.123)[1]. The zero-shear-rate viscosity at the reference temperature $T_{\mathrm{ref}} = 463$ K is $\eta_{0,\mathrm{ref}} = 7.146 \cdot 10^3$ Pa·s. The mean relaxation time at the reference temperature is $\lambda_{0,\mathrm{ref}} = 9.32 \cdot 10^{-1}$ s. Figures 5.4, 5.5 and 5.6 show the model predictions of the shear viscosity η, the first normal stress coefficient Ψ_1 and the elongation viscosity η_E as function of the shear and elongation rate for different temperatures. These quantities have been calculated with the viscoelastic parameters given in table 5.4 and the WLF shift parameters in table 5.5. Although for the Leonov model a modal shear stress approximates a constant value, see equation (3.49), the total shear stress reaches a plateau. This is due to the non-zero Newtonian viscosity η_s.

For PS the density slightly decreases and the heat capacity slightly increases with increasing temperature. The thermal conductivity is practically constant for 373 K $< T <$ 473 K. For the anisotropy of the heat conduction tensor of polystyrene the only available experimental

---

[1]The WLF shift factors at the glass transition temperature given by Flaman are $T_{\mathrm{ref}} = T_{\mathrm{g}} = 373$ K, $C_1 = 12.64$ and $C_2 = 53.6$ K. With the help of the formulas $C_2^{\mathrm{ref}} = C_2^{\mathrm{g}} + T_{\mathrm{ref}} - T_{\mathrm{g}}$ and $C_1^{\mathrm{ref}} = C_1^{\mathrm{g}} C_2^{\mathrm{g}} / C_2^{\mathrm{ref}}$ the shift constants C_1^{ref} and C_2^{ref} at an arbitrary reference temperature may be obtained from the shift constants at the glass temperature C_1^{g} and C_2^{g} (see Tanner 1985).

Table 5.4: Viscoelastic properties of PS at $T = 463$ K. Successively the mode number, the modal viscosity and the modal relaxation time are given. The data are from Flaman (1990).

k	η_k(Pa·s)	λ_k(s)
s	$3.501 \cdot 10^1$	
1	$2.049 \cdot 10^3$	$2.68 \cdot 10^0$
2	$3.388 \cdot 10^3$	$3.28 \cdot 10^{-1}$
3	$1.422 \cdot 10^3$	$4.10 \cdot 10^{-2}$
4	$2.516 \cdot 10^2$	$4.46 \cdot 10^{-3}$

Table 5.5: Thermal properties of PS at $T = 463$ K. Successively the density, the linear thermal expansion coefficient, the heat capacity and its temperature dependence, the thermal conductivity in equilibrium and the shift constant for the WLF shift factor are given. The data have been obtained from Flaman (1990).

ρ_{ref}	$1.02 \cdot 10^3$	kg·m^{-3}
α_ρ	$5.13 \cdot 10^{-4}$	K^{-1}
$c_{p,\tau_e,\mathrm{ref}}^{\mathrm{eq}}$	$2.08 \cdot 10^3$	J·kg^{-1}·K^{-1}
α_c	$1.20 \cdot 10^{-3}$	K^{-1}
$\kappa_{\mathrm{eq,ref}}$	$1.7 \cdot 10^{-1}$	W·m^{-1}·K^{-1}
T_{ref}	$4.63 \cdot 10^2$	K
C_1	$4.178 \cdot 10^0$	
C_2	$1.436 \cdot 10^2$	K

Table 5.6: Heat conduction constants of PS in (W·m^{-1}·K^{-1}) for all modes k.

κ_0	$1.36 \cdot 10^{-2}$
$\kappa_{1,k}$	$8.50 \cdot 10^{-3}$
$\kappa_{2,k}$	0

data are given by Washo & Hansen (1969). Figure 2.2 shows that for a relative elongation of $\epsilon = 6$ the anisotropy is still small for polystyrene. Although this is a relatively small elongation ratio and it is not clear which part of the deformation corresponds to the elastic deformation, it seems not likely to assume that the anisotropy is large. For some other polymers the anisotropy is much larger for $\epsilon = 6$. Therefore $\kappa_{1,k} = 0.05 \cdot \kappa_{\mathrm{eq}}$ will be taken for all modal heat conduction constants. The minimum perpendicular thermal conductivity is then $\kappa_0 = 0.80 \cdot \kappa_{\mathrm{eq}}$. The constants have been summarised in table 5.6.

5.2 A fully developed pipe flow

To gain some insight into the importance of the different terms in the system of equations (2.156) the fully developed flow of a viscoelastic fluid will be examined. For this situation the system of equations simplifies considerably due to the fact that all material derivatives, except the pressure derivative, vanish. Because the material derivative of the internal deformation tensor vanishes, the mechanical dissipation also equals the stress work then. In section 4.5 it has been shown that the fully developed flow problem of viscoelastic fluids is described by (4.49-4.52).

The geometry of the flow is shown in figure 5.7. The boundary conditions on the centreline $r = 0$ are $dT/dr = 0$ for the temperature equation and $dw/dr = 0$ for the equations of motion. On the wall $r = R$ the no-slip boundary condition $w = 0$ is assumed to hold for the velocity. For the temperature boundary condition on the wall a Dirichlet condition $T = T_{\mathrm{w}}$ will be prescribed. In the simulations the wall temperature T_{w} is set at $T_{\mathrm{w}} = 423$ K and the tube
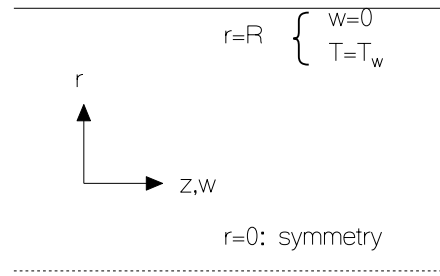
Figure 5.7: Flow geometry and boundary conditions for the fully developed axisymmetrical flow.

radius is taken to be $R = 0.02$ m. They have been chosen such that both viscoelastic and temperature effects are important.

For a given flow rate Q the behaviour of the velocity and temperature will be examined. The important dimensional numbers are the Deborah number De and the Brinkman number Br. For the reference temperature T_{ref} in these numbers the wall temperature will be taken. For the temperature difference in the Brinkman number the maximum temperature difference over the computation domain will be taken.

The iteration process is assumed to be converged if the difference between two subsequent solutions is small, as described in section 4.5. The convergence parameter has been taken $\epsilon = 10^{-4}$. To obtain a convergent solution method it is necessary to use the relaxation parameter introduced in (4.60), particularly for the polystyrene melt where $\kappa_{it} = 0.6$ was needed for the highest Deborah number.

The outline of the remaining part of this section is as follows. The starting point is a temperature equation with isotropic heat conduction, mechanical dissipation and shift factors for the viscosities and relaxation times. Successively the cooling due to the thermal expansion term, the anisotropy of the heat conduction tensor and the temperature dependence of the shear moduli G_k are added then to examine the influence of these terms. The velocity and temperature profiles will be given for some flow rates. The flow rates used and the corresponding Deborah number, the calculated maximum temperature difference, and the Brinkman number have been given in table 5.7 for the LDPE melt and in table 5.8 for PS.

5.2.1 Influence of the mechanical dissipation

In this subsection the fully developed flow equations with mechanical dissipation in the temperature equation and shift factors for the viscosities and relaxation times will be solved. Cooling due to the thermal expansion term, anisotropic heat conduction, and a temperature dependence of the modulus are neglected. In numerical simulations that have appeared in the literature these effects are often not taken into account.

Due to the high viscosity of polymers, which cause large stresses, the mechanical dissipation is often not negligible. Only for small shear rates it may be neglected. For increasing flow rate the mechanical dissipation becomes more and more important, because the Brinkman number increases quadratically with the mean velocity. On the other hand when the flow rate is increased, the viscosity decreases due to the shear thinning as well as the increase of the temperature. This may considerably slow down the temperature rise for increasing flow rate.

Table 5.7: Average velocity W in m·s^{-1}, Deborah number De, maximum temperature difference ΔT in K and Brinkman number Br for LDPE. For situation I only mechanical dissipation and isotropic heat conduction have been taken into account in the temperature equation and shift factors for the relaxation times and viscosities. For situation II the cooling due to the thermal expansion term has been added. For situation III the anisotropy of the heat conduction has also been taken into account. For situation IV the temperature dependence of the shear moduli has been added.

	W	$3.41 \cdot 10^{-5}$	$3.41 \cdot 10^{-4}$	$3.41 \cdot 10^{-3}$	$1.70 \cdot 10^{-2}$	$3.41 \cdot 10^{-2}$	$5.11 \cdot 10^{-2}$
	De	0.100	1.00	10.0	50.0	100	150
I	ΔT	$2.6 \cdot 10^{-4}$	$1.79 \cdot 10^{-2}$	$8.10 \cdot 10^{-1}$	7.54	23.7	40.2
	Br	0.94	1.37	3.03	8.15	10.3	13.7
II	ΔT	$1.0 \cdot 10^{-4}$	$6.74 \cdot 10^{-3}$	$3.02 \cdot 10^{-1}$	2.87	8.69	13.3
	Br	2.5	3.64	8.12	21.4	28.2	41.5
III	ΔT	$1.1 \cdot 10^{-4}$	$8.25 \cdot 10^{-3}$	$4.16 \cdot 10^{-1}$	4.27	13.6	21.7
	Br	2.2	2.97	5.88	14.4	18.0	25.4
IV	ΔT	$1.1 \cdot 10^{-4}$	$8.25 \cdot 10^{-3}$	$4.16 \cdot 10^{-1}$	4.27	13.6	21.4
	Br	2.2	2.97	5.88	14.4	18.0	25.8

Table 5.8: Average velocity W in m·s^{-1}, Deborah number De, maximum temperature difference ΔT in K and Brinkman number Br for PS. For situation I only mechanical dissipation and isotropic heat conduction have been taken into account in the temperature equation and shift factors for the relaxation times and viscosities. For situation II the cooling due to the thermal expansion term has been added. For situation III the anisotropy of the heat conduction has also been taken into account. For situation IV the temperature dependence of the shear moduli has been added.

	W	$3.24 \cdot 10^{-5}$	$3.24 \cdot 10^{-4}$	$3.24 \cdot 10^{-3}$	$1.62 \cdot 10^{-2}$	$3.24 \cdot 10^{-2}$	$4.85 \cdot 10^{-2}$
	De	0.100	1.00	10.0	50.0	100	150
I	ΔT	$2.53 \cdot 10^{-3}$	$1.40 \cdot 10^{-1}$	4.21	36.8	66.8	87.6
	Br	1.16	2.10	6.95	19.8	43.8	75.2
II	ΔT	$1.27 \cdot 10^{-3}$	$6.88 \cdot 10^{-2}$	1.98	18.6	41.6	57.3
	Br	2.30	4.25	14.8	39.2	70.3	115
III	ΔT	$1.28 \cdot 10^{-3}$	$7.24 \cdot 10^{-2}$	2.20	20.7	43.6	58.9
	Br	2.29	4.04	13.3	35.3	67.1	112
IV	ΔT	$1.17 \cdot 10^{-3}$	$6.66 \cdot 10^{-2}$	2.01	19.0	41.9	57.7
	Br	2.50	4.39	14.6	38.4	69.8	114

Near the wall τ_{rz} and $\dot{\gamma}$ are large, so that the mechanical dissipation may become large there. At the axis of symmetry the mechanical dissipation vanishes, because the shear rate is $\dot{\gamma} = 0$. Nevertheless, in the steady state the temperature rise near the axis of symmetry is larger than the temperature rise near the wall. This is caused by the redistribution of heat via the heat conduction term.

Although the equations are simplified considerably, they are still too difficult to solve analytically when the shift factors are taken into account. An analytic solution can be calculated for a Maxwell fluid with constant viscosity. For small temperature differences $a_T \simeq 1$ this gives

the following behaviour:

$$\frac{w}{W} = 2(1 - \frac{r^2}{R^2}),$$

$$T = \frac{\eta_{0,\text{ref}} W^2}{\kappa_{\text{eq}}} \left(1 - \frac{r^4}{R^4}\right) + T_{\text{w}},$$

$$W = \frac{Q}{\pi R^2}, \tag{5.1}$$

where W is the mean axial velocity and Q the flow rate. Equation (5.1) shows that the maximum of the temperature is on the axis of symmetry and the temperature decreases monotonically with increasing r. For small $\dot{\gamma}$ the viscoelastic fluid models in appendix A behave like a Maxwell fluid. The mechanical dissipation is small then, thus for low Deborah numbers it is expected that (5.1) is a good approximation.

Low density polyethylene

For LDPE the velocity and the temperature have been given in figure 5.8 for different values of the Deborah number. When the flow rate, or the Deborah number at the wall, is increased
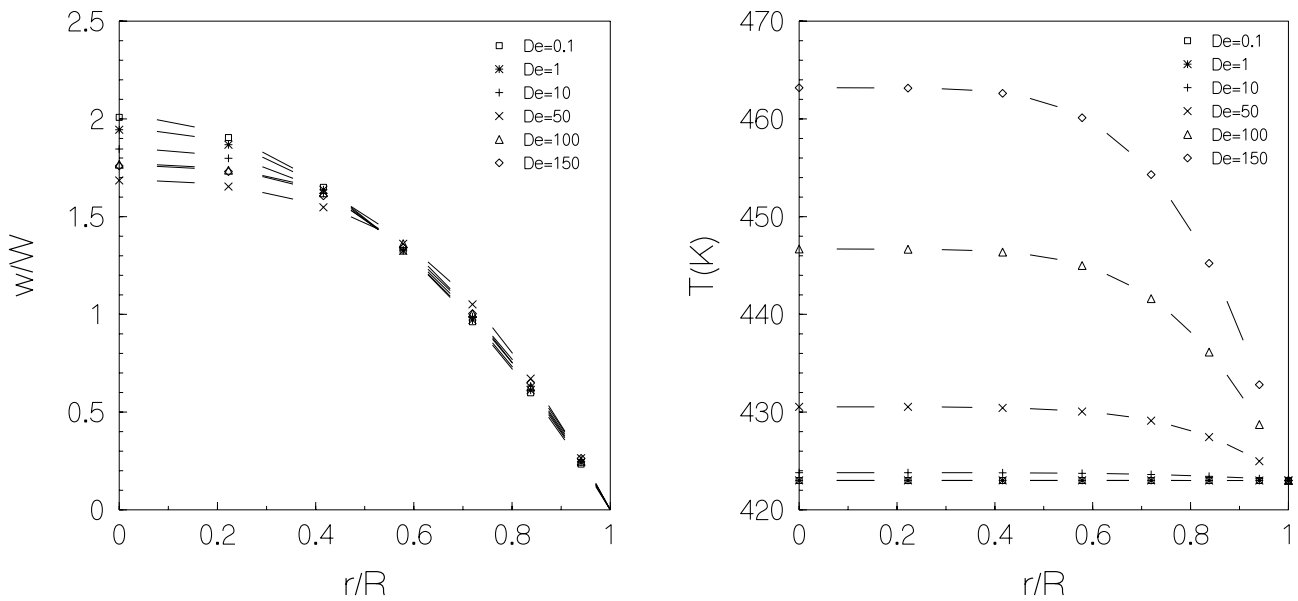
Figure 5.8: The non-dimensional velocity w/W and the temperature against the non-dimensional radius r/R of the LDPE melt for the different values of *De* of table 5.7. Only mechanical dissipation and isotropic heat conduction have been taken into account in the temperature equation.

there are two effects on the viscosity of the fluid. On the one hand the viscosity decreases due to the shear thinning of the fluid. This effect is large near the wall and small near the axis of symmetry. Due to this non-homogeneity the velocity profile shows a tendency to become more flat and on the centreline w/W will decrease. On the other hand the viscosity decreases due to the temperature rise. This effect is large near the centreline and small near the wall. Due to this non-homogeneity the velocity profile shows a tendency to become more steep and on the centreline w/W will increase. Due to the relatively small temperature dependence

of the relaxation times and viscosities, the influence of the temperature rise on the velocity profile is relatively small. For $De = 0.1$ the effect of shear thinning and the effect of the temperature on the viscosity are extremely small. Therefore the velocity profile almost equals the velocity of a Maxwellian fluid (5.1) for which $w/W = 2$ at the centreline. Figure 5.8 shows that for small Deborah numbers the shear thinning is dominant. The minimum of the non-dimensional velocity w/W on the centreline is approximately of $De = 50$. Then the decrease of the viscosity due to the temperature rise at the centreline becomes more important and w/W increases somewhat. The temperature profiles in figure 5.8 may roughly be divided into three parts: a plateau near the centreline, an almost linear part near the wall and a transition zone. For higher flow rates the plateau becomes smaller and the gradient at the wall increases.

Polystyrene

For PS the velocity and the temperature are given in figure 5.9 for different values of the Deborah number. The temperature dependence of the relaxation times and the viscosities for
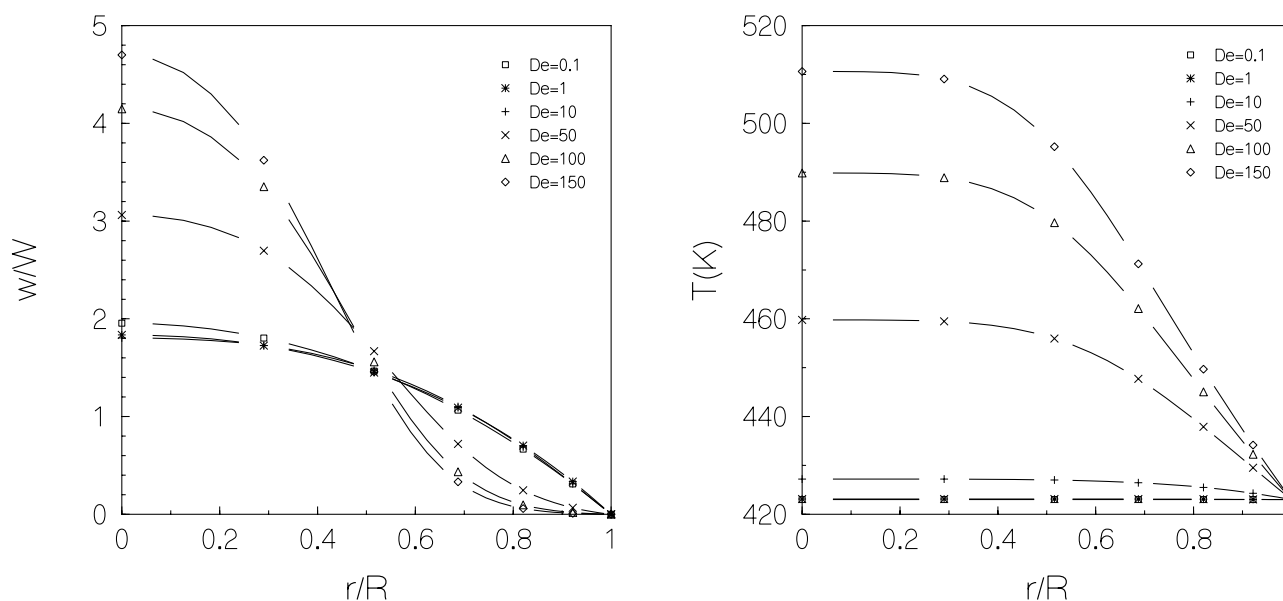
Figure 5.9: The non-dimensional velocity w/W and the temperature against the non-dimensional radius r/R of PS for the different values of De of table 5.8. Only mechanical dissipation and isotropic heat conduction have been taken into account in the temperature equation.

PS is much stronger than for LDPE. This results in completely different velocity profiles for the higher flow rates, see figure 5.9. For $De = 0.1$ the velocity profile almost equals the velocity of a Maxwellian fluid (5.1). For small flow rates the shear thinning is still dominant. However, the influence of the temperature becomes more and more dominant when the flow rate is increased. This results in a velocity ratio on the centreline of $w/W \simeq 4.8$ for $De = 150$. Near the wall the velocity decreases correspondingly. For $De = 150$ the flow almost stagnates in the region $0.8 < r/R < 1$. As for the LDPE melt, the temperature profiles for PS in 5.9 show a plateau near the centreline, a linear part near the wall and a transition zone. Compared to figure 5.8 the linear part near the wall is much larger, while both the plateau and the transition zone are smaller.

5.2.2   Influence of the thermal expansion term

In section 2.6 it has been noticed that although the cooling due to the thermal expansion term is relatively small compared to the mechanical dissipation, this term may not be neglected in shear flows. Contrary to the mechanical dissipation, which is small near the centreline and large near the wall, the cooling due to the thermal expansion term is large near the centreline and small near the wall. Dependent on the value of α_ρ the temperature profiles may change drastically when this term is taken into account. At the wall the velocity vanishes, thus there the thermal expansion term does not contribute to the temperature change. At the axis of symmetry the velocity w is relatively large and there the thermal expansion term will cause a decrease of the temperature, compared to the situation when only mechanical dissipation has been taken into account. It is possible to obtain an analytic solution when the viscosity is constant and $T = T_{\mathrm{w}}$ in the thermal expansion term. For the boundary conditions given in the beginning of this section the temperature becomes

$$T = \frac{\eta_{0,\mathrm{ref}} W^2}{\kappa_{\mathrm{eq}}} \left(1 - \frac{r^4}{R^4} - \alpha_\rho T_{\mathrm{w}} (1 - \frac{r^2}{R^2})(3 - \frac{r^2}{R^2}) \right) + T_{\mathrm{w}}, \tag{5.2}$$

where W is given by (5.1). The maximum temperature is no longer on the axis of symmetry, but at the non-dimensional coordinate $r/R = \sqrt{2\alpha_\rho T_{\mathrm{w}}/(1 + \alpha_\rho T_{\mathrm{w}})}$. The larger $\alpha_\rho T_{\mathrm{w}}$ the more the maximum will shift towards the wall. If $\alpha_\rho T_{\mathrm{w}} \geq 1$ the maximum is at the wall. For the LDPE melt ($\alpha_\rho = 7.02 \cdot 10^{-4}$ K^{-1}) the maximum is predicted at $r/R = 0.68$ and for PS ($\alpha_\rho = 5.13 \cdot 10^{-4}$ K^{-1}) the maximum is predicted at $r/R = 0.60$. The temperature at the centreline T_{ax} is

$$T_{\mathrm{ax}} - T_{\mathrm{w}} = \frac{\eta_{0,\mathrm{ref}} W^2}{\kappa_{\mathrm{eq}}} \left(1 - 3\alpha_\rho T_{\mathrm{w}} \right). \tag{5.3}$$

For $\alpha_\rho T_{\mathrm{w}} = 1/3$ the temperature at the centreline equals the temperature on the wall. For $\alpha_\rho T_{\mathrm{w}} > 1/3$ the temperature T_{ax} is even smaller than the wall temperature and the minimum temperature is at the axis of symmetry then. For the calculations the temperature will in general not be close to the temperature profile (5.2) due to the strong temperature dependence of $\eta_{0,\mathrm{ref}}$. Only for $T(r) \simeq T_{\mathrm{w}}$ it may be used as a first approximation.

Low density polyethylene

For the LDPE melt the velocity and the temperature are given in figure 5.10 for different values of the Deborah number. Figure 5.10 shows that the effects on the temperature profile are large. Not only the maximum temperature is much smaller, 25 K for the highest Deborah number, but it is also at a completely different position. For all the Deborah numbers the maximum is in the region $0.68 \leq r/R \leq 0.75$. On the centreline the temperature is close to the wall temperature. Only for $De = 150$ it is a little less. Nevertheless, the velocity profiles are almost equal to figure 5.8, where only the mechanical dissipation was taken into account in the temperature equation. Only for the high Deborah numbers the centreline velocity w/W is somewhat smaller.

Polystyrene

For PS the velocity and the temperature are given in figure 5.11 for different values of the Deborah number. As expected, the influence of the cooling due to the thermal term on the temperature profiles is less than for LDPE. The linear expansion coefficient of PS is about 35 % smaller than for LDPE. In figure 5.11 the difference between the maximum temperature and
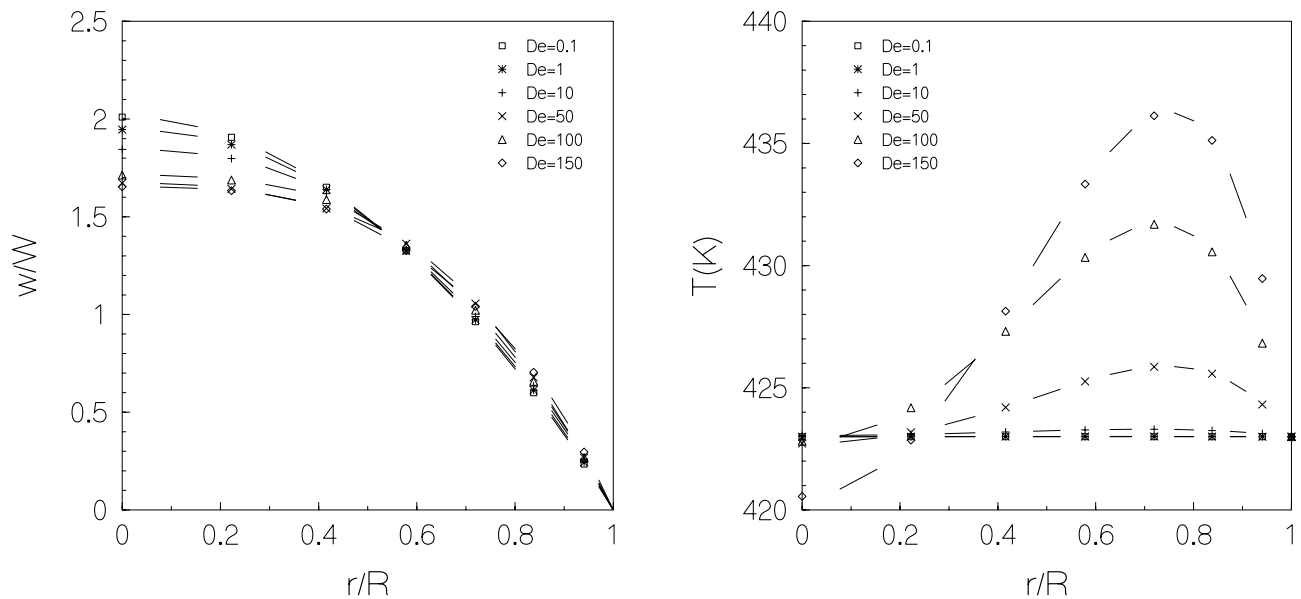
Figure 5.10: The non-dimensional velocity w/W and the temperature against the non-dimensional radius r/R of the LDPE melt for the different values of De of table 5.7. Mechanical dissipation, cooling due to the thermal expansion term and, isotropic heat conduction have been taken into account in the temperature equation.
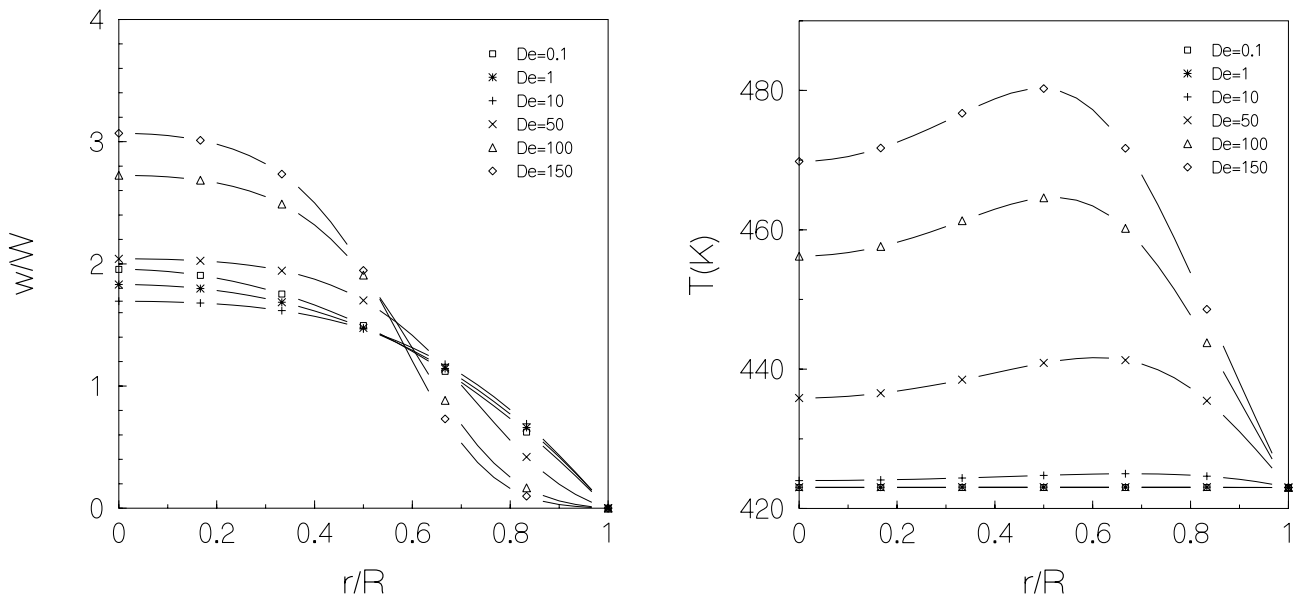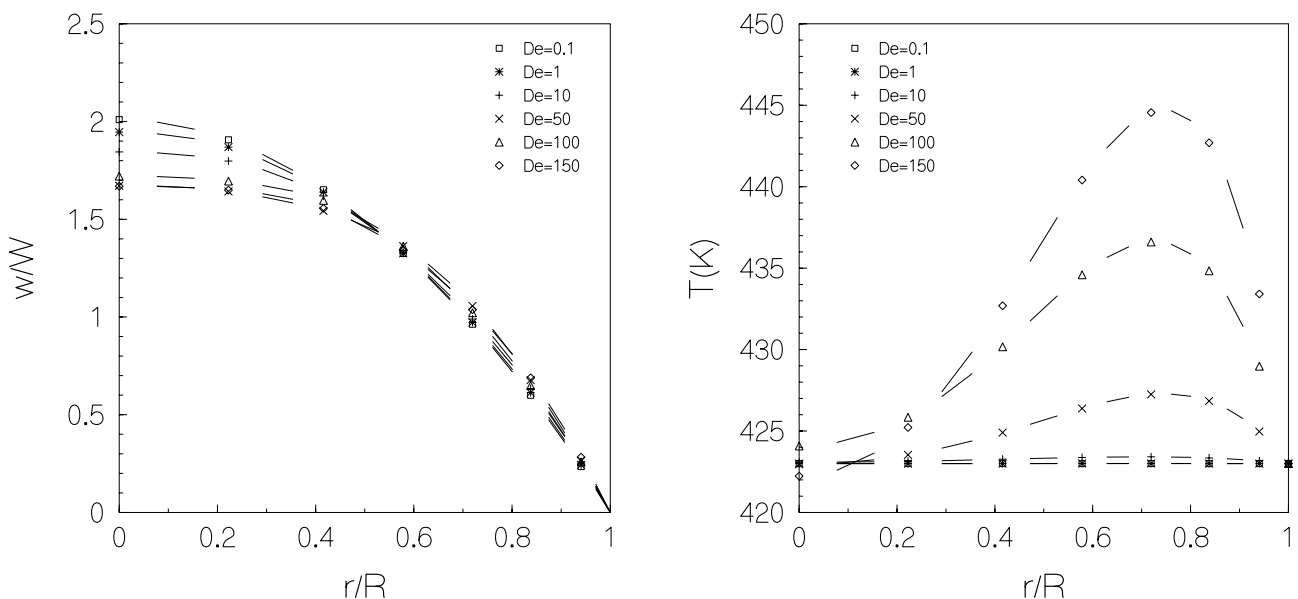

Figure 5.11: The non-dimensional velocity w/W and the temperature against the non-dimensional radius r/R of PS for the different values of De of table 5.8. Mechanical dissipation, cooling due to the thermal expansion term, and isotropic heat conduction have been taken into account in the temperature equation.

the temperature on the centreline is relatively small compared to the maximum temperature difference. Furthermore the maximum temperature is closer to the centreline. Dependent on the flow rate it is somewhere in the interval $0.5 < r/R < 0.65$. With increasing flow rate the maximum is closer to the axis of symmetry. Compared to figure 5.9, where the cooling due to the thermal expansion term was not taken into account, the temperature near the centreline

is much smaller: for the highest Deborah number about 40 K. However, near the wall the differences are small even for the large flow rates.

The influence of the temperature on the velocity profile is still large for the large flow rates. However, due to the smaller temperatures near the axis of symmetry, the centreline velocities are smaller than in figure 5.9. Particularly for the high Deborah numbers the effect is clear. On the centreline the non-dimensional velocity is $w/W \simeq 3$, compared to $w/W \simeq 4.8$ in figure 5.9, for the highest Deborah number. Because the shear stress and the shear viscosity have a fixed sign in a fully developed shear flow, the shear rate also has a fixed (negative) sign. Therefore the maximum velocity remains on the axis of symmetry, although the maximum temperature does not. The region near the wall where the flow stagnates is $0.9 < r/R < 1$, which is half of the length of the region in figure 5.9.

5.2.3   Influence of the anisotropic heat conduction

In section 2.4 it has been noticed that the anisotropy of the heat conduction tensor may be important. For a fully developed flow only the component perpendicular to the flow κ_{rr} appears in the temperature equation. In chapter 3 it has been shown that the model (2.113), in combination with the Giesekus or the Leonov model, is able to predict a lower perpendicular thermal conductivity when κ_0 and $\kappa_{1,k}$ are constants. The decrease of the parallel thermal conductivity of course leads to higher temperatures.

Low density polyethylene

For the LDPE melt the velocity and the temperature are given in figure 5.12 for different values of the Deborah number. On the axis of symmetry there is no decrease of the perpendicular ther-
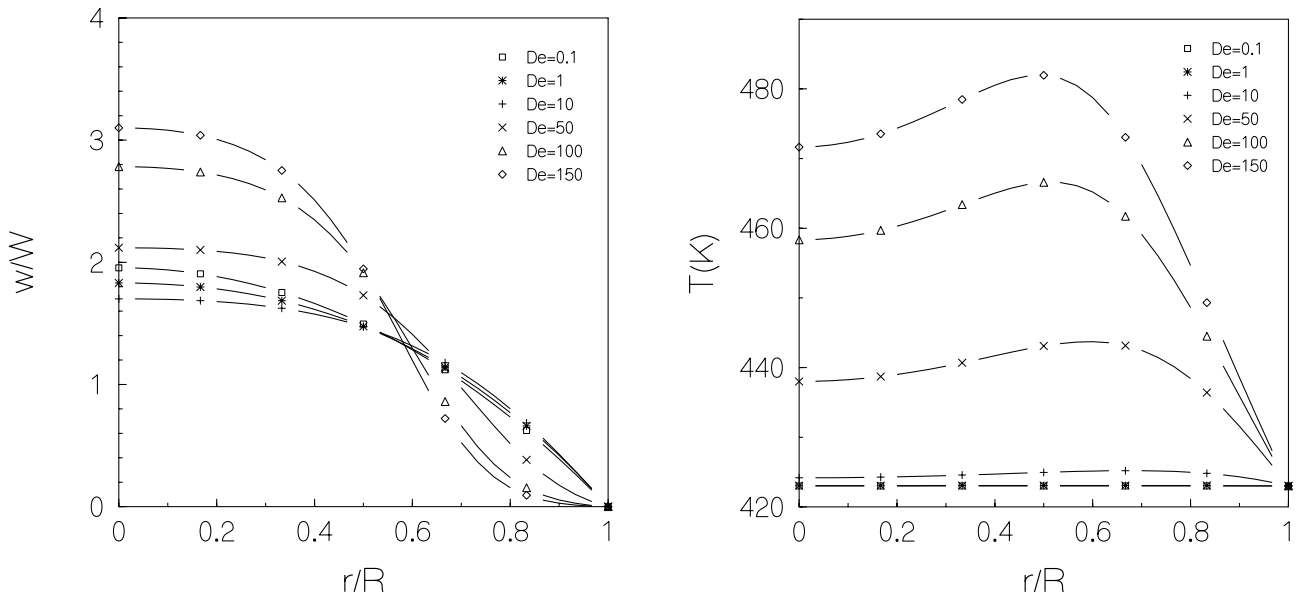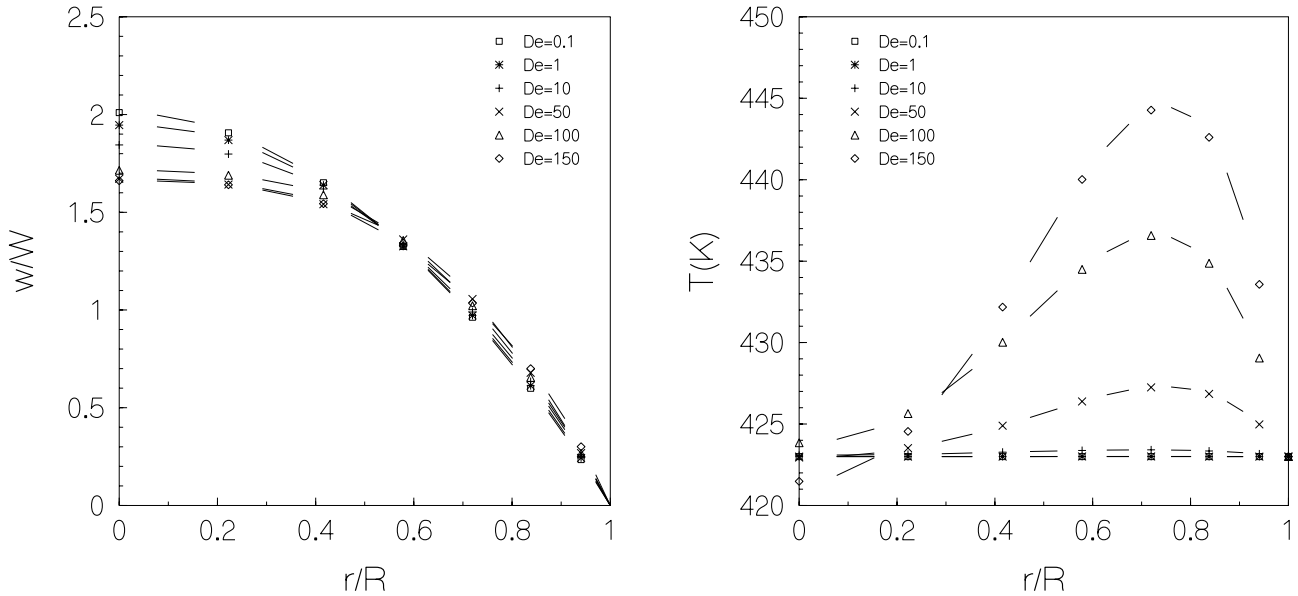

Figure 5.12: The non-dimensional velocity w/W and the temperature against the non-dimensional radius r/R of the LDPE melt for the different values of De of table 5.7. Mechanical dissipation, cooling due to the thermal expansion term, and anisotropic heat conduction have been taken into account in the temperature equation.

mal conductivity, because $b_{rr,k} = 1$. In the neighbourhood of the wall $b_{rr,k} < 1$ for the Giesekus model, thus the perpendicular thermal conductivity decreases there. Because of the smaller

conductivity less heat can be removed from the fluid which results in higher temperatures. The temperature profiles in figure 5.12 show that, compared to figure 5.2.2, the temperature rise is mainly near the temperature maximum: about 10 K for the highest flow rate. Close to the centreline the temperature rise is only 1 K. The increase of the temperature maximum has hardly any effect on the velocity profiles. The velocity profiles in figure 5.10 and figure 5.12 are almost identical.

Polystyrene

For PS the velocity and the temperature are given in figure 5.13 for different values of the Deborah number. For the three lowest Deborah numbers the velocity and the temperature do
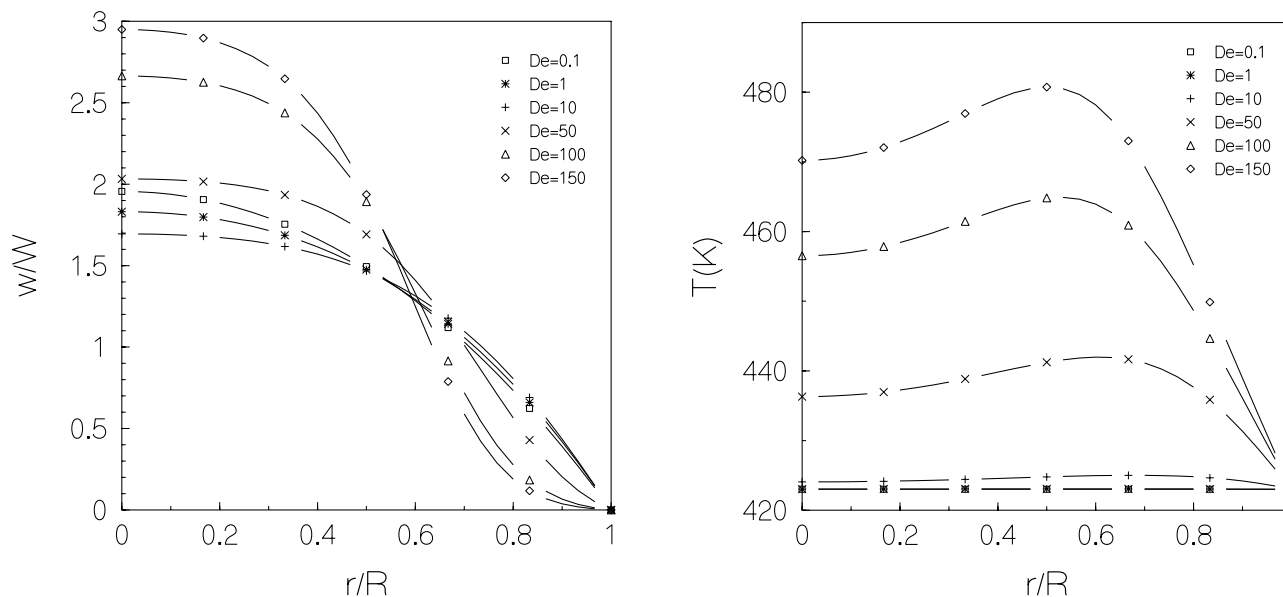

Figure 5.13: The non-dimensional velocity w/W and the temperature against the non-dimensional radius r/R of PS for the different values of De of table 5.8. Mechanical dissipation, cooling due to the thermal expansion term, and anisotropic heat conduction have been taken into account in the temperature equation.

not show any perceptible difference with figure 5.11. For the three highest Deborah numbers the temperature is somewhat higher compared to the temperature in figure 5.11. Left of the maximum the temperature difference is about $1-2$ K, right of the maximum it is between $0-1$ K. Because the temperature rise near the axis of symmetry is slightly larger, the velocity near the centreline increases slightly compared to figure 5.11.

5.2.4 Influence of the temperature dependence of the modulus

In section 2.6 it has been noticed that the influence of the temperature on the modulus is small and may often be neglected for the calculation of the stress in (2.19). Now it will be checked whether this is permissible. The density is assumed to be constant, so that (2.126) reduces to $G_k = G_{k,\text{ref}} T/T_{\text{ref}}$. If the temperature dependence of the density is also taken into account the influence of the temperature on the moduli is still smaller, because the density decreases with

increasing temperature.

Low density polyethylene

For the LDPE melt the velocity and the temperature are given in figure 5.14 for different values of the Deborah number. Figure 5.14 shows that the influence of the temperature dependence of

Figure 5.14: The non-dimensional velocity w/W and the temperature against the non-dimensional radius r/R of the LDPE melt for the different values of De of table 5.7. Besides the mechanical dissipation, the cooling due to the thermal expansion term and the anisotropic conduction, the temperature scaling of the modulus has been taken into account.

the modulus on the velocity and the temperature field is very small. Only the temperature profiles are a little different. On the left-hand side of the temperature maximum the temperatures are slightly smaller and on the right-hand side slightly larger compared to the temperature distributions in figure 5.12. However, even for the highest Deborah number the differences are smaller than 0.5 K. The velocity profiles are completely identical.

Polystyrene

For PS the velocity and the temperature are given in figure 5.15 for different values of the Deborah number. The influence is somewhat larger than for the LDPE melt. This is mainly caused by the difference in the wall temperature of 423 K and the reference temperature of 463 K. However, comparison of the temperature distributions in figure 5.15 and 5.13 shows that the differences are small (at most about 1.5 K for the highest Deborah number). Only on the right-hand side of the maximum the temperature is somewhat higher. The linear scaling of the shear modulus with the temperature decreases the viscosity for regions where the temperature is relatively low. For the high Deborah numbers the temperature differences in the flow are large. Then the velocity near the wall has slightly increased and the velocity near the centreline has slightly decreased compared to the velocity in figure 5.13.

Figure 5.15: The non-dimensional velocity w/W and the temperature against the non-dimensional radius r/R of PS for the different values of De of table 5.8. Besides the mechanical dissipation, the cooling due to the thermal expansion term and the anisotropic conduction, the temperature scaling of the modulus has been taken into account.

5.2.5 Comparison with the isothermal flow

In this section the results of the nonisothermal flows will be compared with the isothermal flow at the wall temperature $T_w = 423$ K. The isothermal flow will be denoted by situation 0, the nonisothermal flows by the situations I-IV of table 5.7 for LDPE and table 5.8 for PS.

Low density polyethylene

Comparison of the isothermal flow at 423 K with the situations I-IV of table 5.7 shows small differences, even for the higher Deborah numbers (flow rates). The maximum temperature and the pressure gradient $\partial p/\partial z$ have been depicted in figure 5.16. For the three lowest flow rates the temperature is still close to 423 K. Then there are no significant differences for the velocity, the stresses and the pressure gradient. For the three highest flow rates the temperature distribution differs considerably from the isothermal situation. However, the differences for the velocity, the stresses and the pressure are still relatively small. For the highest flow rate the stresses and pressure gradient of the nonisothermal flow with mechanical dissipation are about 10 % smaller than the isothermal flow. For the other nonisothermal flows the differences are smaller, because the temperature is lower then. For situation IV the differences are about 4 %. The velocity at the centreline differs slightly from the isothermal case, even for the highest flow rate. Then the difference is about 5 % for situation I. Otherwise the difference is less than 1 %.

Polystyrene

Comparison of the isothermal flow at 423 K with the situations I-IV of table 5.8 shows large differences for the higher Deborah numbers (flow rates). Particularly the stresses and the pressure gradients are much smaller for the nonisothermal flows. For the highest Deborah
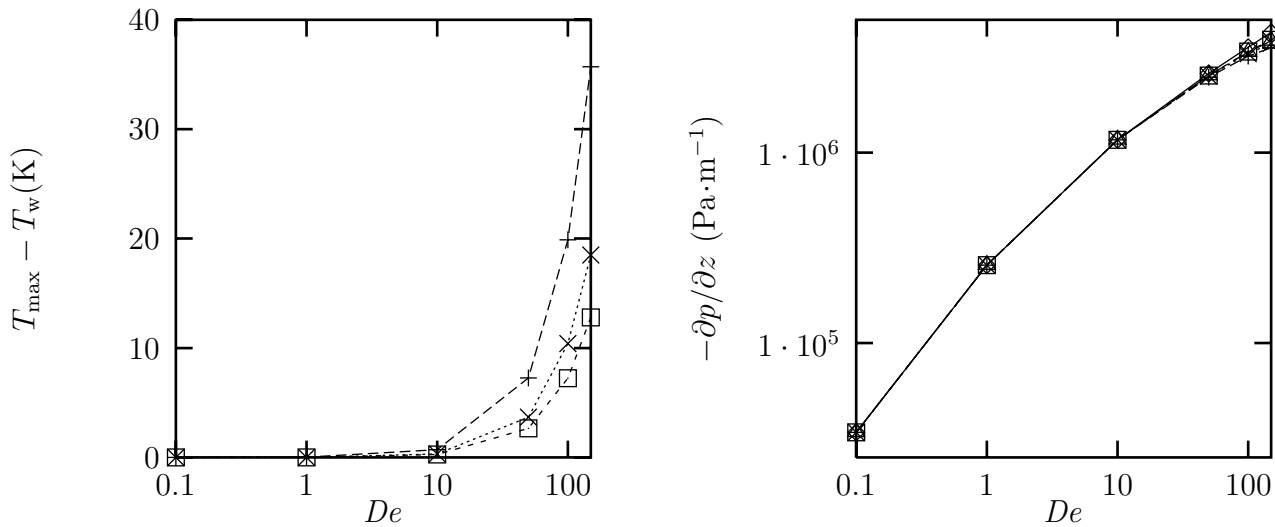
Figure 5.16: Maximum temperature $T_{\max}$ relative to the wall temperature T_{w} and pressure gradient $\partial p/\partial z$ for the fully developed flow of LDPE. $\diamond$ = Situation 0, $+$ = Situation I, $\square$ = Situation II, $\times$ = Situation III, $\triangle$ = Situation IV.

number the stresses and pressure gradients are about one decade lower. Figures 5.17, 5.18 and 5.19 also show that until $De \simeq 10$ the differences between the five situations are small.
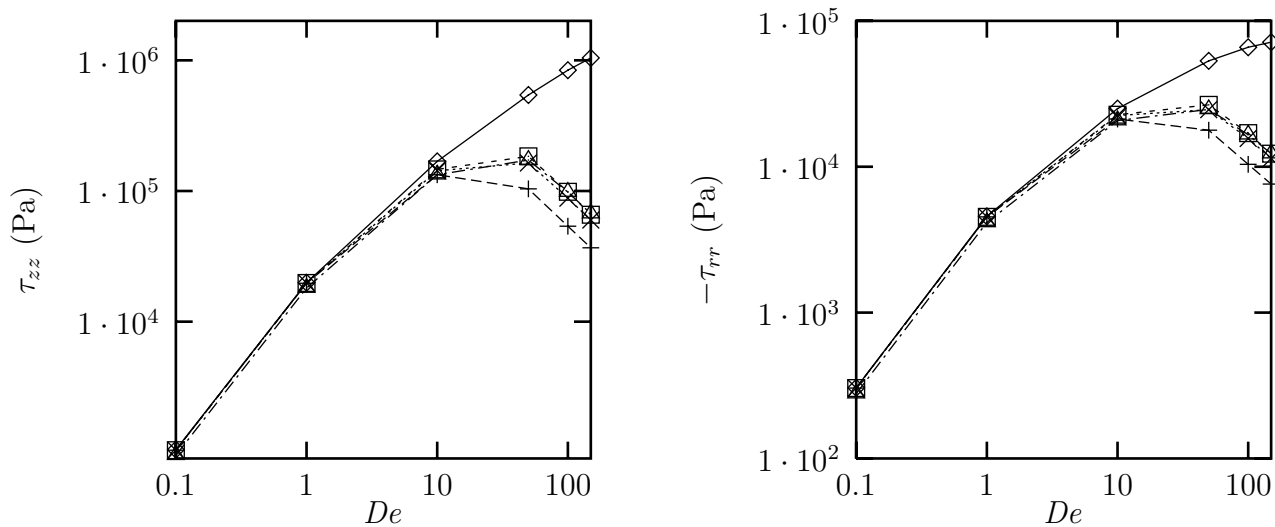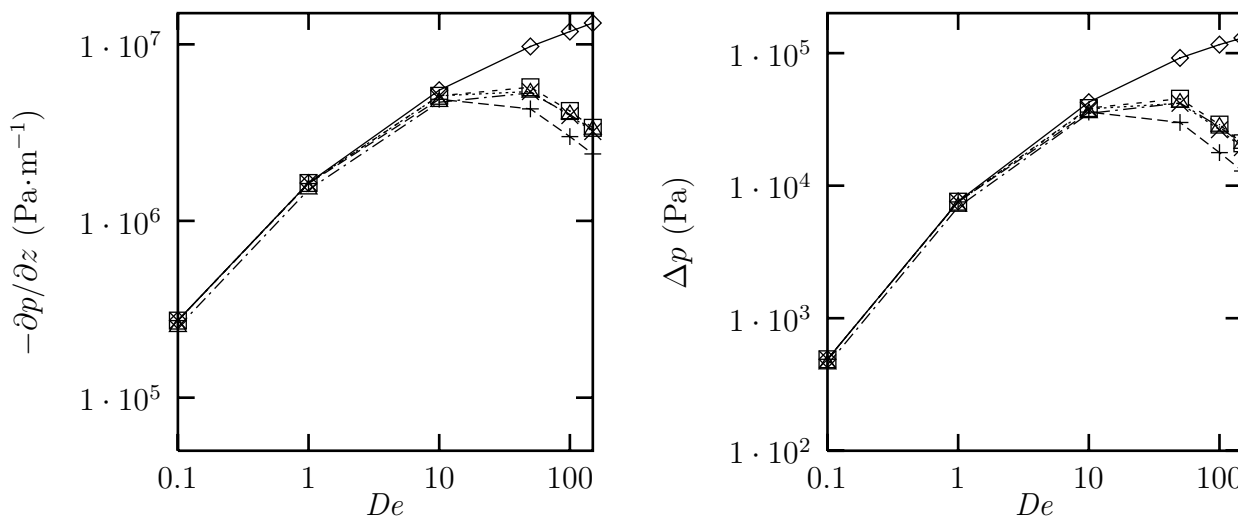

Figure 5.17: Normal stress τ_{zz} at the wall and normal stress τ_{rr} at the wall for the fully developed flow of PS. $\diamond$ = Situation 0, $+$ = Situation I, $\square$ = Situation II, $\times$ = Situation III, $\triangle$ = Situation IV.

This can easily be explained by examining figure 5.20, which shows that the temperature rise on the centreline, about $1-4$ K, and the maximum temperature rise, about $2-4$ K, are still relatively small then. For the three highest Deborah numbers the temperature rises are about $20-90$ K. These large temperature rises also causes a large increase of the relative velocity at the centreline, while it keeps decreasing for the isothermal flow.
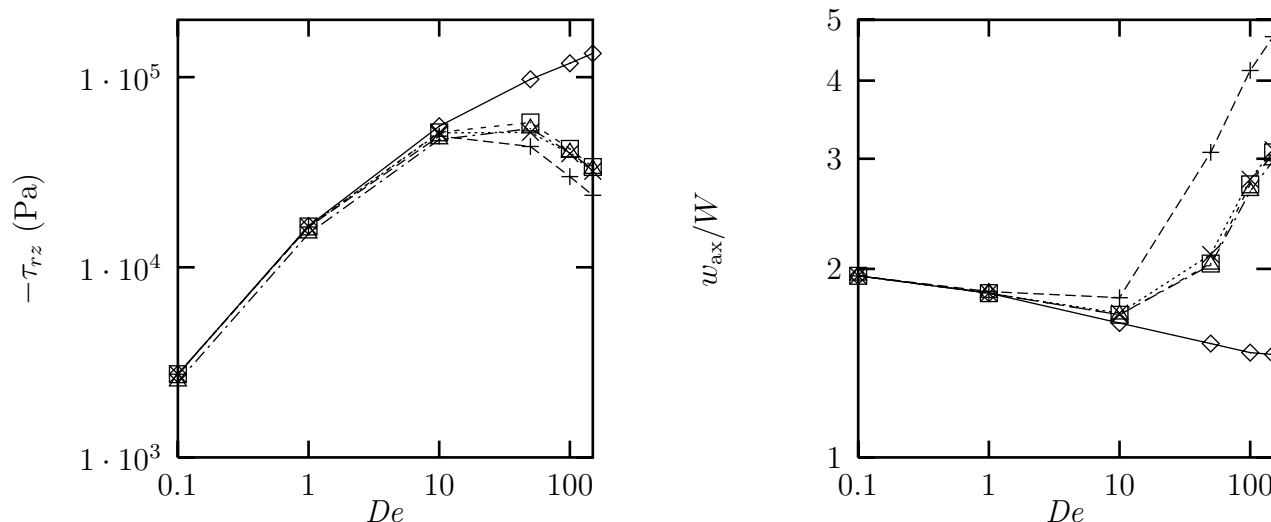
Figure 5.18: Shear stress τ_{rz} at the wall and normalised velocity w_{ax}/W at the axis of symmetry for the fully developed flow of PS. $\diamond$ = Situation 0, + = Situation I, $\square$ = Situation II, $\times$ = Situation III, $\triangle$ = Situation IV.

Figure 5.19: Pressure gradient $\partial p/\partial z$ and pressure difference Δp between the axis of symmetry and the wall for the fully developed flow of PS. $\diamond$ = Situation 0, + = Situation I, $\square$ = Situation II, $\times$ = Situation III, $\triangle$ = Situation IV.

Mutually the nonisothermal situations II, III and IV do not differ very much. However, the relatively high temperature for situation I, without the thermal expansion term, results in lower stresses and pressure gradients. Compared to the other nonisothermal flows they are a factor $1.5-2$ smaller. Due to the high temperatures near the centreline, the relative velocity on the centreline is also much larger for situation I than for the other nonisothermal situations.
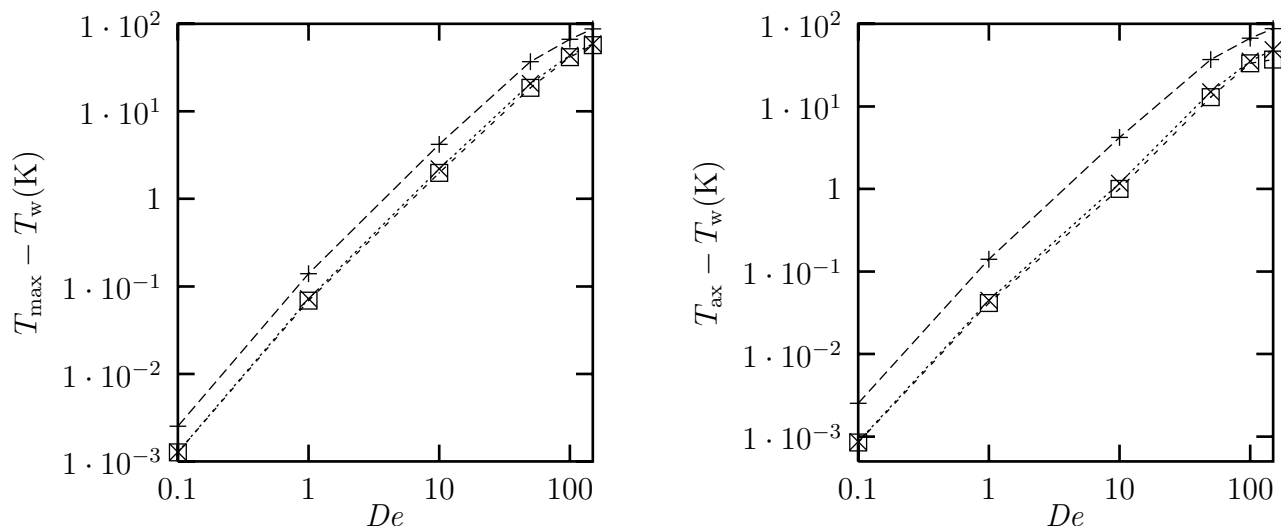
Figure 5.20: Maximum temperature $T_{\max}$ and temperature T_{ax} at $r = 0$ relative to the wall temperature T_{w} for the fully developed flow of PS. $+$ = Situation I, $\square$ = Situation II, $\times$ = Situation III, $\triangle$ = Situation IV.

5.3 A Graetz–Nusselt problem

To examine the influence of the wall cooling a variant of the Graetz–Nusselt problem will be discussed. The polymer melt flows in a pipe with a sudden temperature jump at the wall. It will be treated as an introductory example for the more difficult problem of a flow through a contraction with a temperature jump at the wall. To avoid phase changes and possible problems with the convergence of the solution method the cooling temperature at the wall has been taken well above T_{g} in the simulations. For the velocity it has been assumed that the no-slip boundary condition holds at the fixed wall. At the inflow fully developed Dirichlet boundary conditions have been imposed for the velocity, the modal stresses and the temperature. At the outflow fully developed Neumann boundary conditions have been imposed for the equations of motion and the temperature equation. Refer to section 4.5 for the details. The geometry of the flow has been depicted in figure 5.21. The inflow length has been taken $20\,R$ and the outflow length
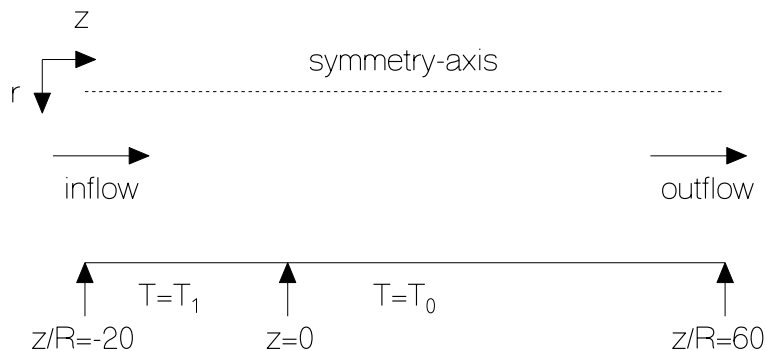
Figure 5.21: Flow geometry and temperature boundary conditions for the Graetz–Nusselt problem. The first part of the wall $-20 \leq z/R < 0$ has been kept at temperature T_1, the last part of the wall $0 \leq z/R \leq 60$ at temperature $T_0 < T_1$.

60 R, as in the isothermal computations for a 4:1 contraction of Hulsen & van der Zanden (1991). For the radius of the pipe $R = 5.0 \cdot 10^{-3}$ m has been taken. The part of the mesh near the temperature jump has been depicted in figure 5.22. Near the temperature jump at $z = 0$,
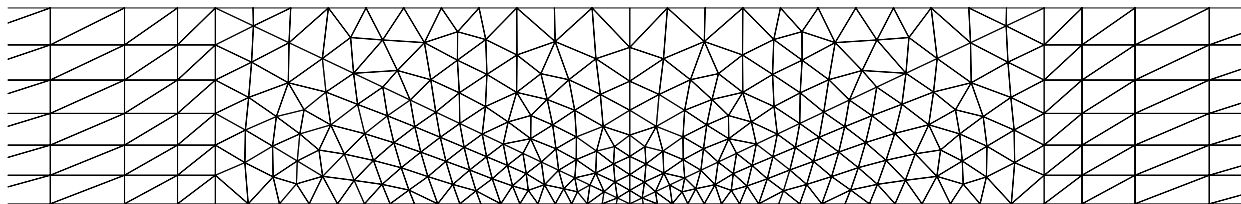

Figure 5.22: A part of the finite element mesh for the Graetz–Nusselt problem near the temperature jump: $-3 \leq z/R \leq 3$.

where the gradients are large, the mesh is relatively fine. Towards the inflow and the outflow the grid has been taken coarser, because the gradients are much smaller there.

For the fully developed flows the only non-dimensional numbers were the Deborah number and the Brinkman number. For the Graetz–Nusselt problem the convective terms do not vanish anymore in the equation of motion and the temperature equation. Due to the large viscosity of the polymers the Reynolds number Re does not play an important role in most problems. However, the convective term in the temperature equation is often dominant due to the large values of the density and the heat capacity for polymeric materials.

In section 5.2, describing the fully developed flows, it has been shown that for the polystyrene melt small temperature differences may result in large differences in the velocity and stress profiles. For LDPE, however, small temperature differences have hardly any effect on the velocity and stress profiles. Then, however, the anisotropy of the heat conduction tensor may play an important role. Therefore the following examples for polystyrene will be more focused on the influence of the temperature on the velocity and the examples for low density polyethylene on the anisotropy of the heat conduction tensor.

Polystyrene

For the polystyrene melt a Graetz–Nusselt problem will be considered, for which the temperature jump is $\Delta T = T_1 - T_0 = 40$ K, where $T_1 = 463$ K and $T_0 = 423$ K. The flow rate will be varied to examine the influence of the Deborah and Péclet number. The average velocities and the non-dimensional parameters for the simulations have been summarised in table 5.9. For the temperature difference in the Brinkman number the imposed temperature jump at

Table 5.9: Average velocity W in m·s^{-1}, Deborah number De, Péclet number Pe, Brinkman number Br and Reynolds number Re for PS.

W	$8.09 \cdot 10^{-6}$	$8.09 \cdot 10^{-5}$	$8.09 \cdot 10^{-4}$	$4.05 \cdot 10^{-3}$
De	0.100	1.00	10.0	50.0
Pe	$4.86 \cdot 10^{-1}$	4.86	$4.86 \cdot 10^{1}$	$2.43 \cdot 10^{2}$
Br	$4.57 \cdot 10^{-6}$	$4.57 \cdot 10^{-4}$	$4.57 \cdot 10^{-2}$	1.14
Re	$8.70 \cdot 10^{-11}$	$8.70 \cdot 10^{-10}$	$8.70 \cdot 10^{-9}$	$4.35 \cdot 10^{-8}$

the wall of $\Delta T = 40$ K has been taken. For these problems the Reynolds number is small:

$Re \leq 5 \cdot 10^{-8}$ for the highest flow rate. In the temperature equation the Péclet number does play an important role, due to the large value of the diffusivity $\rho c_{p,\tau_e}^{\text{eq}}/\kappa_{\text{eq}}$ for polystyrene. For the simulations the following contributions to the temperature equation have been taken into account: isotropic heat conduction, a constant shear modulus (i.e. entirely energy elastic) and the cooling due to the thermal expansion term. Due to the relatively small Brinkman numbers the mechanical dissipation and the cooling due to the thermal expansion term do not play an important role. When these terms are neglected, the temperature and velocity profiles do not change significantly.

During the calculations the following subjects came to light. For the highest flow rate the convergence becomes very slow. Until $\epsilon_{v,\text{res}} \simeq 4 \cdot 10^{-2}$ the convergence of the iteration process is good. The ratio of two residuals of two subsequent iteration steps is then somewhere between 0.5 and 0.9. Afterwards the ratio of two residuals of two subsequent iteration steps is about $0.990 - 0.998$. It is true that the convergence criteria for the equations of motion and the temperature equation $\epsilon_{v,\text{res}} = \epsilon_{T,\text{res}} = \epsilon_{v,\text{inc}} = \epsilon_{T,\text{inc}} = 10^{-3}$ could be achieved for the mesh depicted in figure 5.22, but the radial velocity and all stress components showed relatively large wiggles near $z = 0$. The wiggles for the axial velocity were somewhat smaller. Mesh refinement with a factor two solved this problem. If the mesh was refined once more, the results did not change significantly. The iteration process has been stopped when $\epsilon_{v,\text{res}} = \epsilon_{T,\text{res}} = \epsilon_{v,\text{inc}} = \epsilon_{T,\text{inc}} = 5 \cdot 10^{-3}$ was fulfilled. Except at the temperature jump the differences for the velocity, stress and temperature profiles were at most about 1 %. For the iteration viscosity $\eta_{\text{it}} = 2\eta_0$ and the extra viscosity $\eta_{\text{it}} = \eta_0 - \eta_s$, both at the temperature of the wall at the outflow section, have been taken in the equations of motion. Other values of these parameters did not give a better convergence of the solution method for the highest flow rate. An attempt to accelerate the convergence by taking the same temperature dependence as the modal viscosities η_k for $\eta_{\text{it}} = 2\eta_0(T)$ and $\eta_{co} = \eta_0(T) - \eta_s(T)$ failed. Contrary to a Newtonian fluid, where a temperature dependent η_{it} accelerated the convergence considerably, the method did not converge for viscoelastic fluids. For the temperature equation the SUPG method, see section 4.3, has been used to handle the large Péclet numbers. An iteration diffusivity of $\kappa_{\text{it}} = \kappa_{\text{eq}}$ for the three lowest flow rates and $\kappa_{\text{it}} = 2\kappa_{\text{eq}}$ for the highest flow rate has been used to slow down the iteration process. Then a value of $\kappa_{\text{it}} = \kappa_{\text{eq}}$ was insufficient to obtain a convergent solution method.

The temperature profiles for the various situations in table 5.9 have been given in figure 5.23. For the lowest flow rate, with $Pe = 4.86 \cdot 10^{-1}$ the diffusive transport of heat is dominant. Even upstream of the temperature jump the temperature decreases, particularly near the centreline. Just after the jump, at about $z/R = 2.5$ the temperature distribution is almost homogeneous again. For the flow rate with $Pe = 4.86$ the temperature decrease upstream of the jump is much smaller and it takes much longer (about $z/R = 9$) before the temperature distribution is almost homogeneous again. For the next flow rate this effect is still increased. Although the temperature differences at $z/R = 60$ are already relatively small for the flow rate with $Pe = 4.86 \cdot 10^1$, the convective transport is so large that the temperature distribution still differs from the fully developed profile. Upstream of $z = 0$ the temperature only decreases somewhat close to the wall. Near the centreline, where the velocity is large, the temperature decreases only for $z/R > 2$. For the highest flow rate the temperature at the outflow is far from its fully developed profile. At the centreline the temperature is still larger than 450 K, while
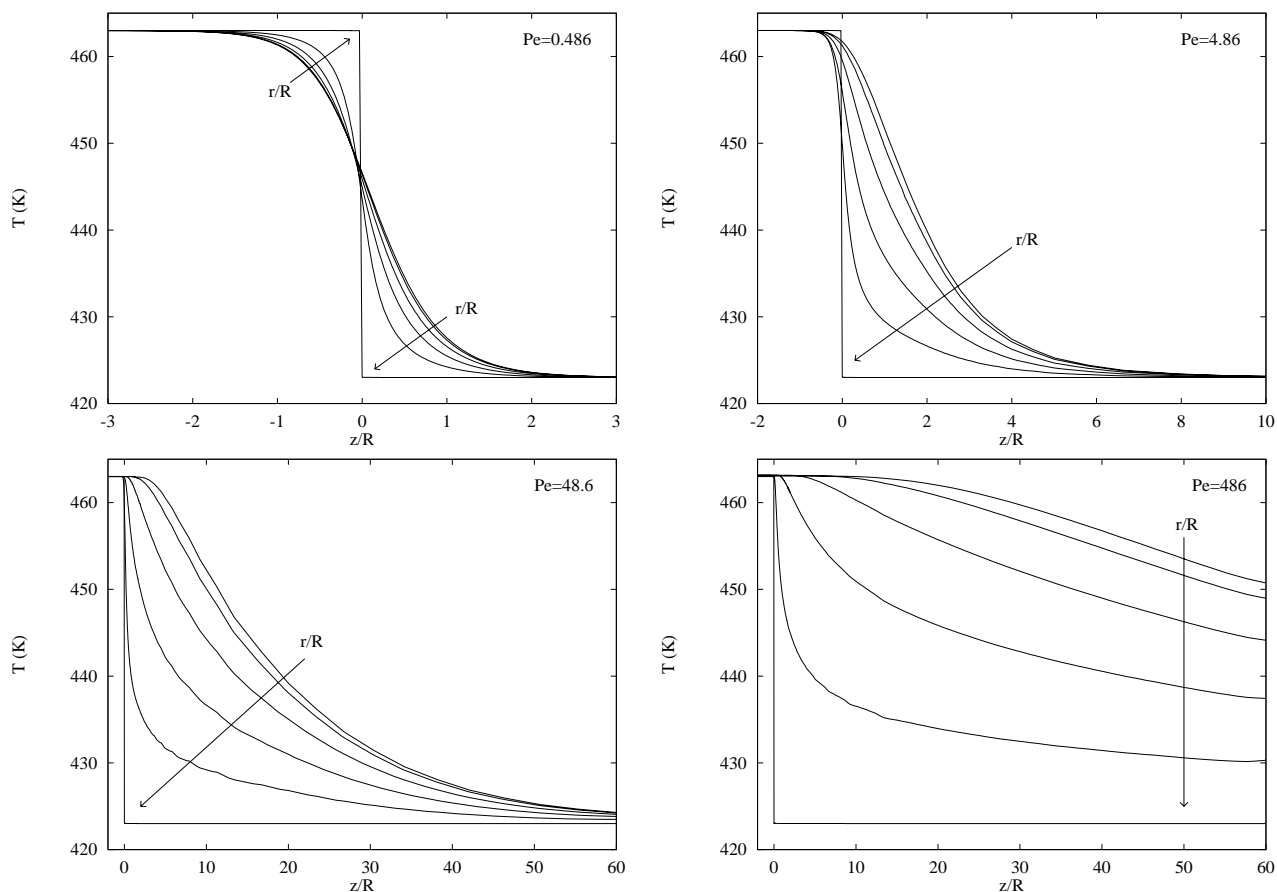
Figure 5.23: Temperature profiles of PS for the Péclet numbers of table 5.9, arranged from low to high flow rates. The temperatures have been given at lines of constant radii: $r/R = 0$, $r/R = 0.2$, $r/R = 0.4$, $r/R = 0.6$, $r/R = 0.8$ and $r/R = 1$. The arrow indicates the direction of increasing r.

the maximum temperature difference for the fully developed profile would be $\Delta T_{\max} \simeq 1$ K.

The corresponding axial velocities w have been depicted in figure 5.24. Due to the relatively large temperature differences upstream of the temperature jump for the lowest flow rate, w firstly decreases near the centreline (relatively low temperatures) and increases near the wall (relatively high temperatures). Downstream of the temperature jump the temperatures near the wall are relatively low compared to the region near the centreline. This results in relatively large velocities near the centreline and low velocities near the wall. On the centreline the maximum velocity is $w_{\mathrm{ax}}^{\max}/W = 2.35$. At about $z/R = 2$ the temperature distribution is approximately homogeneous. The axial velocity is then fully developed as well. For the second flow rate the temperature differences upstream of the jump are too small to influence the velocity field there. Downstream, the maximum velocity near the centreline increases until $w_{\mathrm{ax}}^{\max}/W = 3.30$ and the minimum near the wall decreases, compared to the lowest flow rate. For the third flow rate the maximum velocity at the centreline becomes larger $w_{\mathrm{ax}}^{\max}/W = 3.43$. and shifts downstream to $z/R \simeq 3$. The minimum for $r/R = 0.2$ remains close to $z = 0$. For the highest flow rate the maximum axial velocity becomes somewhat lower: $w_{\mathrm{ax}}^{\max}/W = 3.09$ at $z/R \simeq 11$. This is possibly caused by the influence of the viscoelasticity. The influence of the viscoelasticity on
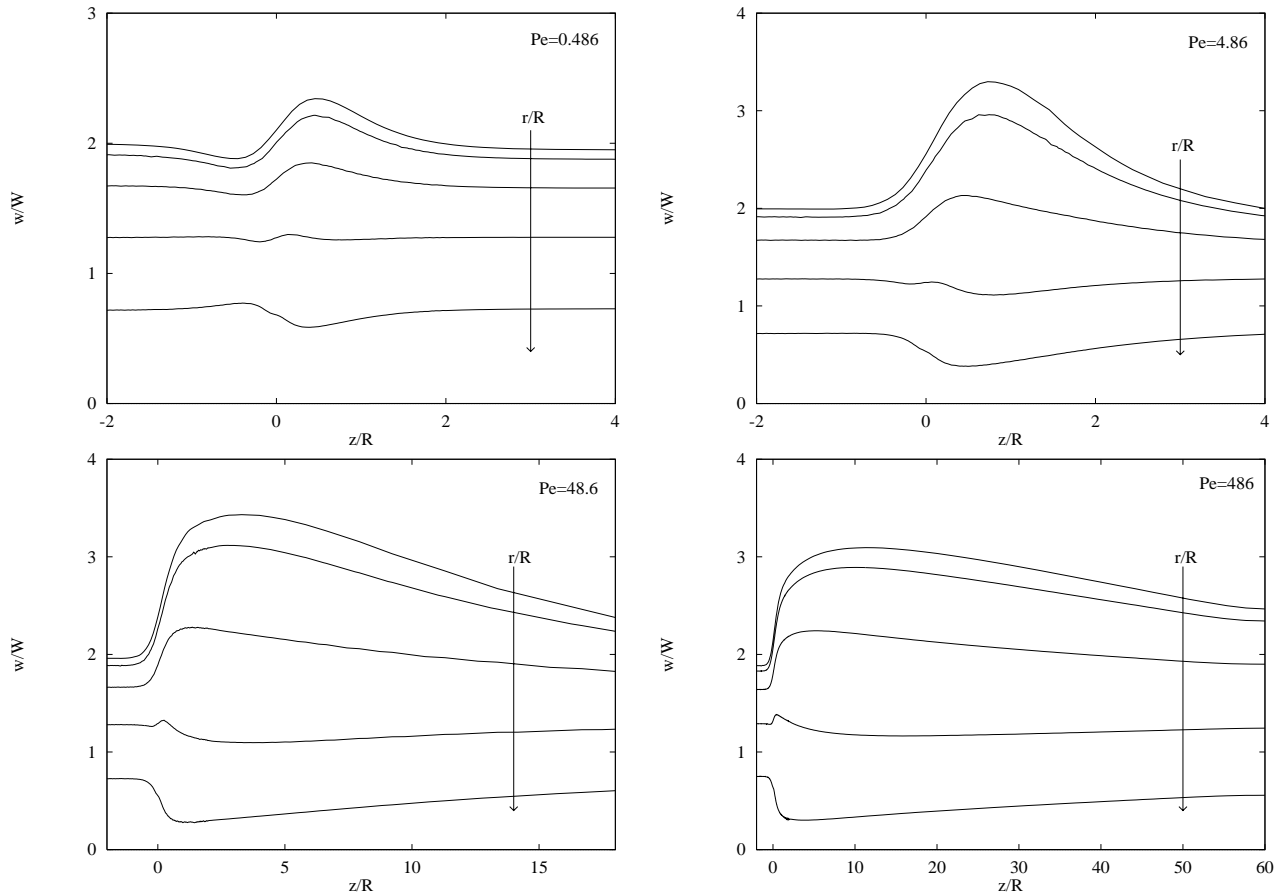
Figure 5.24: Non-dimensional axial velocity w/W of PS for the Péclet numbers of table 5.9. The velocities have been given at lines of constant radii: $r/R = 0$, $r/R = 0.2$, $r/R = 0.4$, $r/R = 0.6$ and $r/R = 0.8$. The arrow indicates the direction of increasing r.

the velocity profile is already considerably at the inflow. The ratio of the axial velocity at $r = 0$ and the mean velocity is about 1.85. For the three lowest flow rates this ratio almost equals the Newtonian value of 2.

Note that the fully developed Neumann boundary conditions are not necessary for the two lowest flow rates. Fully developed Dirichlet boundary conditions will not cause convergence problems or wiggles, because the outflow length is large enough. For the example with $W = 8.09 \cdot 10^{-4}$ m·s^{-1} and particularly for $W = 4.05 \cdot 10^{-3}$ m·s^{-1} the Neumann boundary conditions are necessary to avoid wiggles or even lack of convergence.

Influence of the various terms in the temperature equation.

For the three lowest flow rates the mechanical dissipation, the thermal expansion term and the anisotropy of the heat conduction tensor are too small to cause significant differences in the stress, pressure, velocity and temperature distribution. Only for the highest flow rate these terms cause some small differences. The following situations are considered: isotropic heat conduction and mechanical dissipation $D_{\mathrm{m}}^{\mathrm{ve}}$ (situation I), anisotropic heat conduction and mechanical dissipation $D_{\mathrm{m}}^{\mathrm{ve}}$ (situation II), and anisotropic heat conduction, mechanical dissipation

$D_{\mathrm{m}}^{\mathrm{ve}}$ and a linear dependence of the moduli G_k on the temperature (situation III). For situation III the fluid is entirely entropy elastic, which means that the stress work $\underline{\underline{\tau}} : \underline{\underline{d}}$ contributes completely to the temperature changes. In table 5.10 some of these differences are given at $z/R = 40$. This is far enough from the temperature jump and far enough from the outflow,

Table 5.10: Pressure difference Δp (Pa) between the inflow and $z/R = 40$, normal stress τ_{zz} (Pa) at the wall, shear stress τ_{rz} (Pa) at the wall, temperature T (K) at the centreline and relative velocity $w_{\mathrm{ax}}^{\mathrm{max}}/W$ at the centreline for the polystyrene melt. Stresses, temperature and velocity are at $z/R = 40$. Situation I: isotropic heat conduction and constant moduli, situation II: anisotropic heat conduction and constant moduli, situation III: anisotropic heat conduction and linear temperature dependence of the moduli.

	Δp	τ_{zz}	τ_{rz}	T	$w_{\mathrm{ax}}^{\mathrm{max}}/W$
I	$4.7 \cdot 10^6$	$2.4 \cdot 10^5$	$-6.6 \cdot 10^4$	456.8	2.74
II	$4.6 \cdot 10^6$	$2.2 \cdot 10^5$	$-6.3 \cdot 10^4$	458.1	2.91
III	$4.4 \cdot 10^6$	$2.1 \cdot 10^5$	$-5.9 \cdot 10^4$	458.1	2.89

so that the boundary conditions and stress peaks have no noticeable influence on the solution there. Due to the slightly higher temperatures, particularly near the centreline, for the situations where the anisotropy has been taken into account, the pressure difference and the stresses are somewhat smaller. The velocity near the centreline is a little larger for these situations. If the temperature dependence of the moduli is taken into account, the pressure difference and the stresses, become somewhat smaller. The temperature and the velocity remain almost unchanged.

Low density polyethylene

For the LDPE melt a Graetz–Nusselt problem will be considered, for which the wall temperature at the outflow is 393 K, just above the melting point. Successively the wall temperature at the inflow will be taken 403 K, 433 K and 463 K, so that the temperature jumps are $\Delta T = 10$, $\Delta T = 40$ and $\Delta T = 70$. For the simulations the following contributions to the temperature equation have been taken into account: anisotropic heat conduction, a constant shear modulus (i.e. entirely energy elastic) and the cooling due to the thermal expansion term. For the average velocity $W = 2.56 \cdot 10^{-2}$ m·s^{-1} will be taken, so that the Deborah number at the wall of the outflow equals $De = 300$. The Péclet number then equals $Pe = 4.9 \cdot 10^2$. The Brinkman numbers for the three different temperature jumps at the wall are respectively $Br = 6.1$, $Br = 1.5$ and $Br = 0.88$, with increasing temperature jump.

To obtain a convergent solution method $\eta_{\mathrm{it}} = 2\eta_0$ and $\eta_{\mathrm{co}} = \eta_0 - \eta_s$, both at the temperature at the outflow section, have been taken in the equations of motion. In the temperature equation the iteration diffusivity has been taken $\kappa_{\mathrm{it}} = \kappa_{\mathrm{eq}}$.

The resulting temperature profiles at different distances from the temperature jump have been depicted in figure 5.25. The temperature profiles at $z/R = -10$ seem to differ a lot. However, the different scales give a distorted view. In fact the differences are not that large. The maximum temperature difference at the inflow is about 0.8 K for the highest wall temperature and 1.3 K for the lowest. For the temperature jump of 10 K the maximum slowly moves towards the centreline with increasing z-coordinate. At $z/R = 30$ the maximum is still about $r/R = 0.3$. However, the difference with the temperature at the centreline is already very small then. For the temperature jump of 40 K and the temperature jump of 70 K the maximum is
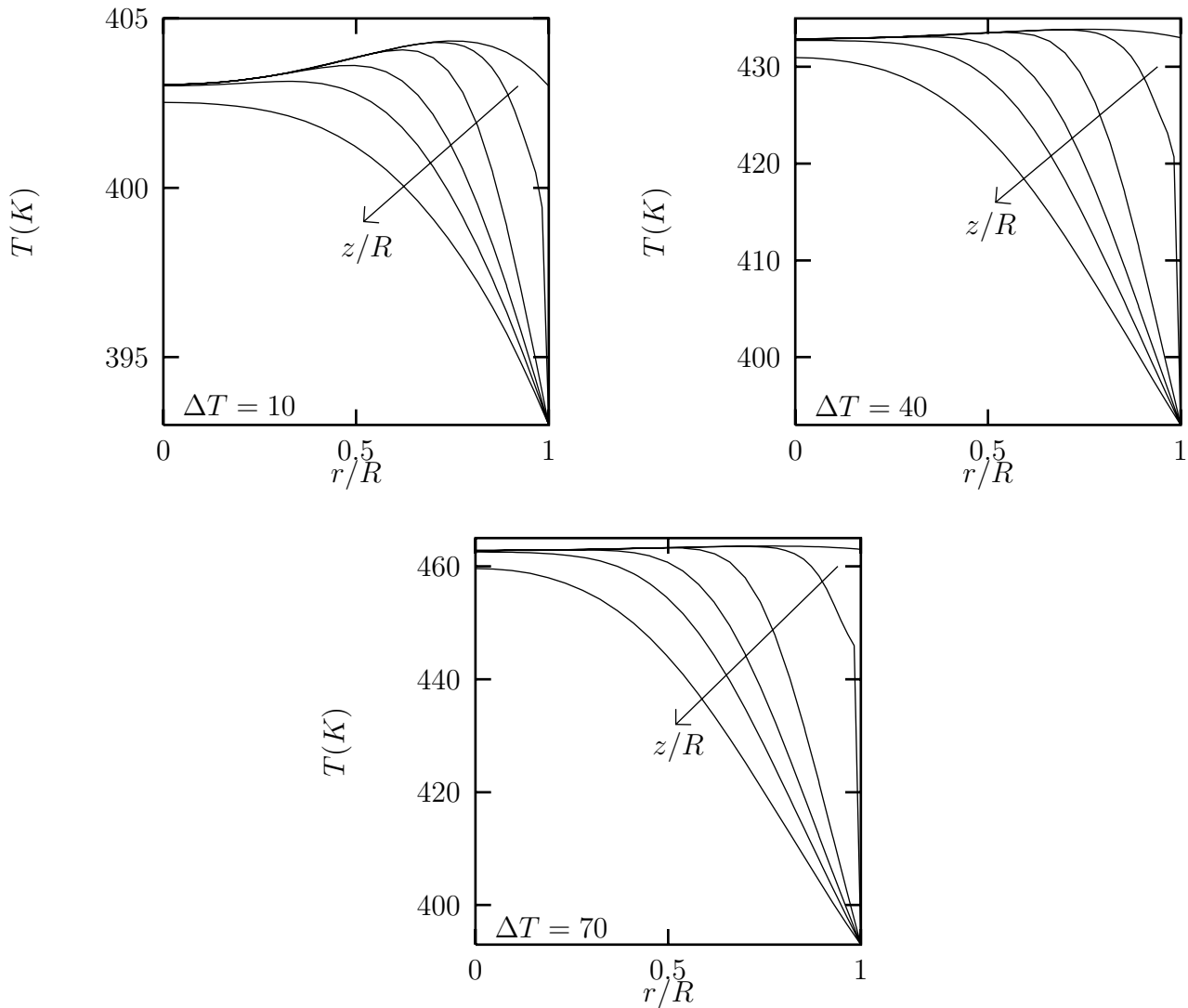
Figure 5.25: Development of the temperature profiles for the Graetz–Nusselt problem for LDPE (arranged from a small to a high temperature jump). The temperatures have been given at lines of constant z: $z/R = -10$, $z/R = 0$, $z/R = 5$, $z/R = 15$, $z/R = 30$ and $z/R = 60$. Near the wall the temperature decreases with increasing z.

sooner at the axis of symmetry, although this is difficult to see in figure 5.25. This is caused by the higher temperature derivative in the radial direction. Note that if the exit length would be much longer, so that the flow would approximate its fully developed profile, the maximum moves again to higher r/R-values (see section 5.2).

The normal stress τ_{zz} at the wall and the velocity at the centreline w_{ax} have been depicted in figure 5.26. Near the temperature jump there are some small wiggles, both for the normal stress and the axial velocity. The temperature jump causes an overshoot in the zz-component of the normal stress. For increasing ΔT the overshoot becomes larger: for $\Delta T = 10$ K the magnitude of the overshoot equals $\Delta\tau = 2 \cdot 10^4$ Pa, for $\Delta T = 40$ K it is $\Delta\tau = 6 \cdot 10^4$ Pa and for $\Delta T = 70$ K it is $\Delta\tau = 1.1 \cdot 10^5$ Pa. After the overshoot the stress increases slowly due to the developing temperature boundary layer. The axial velocity at the centreline also shows an
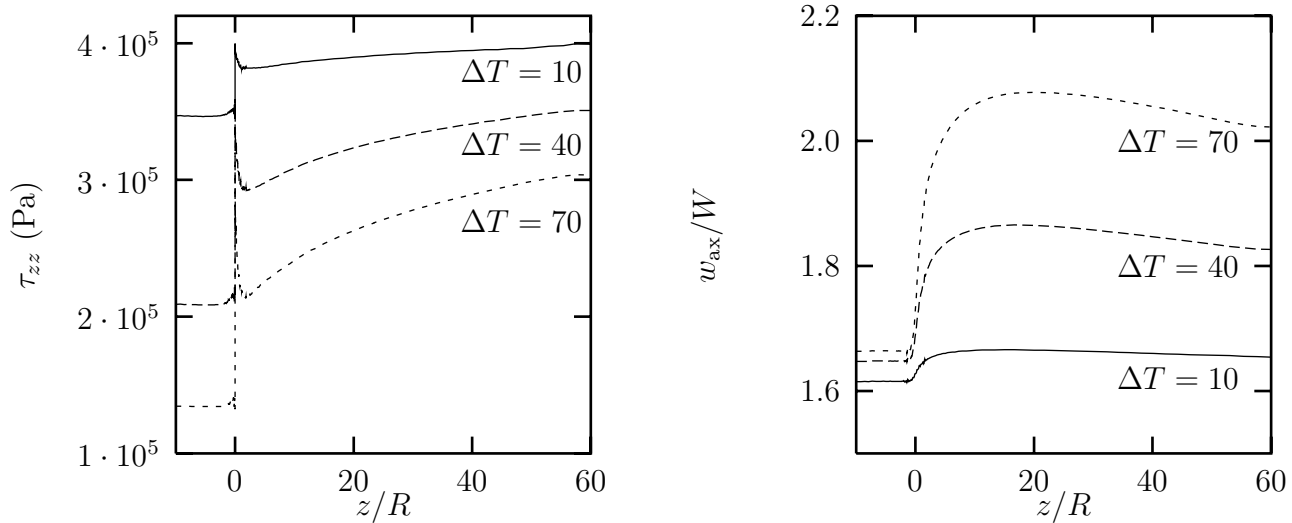
Figure 5.26: Normal stress τ_{zz} of LDPE at the wall and normalised velocity at the centreline for the three different temperature jumps. Solid line: $\Delta T = 10$ K, line with large dashes: $\Delta T = 40$ K, line with small dashes: $\Delta T = 70$ K.

overshoot. However, because the temperature boundary layer develops slowly, the maximum is not at $z = 0$, but somewhere downstream. For $\Delta T = 70$ K for example the maximum velocity only occurs at $z/R = 20$.

The relatively large Deborah number of the flow results in internal deformation tensors which are far from equilibrium. Therefore the anisotropy of the heat conduction tensor may be large. The perpendicular thermal conductivity has been depicted in figure 5.27. Before the temperature jump, the perpendicular thermal conductivity κ_{rr} is the smallest for $\Delta T = 10$ K. Due to the relatively low temperature the relaxation times are higher then. This results in a larger anisotropy of the internal deformation tensors and consequently a larger anisotropy of the heat conduction tensor. At the temperature jump κ_{rr} increases, compared to the fully developed flow. For $\Delta T = 40$ K and $\Delta T = 70$ K there is a sharp peak at the jump. The maximum value is even larger than the equilibrium value. This is caused by the strong temperature boundary layer after $z = 0$. Due to the relatively high viscosity there, the direction of the velocity is not parallel to the wall. Thus also the polymers will not be oriented parallel to the wall then.

The shear component of thermal conductivity has been depicted in figure 5.28. For all three examples the largest deviations from equilibrium are near the temperature jump. In the other part of the flow region the shear component is of the order of the equilibrium conductivity. The angular behaviour after the temperature jump is mainly caused by the first mode, which gives the largest contribution to κ_{rz}. The other modes are relatively smooth.

The parallel thermal conductivity has been depicted in figure 5.29. The maximum conductivity, at the temperature jump, is about 300 times as large as the equilibrium thermal conductivity. This maximum decreases somewhat with increasing temperature jump. For the smallest temperature jump, κ_{zz} is already large before the temperature jump, due to the relatively low temperature. The temperature jump does not cause large differences then. For the other two examples κ_{zz} is much smaller at the inflow. Probably due to the coarser mesh,
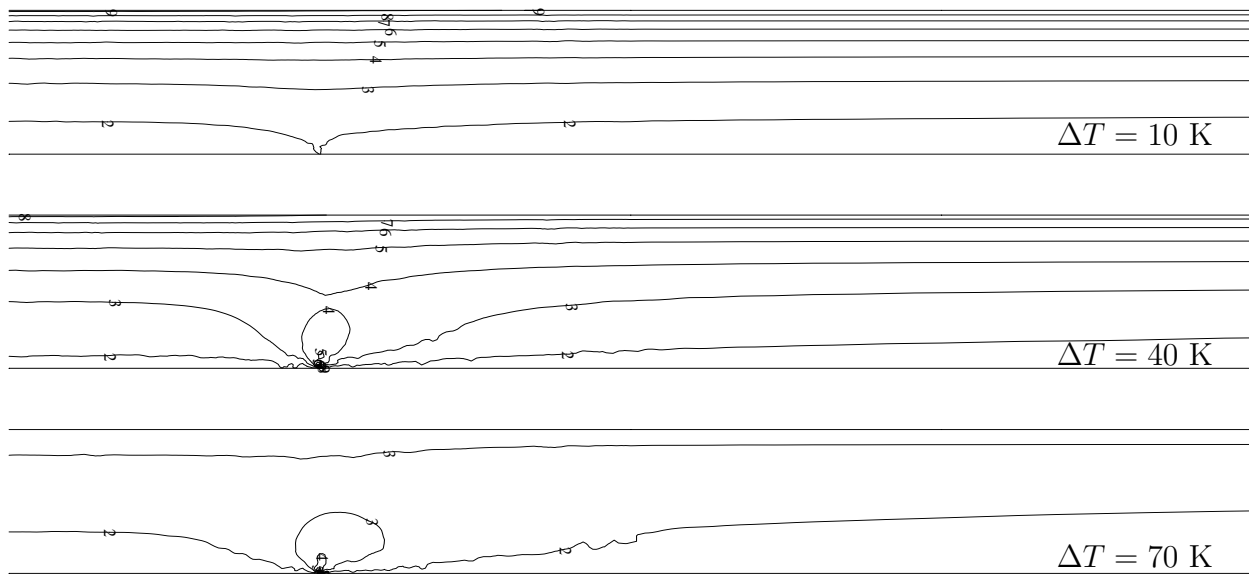
Figure 5.27: Isolines for the perpendicular component of the thermal conductivity $\kappa_{rr}/\kappa_{\text{eq}}$ of LDPE for $\Delta T = 10$ K, $\Delta T = 40$ K and $\Delta T = 70$ K in the area $-2 \leq z/R \leq 6$. For $\Delta T = 10$ K the labels correspond with: $1 = 0.63$ and $10 = 1.00$, for $\Delta T = 40$ K with: $1 = 0.64$ and $10 = 1.06$, and for $\Delta T = 70$ K with: $1 = 0.62$ and $10 = 1.71$. The levels between have been divided in equidistant parts.
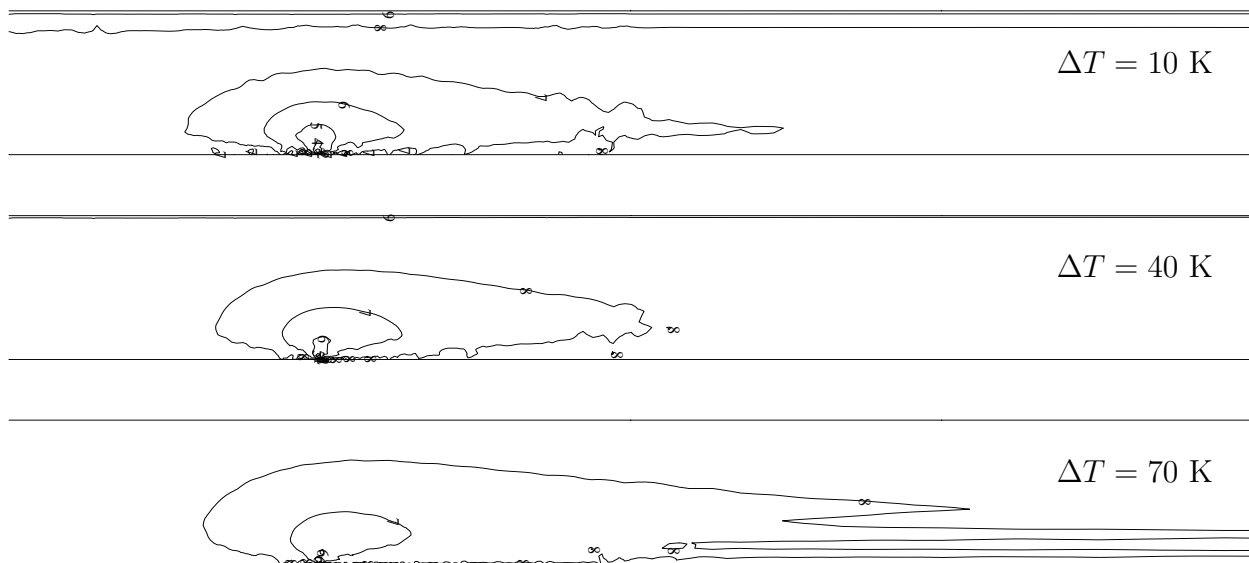

Figure 5.28: Isolines for the shear component of the thermal conductivity $\kappa_{rz}/\kappa_{\text{eq}}$ of LDPE for $\Delta T = 10$ K, $\Delta T = 40$ K and $\Delta T = 70$ K in the area $-2 \leq z/R \leq 6$. For $\Delta T = 10$ K the labels correspond with: $1 = -4.15$ and $10 = 0.0$, for $\Delta T = 40$ K with: $1 = -11.4$ and $10 = 1.04$, and for $\Delta T = 70$ K with: $1 = -17.6$ and $10 = 3.11$. The levels between have been divided in equidistant parts.

the solution becomes more angular near $z/R = 6$. The first and second mode of the internal deformation tensor, which contribute most to the parallel thermal conductivity, show the same angular behaviour near the wall. The other modes are relatively smooth. To give an
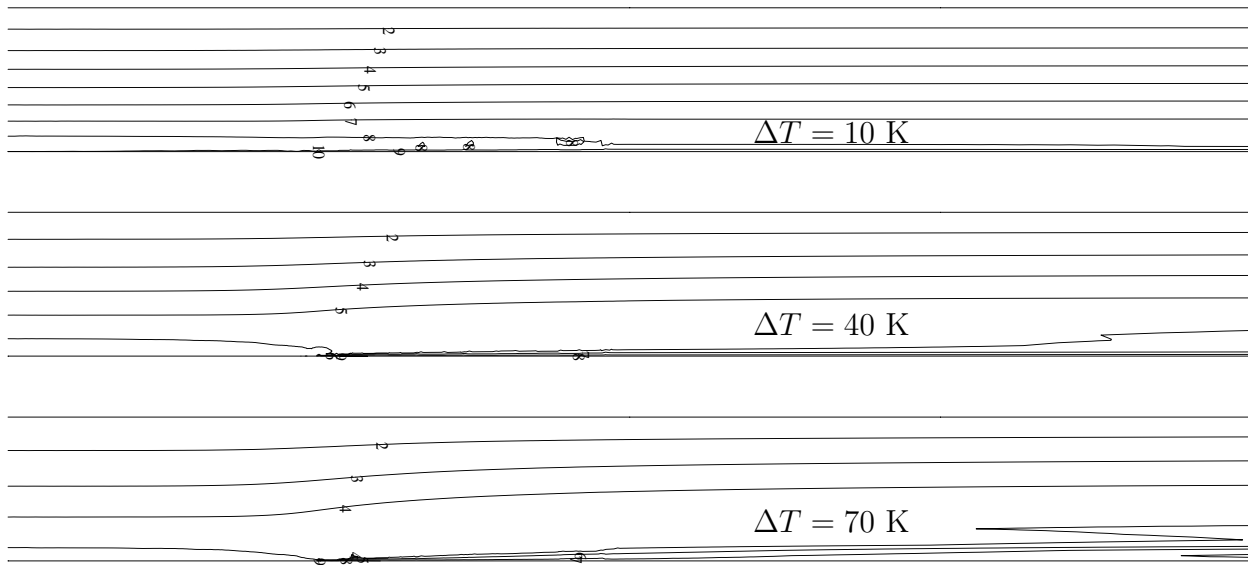
Figure 5.29: Isolines for the parallel component of the thermal conductivity $\kappa_{zz}/\kappa_{\mathrm{eq}}$ of LDPE for $\Delta T = 10$ K, $\Delta T = 40$ K and $\Delta T = 70$ K in the area $-2 \leq z/R \leq 6$. For $\Delta T = 10$ K the labels correspond with: $1 = 0.0$ and $10 = 342$, for $\Delta T = 40$ K with: $1 = 0.0$ and $10 = 316$, and for $\Delta T = 70$ K with: $1 = 0.0$ and $10 = 290$. The levels between have been divided in equidistant parts.

impression of the contributions of the different modes to the heat conduction tensor: the maximum zz-component of the internal deformation tensor equals $b_{zz}^{\max} = 2 \cdot 10^3$ for the first mode, $b_{zz}^{\max} = 5 \cdot 10^2$ for the second mode, and $b_{zz}^{\max} = 5 \cdot 10^1$ for the third mode. Thus the high value of $\kappa_{zz} \simeq 300$ is mainly caused by the first two modes. Whether κ_{zz} may become that large in real flows or this is a deficiency of the model, is of course still open to question.

5.4 Flow through a 4:1 contraction

The isothermal flow through an axisymmetrical contraction has been, and still is, one of the benchmarks for viscoelastic computations. This flow consists of a fully developed flow at the upstream boundary, a sudden contraction and a fully developed flow at the downstream boundary. The 4:1 contraction will be studied here, because it is the most studied contraction flow in the literature. Reviews of both the experimental results and the numerical calculations of contraction flows have been presented by Boger (1987) and White et al. (1987).

In this section the emphasis will be on the nonisothermal flow through a 4:1 contraction. The geometry of the flow and the temperature boundary conditions that will be used for the flow through the contraction have been depicted in figure 5.30. As for the Graetz–Nusselt problem, the inflow length will be taken $20\,R$ and the outflow length $60\,R$, where the radius at the outflow has been taken $R = 5 \cdot 10^{-3}$ m. The wall near the inflow has been kept at a fixed temperature T_1, the other part of the fixed wall has been kept at a fixed temperature $T_0 \leq T_1$. For the equations of motion it will be assumed that on the fixed wall the no-slip boundary condition holds for the velocity. At the inflow boundary fully developed Dirichlet boundary conditions will be prescribed for the velocity, the modal stresses and the temperature. At the

outflow boundary fully developed Neumann boundary conditions for the normal stress and the temperature will be imposed. See section 4.5 for the details of these boundary conditions.

The calculations will be performed on a mesh with 5587 grid points. The part of the mesh near the contraction has been depicted in figure 5.31. Near the sharp corner, where the gradients are large, the mesh is relatively fine. Towards the outflow and inflow boundary the mesh has been taken much coarser, because the gradients are much smaller there.
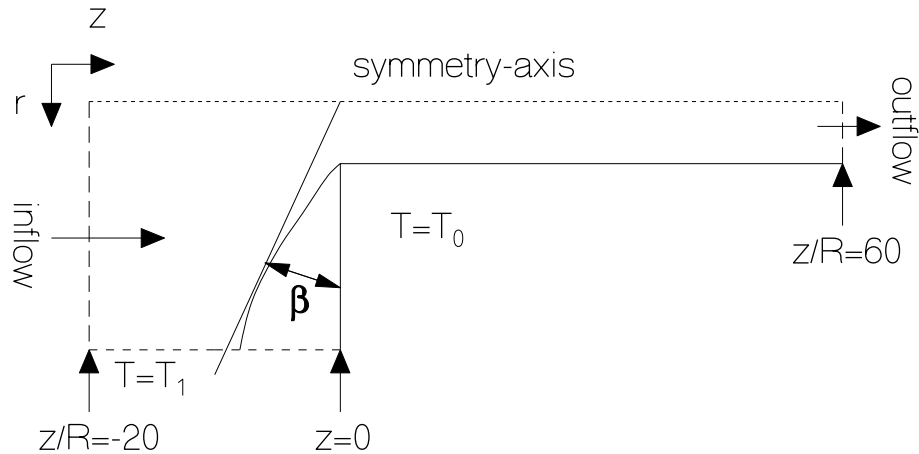

Figure 5.30: Flow geometry, definition of the opening angle β and temperature boundary conditions for the 4:1 contraction. The fixed wall near the inflow (dashed line) has been kept at temperature T_1. The other part of the wall (solid line) has been cooled to T_0.
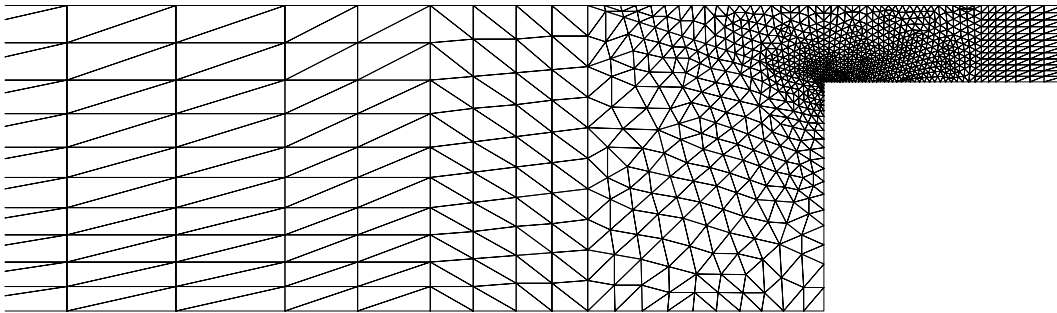

Figure 5.31: A part of the finite element mesh, $-10 \leq z/R \leq 3$, near the sharp corner of the 4:1 contraction.

A characteristic phenomenon of contraction flows of viscoelastic fluids is that a vortex may exist in the entry corner. Two features of this vortex will be examined. Firstly, the opening angle β of the vortex, defined in figure 5.30, which is a measure for the size of the vortex. Secondly, the vortex intensity I_ψ defined by

$$I_\psi = \frac{\psi_{\text{sep}} - \psi_{\text{cen}}}{\psi_{\text{ax}} - \psi_{\text{sep}}}, \tag{5.4}$$

where ψ_{sep} is the value of the stream function at the separating streamline, ψ_{cen} the value at the centre of the vortex and ψ_{ax} the value at the axis of symmetry. The vortex intensity equals

the ratio of the amount of fluid flowing in the vortex and in the main flow.

Before the results of the nonisothermal calculations will be presented, the influence of the viscoelasticity (isothermal) will be examined for the LDPE and PS melt. The isothermal results will be used as a reference for the nonisothermal flow through a 4:1 contraction.

5.4.1 Isothermal flow

Hulsen & van der Zanden (1991) have calculated the flow through a 4:1 and a 5.75:1 contraction for the eight-mode Giesekus model of table 5.1. They have shown that the size of the computed vortex in the edge before the contraction agrees well with experimental results. The size of the vortex strongly depends on the flow. To characterise the flow the Deborah number based on the outflow radius R and the average velocity at the outflow will be used.

Hulsen & van der Zanden (1991) argued that the growth of the vortex is a mechanism to fulfil the balance of momentum in the z-direction:

$$\frac{1}{r}\frac{\partial r\tau_{rz}}{\partial r} + \frac{\partial \tau_{zz}}{\partial z} \simeq 0, \tag{5.5}$$

where the (small) term with the pressure gradient has been neglected. With a larger vortex the build-up of the dominant term in this equation, τ_{zz}, before the contraction can be more gradually. Equation (5.5) indicates that the ratio of the elongational stress and the shear stress is important for the size of the vortex.

Low density polyethylene

The isothermal flow through the 4:1 contraction for the eight-mode Giesekus model has been calculated for the four Deborah numbers of table 5.11. For the computations the iteration

Table 5.11: Vortex intensity I_ψ and opening angle β for various Deborah numbers for the isothermal flow through a 4:1 contraction of the LDPE melt.

De	$I_\psi(\%)$	$\beta(\deg)$
3	2.9	28
15	10.0	43
50	10.9	52
200	11.1	53

viscosity has been taken $\eta_{it} = 2\eta_0$ and the extra viscosity $\eta_{co} = \eta_0 - \eta_s$.

The results for the streamline patterns of the eight-mode Giesekus model have been depicted in figure 5.32. Notice that for relatively small Deborah numbers the opening angle β is already considerable: $\beta = 28$ deg for $De = 3$. For increasing Deborah number the opening angle keeps increasing till $\beta = 53$ deg for the highest Deborah number of $De = 200$. However, for the two highest Deborah numbers the difference are relatively small. The corresponding opening angles β and the vortex intensities I_ψ for the various Deborah numbers have been given in table 5.11. As for the opening angle, the increase of the vortex intensity is large for the low Deborah numbers. For the two highest Deborah numbers there is hardly any difference. The strong increase for the low Deborah numbers can be explained by examining the stresses at the contraction.
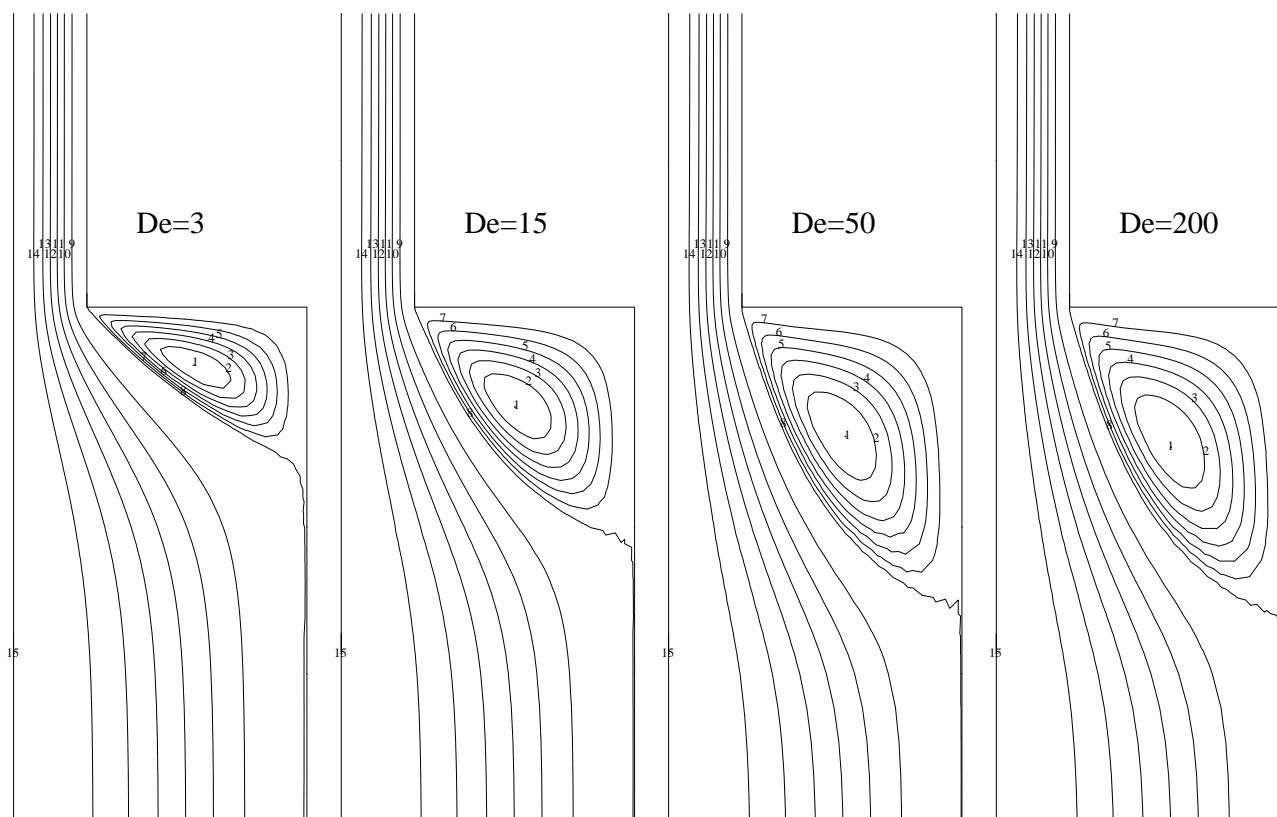
Figure 5.32: Streamline contours of the LDPE melt near the contraction, $-7 \leq z/R \leq 4$, for the various Deborah numbers of table 5.11. Seven contours are evenly spaced from zero to the maximum value and from zero to the minimum value.

The normal stress τ_{zz} and the shear stress τ_{rz} at $z = 0$, have been depicted in figure 5.33. The stresses are relative to the wall shear stress τ_{w} at the outflow for a Deborah number of $De = 200$. Particularly between $De = 3$ and $De = 50$ the increase of τ_{zz} is relatively large. Only for the lowest Deborah numbers the normal stress is almost constant over the whole region. For $De = 15$ a small local maximum arises near $r/R \simeq 0.7$. The local maximum is more clear for the two highest Deborah numbers, where the maximum normal stress is about two times as large as the normal stress at the centreline and at the wall. Also the magnitude of the shear stress decreases more for the low Deborah numbers, although less than τ_{zz}. For all Deborah numbers τ_{rz} remains approximately linear in the core region. Only near the wall there is a sharp decrease preceded by a small increase for the two highest Deborah numbers.

Polystyrene

The isothermal flow through the 4:1 contraction for the four-mode Leonov model has been calculated for the four Deborah numbers of table 5.11, which are the same as for the eight-mode Giesekus model. For the computations the iteration viscosity has been taken $\eta_{\mathrm{it}} = \eta_0$ and the extra viscosity[2] $\eta_{\mathrm{co}} = \eta_0 - \eta_s$. Before proceeding, a remark has to be made on the expected correspondence with experimental results. In the flow of a polymer melt through a

---

[2]The iteration viscosity has to be chosen carefully. For an increase of the iteration factor by a factor two or three the convergence criteria could not be obtained.
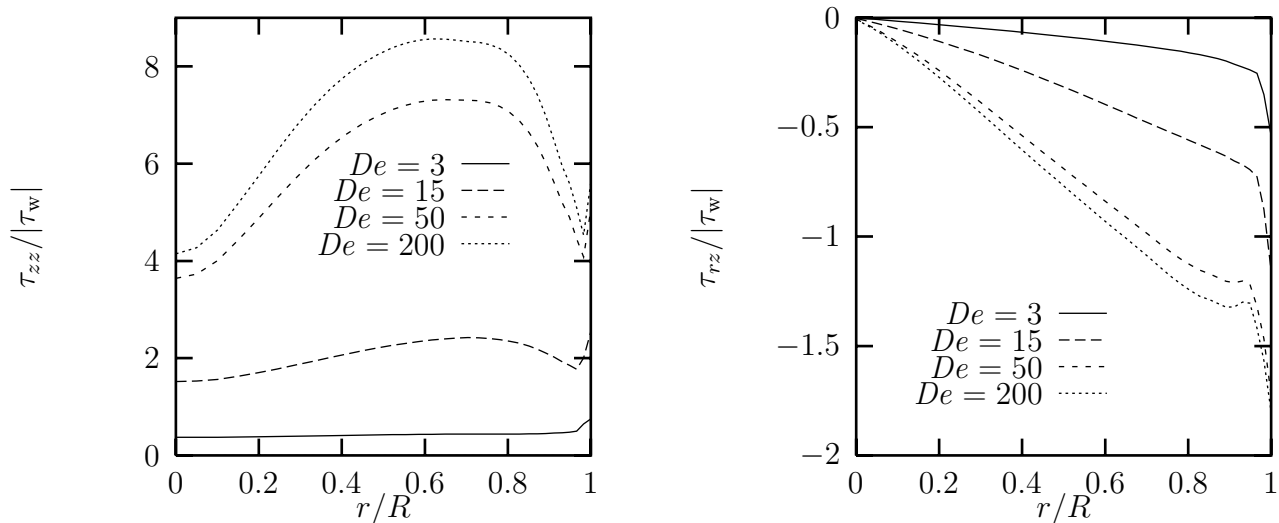
Figure 5.33: Normal stress $\tau_{zz}/|\tau_{\mathrm{w}}|$ and shear stress $\tau_{rz}/|\tau_{\mathrm{w}}|$ at $z = 0$ for various Deborah numbers of the LDPE melt. The stresses have been normalised with the wall shear stress for $De = 200$ at the outflow.

Table 5.12: Vortex intensity I_{ψ} and opening angle β for various Deborah numbers for the isothermal flow through a 4:1 contraction of the PS melt.

De	$I_{\psi}(\%)$	$\beta(\mathrm{deg})$
3	0.7	22
15	2.6	31
50	5.2	40
200	5.4	50

contraction both the (unsteady) elongational behaviour and the (unsteady) shear behaviour are important, see Hulsen & van der Zanden (1991). Because the polystyrene melt has only been characterised in shear flows, it is open to question whether the numerical results of this section correspond well with experimental results. Experiments for a 5.75:1 contraction of White & Kondo (1977/1978) for polyethylene and polystyrene show that the opening angle is smaller for the PS melts, particularly for low Deborah numbers.

For the four-mode Leonov model the obtained streamline patterns for the various Deborah numbers have been depicted in figure 5.34. As for the LDPE melt the size of the vortex may be considerable for the high Deborah numbers. However, it is striking that the size of the vortex is smaller than for the LDPE melt, particularly for the lower Deborah numbers. The corresponding opening angles β and the vortex intensities I_{ψ} have been given in table 5.12. Except for the smaller opening angle, also the vortex intensities for the PS melt are relatively low compared to the LDPE melt.

The normal stress τ_{zz} and the shear stress τ_{rz} at $z = 0$, have been depicted in figure 5.35. The stresses are relative to the wall shear stress τ_{w} at the outflow for a Deborah number of $De = 200$. For the two lowest Deborah numbers the normal stress is almost constant over the whole region. For $De = 50$ a small local maximum arises near $r/R \simeq 0.7$. The local maximum is more clear for the highest Deborah number. Compared to LDPE the strong increase of the
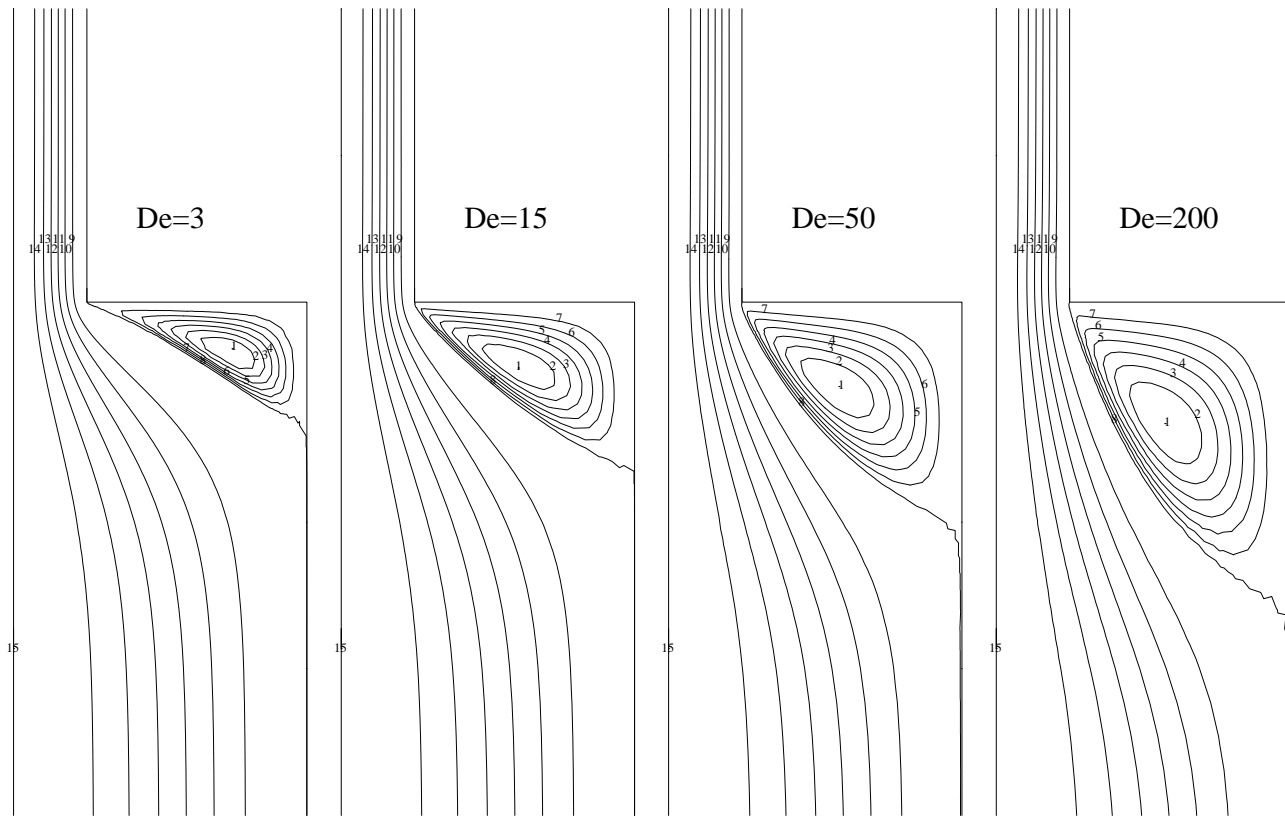
Figure 5.34: Streamline contours of the PS melt near the contraction, $-7 \leq z/R \leq 4$, for the various Deborah numbers of table 5.12. Seven contours are evenly spaced from zero to the maximum value and from zero to the minimum value.
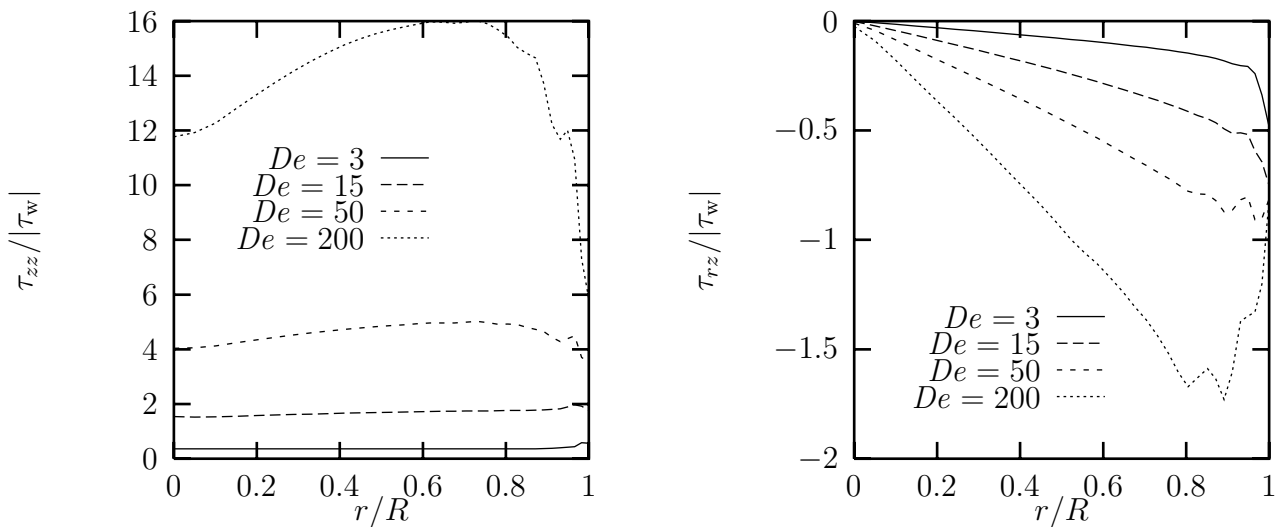

Figure 5.35: Normal stress $\tau_{zz}/|\tau_{\mathrm{w}}|$ and shear stress $\tau_{rz}/|\tau_{\mathrm{w}}|$ at $z = 0$ for various Deborah numbers of the PS melt. The stresses have been normalised with the wall shear stress for $De = 200$ at the outflow.

normal stress τ_{zz} is at higher Deborah numbers. For the LDPE melt the differences between

$De = 50$ and $De = 200$ are just relatively small. Furthermore the large differences between the value of τ_{zz} at the centreline and at the wall are large for PS, while they are almost equal for LDPE. For the two lowest Deborah numbers, the behaviour of the shear stress resembles that for the LDPE melt: approximately linear in the core region and a sharp decrease near the wall. For the two highest Deborah numbers the decrease near the wall vanishes. For $De = 50$ it remains approximately constant and for $De = 200$ it even increases. Near the wall there are also some wiggles in the shear stress then.

5.4.2 Nonisothermal flow

First the isothermal flow will be compared with the nonisothermal flow, without a temperature jump at the wall. Then the results for the 4:1 contraction for which the outflow boundary has been cooled will be presented. All dimensionless numbers, unless explicitly stated, are based on the outflow conditions, i.e. the outflow radius and the temperature and average velocity at the outflow. For the LDPE melt the attention will again be focused on the anisotropy of the heat conduction tensor, while for the PS the emphasis will be on the influence of the temperature on the flow.

Low density polyethylene

For the computations the iteration viscosity has been taken $\eta_{it} = 2\eta_0$ and the extra viscosity $\eta_{co} = \eta_0 - \eta_s$, both at the temperature of the wall at the outflow. The heat conduction tensor will be taken independent of the temperature. Furthermore the heat capacity and the density will be taken constant in the convective term of the temperature equation.

First the influence of the internal heat production has been checked. For a wall temperature of $T_w = 463$ K, a Deborah number of $De = 50$, a Péclet number of $Pe = 523$, and the anisotropy of the heat conduction taken into account, the maximum temperature rise at $z = 0$ was about 0.15 K. At the outflow boundary the maximum temperature rise was about 0.7 K. Since the stresses do not depend very strongly on the temperature, these temperature rises do not have a significant effect on the flow. If the flow rate was increased until $De = 200$, no convergence could be obtained. Probably this problem is caused by the wiggly behaviour of the first mode of the internal deformation tensors near the contraction. If the heat conduction was assumed to be isotropic, or if the anisotropy caused by the first mode was omitted, it was no problem to obtain a convergent solution method. In the following calculations the Deborah number will be taken $De = 50$.

For the second nonisothermal flow of the LDPE melt the anisotropy of the heat conduction tensor will be examined. For the temperature jumps at the wall $\Delta T = 10$ K and $\Delta T = 40$ K will be taken. For the anisotropy the parameters of table 5.3 will be taken again. This means that 4 cases will be distinguished: $\Delta T = 10$ K with isotropic heat conduction (case I), $\Delta T = 10$ K with anisotropic heat conduction (case II), $\Delta T = 40$ K with isotropic heat conduction (case III) and $\Delta T = 40$ K with anisotropic heat conduction (case IV). The isothermal flow at $De = 50$ will be denoted by case 0. The Péclet number for all calculations was $Pe = 93$.

For the four cases the resulting temperature distributions near the contraction have been depicted in figure 5.36. The results can be explained by considering the corresponding anisotropy of the heat conduction tensor. The rr-, the rz- and zz-components have been depicted in figures 5.37 and 5.38. In the entry corner the conduction of heat upstream is much larger when the anisotropy has been taken into account. This is caused by the large values of κ_{zz} in
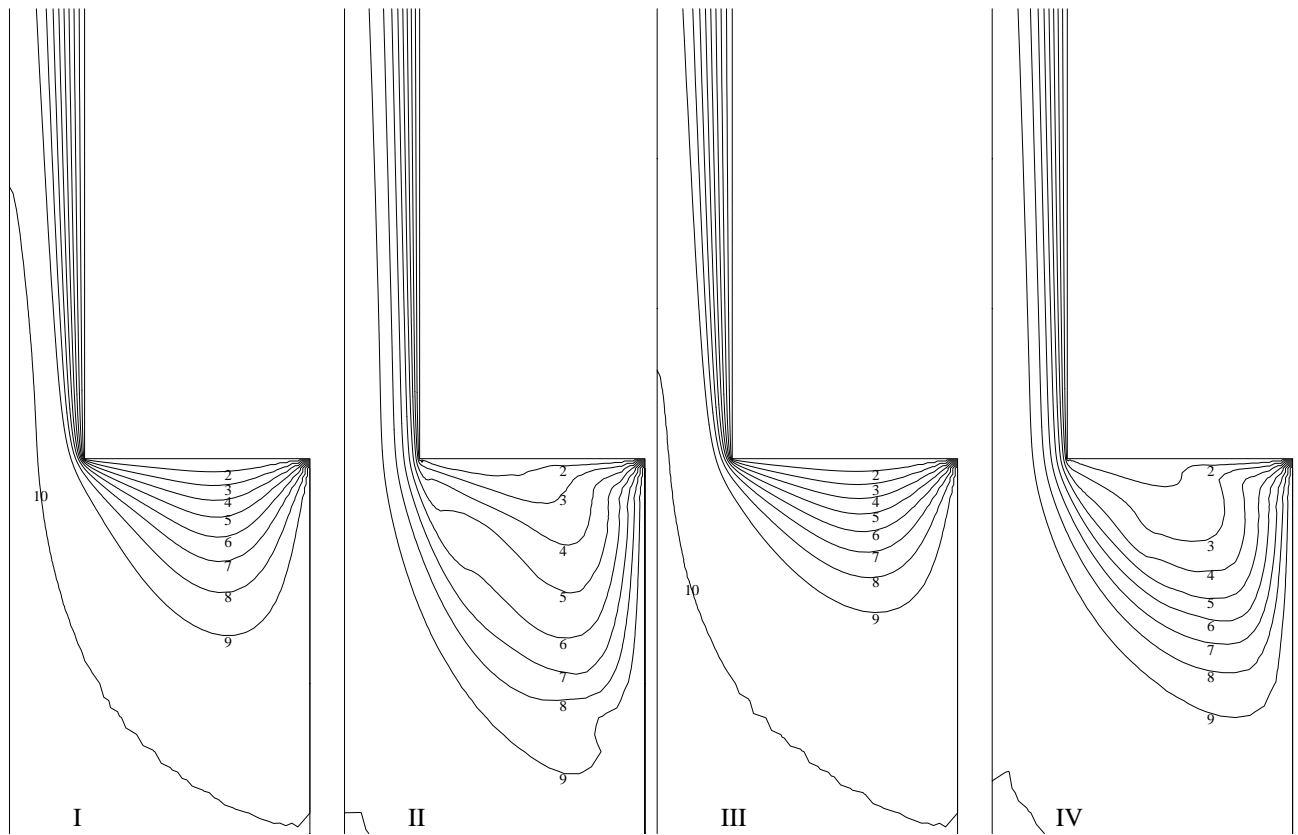
Figure 5.36: Temperature isolines near the contraction, $-5 \leq z/R \leq 6$, of LDPE for various temperature jumps with and without the anisotropy of the heat conduction tensor. Case I-IV of table 5.13 have been depicted. The ten isotherms are evenly spaced between the maximum temperature, 403 K or 433 K, and the minimum temperature 393 K.

the entry corner as can be seen from the small figures in figures 5.37 and 5.38. Along the wall of the outflow a temperature boundary layer develops. At $z = 0$ the boundary layer for the anisotropic cases is about two times as large as for the isotropic cases. Because the cold front develops farther outside the vortex, the convective transport of heat in the core flow provides a larger temperature boundary layer at $z = 0$. Due to the reduced thermal conductivity in the direction perpendicular to the flow in the outflow section (after some z/R when the polymer chains are oriented in the direction of the flow), the boundary layer develops much slower for the anisotropic cases. At $z/R \simeq 6$ (the top side of the figures in 5.36) the sizes of the boundary layers are almost equal. The magnitude of the rz-component of the heat conduction tensor is large (and negative) near the separation line of the vortex, indicating that the polymer chains are oriented in the direction of the flow. The main difference between figure 5.37 for $\Delta T = 10$ K and figure 5.38 for $\Delta T = 40$ K is that the thermal conductivity parallel to the flow is much lower for the latter. This is due to the lower temperature in the core flow, which causes a lower relaxation time and therefore less orientation of the polymer chains. The thermal conductivities in the direction perpendicular to the flow are of comparable magnitude. The minimum is just below $0.7\kappa_{\text{eq}}$, indicating that only the first four modes are active.

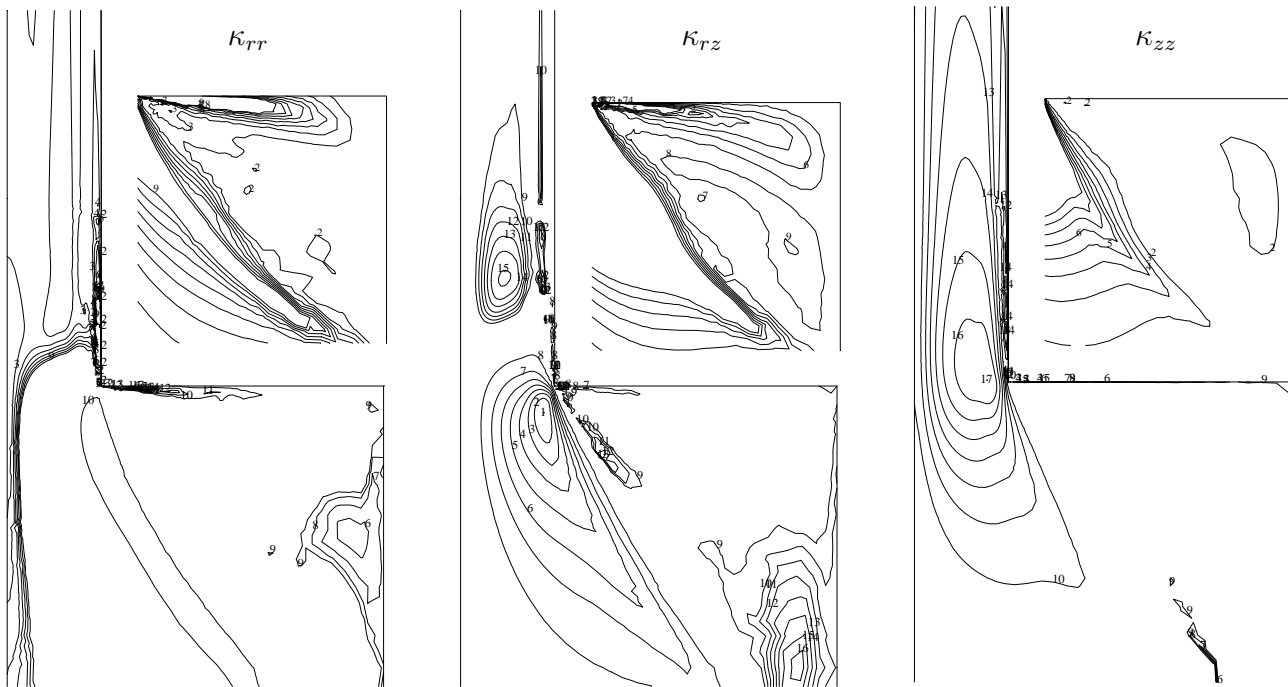Due to the higher temperature near the centre, compared to the isothermal flow for $De = 50$

Figure 5.37: Isolines near the contraction, $-5 \leq z/R \leq 6$, for κ_{rr}, κ_{rz} and κ_{zz} for the LDPE melt. The temperature jump equals $\Delta T = 10$ K (case II of table 5.13). The lines are evenly spaced below and above the isotropic value of the concerned quantity. The isotropic value corresponds to line 8 for κ_{rz} and κ_{zz} and to line 10 for κ_{rz}. The minimum (line 1) and maximum (line 17) values are: $0.68 \leq \kappa_{rr}/\kappa_{\mathrm{eq}} \leq 204$, $-143 \leq \kappa_{rz}/\kappa_{\mathrm{eq}} \leq 3.2$, $0.74 \leq \kappa_{zz}/\kappa_{\mathrm{eq}} \leq 791$. For the figures of the entry corner, $-3 \leq z/R \leq 0$ and $1 \leq r/R \leq 4$, the minimum (line 1) and maximum (line 9) values are evenly spaced between: $0.68 \leq \kappa_{rr}/\kappa_{\mathrm{eq}} \leq 24$, $-16 \leq \kappa_{rz}/\kappa_{\mathrm{eq}} \leq 3.2$, $0.74 \leq \kappa_{zz}/\kappa_{\mathrm{eq}} \leq 89$.

at $T = 393$ K, the magnitude of the stresses is also smaller. The influence on the normal stress τ_{zz} and the shear stress τ_{rz} at $z = 0$ has been depicted in figure 5.39. The stresses are relative to the wall shear stress τ_{w} at the outflow for the isothermal flow of $De = 200$. For comparison the stresses for the isothermal flows with $De = 15$ and $De = 50$ have also been given. The latter corresponds to the Deborah number calculated with the temperature of 423 K at the outflow boundary. The first almost corresponds to the Deborah number calculated with the temperature of 463 K at the inflow boundary ($De(T_1) = 17$). Particularly, the resulting normal stresses τ_{zz} at $z = 0$ are considerably smaller than for the isothermal case at $De = 50$ and larger than the isothermal case at $De(T_1)$. Only at the wall all stresses for the nonisothermal calculations are almost equal to the stresses for the isothermal calculations at $De = 50$. The shear stress shows the same type of behaviour, only the differences are somewhat smaller.

Compared to the influence of the temperature jump, the anisotropy only has a small influence on the stresses, although the temperature at $z = 0$ is considerably lower when the anisotropy of the heat conduction tensor has been taken into account. With increasing magnitude of the temperature jump the differences increase, but only for $\Delta T = 40$ K the magnitude of the stresses near $r/R = 0.8$ are significantly larger when the anisotropy has been taken into account.

In view of the isothermal results for the stresses in figure 5.33, one would expect that the
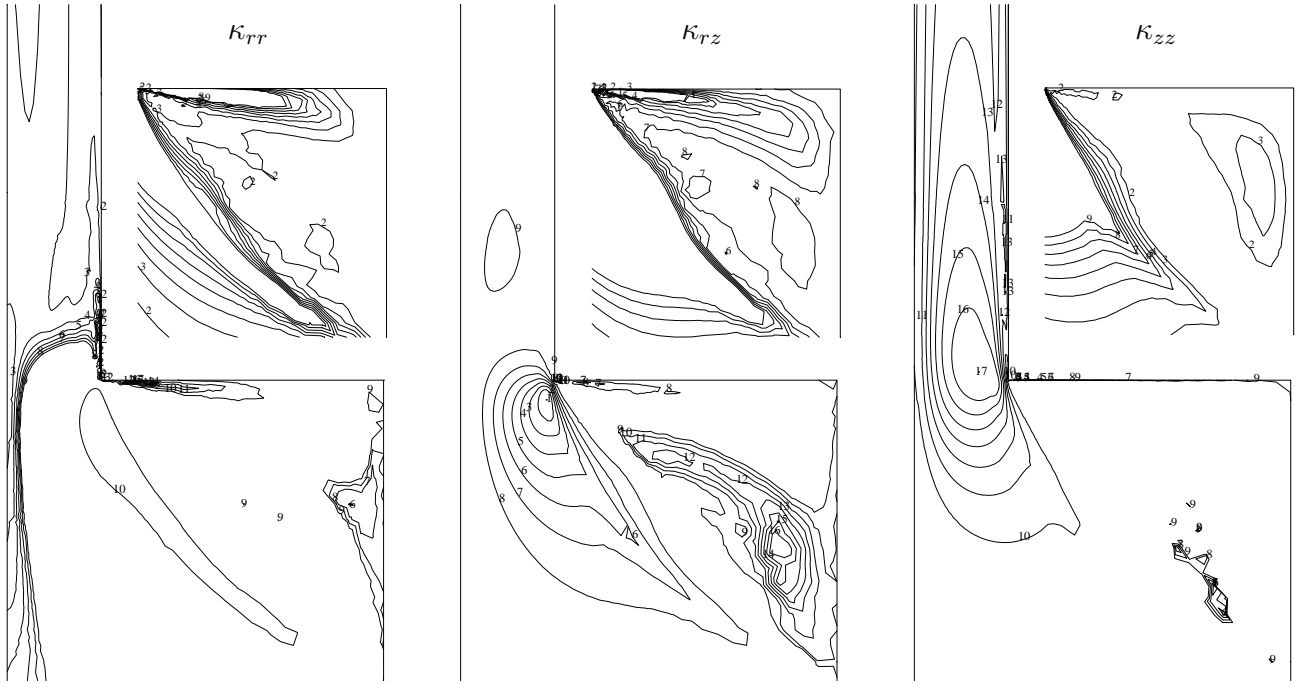
Figure 5.38: Isolines near the contraction, $-5 \leq z/R \leq 6$, for κ_{rr}, κ_{rz} and κ_{zz} for the LDPE melt. The temperature jump equals $\Delta T = 40$ K (case IV of table 5.13). The lines are evenly spaced below and above the isotropic values of the concerned quantity. The isotropic value corresponds to line 8 for κ_{rz} and κ_{zz} and to line 10 for κ_{rz}. The minimum (line 1) and maximum (line 17) values are: $0.69 \leq \kappa_{rr}/\kappa_{\mathrm{eq}} \leq 175$, $-109 \leq \kappa_{rz}/\kappa_{\mathrm{eq}} \leq 3.4$, $0.75 \leq \kappa_{zz}/\kappa_{\mathrm{eq}} \leq 478$. For the figures of the entry corner, $-3 \leq z/R \leq 0$ and $1 \leq r/R \leq 4$, the minimum (line 1) and maximum (line 9) values are evenly spaced between: $0.69 \leq \kappa_{rr}/\kappa_{\mathrm{eq}} \leq 20$, $-12 \leq \kappa_{rz}/\kappa_{\mathrm{eq}} \leq 3.4$, $0.75 \leq \kappa_{zz}/\kappa_{\mathrm{eq}} \leq 54$.

decrease of the stresses in the nonisothermal flow also decreases the vortex intensity and the opening angle. The resulting opening angles β and the vortex intensities I_ψ have been given in table 5.13. The opening angle does not differ much from the isothermal calculations, with the

Table 5.13: Vortex intensity I_ψ, opening angle β and the Deborah number at the temperature at the inflow boundary for the LDPE melt. For the various temperature jumps at the wall, the influence of the anisotropy of the heat conduction tensor has been given. The Deborah number based on the outflow equals $De = 50$.

	ΔT (K)		$I_\psi(\%)$	β(deg)	$De(T_1)$
	0	isotherm	10.9	52	50
I	10	isotropic	10.4	50	38
II	10	anisotropic	10.9	50	38
III	40	isotropic	6.8	42	17
IV	40	anisotropic	7.9	43	17
	0	isotherm	10.0	43	15

Deborah number evaluated at the temperature of the wall at the inflow. The vortex intensities, however, may become considerably smaller. For the isothermal calculations at $De = 15$ the vortex intensity was $I_\psi = 10\,\%$. For the nonisothermal calculations with $\Delta T = 40$ K the vortex intensity is about 2-3 % smaller. The local decrease of the temperature in the entry corner,
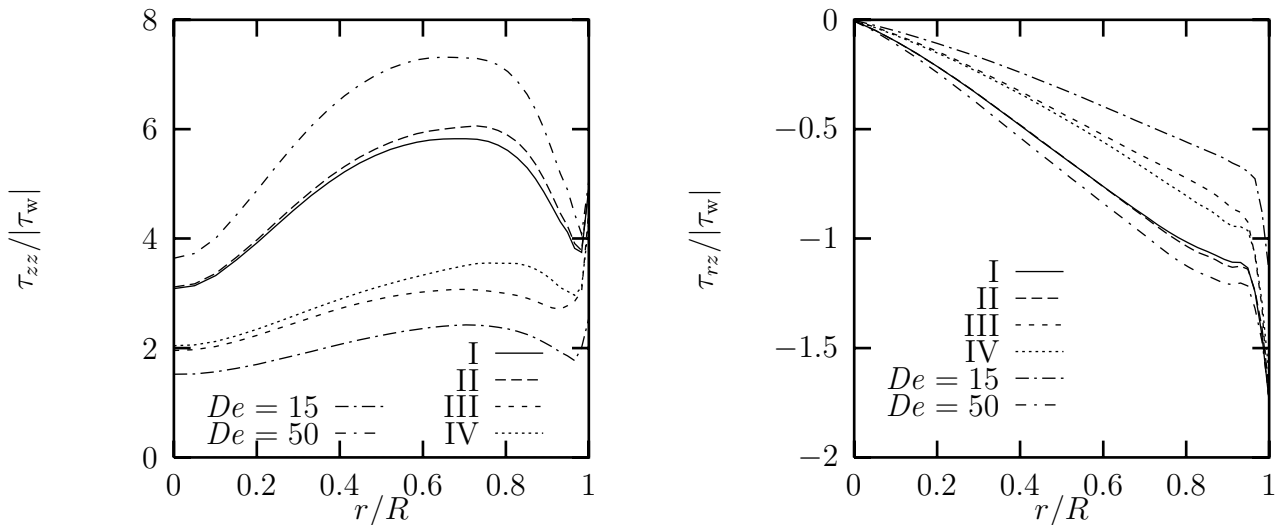
Figure 5.39: Normal stress $\tau_{zz}/|\tau_{\mathrm{w}}|$ and shear stress $\tau_{rz}/|\tau_{\mathrm{w}}|$ of the LDPE melt at $z = 0$ for various temperature jumps ΔT with and without the anisotropy of the heat conduction tensor (see table 5.13). The isothermal stresses for $De = 50$ has been depicted for comparison. The stresses have been normalised with the isothermal wall shear stress τ_{w} at the outflow.

increases the viscosity of the fluid there. If the force of the core flow on the vortex increases less, the temperature is close to $T = T_1$ in almost the complete core flow, this results in a decrease of the vortex intensity.

Polystyrene

For the computations the iteration viscosity has been taken $\eta_{\mathrm{it}} = \eta_0$ and the extra viscosity $\eta_{\mathrm{co}} = \eta_0 - \eta_s$, both at the temperature of the wall at the outflow. The heat conduction tensor will be taken isotropic and independent of the temperature. Furthermore the heat capacity and the density will be taken constant in the convective term of the temperature equation.

For the first problem the influence of the cooling due to expansion and the use of the mechanical dissipation (energy elastic) or the stress work (entropy elastic) will be examined. The Péclet number of the flow equals $Pe = 6.6 \cdot 10^3$ and the temperature at the fixed wall will be taken $T = 463$ K. This means that four cases will be considered: case I with only mechanical dissipation, case II with only the stress work, case III with the mechanical dissipation and the pressure derivative and case IV with the stress work and the pressure derivative.

The temperature isolines for the various examples have been depicted in figure 5.40. Figure 5.40 shows that the cooling due to the pressure decrease, does change the temperature profiles considerably. The temperature in the core flow decreases by 3-4 K and the maximum shifts towards the wall. The influence of the mechanical dissipation, compared to the stress work, is small. Near the contraction the temperature is only a little higher when the stress work is used. This is not because the difference between the mechanical dissipation and the stress work is small. Figure 5.41 shows the differences on lines of constant z near the contraction. Before the contraction the stress work is considerably higher than the mechanical dissipation, particularly for $r/R \leq 0.6$ at $z/R = -1$ where it is about 2.5 time as large. This means that a part of the mechanical energy is stored as elastic energy for case I, while for case II it is stored
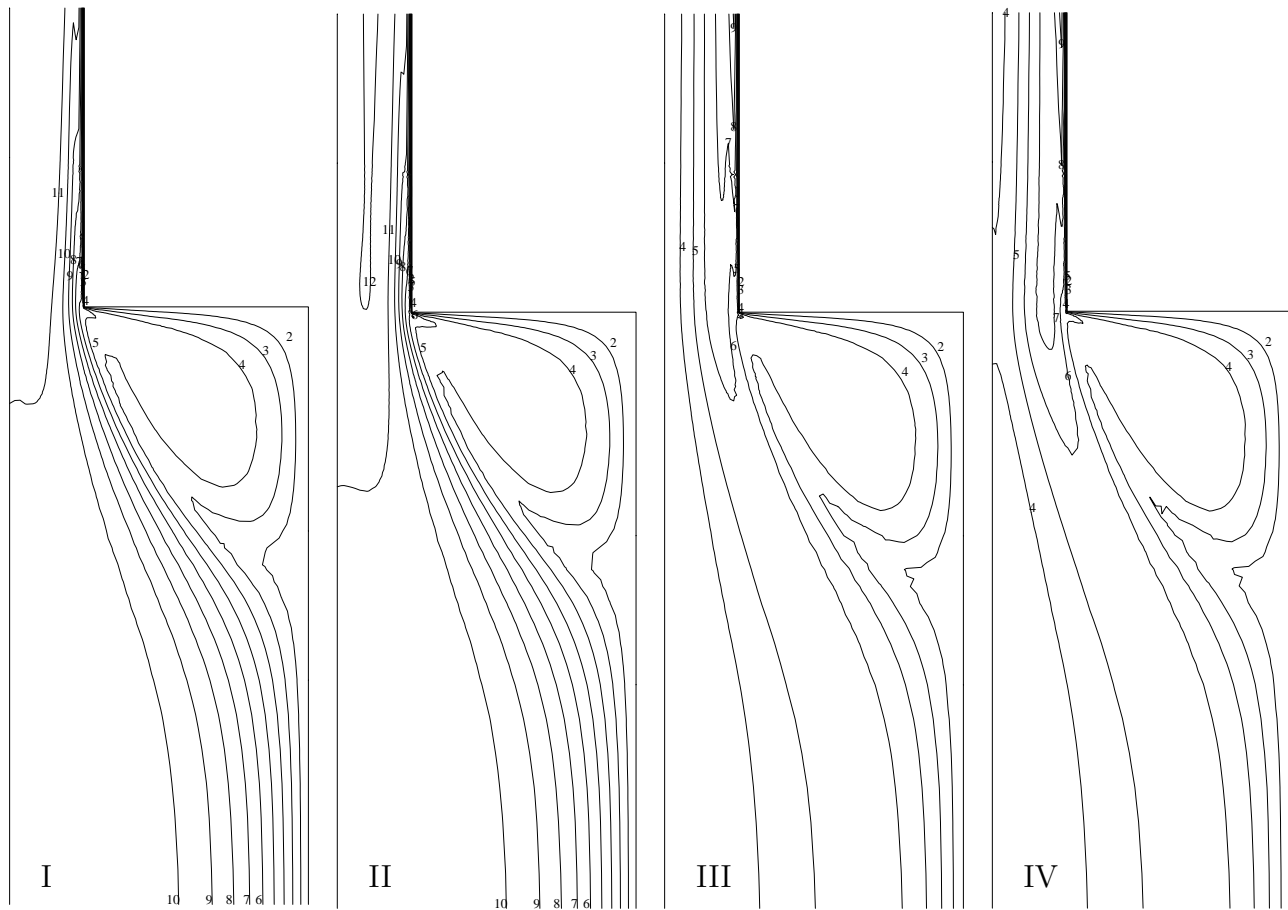
Figure 5.40: Temperature isolines near the contraction, $-8 \leq z/R \leq 4$, of PS for the situations I-IV of table 5.14. The Deborah number equals $De = 200$. The isotherms are evenly spaced between the wall temperature $T_{\mathrm{w}} = 463$ K (line 1) and the maximum temperature $T = 469$ K.

as reversible heat. At $z = 0$ the mechanical dissipation and the stress work have some wiggles and a relatively large peak at $r = 0$. The values have not been shown in figure 5.41 because the large peaks would distort the figure too much. After the contraction the mechanical dissipation decreases relatively slowly in the centre, because the stored elastic energy is released then. The change in the stress work is extremely large between $z/R = -1$ and $z/R = 1$. In contrary to the mechanical dissipation, which has to remain positive, the stress work near the centreline has a rather large negative value. This is caused by the decrease of v_z in the z-direction while the dominant stress τ_{zz} is still positive. Near $r/R = 1$ there is a strong increase near the contraction of both the mechanical dissipation and the stress work. The differences after the contraction, however, are only small. Because of the dominance of the convection, however, even the large differences between the mechanical dissipation and the stress work near the contraction do not result in large temperature differences.

Due to the temperature differences the stresses, which strongly depend on the temperature, will be affected. The normal stress τ_{zz} and the shear stress τ_{rz} at $z = 0$ have been depicted in figure 5.42. As expected the magnitude of the stresses is smaller than for the isothermal
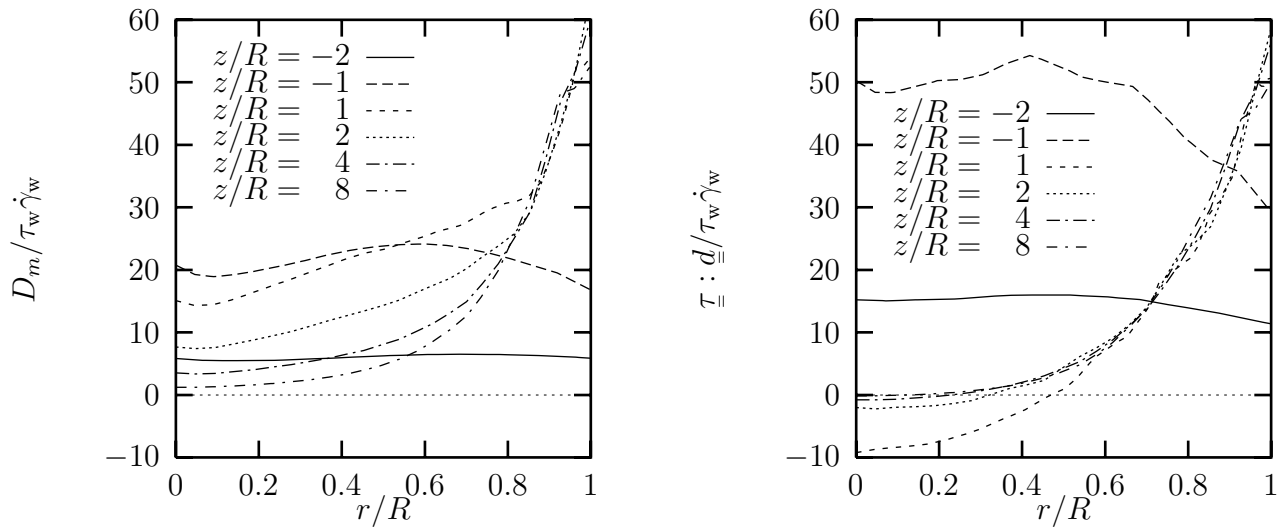
Figure 5.41: Mechanical dissipation (case I) and stress work (case II) at various distances from the contraction for the PS melt. The mechanical dissipation and the stress work have been scaled with the with the isothermal wall shear stress τ_{w} and the isothermal wall shear rate $\dot{\gamma}_{\mathrm{w}}$ at the outflow.
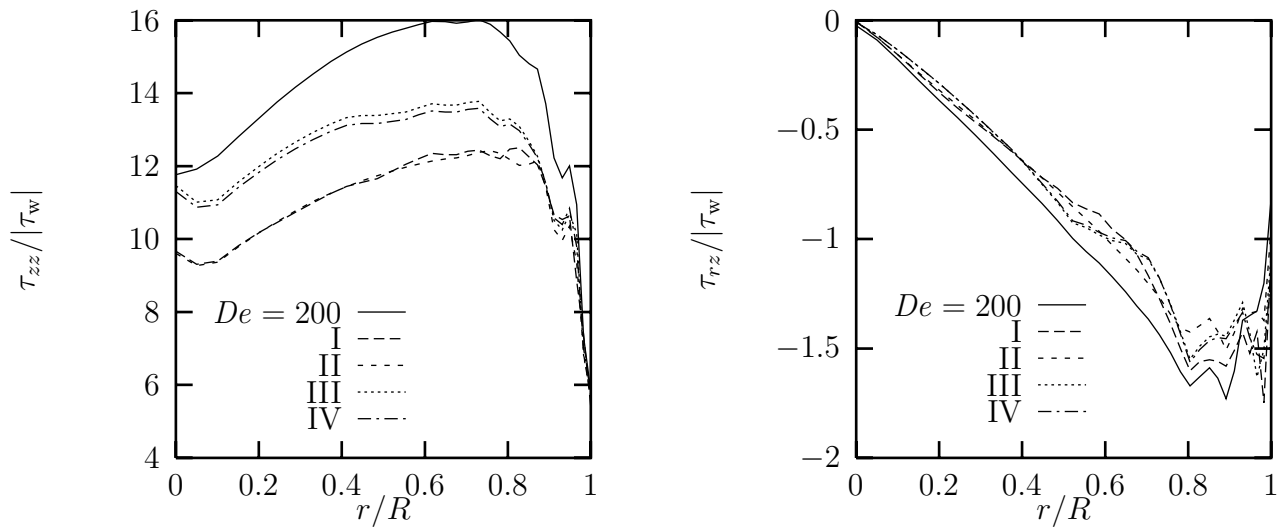

Figure 5.42: Normal stress $\tau_{zz}/|\tau_{\mathrm{w}}|$ and shear stress $\tau_{rz}/|\tau_{\mathrm{w}}|$ at $z = 0$ for the PS melt. The isothermal and nonisothermal flows (case I-IV) for $De = 200$ and $T_{\mathrm{w}} = 463$ have been depicted. The stresses have been normalised with the isothermal wall shear stress τ_{w} at the outflow.

calculation. The shear stress does not differ much for the four nonisothermal calculations. For the normal stress the use of the mechanical dissipation or the stress work has little influence. Compared to the isothermal calculation, however, the normal stresses in the core are considerably lower for the nonisothermal cases. The lower temperatures for case III and IV (with the thermal expansion term) result in higher normal stresses in the core flow, compared to case I and II. Table 5.14 shows the influence of the temperature changes on the vortex intensity and the opening angle. Due to the larger temperature differences between the core flow and the

Table 5.14: Vortex intensity I_ψ, opening angle β, maximum temperature and temperature at the centreline, both at the outflow boundary, for the PS melt. The second column indicates which terms have been taken into account. The Deborah number based on the outflow equals $De = 200$.

		$I_\psi(\%)$	$\beta(\deg)$	$T_{\max} - T_{\mathrm{w}}$ (K)	$T_{\mathrm{ax}} - T_{\mathrm{w}}$ (K)
	isotherm	5.4	50	-	-
I	$D_{\mathrm{m}}^{\mathrm{ve}}$	4.6	47	15.2	5.9
II	$\underline{\underline{\tau}} : \underline{\underline{d}}$	4.4	47	15.3	5.9
III	$D_{\mathrm{m}}^{\mathrm{ve}}, T\alpha_\rho\dot{p}$	5.3	49	13.1	-0.05
IV	$\underline{\underline{\tau}} : \underline{\underline{d}}, T\alpha_\rho\dot{p}$	5.1	49	13.3	-0.04

entry corner the vortex intensities decrease. Particularly for case I and II the decrease is considerable. For case III and IV the temperature difference between the vortex and the core flow is much smaller, which only results in small deviations from the isothermal case. The opening angles for the nonisothermal calculations only decrease weakly compared to $\beta = 50$ deg for the isothermal one. Along the outflow boundary, where the mechanical dissipation and stress work are large, the temperature keeps increasing: about linearly with 1.5 K per $\Delta z = 10R$. The maximum temperatures for all nonisothermal flows are near $r/R = 0.8$, so that the temperature gradient at the wall becomes very large. The width of the peak is about $0.4R$. Near the centreline the temperature remains approximately constant in the z-direction for case I and II. For case III and IV it decreases linearly in the z-direction, about 0.25 K per $\Delta z = 10R$. This means that there is hardly any diffusion of heat towards the centre of the pipe and that there the temperature changes are dominated by the pressure change. The maximum temperature and the temperature at the centreline, both at the outflow boundary, are summarized in table 5.14.

For the second set of calculations the influence of wall cooling has been examined. At the wall along the inflow section three different temperatures have been imposed: $T_1 = 433$ K, $T_1 = 443$ K and $T_1 = 463$ K. The wall at the outflow has been kept at $T_0 = 423$ K so that the resulting temperature jumps at $z = 0$ are $\Delta T = 10$ K, $\Delta T = 20$ K and $\Delta T = 40$ K. These three cases will be denoted by A, B and C respectively. The Péclet number of the flows equals $Pe = 1.0 \cdot 10^3$. For the polystyrene melt the isolines of the temperature have been depicted in figure 5.43. The shape of the boundary layers are similar to the isotropic results for LDPE in figure 5.36. In the entry corner, where the velocity is relatively small, the upstream diffusion is large. Near the corner point at $r = 1$, $z = 0$ the boundary layer is small and the temperature gradient perpendicular to the wall is large. Due to the high Péclet number the boundary layer develops slowly in the outstream section. Because the temperature dependence of the viscosity and the stresses of the polystyrene melt is much stronger than for LDPE, the influence on the normal stress τ_{zz} and the shear stress τ_{rz} is much larger. At $z = 0$ these stresses have been depicted in figure 5.44. The stresses are relative to the wall shear stress τ_{w} at the outflow for the isothermal flow of $De = 200$. For comparison the stresses for the isothermal flow with $De = 3$, which corresponds to the Deborah number calculated with the maximum temperature of 463 K at the inflow boundary, and with $De = 200$, which corresponds to the Deborah number calculated with the temperature of 423 K at the outflow boundary. Particularly, the normal
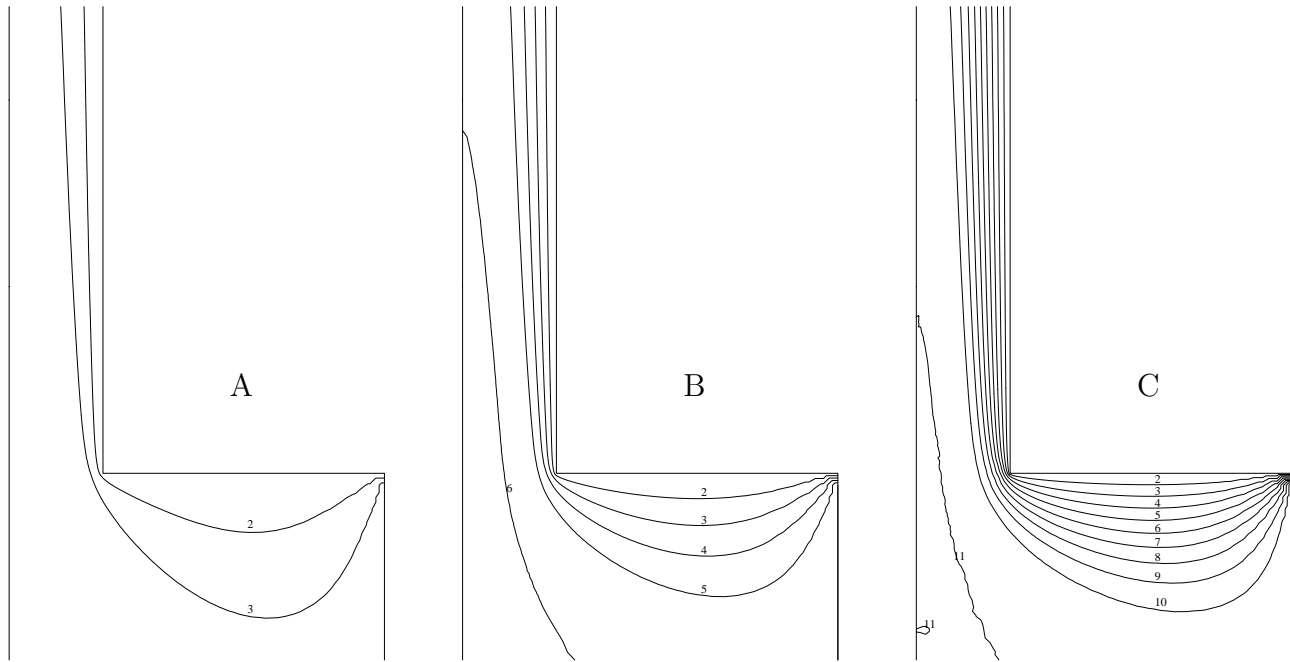
Figure 5.43: Isotherms near the contraction, $-2 \leq z/R \leq 5$, of the PS melt for the various temperature jumps of table 5.15. The temperature at the outflow boundary is $T_0 = 423$ K. Eleven contours are evenly spaced from 423 K (line 1) to 463 K (line 12).
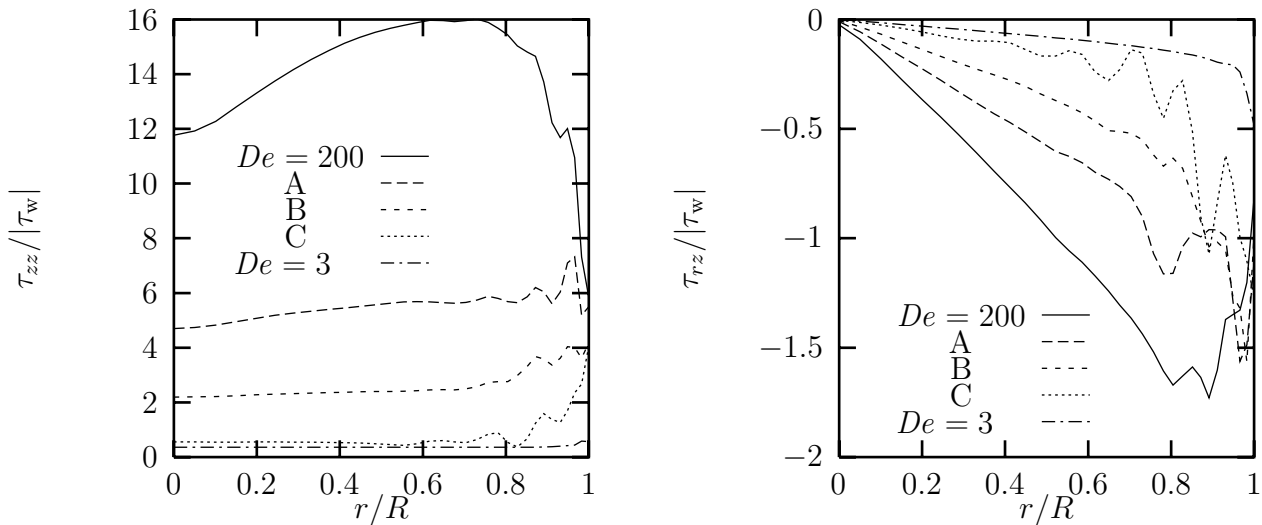
Figure 5.44: Normal stress $\tau_{zz}/|\tau_{\mathrm{w}}|$ and shear stress $\tau_{rz}/|\tau_{\mathrm{w}}|$ at $z = 0$ for the PS melt. Except the nonisothermal flows with the various temperature jumps ΔT, case A-C of table 5.15, the isothermal stresses for $De = 3$ and $De = 200$ have been depicted for comparison. The stresses have been normalized with the isothermal wall shear stress τ_{w} at the outflow.

stress τ_{zz} differs from the isothermal stress profile at a Deborah number of $De = 200$. The local maximum of τ_{zz}, which is present for the isothermal flow with high Deborah numbers, vanishes for the nonisothermal calculations. In the core region the normal stress for $\Delta T = 40$ K

corresponds almost to the isothermal flow at a Deborah number of $De = 3$. Only near the wall, where the temperature is lower, τ_{zz} is significantly larger. The shear stress is also in between the isothermal values of $De = 3$ and $De = 200$. The wiggles are still somewhat larger than for the isothermal calculation at $De = 200$, particularly for the highest temperature jump. Then relatively large wiggles exist near $r/R = 0.5$, where the wiggles are restricted to the region near the wall for the other cases.

The resulting temperature and stress profiles result in the streamline patterns in the entry corner of figure 5.45. The corresponding opening angles β and the vortex intensities I_ψ have

Figure 5.45: Streamline contours of the PS melt for various temperatures of the inflow boundary: successively $T_1 = 423$ K, $T_1 = 433$ K, $T_1 = 443$ K and $T_1 = 463$ K. The temperature at the outflow boundary is $T_0 = 423$ K. Seven contours are evenly spaced from zero to the maximum value and from zero to the minimum value.
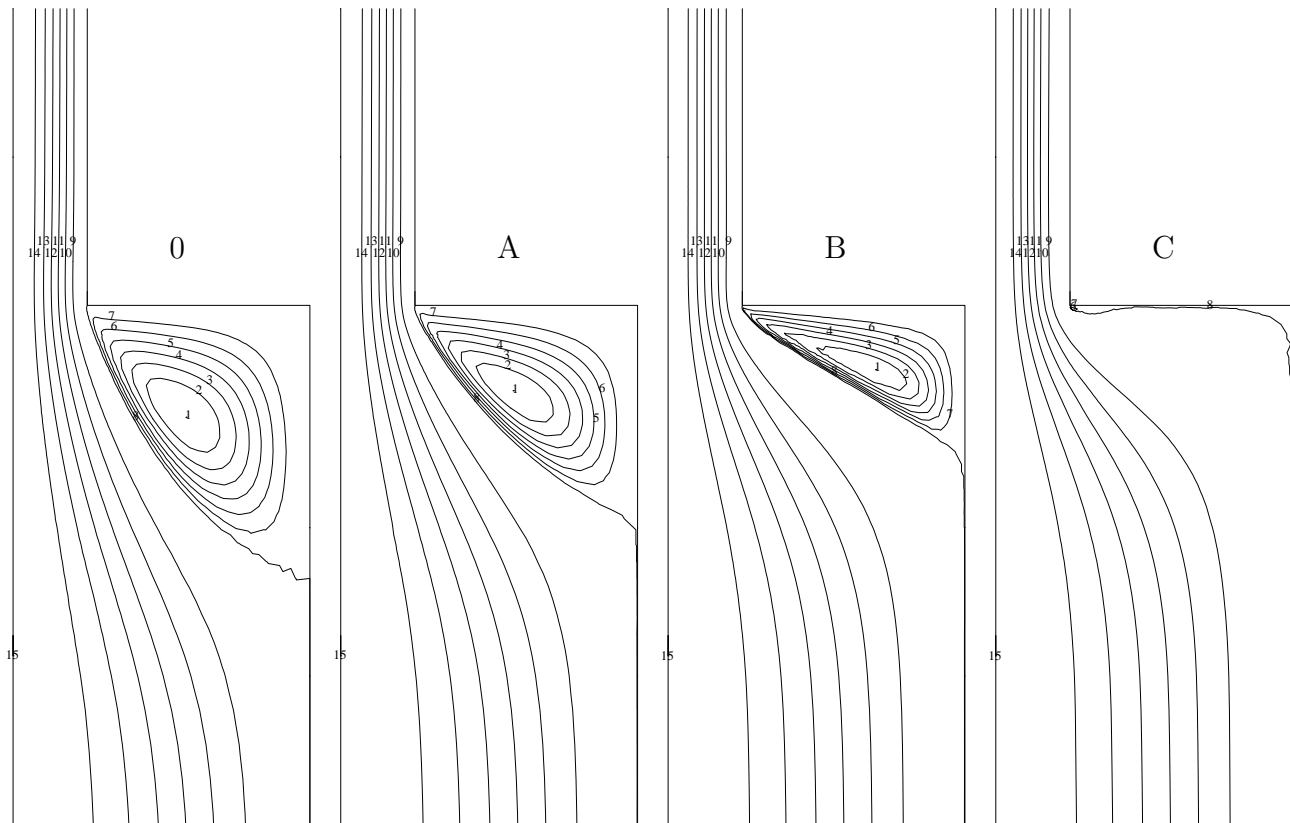
been given in table 5.15. The nonisothermal flow, with a fixed wall temperature of 423 K does not have a significant influence on the vortex compared to the isothermal flow. Only the vortex intensity is somewhat smaller. However, if the inflow boundary is heated, the vortex intensity and the opening angle decrease considerably. This corresponds to the expectations. The temperature distribution near the contraction is strongly non-homogeneous: near the axis of symmetry it is about T_1, the temperature at the wall of the inflow section, and near the wall it is about the wall temperature T_0 at the outflow section. A higher temperature results in smaller relaxation times and, compared to the isothermal flow at $De = 200$, a smaller Deborah number in the core flow. For the isothermal flow of table 5.12 a decrease of the Deborah number corresponded to a decrease of the opening angle and the vortex intensity. However, the vortex

Table 5.15: Vortex intensity I_ψ and opening angle β for different temperatures at the inflow boundary for the flow of the PS melt with $De = 200$. The second column contains the Deborah number $De(T_1)$ for the temperature T_1 at the inflow boundary.

	ΔT (K)	$De(T_1)$	$I_\psi(\%)$	$\beta(\deg)$
0	0	200	5.1	50
A	10	53	3.1	38
B	20	17	0.5	25
C	40	3	–	–

intensity and the opening angle decrease more than could be expected from this analysis. When the temperature jump is increased, the difference becomes larger. At the highest temperature jump of $\Delta T = 40$ K the vortex has even vanished. Probably this is a result of the large temperature gradient near the wall of the contraction at $z = 0$. The relatively large difference in temperature with the main stream cause a much more viscous fluid near the wall (a factor 66 for the highest temperature difference).

5.5 Conclusions

For various flows the influence of the temperature effects has been checked numerically. For LDPE and PS, two polymers with a different temperature dependency of the material functions and a different rheological behaviour, calculations have been performed for a fully developed shear flow, for a Graetz–Nusselt problem and for the flow through a 4:1 contraction, so that a kind of immobile boundary layer near the wall arises.

For the fully developed shear flow the decrease of the temperature due to the thermal expansion term was the most important, compared to the results where only the mechanical dissipation has been taken into account. Particularly for the LDPE melt, for which the thermal expansion coefficient is larger than for PS, the decrease of the temperature near the centreline (until about the wall temperature) was considerable. For the LDPE melt the decrease of the thermal conductivity perpendicular to the flow also caused a considerable temperature rise. For LDPE these large temperature differences did not result in considerable differences in the velocity profiles. The stress profiles did increase somewhat, but by far not as much as for the PS melt, where the decrease of the stress could be more then a decade. Then also the velocity profiles changed. Compared to the isothermal case the velocity at the wall decreases and near the centreline increases correspondingly. The cooling due to the thermal expansion term slightly diminished this effect.

For the Graetz–Nusselt problem the influence of the internal heat production was of minor importance. Due to the dominance of the convection and the cooling at the wall, where the mechanical dissipation may become large, only the convection and the diffusion are important. For PS the changes of the flow rate, and thus the Péclet number, resulted in substantial differences in the temperature and velocity profiles. For the smallest Péclet number the temperature has soon reached its fully developed profile and the maximum velocity on the centreline is close to the temperature jump. For increasing flow rate it takes longer and longer before the temper-

ature profile becomes fully developed. As a consequence the maximum velocity at the axis of symmetry shifts towards the outflow boundary. For the highest flow rate the temperature at the outflow was even far from fully developed. However, still smooth solutions were obtained at he outflow boundary with the help of the special fully developed Neumann boundary conditions. For the flow of LDPE it was remarkable that the thermal conductivity in the direction parallel to the flow became very large. The maximum was about 300 times the thermal conductivity in equilibrium, while the minimum thermal conductivity perpendicular to the flow was about 37 % lower than the equilibrium value.

For the nonisothermal flow through a 4:1 contraction, the temperature changes due to the internal heat production are small for the polyethylene melt. For the polystyrene melt, however, the temperature changes may be considerable. Because the stresses depend strongly on the temperature, the vortex in the entry corner is also influenced. Particularly the vortex intensity decreases compared to the isothermal flow. The use of the stress work or the mechanical dissipation did not have a large effect on the results. The influence of the cooling due to expansion, however, changed the results significantly.

If the wall was cooled from the contraction to the outflow, the magnitude of the vortex and the vortex intensity decreased compared to the isothermal flow. The decrease was even larger than for the corresponding isothermal Deborah number at the highest temperature in the flow. Again the effects were larger for the PS than for the LDPE melt. With the largest temperature difference the vortex even vanished for the polystyrene melt. Compared to an isotropic thermal conductivity, the anisotropy of the thermal conductivity gave a substantial different temperature distribution. In the entry corner the diffusion of heat was larger, which resulted in a larger temperature boundary layer at the start of the outflow section. In the outflow section, however, the temperature boundary layer developed more slowly because of the lower thermal conductivity in the direction perpendicular to the flow.

Chapter 6

Concluding remarks and discussion

In this last section it will be checked how far the objectives have been reached. The objectives mentioned in chapter 1 were twofold. Firstly, the derivation of nonisothermal constitutive equations describing the flow of viscoelastic fluids and secondly the numerical simulation of the obtained equations.

From the thermodynamics of irreversible processes general constitutive equations have been obtained which describe the nonisothermal flow of polymeric fluids. With the introduction of the internal deformation tensors in the thermodynamics, it is possible to obtain the well-known multi-mode differential stress models that have been proposed in the literature and a constitutive equation for the heat flux that is able to describe the anisotropy of the heat conduction. Most of the attention, however, has been paid to the derivation of the temperature equation from the balance of energy for viscoelastic fluids. A good temperature equation is important, because the internal energy production is large due to the high viscosity of polymer melts and concentrated solutions.

The discussion of the results will be split in two parts. Firstly, the various nonisothermal effects which resulted from the thermodynamics, the relations with experiments, and the importance of these terms in the numerical simulations, will be discussed separately. Then the problems in the numerical method for nonisothermal viscoelastic flow will be discussed.

Temperature effects

The various nonisothermal effects resulting from the thermodynamics will be reviewed below. Where possible the influence of these terms in the numerical simulations of chapter 5 will be indicated.

Temperature dependence of the relaxation time and the material functions

The relaxation time and the material functions depend strongly (exponentially) on the temperature (see section 2.5.1) and therefore this dependence is of great importance in nonisothermal flows. For the polystyrene melt, for which the WLF shift factor is valid, the temperature dependence may be extremely large. For the polyethylene melt, for which the Andrade shift factor is valid, the temperature dependence is less strong. Therefore the effects on the stresses and the velocity in the numerical simulations are much larger for the polystyrene melt than for the polyethylene melt. The influence on the velocity field is the most obvious for the fully developed pipe flow (a considerable increase of the velocity near the centreline and a decrease near the wall) and for the flow through a 4:1 contraction. The vortex in the entry corner becomes much smaller when the wall is cooled and even disappears for the highest cooling rate.

Dissipation of mechanical energy

For viscoelastic fluids the mechanical dissipation does not equal the stress work. In section 2.3.3 it has been discussed which part of the mechanical energy is dissipated and which part of the energy is stored reversibly. The right expressions for the mechanical dissipation of the viscoelastic models, including the expressions for incompressible models ($\det \underline{\underline{b}}_k \neq 1$) and for models with a mixed convected derivative, can be determined with the help of the thermodynamics. The results have been summarised in appendix B. A warning is in order here, because in the literature wrong expressions for these type of models have been presented. In the first place one has to be suspicious of the expressions for the incompressible stress models. The contribution of the isotropic term in the relation between the stress and the internal deformation might not be taken into account, which results for example in expressions where the mechanical dissipation does not equal the stress work in steady flows. In the second place one has to be suspicious of the expressions for models with a mixed convected derivative. The non-dissipative slip might contribute to the mechanical dissipation then, but this is not allowed.

Particularly for the fully developed flow, where the convective terms vanish, the influence of the mechanical dissipation is large (a few tens of degrees Kelvin). Although the dissipation of mechanical energy may be large, for both the Graetz–Nusselt problem and the nonisothermal flow through a 4:1 contraction the influence is much smaller, because of the dominance of the convection. Only for the contraction flow of PS without wall cooling the temperature rise was large at the outflow.

Storage of reversible energy

Besides that a part of the mechanical energy is dissipated, another part of is stored reversibly. In section 2.3.3 it has been discussed when the reversible energy may be stored as elastic energy (as for springs) or as reversible entropy (as for rubber bands). For the latter it contributes to the temperature changes (reversibly). For the neo-Hookean stress models this is completely determined by the temperature dependence of the shear modulus. For constant shear moduli all the reversible energy is stored as elastic energy (purely energy elastic). However, if the shear moduli depend linearly on the temperature, the energy is converted into reversible heat (purely entropy elastic).

Only a small amount of experiments (and only on a very few polymers) have been performed to determine whether polymeric fluids are purely entropy elastic, purely energy elastic or something in between. In the purely entropic case the total heat production corresponds exactly to the stress work. Because the difference between the stress work and the mechanical dissipation may be considerable it is important to know the temperature dependence of the moduli for a good description of the nonisothermal flow of viscoelastic fluids. Because it may be difficult to obtain the temperature dependence of the shear modulus from viscometric data, due to the dominating temperature dependence of the relaxation time and viscosity, it might better be measured indirectly. Particularly the relaxation experiment described by Sarti & Esposito (1977/1978) seems a good test for the entropy elasticity, because the temperature must remain constant then, see section 2.5.1. For the other experiment, where they measure the temperature change due to the internal heat production during deformation, things are more difficult because the difference between the mechanical dissipation and the stress work are small for low deformation rates and vanish in steady flows. In the experiments it is not

clear if the difference is large enough. For high deformation rates in unsteady flows, however, it would also be a good test for the energy or entropy elasticity. Another possibility to obtain the temperature dependence of the shear modulus is to measure the anisotropy of the thermal expansion in a deformed polymeric material. For solids this type of experiment has for example been performed by Hellwege et al. (1963), see section 2.5.1. For a neo-Hookean model with a constant modulus, the thermal expansion would be isotropic. A temperature dependent shear modulus, however, causes that the material shrinks in the direction of orientation and it expands in the direction perpendicular to the orientation. It is clear that much more experiments have to be performed to decide whether a polymeric material is energy elastic, entropy elastic or something in between.

In the calculations for the PS melt in a 4:1 contraction with a fixed wall temperature the difference between the stress work and the mechanical dissipation were large near the centreline of the contraction, where the polymer is deformed as in uniaxial elongation. Due to the large convective terms, however, the differences in the temperature distribution were relatively small.

The heat capacity
A subject related to the energy or entropy elasticity is the dependence of the heat capacity on the deformation. As has been shown in section 2.3.3, both effects depend on the existence of cross terms of the internal deformation and the temperature in the free energy. For the neo-Hookean models this means that only when the moduli are constant or when the moduli scale linearly with the temperature and the density, the heat capacity out of mechanical equilibrium equals the heat capacity in equilibrium. Thus only then the heat capacity can be obtained directly from tables with values of the heat capacity at constant pressure. Otherwise, such as for only a linear scaling of the shear moduli with the temperature, the heat capacity depends on the (internal) deformation. Experiments of Sarti & Esposito (1977/1978) showed that for one polymeric material the heat capacity varied during deformation and for some others it remained constant. However, the (elastic) deformation might be too small to obtain measurable effects. It seems recommendable to do some experiments for higher deformation rates, so that the heat capacity difference Δc^{eq}, introduced in section 2.3.3, would be larger.

Temperature changes due to compression and expansion
In section 2.3.3 it has been demonstrated that, just as for gases, the temperature of polymeric fluids changes during expansion (cooling) and compression (heating). Although the effect is not as large as for gases, it is often not negligible for polymeric fluids. Not only in compression or dilatational flows this effect is important, but also in shear flows. In steady shear flows the magnitude of the compression term is about 20 % of the mechanical dissipation, dependent on the magnitude of the thermal expansion coefficient (see section 2.6). In axisymmetrical flows the effect is still more important, because the influence of the cooling term is large near the centreline, where the mechanical dissipation vanishes.

In a fully developed flow this cooling term also causes an of-centreline temperature maximum. The larger the magnitude of the thermal expansion coefficient, the more the maximum moves to the wall and the temperature at the centreline decreases. For LDPE the effects are larger, because its thermal expansion coefficient is larger than for PS. In the convection-dominated Graetz–Nusselt problem and the flow through a 4:1 contraction the influence of this term was small, just as for the mechanical dissipation.

Anisotropy of the heat conduction tensor

In elongational and shear experiments it is observed that the heat conduction is anisotropic in a polymeric fluid, see section 2.4. On the one hand the thermal conductivity in the direction perpendicular to the deformation decreases until a certain lower bound has been reached. On the other hand the thermal conductivity parallel to the deformation increases considerably. In the thermodynamics this anisotropy can be modelled by a dependence of the heat conduction tensor on the elastic deformation (the internal deformation tensors). However, it is difficult to verify the model with experimental results. First of all, the anisotropy has only been measured for a few polymeric fluids. Furthermore, the measurements consist of a relatively small amount of data points either for elongation or for shear flows. This means that it makes no sense to fit the data for multi-mode models, especially when the $(2K + 1)$ heat conduction coefficients are assumed to depend on invariants of the internal deformation tensor. It seems more plausible to take these coefficients as constants. However, then the choice of the stress model becomes important. Most of the stress models predict the increase of the parallel conductivity and the decrease of the perpendicular conductivity in uniaxial elongational flows. In shear flows, however, this type of behaviour may only be described by models having a second normal stress difference, such as the Giesekus, the Leonov and the modified Leonov model. For the most simple anisotropic model, with the anisotropy equally distributed over all modes, the two remaining constants can easily be related to the thermal conductivity in equilibrium and the asymptotic lower bound of the perpendicular thermal conductivity for high deformation rates.

So what is really needed is a good set of measurements of the anisotropy for commonly used polymeric fluids. This means that the anisotropy has to be measured in shear and in elongation flow, because some models predict a different type of behaviour for these flows. Furthermore it is important to obtain the anisotropy for a wide range of deformation rates. Only then a good fit can be made with the multi-mode model described in section 2.4.

In the numerical simulations the relatively small anisotropy of the heat conduction tensor for PS did not have a large influence on the resulting temperature distribution. For the LDPE melt, however, substantial temperature differences were obtained when the anisotropy was taken into account. Except the decrease of the thermal conductivity in the direction perpendicular to the flow, the large values of the parallel thermal conductivity were remarkable.

Nonisothermal rheology

The nonisothermal rheological experiments of Bogue et al. and Sridhar, discussed in section 2.5.2, indicate that the temperature history effect resulting from the temperature dependent relaxation time is not the only thing that matters in the stress constitutive equation. The measurements of Sridhar (on a dilute polymer solution in shear) gave opposite results to the measurements of Bogue et al. (for melts in elongational flow). In the simultaneous heating and shear experiments the stresses were larger than predicted. In the simultaneous cooling and elongational experiment the stresses were also larger than predicted. To obtain clearness in this case the experimental conditions have to be improved and, because of temperature gradients across the fluid, the results have to be compared with the non-isothermal equations including the temperature equation.

Numerical method

Numerical solutions of the flow of viscoelastic fluids could be obtained for flows with high Deborah, Péclet and Brinkman numbers. However, a few problems arose then.

First, the large temperature differences in the flow give some problems. To obtain a convergent solution method for isothermal problems with high Deborah numbers two iteration parameters, an iteration viscosity and an extra viscosity, have been introduced by Hulsen & van der Zanden (1991). For nonisothermal flows with large temperature gradients also an iteration diffusivity, see section 4.3.2, is needed to obtain a convergent solution method. For flows with high Deborah numbers and large temperature gradients a constant iteration viscosity and extra viscosity give some problems. Firstly they have to be chosen very carefully to obtain a convergent solution method at all and when that succeeds the convergence is very slow. Particularly the very temperature dependent polystyrene melt gave rise to problems. The iteration and extra viscosity have to be matched on the lowest temperature, which means that for the high-temperature regions in the flow they are much too large, which causes a very slow convergence. Contrary to the Newtonian model, for which a temperature dependent iteration viscosity gave a considerable acceleration of the convergence rate, a temperature dependent iteration and extra viscosity did not work for the viscoelastic models. So it seems that this problem is inherent in this method for nonisothermal viscoelastic flows.

In the temperature equation the calculation of the mechanical dissipation may cause problems for the models with $\det \underline{\underline{b}}_k \neq 1$. The internal deformation tensor, which is theoretically positive definite, may become indefinite due to numerical errors. Because the mechanical dissipation depends on the inverse of the determinant, this may lead to large errors in the mechanical dissipation. Therefore a method has been developed to calculate the lower bounds of the invariants, see section 3.2. For models with a positive lower bound of the determinant of the internal deformation tensor, the internal deformation tensor may be corrected to a positive definite tensor. For all models described in appendix A, except the 3D Giesekus model, it is possible to find such a lower bound. Then only the stress work of the specific mode can be taken, which makes the Giesekus model less suited for nonisothermal calculations where the mechanical dissipation term is important.

Another problem in the numerical calculations are the high values of the heat capacity and the density of polymeric fluids, which give rise to convection-dominated flows. The first problem concerns the unphysical wiggles for the Galerkin method. As for Newtonian fluids the SUPG upwinding, reviewed in section 4.3, works well. The discontinuity capturing in the direction of the temperature gradient did not work for viscoelastic flows with anisotropic heat conduction. The second problem concerns the outflow boundary conditions. Due to the dominance of the convection, a very long exit length would be required to avoid large wiggles for flows with high Péclet numbers. Furthermore, the simple Neumann boundary conditions for Newtonian fluids (a constant pressure and vanishing normal temperature gradient) do not solve this problem either. Due to the normal stress differences for viscoelastic fluids the constant pressure boundary condition does not work. Therefore an approximation of the normal stress at the outflow boundary has to be calculated somehow. This has been done with the help of a kind of fully developed stress boundary condition at the governing temperature. This procedure results in smooth solutions at the outflow, even for flows with high Deborah and Péclet numbers.

In short, the main difficulty for the numerical simulation of the nonisothermal flow of viscoelastic fluids is not the numerical method itself (for steady flows at least) but the lack of good experimental results. Particularly experimental results of various polymeric materials are needed for the anisotropy of the heat conduction, the entropy or energy elasticity and the dependence of the heat capacity on the deformation. To make a good comparison between the theory and the experiment these experimental results are needed for high deformation rates.

For the numerical simulations itself it seems interesting to consider flows that are less dominated by convection of heat. The influence of the various thermal effects, such as the dissipation of mechanical energy, the cooling due to expansion and the storage of reversible energy, will be much larger then. For the Graetz–Nusselt problem and the flow through a 4:1 contraction these effects were relatively small near the temperature jump and the contraction. Examples could be flows without an inflow and outflow boundary, such as the flow in a Couette viscosimeter and journal bearing lubrication.

References

Akkerman, R. 1993 *Euler–Lagrange simulations of nonisothermal viscoelastic flows.* Dissertation, University of Twente.

Astarita, G. & Sarti, G.C. 1976 The dissipative mechanism in flowing polymers: theory and experiments. *J. Non-Newtonian Fluid Mech.* **1**, 39–50.

Baaijens, F.T.P. 1991 Calculation of residual stresses in injection molded products. *Rheol. Acta* **30**, 284-299.

Barnes, H.A., Hutton, J.F. & Walters, K. 1989 *An introduction to rheology.* Elsevier, Amsterdam.

Beatty, M.F. 1987 Topics in finite elasticity: hyperelasticity of rubber, elastomers and biological tissues – with examples. *Appl. Mech. Rev.* **40**, 1699-1734.

Bird, R.B. 1979 Use of simple molecular models in the study of the mechanical behavior of solutions of flexible macromolecules. *J. Non-Newtonian Fluid Mech.* **5**, 1–12.

Bird, R.B., Armstrong, R.C. & Hassager, O. 1987a *Dynamics of polymeric liquids, vol. 1, Fluid mechanics.* John Wiley & Sons, New York.

Bird, R.B., Curtiss, C.F., Armstrong, R.C. & Hassager, O. 1987b *Dynamics of polymeric liquids, vol. 2, Kinetic theory.* John Wiley & Sons, New York.

Bird, R.B., Stewart, W.E., & Lightfoot, E.N. 1960 *Transport phenomena.* Wiley, New York.

Boger, D.V. 1987 Viscoelastic flows through contractions. *Ann. Rev. Fluid Mech.* **19**, 157-182.

Boyer, R.F. & Spencer, R.S. 1944 *J. Appl. Phys.* **15**, 398–405.

Braun, H. & Friedrich, Chr. 1989 Transient processes in Couette flow of a Leonov fluid influenced by dissipation. *J. Non-Newtonian Fluid Mech.* **33**, 39–51.

Brooks, A. & Hughes, T.J.R. 1982 Streamline upwind/Petrov–Galerkin formulations for convection dominated flows with particular emphasis on the incompressible Navier–Stokes equations. *Comp. Meth. Appl. Mech. Eng.* **32**, 199–259.

Brule, B.H.A.A. van den 1990 The non-isothermal elastic dumbbell: a model for the thermal conductivity of a polymer solution. *Rheol. Acta* **29**, 416-422.

Brule, B.H.A.A. van den & O'Brien S.B.G. 1990 Anisotropic conduction of heat in a flowing polymeric material. *Rheol. Acta* **29**, 580-587.

Bush, M.B. 1989 Prediction of polymer melt extrudate swell using a differential constitutive equation. *J. Non-Newtonian Fluid Mech.* **31**, 179–191.

Callen, H.B. 1960 *Thermodynamics.* John Wiley & Sons, New York.

Carreau, P.J. & Grmela, M. 1991 Conformation tensor rheological models. *Lecture*

Notes in Physics **381**, 126–157.

CHOY, C.L., LUK, W.H. & CHEN, F.C. 1978 Thermal conductivity of highly oriented polyethylene. *Polymer* **19**, 155–162.

CHOY, C.L., ONG, E.L. & CHEN, F.C. 1981 Thermal diffusivity and conductivity of crystalline polymers. *J. Appl. Polym. Sci.* **25**, 2325–2335.

CHRISTIE, I., GRIFFITHS, D.F., MITCHELL, A.R. & ZIENKIEWICZ, O.C. 1976 Finite element methods for second order differential equations with significant first derivatives. *Internat. J. Numer. Meths. Engrg.* **10**, 1389–1396.

CROCHET, M.J. 1989 Numerical simulation of viscoelastic flow: a review. *Rubber Chem. Technol.* **62**, 426–455.

CUVELIER, C., SEGAL, A. & STEENHOVEN, A.A. VAN 1986 *Finite Element Methods and Navier–Stokes Equations.* D. Reidel Publishing Co., Dordrecht.

DIJKSMAN J.F. & KUIKEN, G.D.C. 1995 *Numerical simulation of non-isothermal flow of viscoelastic liquids (proceedings).* Kluwer Academic Publishers, Dordrecht.

FERRY, J.D. 1981 *Viscoelastic properties of polymers (3rd ed.).* Wiley, New York.

FLAMAN, T.A.M. 1990 *Build-up and relaxation of molecular orientation in injection moulding.* Dissertation, Eindhoven University of Technology.

FLAMAN, A.A.M. & VELTMAN, B. 1988 Injection moulding experiments, a challenge to numerical simulation programs. *Rheol. Acta* **26**, 129–131.

FORTIN, A., FORTIN, M. & GERVAIS, J.J. 1991 Complex transition to chaotic flow in a periodic array of cylinders. *Theoret. Comput. Fluid Dynamics* **3**, 79–93.

FORTIN, M. & FORTIN, A. 1985 A generalization of Uzawa's algorithm for the solution of the Navier–Stokes equations. *Communications in Applied Numerical Methods* **1**, 205–208.

GIESEKUS, H. 1982 A simple constitutive equation for polymer fluids on the concept of deformation-dependent tensorial mobility. *J. Non-Newtonian Fluid Mech.* **11**, 69–109.

GODOVSKY, Y.K. 1992 *Thermophysical properties of polymers.* Springer Verlag, Berlin.

GOYAL, S.K., CHU, E. & KAMAL, M.R. 1988 Non-isothermal radial filling of center-gated disc cavities with viscoelastic polymer melts. *J. Non-Newtonian Fluid Mech.* **28**, 373–406.

GROOT, S. R. DE & MAZUR, P. 1984 *Non-equilibrium thermodynamics.* Dover Publications, New York.

GRMELA, M. & CARREAU, P.J. 1987 Conformation tensor rheological models. *J. Non-Newtonian Fluid Mech.* **24**, 271–294.

GUPTA, R.K. & METZNER, A.B. 1982 Modelling of nonisothermal polymer processes. *J. Rheology* **26**, 181–198.

HANDS, D. 1980 The effect of biaxial orientation on the thermal conductivity of vulcanized and unvulcanized rubber. *Rubber Chem. Technol.* **53**, 80–87.

HELLWEGE, K.H., HENNIG, J. & KNAPPE, W. 1963 Anisotropie der Wärmeausdehnung und Wärmeleitung in einachsig verstreckten amorphen Hochpolymeren. *Kolloid ZZ Poly-*

mere **188**, 121–127.

HUGHES, T.J.R. & BROOKS, A. 1982 A theoretical framework for Petrov-Galerkin methods with discontinuous weighting functions: application to the streamline-upwind procedure. In *Finite elements in fluids.* (eds. Gallagher, R.H., Norrir, D.H., Oden, J.T. & Zienkiewicz, O.C.), Vol. 4, Wiley, New York, pp. 47–65.

HUGHES, T.J.R., MALLET, M. & MIZUKAMI, A. 1986 A new finite element formulation for computational fluid dynamics: II. beyond SUPG. *Comp. Meth. Appl. Mech. Eng.* **54**, 341–355.

HULSEN, M.A. 1988a *Computation of a developed flow for non-Newtonian fluids.* Delft University of Technology, Dept. Mech. Eng. & Marine Tech. MEAH79.

HULSEN, M.A. 1988b Some properties and analytical expressions for plane flow of Leonov and Giesekus models. *J. Non-Newtonian Fluid Mech.* **30**, 85–92.

HULSEN, M.A. & VAN DER ZANDEN, J.P.P.M. 1988 Mathematical and physical requirements for successful computations with viscoelastic fluid models. *J. Non-Newtonian Fluid Mech.* **29**, 93–117.

HULSEN, M.A. 1990a *A numerical method for solving steady 2D and axisymmetrical viscoelastic flow problems with an application to inertia effects in contraction flows.* Delft University of Technology, Dept. Mech. Eng. & Marine Tech. MEMT11.

HULSEN, M.A. 1990b A sufficient condition for a positive definite configuration tensor in differential models. *J. Non-Newtonian Fluid Mech.* **38**, 93–100.

HULSEN, M.A. & VAN DER ZANDEN, J.P.P.M. 1991 Numerical simulation of contraction flows using a multi-mode Giesekus model. *J. Non-Newtonian Fluid Mech.* **38**, 183–221.

JONGSCHAAP, R.J.J. 1991 Towards a unified formulation of microrheological models. *Lecture Notes in Physics* **381**, 215–247.

JONGSCHAAP, R.J.J., DE HAAS, K.H. & DAMEN, C.A.J. 1994 A generic matrix representation of configuration tensor rheological models. *J. Rheology* **38**, 769–796.

JOSHI, V.S. & BOGUE, D.C. 1990 Nonisothermal rheological response in amorphous polymers. *J. Rheology* **34**, 1161–1179.

KADIJK, S.E. & BRULE, B.H.A.A. VAN DEN 1994 On the pressure dependence of the viscosity of molten polymers. *Polym. Eng. Sci.* **34**, 1535–1546.

KEUNINGS, R. 1989 Simulation of viscoelastic fluid flow. In *Fundamentals of computer modeling for polymer processing.* (ed. Tucker, C.L. III), Carl Hanser Verlag, pp. 403–469

KREVELEN, D. W. VAN & HOFTYZER, P.J. 1976 *Properties of polymers.* Elsevier, Amsterdam.

KUIKEN, G.D.C. 1994 *Thermodynamics of irreversible processes.* Wiley, Chichester.

LARSON, R.G. 1988 *Constitutive equations for polymer melts and solutions.* Butterworths, Boston.

LEONOV, A.I. 1976 Non-equilibrium thermodynamics and rheology of viscoelastic polymer

media. *Rheol. Acta* **15**, 85–98.

Leonov, A.I. 1987 On a class of constitutive equations for viscoelastic liquids. *J. Non-Newtonian Fluid Mech.* **25**, 1–59.

Leonov, A.I. 1992 Analysis of simple constitutive equations for viscoelastic fluids. *J. Non-Newtonian Fluid Mech.* **42**, 323–350.

Matsui, M. & Bogue, D.C. 1977 Studies in non-isothermal rheology. *Trans. Soc. Rheol.* **21**, 133–148.

Matsumoto, T. & Bogue, D.C. 1977 Non-isothermal rheological response during elongational flow. *Trans. Soc. Rheol.* **21**, 453–468.

McClelland, M.A. & Finlayson, B.A. 1988 Heat transfer effects in extrudate swell of elastic liquids. *J. Non-Newtonian Fluid Mech.* **27**, 363–374.

Nikoleris, T. & Darby, R. 1989 Numerical simulation of the non-isothermal flow of a nonlinear viscoelastic fluid in a rectangular channel. *J. Non-Newtonian Fluid Mech.* **31**, 193–207.

Pearson, J.R.A. 1978 Polymer flows dominated by high heat generation and low heat transfer. *Polym. Eng. Sci.* **18**, 222–229.

Peters, G.W.M. 1995 Thermorheological modelling of viscoelastic materials. In *Numerical simulation of non-isothermal flow of viscoelastic liquids.* (eds. Dijksman, J.F. & Kuiken, G.D.C.), Kluwer Academic Publishers, pp. 21–35

Picot, J.J.C., Goobie, G.I. & Mawhinney, G.S. 1982 Shear-induced anisotropy in thermal conductivity of a polyethylene melt. *Polym. Eng. Sci.* **22**, 154–157.

Pippard, A.B. 1966 *The elements of classical thermodynamics.* Cambridge University Press, Cambridge.

Sarti, G.C. & Esposito, N. 1977/1978 Testing thermodynamic constitutive equations for polymers by adiabatic deformation experiments. *J. Non-Newtonian Fluid Mech.* **3**, 65–76.

Segal, A. 1984 Sepran manuals, Leidschendam.

Sridhar, T. 1988 Non-isothermal rheology of polymer solutions. In X^{th} *international congress on rheology.* (ed. Uhlherr, P.H.T.), Vol. 2, Australian Society of Rheology, Sydney, pp. 288–291.

Sugeng, F., Phan-Thien, N. & Tanner, R.I. 1987 A study of non-isothermal non-Newtonian extrudate swell by a mixed boundary element an finite element method. *J. Rheology* **31**, 37–58.

Tanner, R.I. 1985 *Engineering rheology.* Clarendon Press, Oxford.

Tirtaatmadja, V. & Sridhar, T. 1993 A filament stretching device for measurements of extensional viscosity. *J. Rheology* **37**, 1081–1102.

Treloar, L. 1975 *Physics of rubber elasticity.* Oxford University Press, Oxford.

Truesdell, C. & Noll, W. 1965 *The non-linear field theories of mechanics.* Springer Verlag, Berlin.

Upadhyay, R.K. & Isayev, A.I. 1984 Nonisothermal elongational flow of polymeric fluids

according to the Leonov model. *J. Rheology* **28**, 581–599.

WALLACE, D.J., MORELAND, C. & PICOT, J.J.C. 1985 Shear dependence of thermal conductivity in polyethylene melts. *Polym. Eng. Sci.* **25**, 70–74.

WASHO, B.D. & HANSEN, D. 1969 Heat conduction in linear amorphous high polymers: orientation anisotropy. *J. Appl. Phys.* **7**, 2423–2427.

WHITE, S.A., GOTSIS, A.D. & BAIRD, D.G. 1987 Review of the entry flow problem: experimental and numerical. *J. Non-Newtonian Fluid Mech.* **24**, 121–160.

WHITE, J.L. & KONDO, A. 1977/1978 Flow patterns in polyethylene and polystyrene melts during extrusion through a die entry region: measurement and interpretation. *J. Non-Newtonian Fluid Mech.* **3**, 41–64.

WIEST, J.M. 1989 A differential constitutive equation for polymer melts. *Rheol. Acta* **28**, 4–12.

ZANDEN, J.P.P.M. VAN DER 1989 *Numerical simulation of fluid flow.* Lecture notes, Technical University Delft.

ZANDEN, J.P.P.M. VAN DER 1990 Viscel manual, Leidschendam.

Appendix A

Examples of viscoelastic stress differential models

In this appendix the stress differential equations, which have been implemented in the numerical code, are summarized. They may be written in terms of the internal deformation tensor. The modal stress can be found with the help of (2.19)

$$\underline{\underline{\tau}}_k = \frac{G_k}{1 - \xi_k} \left(B_k \underline{\underline{b}}_k - \underline{\underline{I}} \right). \tag{A.1}$$

The scalar $B_k = 1$ for all models, except for the Larson model. For models having the upper-convected derivative as the convected derivative the parameter ξ_k vanishes: $\xi_k = 0$. A more detailed description of these models and the specific flows for which these models give reasonable predictions, can be found in Tanner (1985) or Larson (1988). The modified Leonov model has been described by Bush (1989).

- *The Johnson–Segalman (quasi-linear) model*

$$\lambda_k \overset{\square}{\underline{\underline{b}}}_k + \underline{\underline{b}}_k - \underline{\underline{I}} = \underline{\underline{0}}. \tag{A.2}$$

  For the special case $\xi_k = 0$ this model reduces to the well-known upper-convected Maxwell model.

- *The Giesekus model*

$$\lambda_k \overset{\triangledown}{\underline{\underline{b}}}_k + \left(\underline{\underline{I}} + \alpha_k \left(\underline{\underline{b}}_k - \underline{\underline{I}} \right) \right) \cdot \left(\underline{\underline{b}}_k - \underline{\underline{I}} \right) = \underline{\underline{0}}, \tag{A.3}$$

  where the mobility parameters $0 \leq \alpha_k < 1$ denote the amount of anisotropic drag, which has been modelled by a dependency on the internal deformation tensor. For $\alpha_k = 0$ the drag is isotropic and the model reduces to the upper-convected Maxwell model. The amount of anisotropy increases with increasing α_k.

- *The Leonov model*

$$\lambda_k \overset{\triangledown}{\underline{\underline{b}}}_k + \frac{1}{2} \left(\underline{\underline{b}}_k^2 - \underline{\underline{I}} - \frac{1}{3} \left(I_{1,k} - I_{2,k} \right) \underline{\underline{b}}_k \right) = \underline{\underline{0}}. \tag{A.4}$$

  This model satisfies the incompressibility condition for the internal deformation tensor, which means that $I_{3,k} = 1$.

- *The modified Leonov model*

$$\lambda_k \overset{\triangledown}{\underline{\underline{b}}}_k + \frac{1}{2} \phi_k (I_{1,k} + I_{2,k}) \left(\underline{\underline{b}}_k^2 - \underline{\underline{I}} - \frac{1}{3} \left(I_{1,k} - I_{2,k} \right) \underline{\underline{b}}_k \right) = \underline{\underline{0}},$$

$$\phi_k^{-1} (I_{1,k} + I_{2,k}) = 1 + \frac{2\alpha_k}{\pi} \arctan \left(\frac{\beta_k}{4} \left(I_{1,k} + I_{2,k} - 6 \right) \right), \tag{A.5}$$

164

where α_k and β_k in the empirical function $\phi_k(I_{1,k} + I_{2,k})$ are parameters to represent elongational flows more realistically than the Leonov model. If $\alpha_k = 0$ or $\beta_k = 0$ the model reduces to the Leonov model. This model also satisfies the incompressibility condition for the internal deformation tensor.

- *The Phan-Thien–Tanner model*

$$\lambda_k \overset{\square}{\underline{\underline{b}}}_k + Y_k(I_{1,k}) \left(\underline{\underline{b}}_k - \underline{\underline{I}}\right) = \underline{\underline{0}}. \tag{A.6}$$

Two forms of Y_k are frequently used:

- The linear Phan-Thien–Tanner model

$$Y_k(I_{1,k}) = 1 + \epsilon_k \left(I_{1,k} - 3\right), \tag{A.7}$$

- The exponential Phan-Thien–Tanner model

$$Y_k(I_{1,k}) = e^{\epsilon_k \left(I_{1,k} - 3\right)}, \tag{A.8}$$

where the constants $\epsilon_k \geq 0$ denotes that longer chains in the network of polymers are destroyed more readily than short ones.

- *The Larson model*[1]

$$\lambda_k \overset{\triangledown}{\underline{\underline{b}}}_k + B_k^{-1}(I_{1,k}) \left(\underline{\underline{b}}_k - \underline{\underline{I}}\right) = \underline{\underline{0}},$$
$$B_k(I_{1,k}) = \left(1 + \frac{\beta_k}{3}\left(I_{1,k} - 3\right)\right)^{-1}. \tag{A.9}$$

Note that the differential equation for the internal deformation tensor is the same as for the linear Phan-Thien–Tanner model. The constants $0 \leq \beta_k \leq 1$ denote the extent of retraction. Polymer chains are supposed to be present in tubelike regions. When the tube has been deformed the chains rapidly retract within the deformed tube. $\beta_k = 0$ corresponds to no retraction (affine motion) and $\beta_k = 1$ to a complete retraction.

---

[1]The representation of the Larson model in terms of the internal deformation tensor can be found by substitution of equation (2.19) in the stress equation described by Larson (1988). The time derivative of the first invariant appearing then, must be eliminated. This can be done by taking the trace of the stress equation and substitution of (2.19). Elimination of the time derivative gives equation (A.9).

Appendix B

The mechanical dissipation of stress differential models

In this appendix a summary will be given of the expression for the mechanical dissipation in (2.64) for the viscoelastic differential models described in appendix A. In fact the results for the differential models of appendix A are identical to the results of a method proposed by Jongschaap (1991,1994)[1]. For that method the positive mechanical dissipation is calculated by splitting the equations in an even and odd part with respect to a macroscopic time reversal.

As will be shown next, the positiveness of the entropy production, and thus the mechanical dissipation, together with the positive definiteness of the internal deformation tensor puts some constraints on the viscosity parameters of the models:

$$
\begin{aligned}
\eta_s &\geq 0, \\
\eta_k &\geq 0.
\end{aligned}
\tag{B.1}
$$

For some non-linear models the positiveness of the dissipation also puts some restrictions on the parameters of the non-linear terms. These restrictions will be mentioned separately for the different models.

- *The Johnson–Segalman (quasi-linear) model*

$$
D_{\mathrm{m}}^{\mathrm{ve}} = 2\eta_s \underline{\underline{d}} : \underline{\underline{d}} + \sum_{k=1}^{K} \frac{G_k}{2(1-\xi_k)^2 \lambda_k} \left(I_{1,k} + \operatorname{tr} \underline{\underline{b}}_k^{-1} - 6 \right),
\tag{B.2}
$$

for $\xi_k \neq 1$. With the help of linear irreversible thermodynamics the mechanical dissipation of the linear model, with the material derivative instead of the convected derivative:

$$
\lambda_k \underline{\underline{\dot{b}}}_k + (\underline{\underline{b}}_k - \underline{\underline{I}}) = \underline{\underline{0}},
\tag{B.3}
$$

can be calculated exactly: $2\lambda_k/G_k D_{\mathrm{m},k}^{\mathrm{ve}} = \operatorname{tr}\left(\underline{\underline{b}}_k - \underline{\underline{I}}\right)^2 = \operatorname{tr}\underline{\underline{b}}_k^2 - 2I_{1,k} + 3$. This is different from expression (B.2), which equals $2\lambda_k/G_k D_{\mathrm{m},k}^{\mathrm{ve}} = \operatorname{tr}\left(\underline{\underline{b}}_k^{-1} \cdot (\underline{\underline{b}}_k - \underline{\underline{I}})^2\right)$. For small deviations from equilibrium $\underline{\underline{b}}_k = \underline{\underline{I}} + \underline{\underline{B}}_k$, with small $\underline{\underline{B}}_k$, the quadratic terms in the convected derivative of the quasi-linear model are small and in the first order approximation it reduces to the linear model. The mechanical dissipation of the linear model then reduces to $2\lambda_k/G_k D_{\mathrm{m},k}^{\mathrm{ve}} = \underline{\underline{B}}_k^2$ and the mechanical dissipation of the quasi-linear model to $2\lambda_k/G_k D_{\mathrm{m},k}^{\mathrm{ve}} = \underline{\underline{B}}_k^2 + \mathcal{O}(\underline{\underline{B}}_k^3)$.

---

[1]Leonov (1992) also gives expressions for the mechanical dissipation of some differential stress models. For the models with $I_{3,k} \neq 1$ his expressions are in error, because he doesn't take into account the isotropic term in 2.19. As a consequence the mechanical dissipation doesn't equal the stress work in fully developed flows then.

Decomposition on the principal axis immediately shows that, for a positive definite internal deformation tensor, the term between the brackets in (B.2) is non-negative (the function $x + 1/x - 2$ is non-negative for $x > 0$). Then it follows from $D_{\mathrm{m}}^{\mathrm{ve}} \geq 0$ that $G_k/\lambda_k = \eta_k/\lambda_k^2$ should be non-negative.

- *The Giesekus model*

$$D_{\mathrm{m}}^{\mathrm{ve}} = 2\eta_s \underline{\underline{d}} : \underline{\underline{d}} + \sum_{k=1}^{K} \frac{G_k}{2\lambda_k} \left((1 - \alpha_k) \left(I_{1,k} + \mathrm{tr}\, \underline{\underline{b}}_k^{-1} - 6 \right) + \alpha_k \left(\underline{\underline{b}}_k : \underline{\underline{b}}_k - 2I_{1,k} + 3 \right) \right). \quad \text{(B.4)}$$

As for the Johnson–Segalman model the term $I_{1,k} + \mathrm{tr}\, \underline{\underline{b}}_k^{-1} - 6$ is always non-negative for a positive definite internal deformation tensor. Decomposition on the principal axis also shows that the last term in (B.4) between the brackets is non-negative (the function $x^2 - 2x + 1$ is non-negative for $x > 0$). This means that if $G_k/\lambda_k = \eta_k/\lambda_k^2$ is non-negative, it follows from $D_{\mathrm{m}}^{\mathrm{ve}} \geq 0$ that $0 \leq \alpha_k \leq 1$. This condition is fulfilled by the constraint given in appendix A for the Giesekus model.

- *The Leonov model*

$$D_{\mathrm{m}}^{\mathrm{ve}} = 2\eta_s \underline{\underline{d}} : \underline{\underline{d}} + \sum_{k=1}^{K} \frac{G_k}{4\lambda_k} \left(\underline{\underline{b}}_k : \underline{\underline{b}}_k - 3 + \frac{I_{1,k}}{3} \left(I_{2,k} - I_{1,k} \right) \right). \quad \text{(B.5)}$$

With the help of the decomposition on the principal axis, and using $I_{3,k} = 1$ and the results of section 3.2.2 that $I_{1,k} \geq 3$ and $I_{2,k} \geq 3$, it can be shown that the term between the brackets in (B.5) is non-negative. From $D_{\mathrm{m}}^{\mathrm{ve}} \geq 0$ it then follows that $G_k/\lambda_k = \eta_k/\lambda_k^2$ should be non-negative.

- *The modified Leonov model*

$$D_{\mathrm{m}}^{\mathrm{ve}} = 2\eta_s \underline{\underline{d}} : \underline{\underline{d}} + \sum_{k=1}^{K} \frac{G_k \phi_k (I_{1,k} + I_{2,k})}{4\lambda_k} \left(\underline{\underline{b}}_k : \underline{\underline{b}}_k - 3 + \frac{I_{1,k}}{3} \left(I_{2,k} - I_{1,k} \right) \right). \quad \text{(B.6)}$$

As for the Leonov model the term between the brackets is always non-negative, because $I_{1,k} \geq 3$ and $I_{2,k} \geq 3$. This means that when $G_k/\lambda_k = \eta_k/\lambda_k$ is non-negative it follows from $D_{\mathrm{m}}^{\mathrm{ve}} \geq 0$ that the function $\phi_k(I_{1,k} + I_{2,k})$ should be non-negative. From (A.5), the definition of ϕ_k, it then follows that $\alpha_k \beta_k \geq 0$.

- *The Phan-Thien–Tanner model*

$$D_{\mathrm{m}}^{\mathrm{ve}} = 2\eta_s \underline{\underline{d}} : \underline{\underline{d}} + \sum_{k=1}^{K} \frac{G_k}{2(1 - \xi_k)^2 \lambda_k} Y_k(I_{1,k}) \left(I_{1,k} + \mathrm{tr}\, \underline{\underline{b}}_k^{-1} - 6 \right), \quad \text{(B.7)}$$

for $\xi_k \neq 1$. As for the Johnson–Segalman model the term $I_{1,k} + \mathrm{tr}\, \underline{\underline{b}}_k^{-1} - 6$ is always non-negative for a positive definite internal deformation tensor. From the positiveness of the dissipation it then follows that $\epsilon_k \geq 0$ for the linear model, which corresponds to the constraint in appendix A. For the exponential model no constraint on ϵ_k can be obtained, because the exponential function Y_k is always positive.

- *The Larson model*

$$D_{\mathrm{m}}^{\mathrm{ve}} = 2\eta_s \underline{\underline{d}} : \underline{\underline{d}} + \sum_{k=1}^{K} \frac{G_k}{2\lambda_k} \left(I_{1,k} - 3 + B_k^{-1}(I_{1,k}) \left(\mathrm{tr}\, \underline{\underline{b}}_k^{-1} - 3 \right) \right). \tag{B.8}$$

After substitution of the definition of B_k, $(A.9)_2$, and reordering of the terms, it follows that the term between the brackets can be written as $(1 - \beta_k) \left(I_{1,k} + \mathrm{tr}\, \underline{\underline{b}}_k^{-1} - 6 \right) + \beta_k \left(\mathrm{tr}\, \underline{\underline{b}}_k^{-1} I_{1,k}/3 - 3 \right)$. As for the Johnson–Segalman model the term $I_{1,k} + \mathrm{tr}\, \underline{\underline{b}}_k^{-1} - 6$ is always non-negative for a positive definite internal deformation tensor. Furthermore it is easy to show that $\mathrm{tr}\, \underline{\underline{b}}_k^{-1} I_{1,k}/3 - 3$ is non-negative. Then it follows that for $0 \le \beta_k \le 1$, which corresponds to the condition mentioned in appendix A, the restriction that the dissipation has to be non-negative is fulfilled.

For plane flow the Giesekus stress model with $\alpha_k = \frac{1}{2}$ equals the Leonov stress model ($I_{1,k} = I_{2,k}$). The mechanical dissipation for the Giesekus model then becomes

$$D_{\mathrm{m}}^{\mathrm{ve}} = 2\eta_s \underline{\underline{d}} : \underline{\underline{d}} + \sum_{k=1}^{K} \frac{G_k}{4\lambda_k} \left(\underline{\underline{b}}_k : \underline{\underline{b}}_k - 3 \right), \tag{B.9}$$

which equals the mechanical dissipation for the Leonov model for plane flow.

Appendix C

Material functions of the modified Leonov model

Bush (1989) claims that the material functions of LDPE melt I may be fitted with a seven-mode modified Leonov model. He gives the parameters $\alpha_k = 3$ and $\beta_k = 4$ for all modes. Figure C.1 shows the shear viscosity, the first normal stress coefficient, and the elongational viscosity for the reference temperature $T = 423$ K. These material functions have been calculated numerically, by solving the fully developed flow equations described in chapter 3. The material functions show relatively large wiggles. This kind of behaviour is not in agreement with the experimental data of LDPE used by Bird et al. (1987a) to fit the eight-mode Giesekus model.
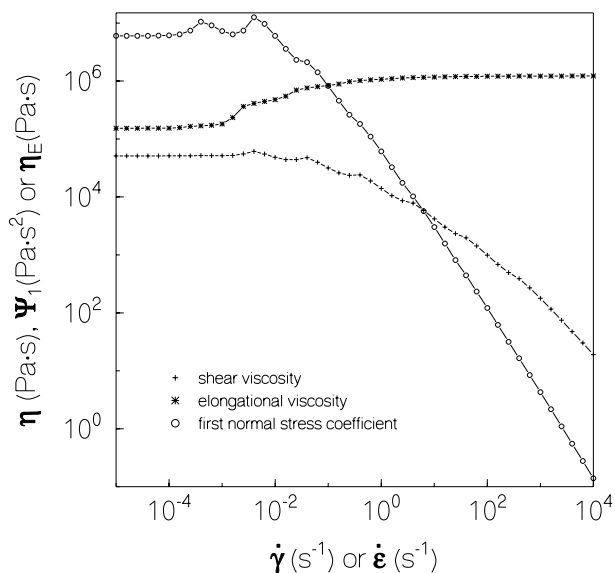

Figure C.1: Material functions of LDPE calculated with the seven-mode modified Leonov model described by Bush (1989). Shear viscosity η and first normal stress coefficient Ψ_1 as a function of the shear rate, and the elongational viscosity η_E as a function of the elongation rate.
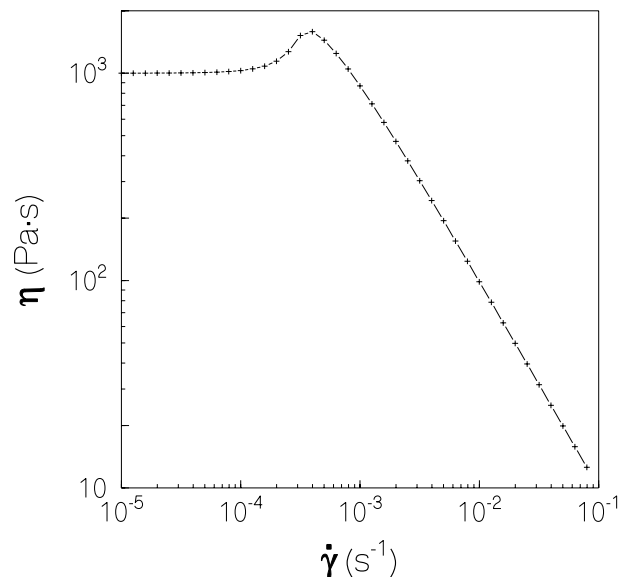
Figure C.2: Calculated shear viscosity η of the first mode of the seven-mode modified Leonov model, described by Bush (1989), as a function of the shear rate.

For the modified Leonov model it is impossible to calculate the shear viscosity explicitly as a function of the shear rate. However, it is possible to show that for small shear rates the shear viscosity increases. For convenience only a one-mode modified Leonov model will be considered. Then the derivative of the shear viscosity is given by

$$\frac{d\eta}{d\dot{\gamma}} = G\frac{db_{12}/\dot{\gamma}}{d\dot{\gamma}} = \frac{G}{\dot{\gamma}}\left(\frac{\lambda(1-b_{12}^2)}{b_{12}d\phi/db_{12} + \phi + 2\lambda\dot{\gamma}b_{12}} - \frac{b_{12}}{\dot{\gamma}}\right), \tag{C.1}$$

169

where the function ϕ defined in (A.5), its derivative with respect to b_{12}, and the shear rate may be written as a function of b_{12} only:

$$\phi^{-1} = 1 + \frac{2\alpha}{\pi} \arctan\left(\beta\left(\frac{1}{\sqrt{1 - b_{12}^2}} - 1\right)\right),$$

$$\frac{d\phi}{db_{12}} = -\phi^2 \frac{2\alpha\beta}{\pi} \frac{1}{1 + \beta^2\left(1 - 1/\sqrt{1 - b_{12}^2}\right)^2} \frac{b_{12}}{(1 - b_{12}^2)^{3/2}} > 0,$$

$$\dot{\gamma} = \frac{\phi}{\lambda} \frac{b_{12}}{1 - b_{12}^2}. \tag{C.2}$$

To write ϕ as a function of b_{12} only the relation $b_{11} + b_{22} = 2/b_{22} = 2/\sqrt{1 - b_{12}^2}$ has been used. The relation between b_{12} and I_1 follows easily from the first two equations in (3.48) and $I_3 = 1$. For small $\lambda\dot{\gamma}$ holds $b_{12} \simeq \lambda\dot{\gamma}$. The derivative of the viscosity (C.1) then equals approximately

$$\frac{d\eta}{d\dot{\gamma}} \simeq \frac{\lambda G}{\dot{\gamma}}\left(\frac{1 - (\lambda\dot{\gamma})^2}{1 + (2 - 3\alpha\beta/\pi)(\lambda\dot{\gamma})^2} - 1\right), \tag{C.3}$$

which is positive for $\alpha\beta > \pi$.

Figure C.2 shows the behaviour of the shear viscosity for one mode. For the first mode only, the shear viscosity has been depicted. Before the shear viscosity becomes less than the zero-shear-rate viscosity at about $\lambda\dot{\gamma} \simeq 1.0$, there is a hump in the shear viscosity with a maximum at $\lambda\dot{\gamma} \simeq 0.5$. The maximum is about 60% higher than the zero-shear-rate viscosity.

Numerical calculations for various values of β gave the following results for the shear viscosity and the first normal stress coefficient. If β is decreased until $\alpha\beta = 2$ the shear viscosity and the first normal stress coefficient are monotonically decreasing functions of the shear rate. If β is decreased until $\alpha\beta = 3$ the shear viscosity is still a monotonically decreasing function of the shear rate. The first normal stress coefficient, however, increased for small $\lambda\dot{\gamma}$. The maximum is about 10% larger then the value of Ψ_1 at $\dot{\gamma} = 0$. If β is decreased until $\alpha\beta = 3.15$ the shear viscosity also increases for small shear rates.

The numerical calculations of the shear viscosity show that one has to be cautious by choosing the parameters α and β. To avoid shear thickening the restriction $\alpha\beta \leq \pi$ has to be fulfilled. To avoid an increase of the first normal stress coefficient $\alpha\beta$ still has to be smaller.

Curriculum vitae

Peter Wapperom werd geboren op 13 december 1967 te Dordrecht.

Het voorbereidend onderwijs werd gevolgd gedurende:

1980 - 1986	Scholengemeenschap Noordendijk te Dordrecht. Het VWO diploma werd behaald in mei 1986.
1986 - 1990	Studie Technische Wiskunde aan de Technische Universiteit Delft; afgestudeerd bij de vakgroep Mathematische Fysica van prof. dr. ir. A.J. Hermans; afstudeerwerk bij TNO-Delft Dienst Grondwaterverkenning met als onderwerp de 3D numerieke simulatie van het opkegelen van water bij de winning van olie uit een olie-waterreservoir. Het diploma werd behaald in november 1990.
1991 - 1995	Assistent in opleiding bij de vakgroep Stromingsleer van de faculteit Werktuigbouwkunde en Maritieme Techniek van de Technische Universiteit Delft. Onder leiding van dr. ir. G.D.C. Kuiken werd onderzoek gedaan naar niet-isotherme stromingen van visco-elastische materialen.